Life in (Fluorescent) Color: Developing Tools for Studying Kinase Activity in Plants

By

Kati A. Seitz

A dissertation submitted in partial fulfillment of

the requirements for the degree of

Doctor of Philosophy

(Genetics)

At the

University of Wisconsin-Madison

2020

Date of final oral examination: August 6th, 2020

This dissertation is approved by the following members of the Final Oral Committee:
Patrick Krysan, Professor, Horticulture
Patrick Masson, Professor, Genetics
Simon Gilroy, Professor, Botany
Marisa Otegui, Professor, Botany
Matthew Merrins, Professor, Medicine

Acknowledgements

I would like to express my sincere gratitude to my research mentor Dr. Patrick Krysan. Thank you for always steering me in the right direction and making sure I never got too far off course. Thank you for letting me be goofy and always checking in when I needed it. Thank you for teaching me the skills to be a better researcher, writer, and person. I am forever grateful that you gave me the opportunity to join your lab—I had a wonderful time.

I would also like to thank the members of my committee for their continuous advice and support. Their feedback has been invaluable for my growth as a researcher. Special thanks to Dr. Patrick Masson, who generously allowed me to perform experiments in his lab, came to so many of my talks, and always had a kind email regarding my progress.

I'd like to thank all of the members of the Krysan lab, both past and present. Thanks to John Seagrist, for being such a wonderful friend and person. I never laughed as much in lab until you came along. Thanks to Nicole Gibbs, who helped me to navigate graduate school and made the Hawaii conference so very enjoyable. Thank you Shih-heng Su, for your mentorship and kindness, your BBQs and funny texts. You always let me know things were going to be okay. And thank you, Chandler Meyer. You are such a joy to work with and I love talking to you about our progress or life in general. You are an awesome graduate student and person and I'm happy I get to be around you for at least a little while longer.

Thanks to my genetics class and the year above, for being such a wonderful support group as we made our way through graduate school. Thank you, Megan Frayer, for always taking the time to chat with me about dogs and Jake from State Farm. Thank you, Joel Serre, for being so upbeat and fun to be around. Thank you, Nik Santistevan, for letting me beat you at trivia, inviting me to your wedding and being the most resilient and empathetic person I know. Thank you Tony Bortolazzo, for your wonderful conversations and sticking with me in plant research. Thank you, Devi Santhosh, for always inviting me to get out of lab and enjoy myself once in a while. Thank you Kassi Crocker and Ali Thompson, for loving Cardinals Baseball and being such wonderful reminders of home. And thank you Khailee Marischuk, in so many ways. Thank you for the book discussions and the Library meetings and the text messages. You have always spread sunshine into my life. I don't know what I did to deserve your friendship, but I'm so glad to have met you. I wish you wonderful times in D.C.

My sincerest gratitude to all the other members of the UW Genetics program for allowing me to pursue a PhD. Special thanks to Martha Reck, for being such a wonderful coordinator. Thank you for assuaging my fears, always being willing to listen, and all the delicious Girl Scout Cookies. You always reminded me it was okay to be a human.

Thanks to the Necomb Imaging Center and Sarah Swanson. Without you, I would not have been able to generate the data necessary for this thesis. Thanks for allowing me to monopolize the

microscope far more than I probably should have and always being willing to help me troubleshoot.

Special thanks to Brian Carrick and Haley Brown. Brian, you are such an empathetic, mature and fun person to be around. I always looked forward to seeing you Tuesday nights for trivia and steak. I wish you all the luck in the world and hope we can see each other in person again soon. Haley, thanks you so much for the dragon cake and always checking in to see how I was doing. I hope things are going well and you're doing great!

Thank you to all of my Como friends for sticking with me through thick and thin. To Chris Soucy, for the movie nights and endless sweets. I will always remember the goldfish and warhead incidents. To Erynn Crawford, for listening to my woes and reminding me to laugh. I'm so glad you were my first real college friend. Special shout-out to Valerie and Gary Crawford, you always made our trips to Chicago wonderful. To Madeline Hodek, for indulging in my silliness and sticking up for me when I couldn't. I am forever in awe of your artistic ability, wit and excellent taste. And to Megan Dowdle. Thank you for the anime nights, soccer matches and endless conversations. Thank you for gushing with me over mutual interests and debating with me when we disagreed. Thank you for introducing me to Brian and Hailey and so many of your wonderful friends. While I never imagined we would end up going to the same graduate school, I'm really glad we did.

And finally, I would like to thank all of my family members for their unwavering support and kind words throughout the years. To Bill and Anne, for always being willing to talk about science or life advice. To Anne and Kai, for opening your home to me in Madison. I really enjoyed getting to know you and everyone else so much more, and you really made me feel like I had a second home. To Grandpa, for reminding me that learning and discovery are endless sources of joy. To Grandma, for your wonderful blankets that kept me warm at night. To Bagel, for always giving me a reason to get up in the morning and to go home at night. To Dad, for stroking my love of baseball and nature—I will always remember those quiet evenings we spent, fishing and chatting. To Tedi, for our mutual rant sessions, your endless support, and always being kind even when it is hard. To Steven, for our gaming sessions, philosophical musings and just being a pretty cool dude. You are both the best younger siblings I could have ever asked for. I am so happy to have gotten the chance to witness the wonderful people you have become and cannot wait to see what you'll do next. To you, Mom. Words will never be able to express how glad I am to have had you as a mother. I always joke about how I literally never would have made it this far without you, but your support, advice and love have kept me afloat in more ways than one. I hope I made you proud, because you inspire me every single day.

Table of Contents

List of Figures

Chapter 1

Chapter 2

Chapter 3

Chapter 4

Chapter 5

List of Tables

Chapter 3

Chapter 4

Life in (Fluorescent) Color: Developing Tools for Studying Kinase Activity in Plants

Kati Seitz
Under the supervision of Dr. Patrick Krysan
University of Wisconsin-Madison

Abstract

Comprehension of the signaling and metabolic networks that underlie the inner workings of a cell relies upon elucidating the complex interactions between the components in an intact biological context. However, conventional methods for studying the inner workings of a cell tend to be destructive and lack the necessary resolution to fully interrogate signaling network dynamics. The imaging of fluorescent proteins in live cells has arisen as a popular alternative approach, allowing minimally intrusive illumination of biological processes through live-cell microscopy. In Chapter 1, I introduce fluorescent biosensors, genetically encoded chimeric proteins that exhibit modulations in fluorescent signal upon recognizing a parameter of interest. Different variants of these biosensors have been used to shed light on the dynamic concentrations of small molecules and metabolites, protein localization and conformation, and even the activity of enzymes such as Mitogen-activated Protein Kinases (MAPKs). Kinase biosensors had been widely employed in numerous model organisms and have provided novel insight into the mechanisms underlying kinase kinetics. However, these tools had not yet been employed within plants. Because of this situation, the Krysan lab initiated a project aimed at developing the first fluorescence-based biosensor for studying kinase activity within *Arabidopsis thaliana*. In order to effectively use this reporter to study MAPK activation in live

plants, however, it was first necessary to the establish an experimental system that allowed live plant samples to be imaged in a minimally stressful environment.

In Chapter 2, I describe a solution to the challenge of establishing an imaging system suitable for studying MAPK activation in Arabidopsis. This work involved repurposing a microfluidic device in order to allow living plant tissue expressing fluorescent biosensors to be gently suspended in an aqueous environment while also allowing for the addition of chemical elicitors during the imaging process. While numerous devices exist to maintain plant tissue in a minimally stressful environment while also allowing application of a solution designed to induce a response, few are designed for rapid addition of consecutive treatments, which can be used to further explore the dynamics of a plant MAPK biosensor. Through repurposing of the HybriWell™, a commercially available device, Arabidopsis whole seedlings, cotyledons, and leaves can be subjected to multiple successive chemical treatments during the process of live-cell confocal imaging. The process of passive pumping allows a complete and swift exchange of the solution surrounding the sample without disturbing the sample or requiring removal from the microscope. In tandem with fluorescent biosensors, our HybriWells™-based imaging protocol allows further exploration of plant MAPK spatiotemporal dynamics by facilitating imaging of signaling networks in both resting and activated states.

Chapter 3 details the work done to create Sensor Of MAPK in Arabidopsis, or SOMA, a Förster resonance energy transfer (FRET) based biosensor. We utilize both *in vitro* and *in vivo* experiments to illustrate how MAPKs can interact with and phosphorylate SOMA. Phosphorylation induces conformation changes that modify the fluorescent properties of SOMA, which can then serve as an indirect measurement of kinase activity. Experiments

utilizing a chemical switch for an inhibitor-sensitive allele of Mitogen-activated Protein Kinase 6 (MPK6) demonstrated NaCl-induced changes in the FRET efficiency of SOMA appear solely derived from MPK3/6 activity, which demonstrates the potential of SOMA to specifically report changes in MAPK activity in living plants. When the FRET behavior of SOMA was observed in response to treatment with biotic and abiotic chemical stressors implicated in MAPK activation, heterogenous changes to the fluorescence signal ratio were observed at the cellular and subcellular levels, illustrating how SOMA can provide novel insights regarding kinase regulation *in planta*. While SOMA serves as a compelling proof-of-concept plant MAPK biosensor, the specificity and performance of this tool could be further improved.

Chapter 4 details the research I performed to create an experimental pipeline for the rapid and efficient development of plant MAPK fluorescent biosensors. The first part of the pipeline is an *in vitro* FRET assay that simplified the biosensor design process such that candidate MAPK docking domain sequences could be inserted into a pre-optimized FRET-based backbone, which we describe as a plant MAPK docking domain trap. Candidate constructs that exhibited a favorable increase in FRET efficiency in response to a MAPK isoform could then be used as a FRET-based biosensor *in vivo*. Application of this docking domain trap offers a potential means to rapidly and efficiently develop new FRET-based biosensors that can be tailored for specific criteria, such as specificity towards specific MAPK isoforms. The second part of this chapter focuses on the development of a fluorescent translocation biosensor for use in Arabidopsis. Translocation biosensors possess a synthetic bipartite Nuclear Localization Signal/Nuclear Exclusion Signal (bNLS/NES) that promotes nuclear export in response to phosphorylation and nuclear import when dephosphorylated. This type of biosensor includes a

kinase docking domain specific for the kinase of interest that allows the sensor to report the activity of a chosen kinase. In this chapter I present *In vivo* experiments utilizing Kinase Localization Reporter (KLR), a translocation biosensor that we developed for use in plants, demonstrated that KLR could exhibit changes in localization within Arabidopsis cells, with evidence strongly suggesting said shift was due to phosphorylation of the reporter. Additionally, incorporating a plant MAPK docking domain verified by the plant MAPK docking domain trap into the KLR backbone culminated in the resulting translocation biosensor exhibiting shifts in localization in response to chemical elicitors known to induce MAPK activity, demonstrating the modularity of the plant MAPK docking domains identified by this method. While more work is needed to determine if KLR specifically reports MAPK activation, these *in vivo* experiments illustrate the potential of this experimental pipeline to expand the toolkit of fluorescent biosensors available for plant MAPK research.

This work encapsulates both the rigorous development, testing, and practical testing necessary to create suitable fluorescent-based biosensors for measuring MAPK activity in Arabidopsis, as well as illustrating how these tools can provide novel insight into the highly dynamic spatiotemporal kinetics of kinase activation in an intact cellular context. The continued development and application of these tools has the potential to further deepen our understanding of the role MAPKs play in plant immunity, development, growth, and other processes, while also potentially offering insight into the complex interactions between these protein kinases and other signaling and metabolic processes.

Chapter 1: The history of genetically encoded fluorescent biosensors

Abstract

Conventional strategies for studying signaling networks have prioritized identification of key players within these pathways. However, in order to fully elucidate the complex mechanism that govern cell function and fate, methods capable of documenting the spatiotemporal dynamics of these molecular components has become more prominent. One such method involves the use of genetically encoded fluorescent biosensors. By serving as visual indicators for a parameter of interest, these tools can illuminate cellular networks in living cells and organisms in real time. Multiple types of fluorescent biosensors have been developed, including single fluorophore protein biosensors, Förster Resonance Energy Transfer (FRET)-based biosensors, and translocation biosensors. These reporters have been used to shed light on a variety of molecular processes, including the activity of protein kinases. Fluorescent biosensors have highlighted the complex regulatory mechanisms by which these ubiquitous proteins are governed in numerous model organisms, including the recent publication of a FRET-based biosensor for studying mitogen-activated protein kinase (MAPK) in Arabidopsis. However, there remains a number of unexplored avenues for further application of MAPK fluorescent biosensors *in planta.*

The work described within this thesis covers the development of the first generation of plant fluorescent biosensors for studying MAPK activity in *Arabidopsis thaliana*. An overview of a select few types of fluorescent biosensors that have been used for studying signal transduction are summarized in this introduction, along with their role in characterizing kinase and MAPK activation and how those benefits may be beneficial for plant MAPK research.

Introduction

In living cells, dynamic interactions between proteins are thought to play a key role in the ability of a cell to relay information regarding pertinent external signals. While many of the key players in these signaling pathways have been identified, questions still remain regarding how the mechanisms by which signal translation is regulated, as differences in the duration, location, or intensity of an initial signal can impact the eventual downstream response (Pozzan et al., 2003; Mehta & Zhang, 2011; Sample et al., 2014). As such, the temporal and spatial context of these pathways is likely an important component of the signaling process. While multiple methods have arisen to contextualize the contents of a cell, such as flow cytometry (Lugli et al., 2010; Aghaeepour et al., 2013; Pedreira et al., 2013; Han et al., 2016) or mass spectrometry (Aebersold & Mann, 2003; Picotti et al., 2012), the crude and destructive nature of these methods can lead to a loss of cellular context and weak or transient signals (Picotti et al., 2012; Han et al., 2016). An alternative method that circumvents these issues involves the use of genetically encoded fluorescent biosensors.

The origin of genetically encoded fluorescent biosensors

A biosensor, in a broad general description, consists of an engineered molecule or cell that can recognize a signal of interest and convert that signal to a visually observable quantity (Mehrotra et al., 2016). Biosensors are generally comprised of two components: a sensory domain and a reporter domain. Detection of the parameter of interest by the sensory domain triggers an adjustment of the reporter domain, which is represented as a quantifiable visual

signal. As such, one of the requirements for a biosensor to function correctly is to be unmodifiable by parameters other than what they are designed to measure. Historically, biosensors have been derived from a range of materials, including enzymes, antibodies, nucleic acids and microbes (Eggeling et al., 2015; Mehrotra et al., 2016; Coulet et al., 2019; Chen & Wang, 2020). However, it was not until the discovery and characterization of fluorescent proteins that the possibility of fluorescent biosensors began to be explored.

Fluorescent proteins are proteins that can emit photons upon excitation at a specific wavelength (Lakowicz, 2013). In the early 1960s, Dr. Osamu Shimomura was researching *Aequorea victoria*, a jellyfish species capable of producing green fluorescence. After isolation and purification, he discovered the bioluminescent aequorin protein. In the presence of Ca2+, purified aequorin produced blue light. However, this emission peak in the blue part of the visible spectrum was decidedly different from the distinct green color of the bioluminescent jellyfish the aequorin was derived from. Shimomura postulated this color change likely derived from another protein, which he had discovered as a byproduct of aequorin isolation and was found highly concentrated together with aequorin in photogenic cells (Shimomura, 1962). As such, it was eventually named Green Fluorescence Protein (GFP) (Hastings & Morin, 1969).

Upon discovery, the utility of GFP as a research tool quickly became apparent. Due to the ability of the protein to spontaneously form a chromophore, GFP fluorescence only required oxygen and did not depend on the presence of enzymes or other auxiliary factors. Additionally, GFP was non-toxic and able to emit on a nanosecond scale (Chalfie et al., 1994). With these attributes, GFP could be used to visualize the essential features of the interior of living cells, real-time, in a non-destructive manner. These benefits resulted in GFP application as

an *in-situ* label for bioactive molecules (Xue et al., 2015). However, this type of labeling possessed several limitations. Experiments involving exogenously applied GFP required samples to be fixed, providing only a single temporal snapshot. It was also difficult to target GFP to a specific location or control penetration into a sample, hindering the fluorophore's ability to reflect target molecule heterogeneity at the cellular or subcellular level. It was not until the cDNA of GFP was sequenced in 1992 (Prasher et al., 1992) and expressed in exogenous organisms in 1994 (Chalfie et al., 1994; Inouye & Tsuji, 1994) that the potential of these proteins could be fully taken advantage of.

Dr. Roger Tsien, one of the leading researchers on fluorescent proteins, demonstrated that select mutations in key residues of GFP could enhance brightness and photostability, as well as modify the emission and excitation range (Heim et al., 1995; Tsien, 1998; Matz et al., 2002). This, along with the development of red fluorescent protein DsRED (Matz et al., 1999; 2002; Campbell et al., 2002) gave rise to a whole array of new fluorescent proteins that together covered a rainbow of colors. This expansion in fluorescent proteins greatly enhanced their ability to be applied in different cellular environments, as well as allowing multiplexing of different fluorescent proteins in the same system (Depry et al., 2013). Dr. Tsien also saw the potential in fluorescent proteins as a way to observe signal dynamics in living cells, publishing the first fluorescent protein biosensor, Cameleon (Miyawaki et al., 1997).

Cameleon is a Genetically Encoded Calcium Indicator (GECI) (Miyawaki et al., 1997) comprised of the calcium binding protein calmodulin, the calmodulin-binding peptide M13, and two fluorescent proteins, CFP and YFP. Binding of Ca2+ to Cameleon induced a quantifiable fluorescent signal change, allowing for the monitoring of free calcium levels within living tissue.

By localizing Cameleon to different subcellular domains, Dr. Tsien was able to document variations in calcium levels among these compartments at a high resolution, illuminating the heterogeneity within these free calcium concentrations and offering insight into how Ca2+ may be involved in network function (Miyawaki et al., 1997). The initial work done with Cameleon demonstrated the potential of fluorescent-based biosensors to illuminate previously unseen aspects of complex signaling networks, and further refinement of Cameleon (including reversible Ca2+ binding) (Miyawaki et al., 1999; Allen et al., 1999) enhanced the biosensor's capabilities.

Fluorescent biosensors contain both a sensory domain and a reporter domain

The initial success of Cameleon led to widespread development and application of fluorescent biosensors. Fluorescent biosensors are fluorescent proteins (the reporter domain) attached to an additional protein sequence (the sensory domain) that induce sensitivity to small biomolecules or other intracellular processes. The sensory domain generally consists of endogenous proteins that naturally interact with the molecule of interest, however, researchers have also successfully engineered new interactive proteins, or modified existing interaction partners to be more selective when necessary. The reporter domain is made up of one or more fluorophores, which can exhibit a change in fluorescent emission (such as intensity, localization, or emission range) in response to the sensory domain coming into contact with the parameter of interest.

Fluorescent-based biosensors that contain discrete fluorophore and sensory domains and are called extrinsic biosensors, as the fluorescent protein needs an extrinsic factor (the

sensory domain) to induce a change in fluorescent signal. There also exists a class in which the fluorescent protein has been engineered to act as both the sensory and reporter domain, known as intrinsic biosensors. The fluorophore of these biosensors can intrinsically interact with some facet of the environment and adjust fluorescent signal in response. An example of these intrinsic biosensors is the pHlourin biosensor, which utilizes a GFP variant capable of exhibiting an alteration in fluorescence in response to pH changes (Miesenböck et al., 1998). As intrinsic fluorescent protein biosensors are not as widely used, the majority of this dissertation will focus on the extrinsic variety. There have been numerous reviews published that cover the field of fluorescent biosensors in extensive detail (Frommer et al., 2009; Okumoto, 2010; Mehrotra, 2016; Bolbat & Schultz, 2017; Ni et al., 2018; Greenwald et al., 2018) so this Chapter will instead focus on three three varieties that are important to my research: single fluorophore biosensors, Förster resonance energy transfer (FRET)-based biosensors, and translocation biosensors.

Single fluorophore biosensors

Single fluorophore biosensors generally consist of a fluorescence protein that that can switch between a fluorescent or non-fluorescent state, such as through circular permutation (cpFP) (Figure 1A). This change is mediated by the sensory domain, which can be further broken into a receiver and a “switch” domain. Interaction between the receiver domain and parameter of interest prompts the “switch” domain to trigger a conformation change in the biosensor. This conformation change results in the cpFP converting from a non-fluorescent to fluorescent state. This conformation change is usually reversible through removal or dissociation of the

parameter of interest, allowing the single fluorescent protein biosensor to reflect both upregulation and downregulation of the parameter of interest.

The conformation change single fluorophore biosensors undergo is relatively rapid—generally on the scale of nanoseconds (hence the colloquial name “nanosensors”), which results in temporal resolution capable of document very transient events, such as calcium signaling cascades (Baird et al., 1999; Nagai et al., 2001; Nakai et al., 2001; Tang et al., 2011). Additionally, as single fluorophore biosensors are only dependent on changes in the signal of a single fluorescent protein (i.e. intensiometric), they can achieve a wide dynamic range (the difference between the resting fluorescent signal and maximum fluorescent signal possible) and high single-to-noise ratio (Hanson et al., 2002). This can result in highly sensitive biosensors, able to provide a fluorescent readout in response to minute changes in the parameter of interest. However, detecting changes in only a single emission range can also be disadvantageous. Due to the lack of an internal control, single fluorophore biosensors tend to be susceptible to optical aberrations or changes in expression or the local environment (Chen et al., 2013; Deng et al., 2015; Ding et al., 2015; Kato et al., 2015). As such, single fluorophore biosensors do not provide absolute quantitative information and can only report relative changes.

Along with calcium, single fluorophore biosensors have been used as reporters of voltage (Siegel & Isacoff 1997; Knöpfel et al., 2003; Barnett et al., 2012; St-Pierre et al., 2014), pH (Bizzarri et al., 2006; Martinière et al., 2013), 3’,5’-cyclic adenosine monophosphate (cAMP) (Kitaguchi et al., 2013; Tewson et al., 2016; Harada et al., 2017), and more recently kinases (Mehta et al., 2018). There have also been single fluorophore biosensors targeted to biological

components unique to plants, such as phytohormones (Brunoud et al., 2012; Larrieu et al., 2015) and activity of some transceptors (De Michele et al., 2013; Ast et al., 2017). Overall, the modular design, ability to be multiplexed, and sensitivity of these biosensors has made them a popular tool for studying signaling dynamics in a number of model organisms.

FRET-based fluorescent biosensors

The second class of fluorescent protein biosensors I will call attention to utilize the principle of Förster (or Fluorescent) Resonance Energy Transfer, or FRET, to report on a parameter of interest. FRET, first described in 1948 (Förster, 1948), describes an exchange of energy between two fluorophores through direct dipole-dipole couplings. In simplified terms, if an excited fluorophore (termed the donor) has an emission range that overlaps with another fluorophore's (the acceptor) excitation range, some of the energy from the donor can transfer to the acceptor in a non-radiative fashion, resulting in acceptor emission without the need for emission of visible light from the donor. The efficiency of that energy transfer (also known as the FRET efficiency) can therefore be defined as the proportion of donor molecules that have transferred excitation state energy to the acceptor molecules (Chen et al., 2006; Frommer et al., 2009). As expected, this ratio is dependent on several factors such as fluorophore orientation and increases as the distance between the acceptor and donor fluorophores decreases (Selvin, 2000; Heyduk et al., 2002, Marx, 2017). The dependency of FRET efficiency on relative distance between fluorophores allows this process to be co-opted for use in fluorescent protein biosensors (Newman et al., 2011; Cardullo, 2013).

In a FRET-based biosensor, the donor-acceptor fluorophores comprise the reporter region, while the sensory region generally contains a sensory domain, which senses the signal of interest, and a "ligand" domain, which possesses affinity for the sensory domain. Each biosensor is designed such that one fluorophore is attached to the sensory domain, and the other is attached to the ligand domain. When the sensory domain interacts with the parameter of interest, this causes an increase in the affinity of the ligand domain for the sensory domain. The ligand and sensory domains are brought into close contact and, subsequently, so are the acceptor and donor fluorophores. This decrease in distance leads to a quantifiable increase in the FRET efficiency of the two fluorophores. Thus, FRET-based imaging can be used to assess fluorophore proximity, and by inference, parameters of interest that can induce shifts in FRET efficiency. Like single fluorescent protein biosensors, this process is usually reversible through removal or dissociation of the targeted signal (Piljić et al., 2011), allowing FRET biosensors to fully document fluctuations in the parameter of interest.

Unlike the intensiometric single fluorescent protein biosensors, FRET-based biosensors are ratiometric: having two fluorophores creates an internal control, normalizing for changes in expression or optical aberrations and allowing for robust quantification of the parameter being detected (Spiering et al., 2013). However, this two-fluorophore design results in FRET-based biosensors tending to possess lower dynamic range and detection sensitivity compared to single fluorophore biosensors (Piljić et al., 2011; Lindenburg & Merkx, 2014). Additionally, FRET-based biosensors require quantification of the emission ranges for two fluorophores, which can require more stringent microscope filters and limits the opportunities for analyzing multiple signaling events within the same cell. Finally, the stringent criteria for a pair of fluorophores to

be capable of undergoing FRET limits the number of available donor-acceptor pairs, although this pool continues to increase due to the development and publication of novel fluorophore variants (Rodriguez et al., 2017). Despite these limitations, however, FRET-based biosensors have been established as valuable tools for quantifying the spatiotemporal dynamics of key components within cellular networks. Currently, FRET-based biosensors can be classified into two groups: intermolecular or intramolecular.

The two types of FRET-based biosensors: intermolecular and intramolecular

For intermolecular FRET biosensors, the two fluorophores are linked to different molecules; each fluorophore is separately connected to either the ligand or sensory domain (Figure 1B). Association with the parameter of interest increases the attraction between the ligand and sensory domains and brings the two fluorophores together. Intermolecular FRET-based biosensors have been used to study apoptosis and cancer (Zlobovskaya et al., 2016), phosphatidylinositol biphosphatate metabolism (Cicchetti et al., 2004), and G-protein-mediated cell signaling (Bu & Callway, 2011). A major benefit of the intermolecular approach is sensitivity—the dynamic range tends to be comparable with that of single fluorescent protein biosensors (Ibraheem & Campbell, 2010). However, expression of the two fusion proteins can differ, or localize asymmetrically to different parts of the cell, which can affect the FRET efficiency (Bajar et al., 2016). Additionally, if the distance and orientation of the fluorophores is not optimal, FRET may not occur even if the two proteins form a complex.

For intramolecular FRET biosensors, the two fluorophores are conjoined to the same molecule (Figure 1C). When the parameter of interest is absent, the biosensor exists in an

"open" conformation—the two fluorophores are kept relatively far apart, and excitation of the donor fluorophore results in low FRET efficiency. However, detection of the targeted signal by the sensory domain results in the biosensor undergoing a conformation change, bringing the donor and acceptor fluorophores closer together. This increase in proximity causes an increase in the FRET efficiency of the biosensor to take place, resulting in a quantifiable indicator of the parameter of interest. Because the biosensor is transcribed as a single mRNA, the ratio of acceptor to donor fluorophore is always equal. However, the larger size of these biosensors can impede localization to some subcellular loci. Intramolecular FRET biosensors also lack in dynamic range and tend to have lower signal-to-noise ratios in comparison to intermolecular or single fluorophore biosensors (Piljić et al., 2011). Nevertheless, numerous intramolecular FRET biosensors have been developed and implemented (Mohsin et al., 2015), including the Cameleon calcium biosensors discussed previously (Miyawaki et al., 1997; Heim & Griesbeck, 2004; Palmer et al., 2006), protease cleavage biosensors (Heim & Tsien, 1996; Mitra et al., 1996) biosensors for plant hormones such as auxin (Herud-Sikimic et al., 2020), gibberellin (Rizza et al., 2019), and abscisic acid (Jones et al., 2014), and several protein kinases biosensors (Zhang et al., 2007; Sato et al., 2007; Komatsu et al., 2011; Morris, 2013; Oldach & Zhang, 2014; Lin et al., 2019).

Why study protein kinases?

Protein kinases have long been implicated in a wide range of biological processes. The common biochemical activity of all protein kinases is reversible post-translational modification of other proteins. These target proteins, known as substrates, possess specific residues, called

phosphoacceptors, onto which a kinase can add a phosphate group. Phosphorylation of a substrate can induce a variety of potential outcomes, from alterations to activity, changes in localization, degradation, or a number of other outcomes (Cohen, 1985; Barford et al., 1998). As such, phosphorylation represents a critical mechanism for regulating cell fate and function and kinases have been implicated in virtually every facet of eukaryotic life, from gene expression, metabolism, proliferation, defense and immunity, and beyond (Robinson & Cobbs, 1997; Hunter, 2000; Johnson & Lapadat, 2002; McCance & Huether, 2014). The widespread involvement in and critical importance of kinases to signaling networks and signal transduction has given rise to multiple questions regarding how these proteins are regulated. Initial experiments using biochemical and genetic approaches were able to determine some of mechanisms that govern kinase specificity (Kobe & Kemp, 2010), such as recruitment of substrates using scaffolding proteins (Pawson & Scott, 1997; Burack & Shaw, 2000; Morrison & Davis, 2003; Meister et al., 2013; Hu et al., 2015) and modular recognition sites present on both kinases and substrates (Pearson & Kemp, 1990; Kemp & Pearson, 1991; Kobe et al., 2005; Ubersax & Ferrell, 2007). However, many of these methods failed to capture the spatiotemporal dynamics displayed by kinases within these pathways, hindering full interrogation. With the advent of genetically encoded fluorescent biosensors, observing these interactions in a cellular context was much more feasible.

A fluorescent biosensor designed to detect kinase activity possesses a sensory domain consisting of a whole or truncated substrate of the target kinase. This substrate domain must also possess at least one amino acid residue capable of undergoing phosphorylation by the kinase of interest, called a phosphoacceptor site or phosphosite. In some cases, conserved

motifs that facilitate kinase-substrate interactions, called docking domains, (Kemp & Pearson, 1990; Sato et al., 2007; Oldach & Zhang, 2014) are also included in the sensory domain to further increase the affinity of kinases for the biosensor. Phosphorylation of the phosphoacceptor elicits a quantifiable change in fluorescent signal, providing a real-time readout of kinase activation. Additionally, these phosphoacceptor sites are usually accessible by phosphatases, which can remove the phosphate group and reverse the signal change of the biosensor (Oldach & Zhang, 2014; Zhang et al., 2015). As such, kinase biosensors can be more accurately described as reporters of the equilibrium between competing target kinase and phosphatase activity. While kinases have been extensively documented in numerous biological systems and contexts with single fluorescent protein and FRET-based biosensors, another classification of biosensors has recently been tailored to report of kinase activity.

Translocation Biosensors

The term translocation biosensor has been historically applied to a class of biosensors that intrinsically relocate to the site of the target signal. These biosensors were generally used to study the production and distribution of lipid messengers (Burd & Emr, 1998; Watton & Downward, 1999; Vaŕnai & Balla, 1998; Gray et al., 1999; Ellson et al., 2001). However, this approach was somewhat restricted by the limited availability of endogenous binding molecules capable of being recruited by specific intracellular targets to drive translocation. While these tools have undergone a recent renaissance due to the emergence of nanobodies (Gonzalez-Sapienza et al., 2017), I will focus on the other classification that utilizes the term: biosensors that, upon detecting the target signal, relocate to a predetermined subcellular destination. To

facilitate this shift in localization, translocation biosensors possess a subcellular localization signal some kind, along with the requisite fluorescent protein reporter domain and sensory domain (Figure 1D). While these tools have been used investigate protease activity and protein-protein interactions (Knauer et al., 2005; Knauer & Stauber, 2005, Spencer et al., 2013), the majority of their utilization has been geared towards detecting phosphorylation (Gu et al., 2004; Kosugi et al., 2008; Regot et al., 2014; Maryu et al., 2016; de la Cova et al., 2017). Due to the presence of modified Nuclear Localization Signals (NLS) and/or Nuclear Exclusion Signals (NES), phosphorylation of a kinase translocation biosensor triggers export of the sensor from the nucleus, while dephosphorylation results in its import to the nucleus. Thus, a phosphorylation-induced change in biosensor localization can serve as a proxy for kinase activity.

The first example of a kinase translocation biosensor was for the mammalian kinase Akt (also known as Protein kinase B) (Gu et al., 2004). This biosensor took advantage of naturally occurring phosphorylation-mediated translocation in the Akt substrate protein PROTEINASE 3 (PR3). Due to this domain, phosphorylation of the Akt biosensor resulted in shuttling from the nucleus to the cytoplasm in response to Akt activity, allowing rapid visualization of Akt activation kinetics (Gu et al., 2004). While a few other translocation biosensors took advantage of this phenomenon (Kosugi et al., 2008; Gross & Rotwein 2015; Maryu et al., 2016), it was not until 2014, when the Regot lab published Kinase Translocation Reporters (KTRs), that an artificially engineered mechanism to facilitate phosphorylation-induced nuclear/cytoplasmic shuttling was described (Regot et al., 2014).

KTR biosensors utilize a unique bipartite nuclear localization signal/nuclear exclusion signal (bNLS/NES) cassette to redirect sensor localization in response to kinase activity, of which the bNLS region contains two phosphorylation sites. In an unphosphorylated state, the bNLS maintains a strong nuclear important signal and KTR fluorescence emission is observed in the nuclei of cells. Phosphorylation of the phosphoacceptor sites negatively regulates the bipartite NLS while also enhancing NES export rate, resulting in KTR fluorescence emission being excluded from the nucleus. Dephosphorylation increases the nuclear import rate and decrease the nuclear export rate, and KTR to return to the nucleus. Localization of KTR can thus be described as a continuous tug-of-war between nuclear localization and nuclear exclusion, with phosphorylation status tipping the balance (Regot et al., 2014)

Translocation biosensors possess several of the same advantages as single fluorescent protein biosensors, offering a generally higher dynamic range and signal-to-noise ratio than FRET-based biosensors. Additionally, translocation biosensors are potentially able to respond more rapidly to downregulation of kinase activity than FRET-based biosensors due to easier access to phosphoacceptor sites for phosphatases (Regot et al., 2014; Sparta et al., 2015). However, these tools are limited by their inability to provide kinase activity measurements in specific subcellular sections, or during degradation of the nucleus. While these biosensors were first demonstrated in mammalian cell lines (Regot et al., 2014; Durandau et al., 2015), recent papers have reported success using translocation biosensors in the additional model organisms *C. elegans* (de la Cova et al., 2017) and zebrafish (Mayr et al., 2018), indicating the bNLS/NES localization system may be applicable to other biological systems such as plants.

When taken as a whole, the application of fluorescent biosensors to kinases in animal model organisms has resulted in the discovery of multiple novel aspects of protein kinases behavior and regulation, including heterogeneity at the subcellular level or within a population of cells (Aoki et al., 2013; Handley et al., 2015; Ma et al., 2019; Lin et al., 2019), alterations in duration, location, or amplitude (Lalonde et al., 2005; Zhang & Allen, 2007), and multiple types of activity profiles, including oscillations, attenuation, ultrasensitivity or switch-like, and graded (Morris, 2013; Lin et al., 2019). However, application of fluorescent biosensors to kinase activity *in planta* has yet to be explored. Physiological differences at the micro- (chlorophyll, chloroplast autofluorescence (Rost, 1995)) or macro- (plant cell wall, vacuole, waxy cuticle) pose significant challenges both for developing novel plant fluorescent biosensors or smoothly transitioning biosensors pioneered in animal systems to *in planta* (Gjetting et al., 2013; Uslu & Grossman, 2016). Despite these challenges, however, as previously mentioned fluorescent protein biosensors for signaling components other than kinases have been established in plants (Sadanandom & Napier, 2010; Martinière et al., 2013; Jones et al., 2013; Walia et al., 2018; Hilleary et al., 2018), including several reporters of plant-specific cellular processes (Jones et al., 2013; Ast et al., 2017). Therefore, in order to import these advantageous tools to the plant kinase research community, the work described in this thesis covers the development of two genetically encoded fluorescent biosensors, a FRET-based biosensor for studying Mitogen-activated Protein Kinase (MAPK) in Arabidopsis (Zaman et al., 2019) and a translocation biosensor for studying protein kinase activity in Arabidopsis (Seitz & Krysan, under review).

Mitogen-activated Protein Kinases (MAPK)

MAPKs are highly conserved kinases that phosphorylate serine or threonine residues (Biondi & Nebreda, 2003). MAPKs belong to a conserved three-tier cascade of kinases which assist in translating of external environmental signals into eventual alterations in cell function and fate (Khokhlatchev et al., 1998). This process begins upon detection of a relevant signal by the appropriate receptor, usually located on the surface of the cell. Interaction between the initial signal and receptor triggers signal transmission to the inner workings of the cell, usually mediated through intermediary signaling molecules. This transmission eventually activates the to the first tier of the appropriate MAPK cascade, which consists of MAPK Kinase Kinase (MAPKKK) proteins. MAPKKKs target and phosphorylate MAPK Kinases (MAPKK), which in turn phosphorylate MAPKs. Activated MAPKs then phosphorylate specific substrates such as transcription factors, which in turn activate the proper downstream response (Chang & Karin, 2001; Jonak et al., 2002). The nature of this signaling cascade is such that the original signal is amplified at each stage, boosting relevant signals and guarding against noise (Ferrell, 1998; Markevich et al., 2004).

Within plants, MAPKs have been implicated in numerous signaling pathways, including those that regulate cell division (Müller et al., 2010; Xu & Zhang, 2015), abiotic and biotic stress responses (Mizoguchi et al., 1996; Felix et al., 1999; Ichimura et al., 2000; Gómez-Gómez & Boller, 2000; Petersen et al., 2001; Frye et al., 2001; Asai et al., 2002; Droillard et al., 2002; 2004; Ahlfors et al., 2004; Teige et al., 2004; Miya et al., 2007; Rasmussen et al., 2012; Meng et al., 2013), developmental patterning (Shinkai et al., 2002; Wang et al., 2008; López-Bucio et al., 2014) and stomatal closure (Liu et al., 2010; Lee et al., 2016). Considering the importance of MAPK signaling for these cellular processes, further interrogation of these protein kinases

should offer insight into the mechanisms by which plant MAPKs function. While the behavior of MAPKs has been widely studied using fluorescent protein biosensors in animal systems (Ma et al., 2019), the use of MAPK-targeted fluorescent protein biosensors in plants had been relatively unexplored (Krysan & Colcombet 2018).

My thesis research covers the design, testing, and application of both a FRET-based MAPK biosensor (Zaman et al., 2019) and a kinase translocation biosensor (Seitz & Krysan, under review) for studying MAPK activity in *Arabidopsis thaliana*. This work represents the first generation of biosensors for studying kinase activation in plants. In addition, I also describe two strategies for facilitating the utilization and further development of these biosensors: a commercially available microfluidic device that can be used as an imaging chamber to apply consecutive chemical treatments to live plant samples during microscopy (Vang et al., 2018), and an *in vitro* FRET-based assay that utilizes a plant MAPK docking domain trap to identify plant MAPK docking domains for use in fluorescent biosensors (Seitz & Krysan, under review). Taken together, the research performed for this thesis resulted in a host of new tools for studying signal transduction in plants, each offering the potential to shed light on MAPK kinetics in Arabidopsis and deepen our understanding of plant signaling networks as a whole.

References

Aebersold, R.; Mann, M. Mass spectrometry-based proteomics. *Nature*. **2003**, *422*, 198-207.

Aghaeepour, N.; Finak, G.; Hoos, H.; Mosmann, T. R.; Brinkman, R.; Gottardo, R.; Scheuermann, R. H. Critical assessment of automated flow cytometry data analysis techniques. *Nature Methods*. **2013**, *10*, 228-238.

Ahlfors, R.; Macioszek, V.; Rudd, J.; Brosché, M.; Schlichting, R.; Scheel, D.; Kangasjärvi, J. Stress hormone-independent activation and nuclear translocation of mitogen-activated

protein kinases in *Arabidopsis thaliana* during ozone exposure. *The Plant Journal*. **2004**, *40*, 512-522.

Allen, G. J.; Kwak, J. M.; Chu, S. P.; Llopis, J.; Tsien, R. Y.; Harper, J. F.; Schroeder, J. I. Cameleon calcium indicator reports cytoplasmic calcium dynamics in Arabidopsis guard cells. *The Plant Journal*. **1999**, *19*, 735-747.

Aoki, K.; Kamioka, Y.; Matsuda, M. Fluorescence resonance energy transfer imaging of cell signaling from *in vitro* to *in vivo*: basis of biosensor construction, live imaging, and image processing. *Development, Growth & Differentiation*. **2013**, *55*, 515-522.

Asai, T.; Tena, G.; Plotnikova, J.; Willmann, M.R.; Chiu, W.L.; Gómez-Gómez, L.; Boller, T.; Ausubel, F.M.; Sheen, J. MAP kinase signalling cascade in Arabidopsis innate immunity. *Nature*. **2002**, *415*, 977-983.

Ast, C.; De Michele, R.; Kumke, M. U.; Frommer, W. B. Single-fluorophore membrane transport activity sensors with dual-emission read-out. *Elife*. **2015**, *4*, e07113.

Ast, C.; Foret, J.; Oltrogge, L. M.; De Michele, R.; Kleist, T. J.; Ho, C. H.; Frommer, W. B. Ratiometric Matryoshka biosensors from a nested cassette of green-and orange-emitting fluorescent proteins. *Nature Communications*. **2017**, *8*, 1-13.

Baird, G. S.; Zacharias, D. A.; Tsien, R. Y. Circular permutation and receptor insertion within green fluorescent proteins. *Proceedings of the National Academy of Sciences*. **1999**, *96*, 11241-11246.

Bajar, B. T.; Wang, E. S.; Zhang, S.; Lin, M. Z.; Chu, J. A guide to fluorescent protein FRET pairs. *Sensors*. **2016**, *16*, 1488.

Barford, D.; Das, A. K.; Egloff, M. P. The structure and mechanism of protein phosphatases: insights into catalysis and regulation. *Annual Review of Biophysics and Biomolecular Structure*. **1998**, *27*, 133-164.

Barnett, L.; Platisa, J.; Popovic, M.; Pieribone, V. A.; Hughes, T. A fluorescent, genetically-encoded voltage probe capable of resolving action potentials. *PloS one*. **2012**, *7*, e43454.

Biondi, R. M.; Nebreda, A. R. Signalling specificity of Ser/Thr protein kinases through docking-site-mediated interactions. *Biochemical Journal*. **2003**, *372*, 1-13.

Bizzarri, R.; Arcangeli, C.; Arosio, D.; Ricci, F.; Faraci, P.; Cardarelli, F.; Beltram, F. Development of a novel GFP-based ratiometric excitation and emission pH indicator for intracellular studies. *Biophysical Journal*. **2006**, *90*, 3300-3314.

Bolbat, A.; Schultz, C. Recent developments of genetically encoded optical sensors for cell biology. *Biology of the Cell*. **2017**, *109*, 1-23.

Brunoud, G.; Wells, D.M.; Oliva, M.; Larrieu, A.; Mirabet, V.; Burrow, A.H.; Beeckman, T.; Kepinski, S.; Traas, J.; Bennett, M.J.; Vernoux, T. A novel sensor to map auxin response and distribution at high spatio-temporal resolution. *Nature*. **2012**, *482*, 103-106.

Bu, Z.; Callaway, D. J. Proteins move! Protein dynamics and long-range allostery in cell signaling. In *Advances in protein chemistry and structural biology.* **2011**, *83*, 163-221.

Burack, W. R.; Shaw, A. S. Signal transduction: hanging on a scaffold. *Current Opinion in Cell Biology*. **2000**, *12*, 211-216.

Burd, C. G.; Emr, S. D. Phosphatidylinositol (3)-phosphate signaling mediated by specific binding to RING FYVE domains. *Molecular Cell*. **1998**, *2*, 157-162.

Campbell, R. E.; Tour, O.; Palmer, A. E.; Steinbach, P. A.; Baird, G. S.; Zacharias, D. A.; Tsien, R. Y. A monomeric red fluorescent protein. *Proceedings of the National Academy of Sciences*. **2002**, *99*, 7877-7882.

Cardullo, R. A. Theoretical principles and practical considerations for fluorescence resonance energy transfer microscopy. In *Methods in Cell Biology*. **2013**, *114*, 441-456

Chalfie, M.; Tu, Y.; Euskirchen, G.; Ward, W. W.; Prasher, D. C. Green fluorescent protein as a marker for gene expression. *Science*. **1994**, *263*, 802-805.

Chang, L.; Karin, M. Mammalian MAP kinase signalling cascades. *Nature*. **2001**, *410*, 37-40.

Chen, C.; Wang, J. Optical biosensors: an exhaustive and comprehensive review. *Analyst*. **2020**, *145*, 1605-1628.

Chen, T.W.; Wardill, T.J.; Sun, Y.; Pulver, S.R.; Renninger, S.L.; Baohan, A.; Schreiter, E.R.; Kerr, R.A.; Orger, M.B.; Jayaraman, V.; Looger, L.L. Ultrasensitive fluorescent proteins for imaging neuronal activity. *Nature*. **2013**, *499*, 295-300.

Cheng, P. C. The contrast formation in optical microscopy. *Handbook of Biological Confocal Microscopy*. **2006.**

Cho, J.H.; Swanson, C.J.; Chen, J.; Li, A.; Lippert, L.G.; Boye, S.E.; Rose, K.; Sivaramakrishnan, S.; Chuong, C.M.; Chow, R.H. The GCaMP-R family of genetically encoded ratiometric calcium indicators. *ACS Chemical Biology*. **2017**, *12*, 1066-1074.

Cicchetti, G.; Biernacki, M.; Farquharson, J.; Allen, P. G. A ratiometric expressible FRET sensor for phosphoinositides displays a signal change in highly dynamic membrane structures in fibroblasts. *Biochemistry*. **2004**, *43*, 1939-1949.

Cohen, P. The role of protein phosphorylation in the hormonal control of enzyme activity. *European Journal of Biochemistry*. **1985**, *151*, 439-448.

Coulet, P. R.; Blum, L. J. (Eds.). Biosensor principles and applications. *CRC Press*. **2019**.

Cristina, M. S.; Petersen, M.; Mundy, J. Mitogen-activated protein kinase signaling in plants. *Annual review of Plant Biology*. **2010**, *61*, 621-649.

de la Cova, C.; Townley, R.; Regot, S.; Greenwald, I. A real-time biosensor for ERK activity reveals signaling dynamics during *C. elegans* cell fate specification. *Developmental Cell*. **2017**, *42*, 542-553.

De Michele, R.; Ast, C.; Loqué, D.; Ho, C.H.; Andrade, S.L.; Lanquar, V.; Grossmann, G.; Gehne, S.; Kumke, M.U.; Frommer, W.B. Fluorescent sensors reporting the activity of ammonium transceptors in live cells. *Elife*. **2013**, *2*, e00800.

Deng, H.; Gerencser, A. A.; Jasper, H. Signal integration by Ca 2+ regulates intestinal stem-cell activity. *Nature*. **2015**, *528*, 212-217.

Depry, C.; Mehta, S.; Zhang, J. Multiplexed visualization of dynamic signaling networks using genetically encoded fluorescent protein-based biosensors. *Pflügers Archiv-European Journal of Physiology*. **2013**, *465*, 373-381.

Ding, G.; Zou, W.; Zhang, H.; Xue, Y.; Cai, Y.; Huang, G.; Chen, L.; Duan, S.; Kang, L. *In vivo* tactile stimulation-evoked responses in *Caenorhabditis elegans* amphid sheath glia. *PloS one*. **2015**, *10*, e0117114.

Droillard, M. J.; Boudsocq, M.; Barbier-Brygoo, H.; Laurière, C. Different protein kinase families are activated by osmotic stresses in *Arabidopsis thaliana* cell suspensions: involvement of the MAP kinases AtMPK3 and AtMPK6. *FEBS Letters*. **2002**, *527*, 43-50.

Droillard, M. J.; Boudsocq, M.; Barbier-Brygoo, H.; Laurière, C. Involvement of MPK4 in osmotic stress response pathways in cell suspensions and plantlets of *Arabidopsis thaliana*: activation by hypoosmolarity and negative role in hyperosmolarity tolerance. *FEBS Letters*. **2004**, *574*, 42-48.

Durandau, E.; Aymoz, D.; Pelet, S. Dynamic single cell measurements of kinase activity by synthetic kinase activity relocation biosensors. *BMC Biology*. **2015**, *13*, 55.

Eggeling, L.; Bott, M.; Marienhagen, J. Novel screening methods—biosensors. *Current Opinion in Biotechnology*. **2015**, *35*, 30-36.

Ellson, C. D.; Anderson, K. E.; Morgan, G.; Chilvers, E. R.; Lipp, P.; Stephens, L. R.; Hawkins, P. T. Phosphatidylinositol 3-phosphate is generated in phagosomal membranes. *Current Biology*. **2001**, *11*, 1631-1635.

Felix, G.; Duran, J. D.; Volko, S.; Boller, T. Plants have a sensitive perception system for the most conserved domain of bacterial flagellin. *The Plant Journal*. **1999**, *18*, 265-276.

Ferrell Jr, J. E. How regulated protein translocation can produce switch-like responses. *Trends in Biochemical Sciences*. **1998**, *23*, 461-465.

Förster, T. Intermolecular energy migration and fluorescence test. *Annalen der Physik*. **1948**, *2*, 55-75

Frommer, W. B.; Davidson, M. W.; Campbell, R. E. Genetically encoded biosensors based on engineered fluorescent proteins. *Chemical Society Reviews*. **2009**, *38*, 2833-2841.

Frye, C. A.; Tang, D.; Innes, R. W. Negative regulation of defense responses in plants by a conserved MAPKK kinase. *Proceedings of the National Academy of Sciences*. **2001**, *98*, 373-378.

Frye, C. A.; Tang, D.; Innes, R. W. Negative regulation of defense responses in plants by a conserved MAPKK kinase. *Proceedings of the National Academy of Sciences*. **2001**, *98*, 373-378.

Gjetting, S. K.; Schulz, A.; Fuglsang, A. T. Perspectives for using genetically encoded fluorescent biosensors in plants. *Frontiers in Plant Science*. **2013**, *4*, 234.

Gómez-Gómez, L.; Boller, T. FLS2: an LRR receptor–like kinase involved in the perception of the bacterial elicitor flagellin in Arabidopsis. *Molecular Cell*. **2000**, *5*, 1003-1011.

Gonzalez-Sapienza, G.; Rossotti, M. A.; Tabares-da Rosa, S. Single-domain antibodies as versatile affinity reagents for analytical and diagnostic applications. *Frontiers in Immunology*. **2017**, *8*, 977.

Gray, A.; Vanderkaay, J.; Downes, C. P. The pleckstrin homology domains of protein kinase B and GRP1 (general receptor for phosphoinositides-1) are sensitive and selective probes for the cellular detection of phosphatidylinositol 3, 4-bisphosphate and/or phosphatidylinositol 3, 4, 5-trisphosphate in vivo. *Biochemical Journal*. **1999**, *344*, 929-936.

Greenwald, E. C.; Mehta, S.; Zhang, J. Genetically encoded fluorescent biosensors illuminate the spatiotemporal regulation of signaling networks. *Chemical Reviews*. **2018**, *118*, 11707-11794.

Gross, S. M.; Rotwein, P. Akt signaling dynamics in individual cells. *Journal of Cell Science*. **2015**, *128*(14), 2509-2519.

Gu, J.; Xia, X.; Yan, P.; Liu, H.; Podust, V. N.; Reynolds, A. B.; Fanning, E. Cell cycle-dependent regulation of a human DNA helicase that localizes in DNA damage foci. *Molecular Biology of the Cell*. **2004**, *15*, 3320-3332.

Han, Y.; Gu, Y.; Zhang, A. C.; Lo, Y. H. Imaging technologies for flow cytometry. *Lab on a Chip*. **2016**, *16*, 4639-4647.

Handly, L. N.; Pilko, A.; Wollman, R. Paracrine communication maximizes cellular response fidelity in wound signaling. *Elife*. **2015**, *4*, e09652.

Hanson, G.T.; McAnaney, T.B.; Park, E.S.; Rendell, M.E.; Yarbrough, D.K.; Chu, S.; Xi, L.; Boxer, S.G.; Montrose, M.H.; Remington, S.J. Green fluorescent protein variants as ratiometric dual emission pH sensors. 1. Structural characterization and preliminary application. *Biochemistry*. **2002**, *41*, 15477-15488.

Harada, K.; Ito, M.; Wang, X.; Tanaka, M.; Wongso, D.; Konno, A.; Hirai, H.; Hirase, H.; Tsuboi, T.; Kitaguchi, T. Red fluorescent protein-based cAMP indicator applicable to optogenetics and in vivo imaging. *Scientific Reports*. **2017**, *7*, 1-9.

Hastings, J. W.; Morin, J. G. Comparative Biochemistry of Calcium-Activated Photoproteins from Ctenophore, Mnemiopsis and Coelenterates Aequorea, Obelia, Pelagia and Renilla. In *Biological Bulletin.* **1969**, *137*, 402.

Heim, N.; Griesbeck, O. Genetically encoded indicators of cellular calcium dynamics based on troponin C and green fluorescent protein. *Journal of Biological Chemistry*. **2004**, *279*, 14280-14286.

Heim, R.; Tsien, R. Y. Engineering green fluorescent protein for improved brightness, longer wavelengths and fluorescence resonance energy transfer. *Current Biology*. **1996**, *6*, 178-182.

Heim, R.; Cubitt, A. B.; Tsien, R. Y. Improved green fluorescence. *Nature*. **1995**, *373*, 663-664.

Herud-Sikimic, O.; Stiel, A. C.; Ortega-Perez, M.; Shanmugaratnam, S.; Höcker, B.; Jürgens, G. Design of a biosensor for direct visualisation of auxin. *BioRxiv*. **2020**

Heyduk, T. Measuring protein conformational changes by FRET/LRET. *Current Opinion in Biotechnology*. **2002**, *13*, 292-296.

Hilleary, R.; Choi, W. G.; Kim, S. H.; Lim, S. D.; Gilroy, S. Sense and sensibility: The use of fluorescent protein-based genetically encoded biosensors in plants. *Current Opinion in Plant Biology*. **2018,** *46*, 32-38.

Hu, J.; Neiswinger, J.; Zhang, J.; Zhu, H.; Qian, J. Systematic prediction of scaffold proteins reveals new design principles in scaffold-mediated signal transduction. *PLoS Comput Biol*. **2015**, *11*, e1004508.

Hunter, T. Signaling—2000 and beyond. *Cell*. **2000**, *100*, 113-127.

Ibraheem, A.; Campbell, R. E. Designs and applications of fluorescent protein-based biosensors. *Current Opinion in Chemical Biology*. **2010**, *14*, 30-36.

Ichimura, K.; Mizoguchi, T.; Yoshida, R.; Yuasa, T.; Shinozaki, K. Various abiotic stresses rapidly activate Arabidopsis MAP kinases ATMPK4 and ATMPK6. *The Plant Journal*. **2000**, *24*, 655-665.

Inouye, S.; Tsuji, F. I. Aequorea green fluorescent protein: Expression of the gene and fluorescence characteristics of the recombinant protein. *FEBS Letters*. **1994**, *341*, 277-280.

Johnson, G. L.; Lapadat, R. Mitogen-activated protein kinase pathways mediated by ERK, JNK, and p38 protein kinases. *Science*. **2002**, *298*, 1911-1912.

Jonak, C.; Ökrész, L.; Bögre, L.; Hirt, H. Complexity, cross talk and integration of plant MAP kinase signalling. *Current Opinion in Plant Biology*. **2002**, *5*, 415-424.

Jones, A. M.; Grossmann, G.; Danielson, J. Å.; Sosso, D.; Chen, L. Q.; Ho, C. H.; Frommer, W. B. *In vivo* biochemistry: applications for small molecule biosensors in plant biology. *Current Opinion in Plant Biology*. **2013**, *16*, 389-395.

Jones, A. M.; Danielson, J. Å.; ManojKumar, S. N.; Lanquar, V.; Grossmann, G.; Frommer, W. B. Abscisic acid dynamics in roots detected with genetically encoded FRET sensors. *Elife*. **2014**, *3*, e01741.

Kato, S.; Kaplan, H.S.; Schrödel, T.; Skora, S.; Lindsay, T.H.; Yemini, E.; Lockery, S.; Zimmer, M. Global brain dynamics embed the motor command sequence of Caenorhabditis elegans. *Cell*. **2015**, *163*, 656-669.

Kemp, B. E.; Pearson, R. B. Protein kinase recognition sequence motifs. *Trends in Biochemical Sciences*. **1990**, *15*, 342-346.

Khokhlatchev, A. V.; Canagarajah, B.; Wilsbacher, J.; Robinson, M.; Atkinson, M.; Goldsmith, E.; Cobb, M. H. Phosphorylation of the MAP kinase ERK2 promotes its homodimerization and nuclear translocation. *Cell*. **1998**, *93*, 605-615.

Kitaguchi, T.; Oya, M.; Wada, Y.; Tsuboi, T.; Miyawaki, A. Extracellular calcium influx activates adenylate cyclase 1 and potentiates insulin secretion in MIN6 cells. *Biochemical Journal*. **2013**, *450*, 365-373.

Knauer, S. K.; Stauber, R. H. Development of an Autofluorescent Translocation Biosensor System To Investigate Protein− Protein Interactions in Living Cells. *Analytical Chemistry*. **2005**, *77*, 4815-4820.

Knauer, S. K.; Moodt, S.; Berg, T.; Liebel, U.; Pepperkok, R.; Stauber, R. H. Translocation biosensors to study signal-specific nucleo-cytoplasmic transport, protease activity and protein–protein interactions. *Traffic*. **2005**, *6*, 594-606.

Knöpfel, T.; Tomita, K.; Shimazaki, R.; Sakai, R. Optical recordings of membrane potential using genetically targeted voltage-sensitive fluorescent proteins. *Methods*. **2003**, *30*, 42-48.

Kobe, B.; Kemp, B. E. Principles of Kinase Regulation. In *Handbook of Cell Signaling*. **2010**, 559-563.

Kobe, B.; Kampmann, T.; Forwood, J. K.; Listwan, P.; Brinkworth, R. I. Substrate specificity of protein kinases and computational prediction of substrates. *Biochimica et Biophysica Acta (BBA)-Proteins and Proteomics*. **2005**, *1754*, 200-209.

Komatsu, N.; Aoki, K.; Yamada, M.; Yukinaga, H.; Fujita, Y.; Kamioka, Y.; Matsuda, M. Development of an optimized backbone of FRET biosensors for kinases and GTPases. *Molecular Biology of the Cell*. **2011**, *22*, 4647-4656.

Kosugi, S.; Hasebe, M.; Tomita, M.; Yanagawa, H. Nuclear export signal consensus sequences defined using a localization-based yeast selection system. *Traffic*. **2008**, *9*, 2053-2062.

Krebs, M.; Held, K.; Binder, A.; Hashimoto, K.; Den Herder, G.; Parniske, M.; Kudla, J.; Schumacher, K. FRET-based genetically encoded sensors allow high-resolution live cell imaging of Ca2+ dynamics. *The Plant Journal*. **2012**, *69*, 181-192.

Krysan, P. J.; Colcombet, J. Cellular complexity in MAPK signaling in plants: Questions and emerging tools to answer them. *Frontiers in Plant Science*. **2018**, *9*, 1674.

Lakowicz, J. R. Principles of fluorescence spectroscopy. *Springer Science & Business Media*. **2013**.

Lalonde, S.; Ehrhardt, D. W.; Frommer, W. B. Shining light on signaling and metabolic networks by genetically encoded biosensors. *Current Opinion in Plant Biology*. **2005**, *8*, 574-581.

Larrieu, A.; Champion, A.; Legrand, J.; Lavenus, J.; Mast, D.; Brunoud, G.; Oh, J.; Guyomarc'h, S.; Pizot, M.; Farmer, E.E.; Turnbull, C. A fluorescent hormone biosensor reveals the dynamics of jasmonate signalling in plants. *Nature Communications*. **2015**, *6*, 1-9.

Lee, Y.; Kim, Y. J.; Kim, M. H.; Kwak, J. M. MAPK cascades in guard cell signal transduction. *Frontiers in Plant Science*. **2016**, *7*, 80.

Lin, W.; Mehta, S.; Zhang, J. Genetically encoded fluorescent biosensors illuminate kinase signaling in cancer. *Journal of Biological Chemistry*. **2019**, *294*, 14814-14822.

Lindenburg, L.; Merkx, M. Engineering genetically encoded FRET sensors. *Sensors*. **2014**, *14*, 11691-11713.

Liu, Y. K.; Liu, Y. B.; Zhang, M. Y.; Li, D. Q. Stomatal development and movement: the roles of MAPK signaling. *Plant Signaling Behavior*. **2010**, *5*, 1176-1180.

López-Bucio, J.S.; Dubrovsky, J.G.; Raya-González, J.; Ugartechea-Chirino, Y.; López-Bucio, J.; de Luna-Valdez, L.A.; Ramos-Vega, M.; León, P.; Guevara-García, A.A. *Arabidopsis thaliana* mitogen-activated protein kinase 6 is involved in seed formation and modulation of primary and lateral root development. *Journal of Experimental Botany*. **2014**, *65*, 169-183.

Lugli, E.; Roederer, M.; Cossarizza, A. Data analysis in flow cytometry: the future just started. *Cytometry Part A*. **2010**, *77*, 705-713.

Ma, M.; Bordignon, P.; Dotto, G. P.; Pelet, S. Visualizing cellular heterogeneity by quantifying the dynamics of MAPK activity in live mammalian cells with synthetic fluorescent biosensors. *bioRxiv*. **2019**, 760652.

MacKeigan, J. P.; Murphy, L. O.; Dimitri, C. A.; Blenis, J. Graded mitogen-activated protein kinase activity precedes switch-like c-Fos induction in mammalian cells. *Molecular and Cellular Biology*. **2005**, *25*, 4676-4682.

Markevich, N. I.; Hoek, J. B.; Kholodenko, B. N. Signaling switches and bistability arising from multisite phosphorylation in protein kinase cascades. *The Journal of Cell Biology*. **2004**, *164*, 353-359.

Martinière, A.; Desbrosses, G.; Sentenac, H.; Paris, N. Development and properties of genetically encoded pH sensors in plants. *Frontiers in Plant Science*. **2013**, *4*, 523.

Marx, V. Probes: FRET sensor design and optimization. *Nature Methods*. *2017*, *14*, 949-953.

Maryu, G.; Matsuda, M.; Aoki, K. Multiplexed fluorescence imaging of ERK and Akt activities and cell-cycle progression. *Cell Structure and Function*. **2016**, 16007.

Matz, M. V.; Fradkov, A. F.; Labas, Y. A.; Savitsky, A. P.; Zaraisky, A. G.; Markelov, M. L.; Lukyanov, S. A. Fluorescent proteins from nonbioluminescent Anthozoa species. *Nature Biotechnology*. **1999**, *17*, 969-973.

Matz, M. V.; Lukyanov, K. A.; Lukyanov, S. A. Family of the green fluorescent protein: journey to the end of the rainbow. *Bioessays*. **2002**, *24*, 953-959.

Mayr, V.; Sturtzel, C.; Stadler, M.; Grissenberger, S.; Distel, M. Fast dynamic *in vivo* monitoring of Erk activity at single cell resolution in DREKA zebrafish. *Frontiers in Cell and Developmental Biology*. **2018**, *6*, 111.

McCance, K. L.; Huether, S. E. Pathophysiology: The biologic basis for disease in adults and children. *Elsevier Health Sciences.* **2014**.

Mehrotra, P. Biosensors and their applications–A review. *Journal of Oral Biology and Craniofacial Research*. **2016**, *6*, 153-159.

Mehta, S.; Zhang, J. Reporting from the field: genetically encoded fluorescent reporters uncover signaling dynamics in living biological systems. *Annual Review of Biochemistry*. **2011**, *80*, 375-401.

Mehta, S.; Zhang, Y.; Roth, R.H.; Zhang, J.F.; Mo, A.; Tenner, B.; Huganir, R.L.; Zhang, J. Single-fluorophore biosensors for sensitive and multiplexed detection of signalling activities. *Nature Cell Biology*. **2018**, *20*, 1215-1225.

Meister, M.; Tomasovic, A.; Banning, A.; Tikkanen, R. Mitogen-activated protein (MAP) kinase scaffolding proteins: a recount. *International Journal of Molecular Sciences*. **2013**, *14*, 4854-4884.

Meng, X.; Zhang, S. MAPK cascades in plant disease resistance signaling. *Annual Review of Phytopathology*. **2013**, *51*, 245-266.

Miesenböck, G.; De Angelis, D. A.; Rothman, J. E. Visualizing secretion and synaptic transmission with pH-sensitive green fluorescent proteins. *Nature*. **1998**, *394*, 192-195.

Mitra, R. D.; Silva, C. M.; Youvan, D. C. Fluorescence resonance energy transfer between blue-emitting and red-shifted excitation derivatives of the green fluorescent protein. *Gene*. **1996**, *173*, 13-17.

Miya, A.; Albert, P.; Shinya, T.; Desaki, Y.; Ichimura, K.; Shirasu, K.; Narusaka, Y.; Kawakami, N.; Kaku, H.; Shibuya, N. CERK1, a LysM receptor kinase, is essential for chitin elicitor signaling in Arabidopsis. *Proceedings of the National Academy of Sciences*. **2007**, *104*, 19613-19618.

Miyawaki, A.; Griesbeck, O.; Heim, R.; Tsien, R. Y. Dynamic and quantitative Ca2+ measurements using improved cameleons. *Proceedings of the National Academy of Sciences*. **1999**, *96*, 2135-2140.

Miyawaki, A.; Llopis, J.; Heim, R.; McCaffery, J. M.; Adams, J. A.; Ikura, M.; Tsien, R. Y. Fluorescent indicators for Ca 2+ based on green fluorescent proteins and calmodulin. *Nature*. **1997**, *388*, 882-887.

Mizoguchi, T.; Irie, K.; Hirayama, T.; Hayashida, N.; Yamaguchi-Shinozaki, K.; Matsumoto, K.; Shinozaki, K. A gene encoding a mitogen-activated protein kinase kinase kinase is induced simultaneously with genes for a mitogen-activated protein kinase and an S6 ribosomal protein kinase by touch, cold, and water stress in *Arabidopsis thaliana*. *Proceedings of the National Academy of Sciences*. **1996**, *93*, 765-769.

Mohsin, M.; Ahmad, A.; Iqbal, M. FRET-based genetically-encoded sensors for quantitative monitoring of metabolites. *Biotechnology Letters*. **2015**, *37*, 1919-1928.

Morris, M. C. Fluorescent biosensors—probing protein kinase function in cancer and drug discovery. *Biochimica et Biophysica Acta (BBA)-Proteins and Proteomics*. **2013**, *1834*, 1387-1395.

Morrison, D. K.; Davis, R. J. Regulation of MAP kinase signaling modules by scaffold proteins in mammals. *Annual Review of cell and developmental biology*. **2003**, *19*, 91-118.

Müller, J.; Beck, M.; Mettbach, U.; Komis, G.; Hause, G.; Menzel, D.; Šamaj, J. Arabidopsis MPK6 is involved in cell division plane control during early root development, and localizes to the pre-prophase band, phragmoplast, trans-Golgi network and plasma membrane. *The Plant Journal*. **2010**, *61*, 234-248.

Nagai, E.S.; Sawano, T.; Park, A.; Miyawaki, A. Circularly permuted green fluorescent proteins engineered to sense Ca2+. *Proc Natl Acad Sci USA.* **2001**, *98*, 197202.

Nakai, J.; Ohkura, M.; Imoto, K. A high signal-to-noise Ca 2+ probe composed of a single green fluorescent protein. *Nature Biotechnology*. **2001**, *19*, 137-141.

Newman, R. H.; Fosbrink, M. D.; Zhang, J. Genetically encodable fluorescent biosensors for tracking signaling dynamics in living cells. *Chemical Reviews*. **2011**, *111*, 3614-3666.

Ni, Q.; Mehta, S.; Zhang, J. Live-cell imaging of cell signaling using genetically encoded fluorescent reporters. *The FEBS Journal*. **2018**, *285*, 203-219.

Okumoto, S. Imaging approach for monitoring cellular metabolites and ions using genetically encoded biosensors. *Current Opinion in Biotechnology*. **2010**, *21*, 45-54.

Oldach, L.; Zhang, J. Genetically encoded fluorescent biosensors for live-cell visualization of protein phosphorylation. *Chemistry Biology*. **2014**, *21*, 186-197.

Palmer, A. E.; Giacomello, M.; Kortemme, T.; Hires, S. A.; Lev-Ram, V.; Baker, D.; Tsien, R. Y. Ca2+ indicators based on computationally redesigned calmodulin-peptide pairs. *Chemistry & Biology*. **2006**, *13*, 521-530.

Pawson, T.; Scott, J. D. Signaling through scaffold, anchoring, and adaptor proteins. *Science*. **1997**, *278*, 2075-2080.

Pearson, R. B.; Kemp, B. E. [3] Protein kinase phosphorylation site sequences and consensus specificity motifs: Tabulations. In *Methods in Enzymology.* **1991**, *200*, 62-81.

Pedreira, C. E.; Costa, E. S.; Lecrevisse, Q.; van Dongen, J. J.; Orfao, A.; EuroFlow Consortium. Overview of clinical flow cytometry data analysis: recent advances and future challenges. *Trends in Biotechnology*. **2013**, *31*, 415-425.

Petersen, M.; Brodersen, P.; Næsted, H.; Andreasson, E.; Lindhart, U.; Johansen, B.; Nielsen, H.B.; Lacy, M.; Austin, M.J.; Parker, J.E.; Sharma, S.B. Arabidopsis MAP kinase 4 negatively regulates systemic acquired resistance. *Cell*. **2000**, *103*, 1111-1120.

Picotti, P.; Bodenmiller, B.; Aebersold, R. Proteomics meets the scientific method. *Nature Methods*. **2013**, *10*, 24-27.

Piljić, A.; De Diego, I.; Wilmanns, M.; Schultz, C. Rapid development of genetically encoded FRET reporters. *ACS Chemical Biology*. **2011**, *6*, 685-691.

Pozzan, T.; Mongillo, M.; Rudolf, R. Investigating signal transduction with genetically encoded fluorescent probes. *European Journal of Biochemistry*. **2003**, *270*, 2343-2352.

Prasher, D.C.; Eckenrode, V.K.; Ward, W.W.; Prendergast, F.G. Cormier, M.J. Primary structure of the *Aequorea victoria* green fluorescent protein. *Gene*. **1992**, *111*, 229–233.

Rasmussen, M. W.; Roux, M.; Petersen, M.; Mundy, J. MAP kinase cascades in Arabidopsis innate immunity. *Frontiers in Plant Science*. **2012**, *3*, 169.

Regot, S.; Hughey, J. J.; Bajar, B. T.; Carrasco, S.; Covert, M. W. High-sensitivity measurements of multiple kinase activities in live single cells. *Cell*. **2014**, *157*, 1724-1734.

Rizza, A.; Walia, A.; Lanquar, V.; Frommer, W. B.; Jones, A. M. *In vivo* gibberellin gradients visualized in rapidly elongating tissues. *Nature Plants*. **2017**, *3*, 803-813.

Robinson, M. J.; Cobb, M. H. Mitogen-activated protein kinase pathways. *Current Opinion in Cell Biology*. **1997**, *9*, 180-186.

Rodriguez, E.A.; Campbell, R.E.; Lin, J.Y.; Lin, M.Z.; Miyawaki, A.; Palmer, A.E.; Shu, X.; Zhang, J.; Tsien, R.Y. The growing and glowing toolbox of fluorescent and photoactive proteins. *Trends in Biochemical Sciences.* **2017**, *42*, 111-129.

Rost, F.W.D. Autofluorescence in plants, fungi, and bacteria. *Fluorescence Microscopy*. 1995, *2*, 16–39.

Sadanandom, A.; Napier, R. M. Biosensors in plants. *Current Opinion in Plant Biology*. **2010**, *13*, 736-743.

Sample, V.; Mehta, S.; Zhang, J. Genetically encoded molecular probes to visualize and perturb signaling dynamics in living biological systems. *Journal of Cell Science*. **2014**, *127*, 1151-1160.

Sato, M.; Kawai, Y.; Umezawa, Y. Genetically encoded fluorescent indicators to visualize protein phosphorylation by extracellular signal-regulated kinase in single living cells. *Analytical Chemistry*. **2007**, *79*, 2570-2575.

Schuster, C.; Gaillochet, C.; Medzihradszky, A.; Busch, W.; Daum, G.; Krebs, M.; Kehle, A.; Lohmann, J.U. A regulatory framework for shoot stem cell control integrating metabolic, transcriptional, and phytohormone signals. *Developmental Cell*. **2014**, *28*, 438-449.

Selvin, P. R. The renaissance of fluorescence resonance energy transfer. *Nature Structural Biology*. **2000**, *7*, 730-734.

Shimomura, O.; Johnson, F. H.; Saiga, Y. Extraction, purification and properties of aequorin, a bioluminescent protein from the luminous hydromedusan, Aequorea. *Journal of Cellular and Comparative Physiology*. **1962**, *59*, 223-239.

Shinkai, Y.; Satoh, H.; Takeda, N.; Fukuda, M.; Chiba, E.; Kato, T.; Kuramochi, T.; Araki, Y. A testicular germ cell-associated serine-threonine kinase, MAK, is dispensable for sperm formation. *Molecular and Cellular Biology*. **2002**, *22*, 3276-3280.

Siegel, M. S.; Isacoff, E. Y. A genetically encoded optical probe of membrane voltage. *Neuron*. **1997**, *19*, 735-741.

Sparta, B.; Pargett, M.; Minguet, M.; Distor, K.; Bell, G.; Albeck, J. G. Receptor level mechanisms are required for epidermal growth factor (EGF)-stimulated extracellular signal-regulated kinase (ERK) activity pulses. *Journal of Biological Chemistry*. **2015**, *290*, 24784-24792.

Spencer, S. L.; Cappell, S. D.; Tsai, F. C.; Overton, K. W.; Wang, C. L.; Meyer, T. The proliferation-quiescence decision is controlled by a bifurcation in CDK2 activity at mitotic exit. *Cell*. **2013**, *155*, 369-383.

Spiering, D.; Bravo-Cordero, J. J.; Moshfegh, Y.; Miskolci, V.; Hodgson, L. Quantitative ratiometric imaging of FRET-biosensors in living cells. In *Methods in Cell Biology.* **2013**, *114*, 593-609.

St-Pierre, F.; Marshall, J. D.; Yang, Y.; Gong, Y.; Schnitzer, M. J.; Lin, M. Z. High-fidelity optical reporting of neuronal electrical activity with an ultrafast fluorescent voltage sensor. *Nature Neuroscience*. **2014**, *17*, 884-889.

Tang, S.; Wong, H.C.; Wang, Z.M.; Huang, Y.; Zou, J.; Zhuo, Y.; Pennati, A.; Gadda, G.; Delbono, O.; Yang, J.J. Design and application of a class of sensors to monitor Ca2+ dynamics in high Ca2+ concentration cellular compartments. *Proceedings of the National Academy of Sciences*. **2011**, *108*, 16265-16270.

Teige, M.; Scheikl, E.; Eulgem, T.; Dóczi, R.; Ichimura, K.; Shinozaki, K.; Dangl, J.L.; Hirt, H. The MKK2 pathway mediates cold and salt stress signaling in Arabidopsis. *Molecular Cell*. **2004**, *15*, 141-152.

Tewson, P. H.; Martinka, S.; Shaner, N. C.; Hughes, T. E.; Quinn, A. M. New DAG and cAMP sensors optimized for live-cell assays in automated laboratories. *Journal of Biomolecular Screening*. **2016**, *21*, 298-305.

Tsien, R. Y. The green fluorescent protein. *Annual Review of Biochemistry*. **1998**, *67*, 509-544.

Ubersax, J. A.; Ferrell Jr, J. E. Mechanisms of specificity in protein phosphorylation. *Nature reviews Molecular Cell Biology*. **2007**, *8*, 530-541.

Uslu, V. V.; Grossmann, G. The biosensor toolbox for plant developmental biology. *Current Opinion in Plant Biology*. **2016**, *29*, 138-147.

Vang, S.; Seitz, K.; Krysan, P. J. A simple microfluidic device for live cell imaging of Arabidopsis cotyledons, leaves, and seedlings. *Biotechniques*. **2018**, *64*, 255-261.

Várnai, P.; Balla, T. Visualization of phosphoinositides that bind pleckstrin homology domains: calcium-and agonist-induced dynamic changes and relationship to myo-[3H] inositol-labeled phosphoinositide pools. *The Journal of Cell Biology*. **1998**, *143*, 501-510.

Waadt, R.; Krebs, M.; Kudla, J.; Schumacher, K. Multiparameter imaging of calcium and abscisic acid and high-resolution quantitative calcium measurements using R-GECO1-mTurquoise in Arabidopsis. *New Phytologist*. **2017**, *216*, 303-320.

Walia, A.; Waadt, R.; Jones, A. M. Genetically encoded biosensors in plants: pathways to discovery. *Annual review of Plant Biology*. **2018**, *69*, 497-524.

Wang, H.; Nakata, E.; Hamachi, I. Recent progress in strategies for the creation of protein-based fluorescent biosensors. *ChemBioChem*. **2009**, *10*, 2560-2577.

Wang, H.; Liu, Y.; Bruffett, K.; Lee, J.; Hause, G.; Walker, J. C.; Zhang, S. Haplo-insufficiency of MPK3 in MPK6 mutant background uncovers a novel function of these two MAPKs in Arabidopsis ovule development. *The Plant Cell*. **2008** *20*, 602-613.

Watton, S. J.; Downward, J. Akt/PKB localisation and 3' phosphoinositide generation at sites of epithelial cell–matrix and cell–cell interaction. *Current Biology*. **1999**, *9*, 433-436.

Xu, J.; Zhang, S. Mitogen-activated protein kinase cascades in signaling plant growth and development. *Trends in Plant Science*. **2015**, *20*, 56-64.

Zaman, N.; Seitz, K.; Kabir, M.; George-Schreder, L.S.; Shepstone, I.; Liu, Y.; Zhang, S.; Krysan, P.J. A Förster resonance energy transfer sensor for live-cell imaging of mitogen-activated protein kinase activity in Arabidopsis. *The Plant Journal*. **2019**, *97*, 970-983.

Zapata-Hommer, O.; Griesbeck, O. Efficiently folding and circularly permuted variants of the Sapphire mutant of GFP. *BMC Biotechnology*. **2003**, *3*, 5.

Zhang, J.; Allen, M. D. FRET-based biosensors for protein kinases: illuminating the kinome. *Molecular BioSystems*. **2007**, *3*, 759-765.

Zhang, J.; Jensen, M. K.; Keasling, J. D. Development of biosensors and their application in metabolic engineering. *Current Opinion in Chemical Biology*. **2015**, *28*, 1-8.

Zhang, S.; Klessig, D. F. MAPK cascades in plant defense signaling. *Trends in plant science*. **2001**, *6*, 520-527.

Zlobovskaya, O. A.; Sergeeva, T. F.; Shirmanova, M. V.; Dudenkova, V. V.; Sharonov, G. V.; Zagaynova, E. V.; Lukyanov, K. A. Genetically encoded far-red fluorescent sensors for caspase-3 activity. *BioTechniques*. **2016**, *60*, 62-68.

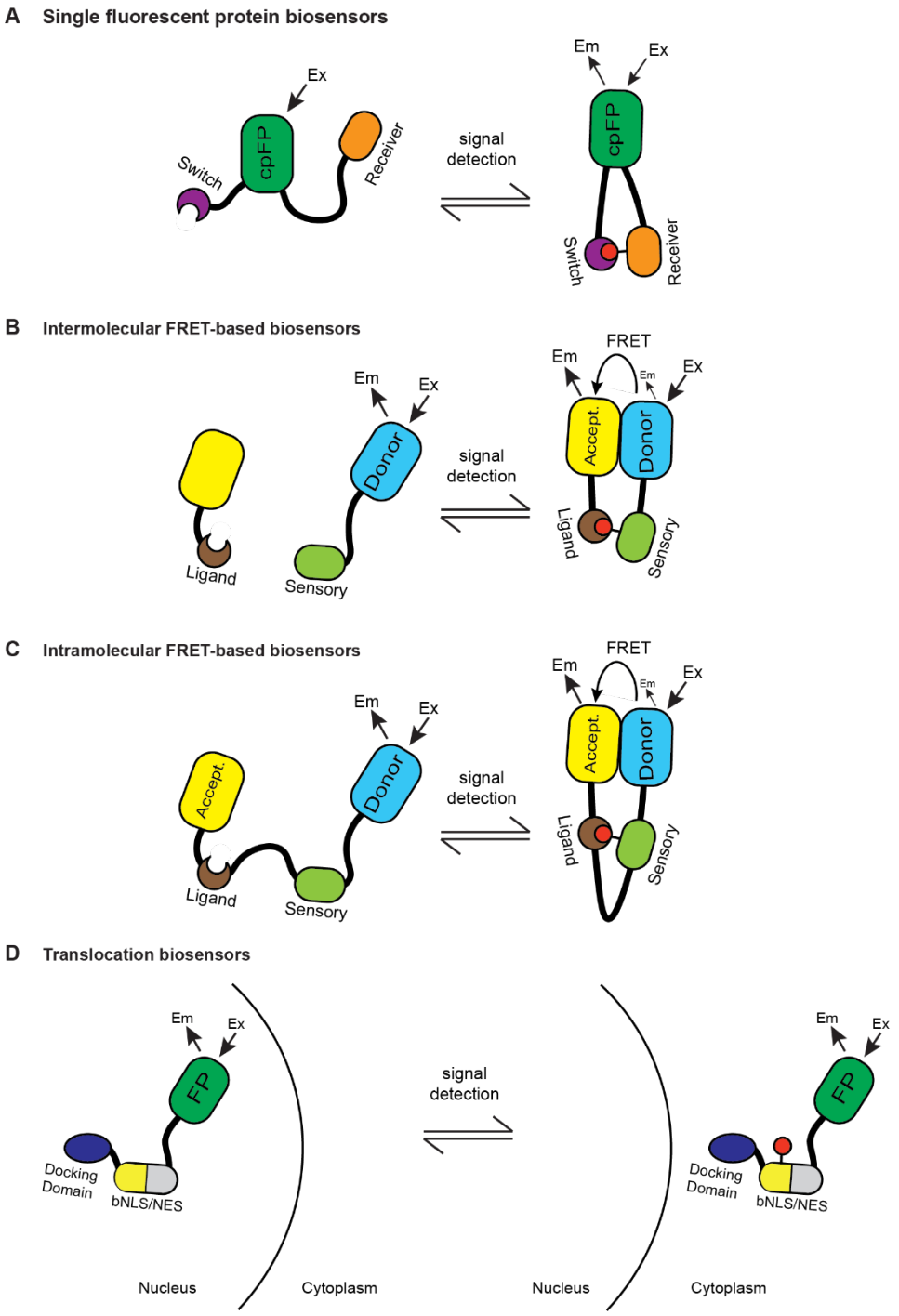

Fig. 1. Different designs of fluorescent biosensors. (a) Schematic model of a generic single fluorescent protein biosensor. A circularly permutated fluorescent protein (cpFP) undergoes a change in fluorescent emission upon interaction with a signal of interest. (b, c) Schematic model of generic intermolecular and intramolecular FRET-based biosensors. Upon detecting the parameter of interest, increased affinity of the ligand domain for the sensory domain brings the donor/acceptor fluorophores closer together, resulting in FRET. (d) Schematic model of a generic translocation biosensor. Interaction with the parameter of interest results in a shift in localization.

Chapter 2: A simple microfluidic device for live cell imaging of Arabidopsis cotyledons and seedlings

My contribution: I performed and analyzed the experiments and created the Figures and Videos for Figure 4 and Supplemental Figures 2 and 3. I also co-authored the Materials and Methods section. I also served as a mentor for the undergraduate student who was first author on the paper.

This chapter was adapted from the following publication: Vang, S.; Seitz, K.; Krysan, P. J. A simple microfluidic device for live cell imaging of Arabidopsis cotyledons, leaves, and seedlings. *Biotechniques*. **2018**, *64*, 255-261.

Abstract

Live cell imaging is a powerful tool for studying a range of biological processes in plants. In order to perform experiments where living tissue is exposed to controlled pulses of a chemical treatment, one must have a system for holding the sample in place during imaging that allows for rapid addition and removal of treatments. Here we report a simple solution to this challenge that involves repurposing a commercially available device called a HybriWell™. This inexpensive, disposable device can be used to create an imaging chamber suitable for Arabidopsis seedlings, detached cotyledons, and leaves. The liquid in the sample chamber can be rapidly exchanged in a manner of seconds to introduce chemical treatments via microfluidic passive pumping. The performance of this device is demonstrated by imaging samples treated with a fluorescent dye. We also show how the HybriWell™ can be used to monitor calcium transients triggered by the bacterial elicitor flg22 using the R-GECO1 calcium indicator in detached Arabidopsis leaves. The HybriWell™ is a simple, cost-effective solution for mounting Arabidopsis samples for live cell imaging. When used in conjunction with fluorescent biosensors, this system should facilitate live cell imaging studies of signal transduction pathways triggered by a range of different treatments.

Introduction

Live cell imaging refers to an experimental approach whereby living samples are observed via microscopy in order to study a biological process at the cellular and/or subcellular level. This approach stands in contrast to traditional microscopy in which non-living, fixed samples are analyzed. Live cell imaging can be used to study cell biology, signal transduction, and a range of other biological phenomena. An important consideration for these experiments is that one needs to have a method available for mounting the sample that keeps it viable and in a stress-free condition throughout the imaging process. In addition, if one wishes to study how the sample responds to a chemical stimulus, the mounting method needs to allow for pulses of chemical treatments to be easily added and removed from the imaging chamber with minimal collateral stress.

Most live cell imaging studies involve the use of fluorescent probes and reporters in conjunction with epifluorescent or confocal microscopy. In the case of plant biology, a recent review highlights the current landscape regarding live cell imaging and biosensors (Grossmann et al., 2018). A number of fluorescent sensors have been developed that allow one to measure the concentrations of glucose, inorganic phosphate, zinc, ATP, hydrogen peroxide, pH, and calcium in living plant tissue, and fluorescent reporters for the plant hormones auxin, gibberellic acid (GA), and abscisic acid (ABA) have also been described (Lanquar et al., 2014; Nagai et al., 2004; Zhao et al., 2011; Rizza et al., 2017; Jones et al., 2014; Waadt et al., 2014; Deuschle et al., 2006; Mukherjee et al., 2015; De Col et al., 2017; Hernandez-Barrera et al., 2015; Gjetting et al., 2012; Brunoud et al., 2012). In addition, fusion proteins tagged with

fluorescent reporters allow one to track the subcellular localization of a protein of interest and monitor its interactions with other proteins (Voss et al., 2013). By using live cell imaging methods, one can observe these factors in real time and also determine how the sample responds to a stimulus.

An elegant method for performing live cell imaging studies of Arabidopsis root tissue has been previously described. This system, called the RootChip, is based on a custom-built microfluidic device that channels the growing primary root of an Arabidopsis seedling into a microfluidic channel fabricated on the surface of a microscope cover glass (Lanquar et al., 2014; Grossmann et al., 2011; Stanley et al., 2017). The microfluidic channels allow one to flow pulses of chemical treatments across the root tissue while the sample is mounted on a microscope for imaging. This strategy has been used to study a range of biochemical and signaling processes in Arabidopsis roots (Lanquar et al., 2014; Rizza et al., 2017; Jones et al., 2014; Grossmann et al., 2011; Stanley et al., 2017).

In the case of studies focused on leaf tissue, a variety of custom imaging chambers have been described that aim to hold the sample in place during microscopy while also allowing chemical treatments to be perfused into the chamber (Keinath et al., 2015; Loro et al., 2016; Salomon et al., 2010). Although effective for imaging experiments, these custom chambers can be challenging to replicate. Therefore developing a simple, reproducible method for mounting Arabidopsis leaves for live cell imaging that could be easily adopted by other labs with minimal effort would be extremely beneficial. This manuscript describes how a commercially available device called a HybriWell™ (Grace Bio-Labs, Bend, OR), which is designed for performing

microarray hybridization experiments, can be repurposed to serve as a live cell imaging chamber for Arabidopsis leaves and seedlings.

Results

Repurposing the HybriWell™ for live cell imaging in Arabidopsis

The HybriWell™ is a disposable plastic device that was originally designed to create low-volume chambers on microscope slides for use in microarray hybridization experiments. HybriWells™ are available in a variety of sizes and shapes, but the one selected for our experiments is a square patch of plastic 25 mm by 25 mm in size with a 20 mm diameter circular chamber in the center (Figure 1A). After peeling the protective cover off of the adhesive side of the HybriWell™, one can press the HybriWell™ down onto the surface of a microscope cover glass to form a chamber 20 mm in diameter and 150 µm deep (Figure 1B). The resulting chamber has an approximate volume of 30 µl. The top of the chamber is clear plastic, and the bottom is formed by the glass cover glass. The sides of the HybriWell™ are held tight to the cover glass by the adhesive. On top of the chamber there are two 1.5 mm diameter ports that are used to introduce liquid into the chamber once it has been mounted on the cover glass.

When using the HybriWell™ to image Arabidopsis samples, one first places the sample in a 5 µl drop of water on a glass cover glass. Next, a HybriWell™ with the adhesive exposed is carefully laid over the top of the sample using a forceps (Figure 1C). Finally, a pipette is used to force water into one of the ports on top of the HybriWell™, thus filling the HybriWell™ with liquid. The sample is gently held in place between the clear plastic top of the HybriWell™ and the cover glass. The 150 µm depth of the chamber works well for mounting detached

Arabidopsis cotyledons and leaves as well as young seedlings up to a few days old. Since the sample is mounted on top of a microscope cover glass, imaging can be performed using an inverted microscope. Because the adhesive material on the HybriWell™ forms a strong bond to the cover glass it is not practical to remove the HybriWell™ from the cover glass once a sample has been mounted. The HybriWell™ is therefore a disposable device that can only be used to analyze one sample before discarding it.

Passive pumping can exchange liquid within the HybriWell™

After determining that the depth of the HybriWell™ chamber was suitable for mounting Arabidopsis samples, we next wanted to test how effectively the liquid in the chamber could be exchanged with fresh solution. Since our ultimate goal is to be able to apply chemical treatments to samples during live cell imaging, it is critical that the liquid within the HybriWell™ can be efficiently exchanged. Fluid movement through the HybriWell™ device can be driven by the microfluidic process of passive pumping (Walker & Beebe, 2002). To achieve passive pumping, one first places a large drop of water over one of the 1.5 mm ports on top of the HybriWell™ (Figure 1D). If liquid is then applied dropwise to the other port, it will be rapidly drawn into the HybriWell™ by passive pumping. Each time a drop of liquid is added to the inlet port, it quickly enters the HybriWell™ and an equal volume of liquid exits the HybriWell™ into the growing drop covering the outlet port. It is important to stress that one does not use positive pressure to force liquid into the inlet port, rather, a drop of liquid is gently dropped into the inlet port, and passive pumping pulls that liquid into the HybriWell™.

In order to visualize the movement of liquid through the HybriWell™ chamber, a detached Arabidopsis cotyledon was mounted in water using a HybriWell™ as described above. A 50 µl drop of water was placed over the outlet port, and then 50 µl of red food coloring solution was introduced dropwise into the inlet port. At time zero, the small green cotyledon can be seen in the center of the clear water in the HybriWell™ chamber. In as little as five seconds, the red food coloring solution has surrounded the cotyledon, and by 20 seconds it has filled the chamber (Figure 2A and Supplemental Video 1) at an approximate flow rate of 3 mm/sec. To demonstrate the ability to perform pulse-chase experiments using the HybriWell™, 50 µl of sterile ultrapure water was added to the chamber that had been filled with red food coloring (Figure 2B and Supplemental Video 2). The clear water quickly replaced the red food coloring in the chamber. It should be noted that when liquid is introduced into the HybriWell™ by passive pumping, there is an interface between the new and old solutions that sweeps across the chamber. Since the chamber volume is ca. 30 µl, adding 50 µl of new solution effectively replaces the old solution in the chamber with the new solution.

Next, we wanted to determine how the HybriWell™ affected seedling growth. For this experiment 3-day-old seedlings were mounted in HybriWells™, and root length was measured at 0 and 6 hours after mounting. For comparison, control seedlings growing on the surface of agar growth media plates were also measured. It was determined that the average growth rate of primary roots in HybriWells™ was 0.38±0.09 mm/hr. (n=6) versus 0.44±0.03 mm/hr. (n=6) for the control samples. This difference was not statistically significant (two-tailed t-test, $p=0.19$).

Epidermal cells are exposed to chemical treatments added to the HybriWell™

The experiments using red food coloring described above demonstrated that the liquid within the HybriWell™ chamber can be efficiently exchanged. When an Arabidopsis sample is mounted in a HybriWell™ for imaging, it is sandwiched between the top of the HybriWell™ and the glass cover glass. If the HybriWell™ is to be used for live cell imaging experiments, it is important that a chemical treatment introduced into the HybriWell™ is able to rapidly reach the surface of the tissue that is being imaged. Therefore it was necessary to determine if liquid added to a HybriWell™ through the inlet port efficiently flows through the space between the cotyledon and the glass cover glass. If the sample were too tightly pressed down upon the cover glass, it might prevent the added treatment from contacting the epidermis.

To address this question, a cotyledon was mounted in water as described above. The sample was then placed on an inverted confocal microscope such that the lens pointed up through the coverglass to the epidermis of the cotyledon. Next, 50 µl of 300 µM propidium iodide (PI) was added to the HybriWell™ through the inlet port. PI is a red fluorescent dye that has been previously shown to stain plant cell walls. In addition, the Arabidopsis seedlings used for this experiment expressed green fluorescent protein (GFP) throughout the cotyledon, which allowed us to visualize the cotyledon epidermis. An image collected one min after PI addition showed strong red fluorescence highlighting the cell walls of a substantial portion of the cotyledon epidermis, and the area of the epidermis stained by PI increased at the 3 min and 5 min time points (Figure 3). The images shown in Figure 3 are maximum intensity projections of Z-stack series focused on the epidermal layer.

In these experiments the red fluorescent signal in the central portion of the cotyledon was routinely observed to be substantially lower than that observed in the outer regions (Figure 3A). These observations suggest that the flow of liquid through the HybriWell™ may be restricted in areas where the cotyledon is pressed tightly against the cover glass. Our observation that a majority of the sample becomes quickly stained, however, indicating that a substantial portion of the cotyledon epidermis is rapidly contacted by chemical treatments introduced into the HybriWell™ by passive pumping. These results suggest that there is a layer of liquid between the epidermis and the cover glass in this imaging setup that allows introduced chemical treatments to easily flow across the sample. It is important to recognize, however, that the entire cotyledon is not likely to be uniformly exposed to the treatment, with the inner portion of the sample less likely to be exposed. Focusing on regions of the epidermis near the margin of the cotyledon provide the best opportunity for exposure to the chemical treatment. In addition, a fluorescent dye could be used in conjunction with the treatment of interest to serve as a tracer for identifying cells that were directly exposed to the treatment.

We next wanted to determine if the HybriWell™ could be used to image Arabidopsis roots. For this experiment intact 3-day-old Arabidopsis seedlings were mounted in the HybriWell™ using the same technique described above for cotyledons. One min after adding 50 µl of 300 µM PI to the HybriWell™ strong PI staining of the entire root was observed (Supplemental Figure 1). The fluorescent signal did not increase in intensity when images were collected at the 3 min and 5 min time-points. These results indicate that the entire root is rapidly exposed to the PI treatment delivered via the HybriWell™. In this experiment 3-day-old seedlings were used so that they could easily fit inside the 20 mm diameter HybriWell™

chamber. It should be noted that larger HybriWells™ are available, including one that creates a 21 mm x 60 mm rectangular chamber. Using this larger size HybriWell™ should allow one to analyze older seedlings.

Imaging flg22-induced Ca^{2+} transients using the R-GECO1 calcium indicator

Fluorescent biosensors that report the concentration or activity of signal transduction molecules are valuable tools for live cell imaging studies. For example, R-GECO1 is an intensiometric calcium indicator in which the intensity of red fluorescence is proportional to free calcium concentration (Zhao et al., 2011; Keinath et al., 2015; Wu et al., 2013). In order to evaluate the utility of the HybriWell™ for studying signal transduction using fluorescent biosensors, the response of true leaves expressing the R-GECO1 calcium indicator to the bacterial elicitor peptide flg22 was tested. flg22 is a conserved sequence from bacterial flagella that has been shown to cause rapid calcium oscillations in Arabidopsis (Keinath et al., 2015; Kwaaitaal et al., 2011; Ranf et al., 2011). True leaves expressing R-GECO1 in HybriWells™ were mounted and collected images every five seconds using a confocal microscope in order to quantify the intensity of red fluorescent emission. Addition of 100 nM flg22 to the HybriWell™ via passive pumping caused a sharp gain in red fluorescence ca. 1 min after treatment, indicative of a rapid increase in free calcium (Figure 4; Supplemental Video 3). Analysis of four different regions of interest (ROIs) in the images revealed similar oscillating patterns of red fluorescence, consistent with previously reported experiments involving flg22 treatment of Arabidopsis leaves expressing R-GECO1 (Keinath et al., 2015). In order to evaluate the reproducibility of the HybriWell™ system for performing live-cell imaging studies, this flg22

experiment was repeated two additional times and observed similar results: a rapid gain in red fluorescence one to two mins after flg22 treatment followed by oscillations in fluorescence intensity (Supplemental Figure 2; Supplemental Videos 4 and 5).

Because calcium signaling is known to be sensitive to mechanical stimulation, we also performed a control experiment where sterile ultrapure water was added to the HybriWell™, rather than flg22 (Supplemental Figure 3; Supplemental Video 6). No strong increase in red fluorescence was observed upon adding sterile ultrapure water to the HybriWell™, demonstrating that the process of passive pumping through the device does not produce any strong mechanical stimulation. This feature of the HybriWell™ suggests that it should be possible to use this device to test the effect of a chemical treatment without confounding effects caused by mechanical stress.

Taken together, our results demonstrate that the HybriWell™ device is able to function as a microfluidic chamber for performing live cell imaging studies of Arabidopsis leaves and seedlings. Observations revealed that samples were able to be maintained in the HybriWell™ chambers for at least 6 hours with no apparent negative effects on growth, indicating that this system is suitable for relatively long-term time-course experiments. Because HybriWell™ devices are low cost and commercially available, it should be straightforward for labs interested in performing live cell imaging of Arabidopsis to adopt them for use in their experimental systems.

Materials and Methods

Chemicals and supplies

Propidium iodide (PI) solution (1 mg/ml in water) was obtained from Sigma-Aldrich (St. Louis, MO) (Cat. # P4864). For flg22 treatment, synthetic flg22 peptide (QRLSTGSRINSAKDDAAGLQIA) was obtained from PhytoTechnology Laboratories (Shawnee Mission, KS) (cat. # P6622). HBW20 HybriWell™ devices were obtained from Grace Bio-labs (Bend, OR) (Cat. # 611102). 45 mm x 50 mm microscope cover glasses 0.16 – 0.19 mm thick were obtained from Fisher Scientific (Waltham, MA) (Cat. # 12-544F).

Plant materials and growth conditions

Arabidopsis thaliana seedlings were grown on 1% agar (w/v) plates containing 0.5x Murashige and Skoog (MS) basal salt mixture under constant light at a light intensity of 115 - 130 µmol/m^2sec at 20- 23°C with the plates in a vertical orientation. A transgenic line expressing the intensiometric calcium indicator R-GECO1 was a kind gift from Melanie Krebs and is described as line #7-8 in (Keinath et al., 2015). Experiments with detached cotyledons used seedlings that were four to six days old. Experiments with intact seedlings used three-day-old seedlings. For experiments using detached true leaves, seedlings were first germinated on agar plates and then transplanted to soil after one week. Leaf samples were then collected from two-week-old plants in soil.

Mounting samples in the HybriWell™

To mount an Arabidopsis cotyledon in a HybriWell™, a 45 mm x 50 mm microscope cover glass was laid on a lab bench. A 5 µl drop of sterile ultrapure water was then placed in the center of the cover glass using a micropipette. Next, a cotyledon was removed from a four- to

six-day-old seedling growing on a 0.5x MS plate by snipping the petiole with a small scissors. The cotyledon was grasped by the petiole using a forceps and gently placed on the water drop with the abaxial surface facing up. Since the cotyledon typically floats on the surface of the water drop, a micropipette was then used to transfer water from below the cotyledon onto the top surface in order to fully wet the cotyledon on both its abaxial and adaxial surfaces. Excess water was then removed using the micropipette, being careful not to damage the cotyledon. The adhesive backing on the HybriWell™ was then exposed by peeling off the protective covering and a forceps was used to gently lower the HybriWell™ down onto the coverglass, positioning it such that the cotyledon is in the center of the HybriWell™ chamber. The back of the forceps is then used to gently press the adhesive portion of the HybriWell™ down onto the cover glass to fully seal the chamber, taking care not to press down on the top of the chamber. To fill the chamber with water, 300 µl of sterile ultrapure water was rapidly dispensed into one of the ports of the HybriWell™ such that water shoots out the second port during the filling process. This approach is necessary in order to minimize the chance of trapping an air bubble in the chamber. If an air bubble is trapped in the chamber, then an additional 300 µl of sterile ultrapure water can be flushed through the HybriWell™ to remove the bubble. Finally, a 200 µl drop of sterile ultrapure water was placed on top of one of the ports of the HybriWell™ to prevent evaporation of the 30 µl of water within the chamber. The HybriWell™ mounted to the cover glass was then placed inside a 100 mm x 15 mm round plastic Petri dish and covered to maintain sterility and humidity.

The same process described above was used to mount intact seedlings, but in this case the seedlings were transferred to the drop of water on the cover glass by gently lifting them off

the growth plate with a sterile plastic 200 µl pipette tip. For mounting true leaves, a single leaf was collected from a plant growing in soil by snipping the petiole with a scissors and grasping the detached leaf by the petiole using a forceps. The same process described above for cotyledons was then used to mount the true leaf samples in HybriWells™, except that the true leaves were placed on the water droplets with their adaxial sides facing up.

Imaging

Samples were mounted as described above and then incubated in the HybriWell™ for 6 to 8 hours prior to imaging. During this time period the samples were maintained under constant light at 20- 23°C at a light intensity of 115 - 130 µmol/m^2sec.

For the experiments using PI and green fluorescent protein (GFP), images were collected by confocal microscopy using a Zeiss LSM 710 with 10x and 20x objectives. PI fluorescence was imaged by laser excitation at 594 nm with emission collected between 600 nm and 643 nm. GFP fluorescence was imaged by laser excitation at 488 nm with emission collected between 500 nm and 541 nm. 3 µm optical sections were collected as a Z-stack covering a total distance of 63 µm. Images were analyzed using Fiji software (Schindelin et al., 2012).

For experiments using R-GECO1, images were collected by confocal microscopy using a Zeiss LSM 780 with a 20x objective. Samples were placed on the microscope and allowed to equilibrate for 30 mins prior to imaging. R-GECO1 fluorescence was imaged by laser excitation at 561 nm with emission collected between 579 nm and 651 nm and an optical slice thickness of 2 µm. Single images were collected every five seconds for the duration of the experiment.

Images were analyzing using Fiji software, and the Fire lookup table was used to false-color the image to reflect fluorescent signal intensity.

Root Growth Rate Measurement

Arabidopsis Col-0 seeds were surface sterilized and stratified on a 0.5x MS plate at 4°C for 2 days. The plate was then placed vertically under constant light at 20-23°C for 3 days. Six seedlings were then mounted in sterile ultrapure water in HybriWells™, one seedling per HybriWell™. Another six seedlings were transferred to a new 0.5x MS plate. The HybriWells™ were incubated horizontally in covered Petri dishes under constant light at 20 - 23°C. The 0.5x MS plates were incubated in a vertical orientation. Images of the seedlings were captured at 0 hour and 6 hour time points using an Epison Perfection V700 Photo Scanner at 4800 dpi resolution. Root length was determined using Fiji software and growth rate was calculated.

References

Brunoud, G.; Wells, D.M.; Oliva, M.; Larrieu, A.; Mirabet, V.; Burrow, A.H.; Beeckman, T.; Kepinski, S.; Traas, J.; Bennett, M.J.; Vernoux, T. A novel sensor to map auxin response and distribution at high spatio-temporal resolution. *Nature*. **2012**, *482*, 103-106.

De Col, V.; Fuchs, P.; Nietzel, T.; Elsässer, M.; Voon, C.P.; Candeo, A.; Seeliger, I.; Fricker, M.D.; Grefen, C.; Møller, I.M. Bassi, A. ATP sensing in living plant cells reveals tissue gradients and stress dynamics of energy physiology. *Elife*. **2017**, *6*, 26770.

Deuschle, K.; Chaudhuri, B.; Okumoto, S.; Lager, I.; Lalonde, S.; Frommer, W. B. Rapid metabolism of glucose detected with FRET glucose nanosensors in epidermal cells and intact roots of Arabidopsis RNA-silencing mutants. *The Plant Cell*. **2006**, *18*, 2314-2325.

Gjetting, S. K.; Ytting, C. K.; Schulz, A.; Fuglsang, A. T. Live imaging of intra-and extracellular pH in plants using pHusion, a novel genetically encoded biosensor. *Journal of Experimental Botany*. **2012**, *63*, 3207-3218.

Grossmann, G.; Guo, W. J.; Ehrhardt, D. W.; Frommer, W. B.; Sit, R. V.; Quake, S. R.; Meier, M. The RootChip: an integrated microfluidic chip for plant science. *The Plant Cell*. **2011**, *23*, 4234-4240.

Grossmann, G.; Krebs, M.; Maizel, A.; Y. Stahl, J.E.M. Vermeer, and T. Ott. Green light for quantitative live-cell imaging in plants. *J Cell Sci*. **2018**, *131*.

Hernández-Barrera, A.; Velarde-Buendía, A.; Zepeda, I.; Sanchez, F.; Quinto, C.; Sánchez-Lopez, R.; Cheung, A.Y.; Wu, H.M. Cardenas, L. Hyper, a hydrogen peroxide sensor, indicates the sensitivity of the Arabidopsis root elongation zone to aluminum treatment. *Sensors*. **2015**, *15*, 855-867.

Jones, A. M.; Danielson, J. Å.; ManojKumar, S. N.; Lanquar, V.; Grossmann, G.; Frommer, W. B. Abscisic acid dynamics in roots detected with genetically encoded FRET sensors. *Elife*. **2014**, *3*, e01741.

Keinath, N. F.; Waadt, R.; Brugman, R.; Schroeder, J. I.; Grossmann, G.; Schumacher, K.; Krebs, M. Live cell imaging with R-GECO1 sheds light on flg22-and chitin-induced transient [Ca2+] cyt patterns in Arabidopsis. *Molecular Plant*. **2015**, *8*, 1188-1200.

Kwaaitaal, M.; Huisman, R.; Maintz, J.; Reinstädler, A.; Panstruga, R. Ionotropic glutamate receptor (iGluR)-like channels mediate MAMP-induced calcium influx in *Arabidopsis thaliana*. *Biochemical Journal*. **2011**, *440*, 355-373.

Lanquar, V.; Grossman, G.; Vinkenborg, J.L.; Merkx, M.; Thomine, S.; Frommer, W.B. Dynamic imaging of cytosolic zinc in Arabidopsis roots combining FRET sensors and RootChip technology. *New Phytol*. **2014**, *202*, 198-208.

Loro, G.; Wagner, S.; Doccula, F.G.; Behera, S.; Weinl, S.; Kudla, J.; Schwarzländer, M.; Costa, A. Zottini, M. Chloroplast-specific *in vivo* Ca2+ imaging using Yellow Cameleon fluorescent protein sensors reveals organelle-autonomous Ca2+ signatures in the stroma. *Plant Physiology*. **2016**, *171*, 2317-2330.

Mukherjee, P.; Banerjee, S.; Wheeler, A.; Ratliff, L.A.; Irigoyen, S.; Garcia, L.R.; Lockless, S.W.; Versaw, W.K. Live imaging of inorganic phosphate in plants with cellular and subcellular resolution. *Plant Physiology*. **2015**, *167*, 628-638.

Nagai, T.; Yamada, S.; Tominaga, T.; Ichikawa, M.; Miyawaki, A. Expanded dynamic range of fluorescent indicators for Ca(2+) by circularly permuted yellow fluorescent proteins. *Proc Natl Acad Sci USA*. **2004**, *101*, 10554-10559.

Ranf, S.; Eschen-Lippold, L.; Pecher, P.; Lee, J.; Scheel, D. Interplay between calcium signalling and early signalling elements during defence responses to microbe-or damage-associated molecular patterns. *The Plant Journal*. **2011**, *68*, 100-113.

Rizza, A.; Walia, A.; Lanquar, V.; Frommer, W.B.; Jones, A.M. *In vivo* gibberellin gradients visualized in rapidly elongating tissues. *Nat Plants*. **2017**, *3*, 803-813.

Salomon, S.; Grunewald, D.; Stüber, K.; Schaaf, S.; MacLean, D.; Schulze-Lefert, P.; Robatzek, S. High-throughput confocal imaging of intact live tissue enables quantification of membrane trafficking in Arabidopsis. *Plant physiology*. **2010**, *154*, 1096-1104.

Schindelin, J.; Arganda-Carreras, I.; Frise, E.; Kaynig, V.; Longair, M.; Pietzsch, T.; Preibisch, S.; Rueden, C.; Saalfeld, S.; Schmid, B.; Tinevez, J.Y. Fiji: an open-source platform for biological-image analysis. *Nature methods*. **2012**, *9*, 676-682.

Stanley, C. E.; Shrivastava, J.; Brugman, R.; Heinzelmann, E.; van Swaay, D.; Grossmann, G. Dual-flow-RootChip reveals local adaptations of roots towards environmental asymmetry at the physiological and genetic levels. *New Phytologist*. **2018**, *217*, 1357-1369.

Voss, U.; Larrieu, A.; Wells, D. M. From jellyfish to biosensors: the use of fluorescent proteins in plants. *International Journal of Developmental Biology*. **2013**, *57*, 525-533.

Waadt, R.; Hitomi, K.; Nishimura, N.; Hitomi, C.; Adams, S. R.; Getzoff, E. D.; Schroeder, J. I. FRET-based reporters for the direct visualization of abscisic acid concentration changes and distribution in Arabidopsis. *Elife*. **2014**, *3*, e01739.

Walker, G. M.; Beebe, D. J. A passive pumping method for microfluidic devices. *Lab on a Chip*. **2002**, *2*, 131-134.

Wu, J.; Liu, L.; Matsuda, T.; Zhao, Y.; Rebane, A.; Drobizhev, M.; Chang, Y.F.; Araki, S.; Arai, Y.; March, K.; Hughes, T.E. Improved orange and red Ca2+ indicators and photophysical considerations for optogenetic applications. *ACS Chemical Neuroscience*. **2013**, *4*, 963-972.

Zhao, Y.; Araki, S.; Wu, J.; Teramoto, T.; Chang, Y.F.; Nakano, M.; Abdelfattah, A.S.; Fujiwara, M.; Ishihara, T.; Nagai, T.; Campbell, R.E. An expanded palette of genetically encoded Ca2+ indicators. *Science*. **2011**, *333*, 1888-1891.

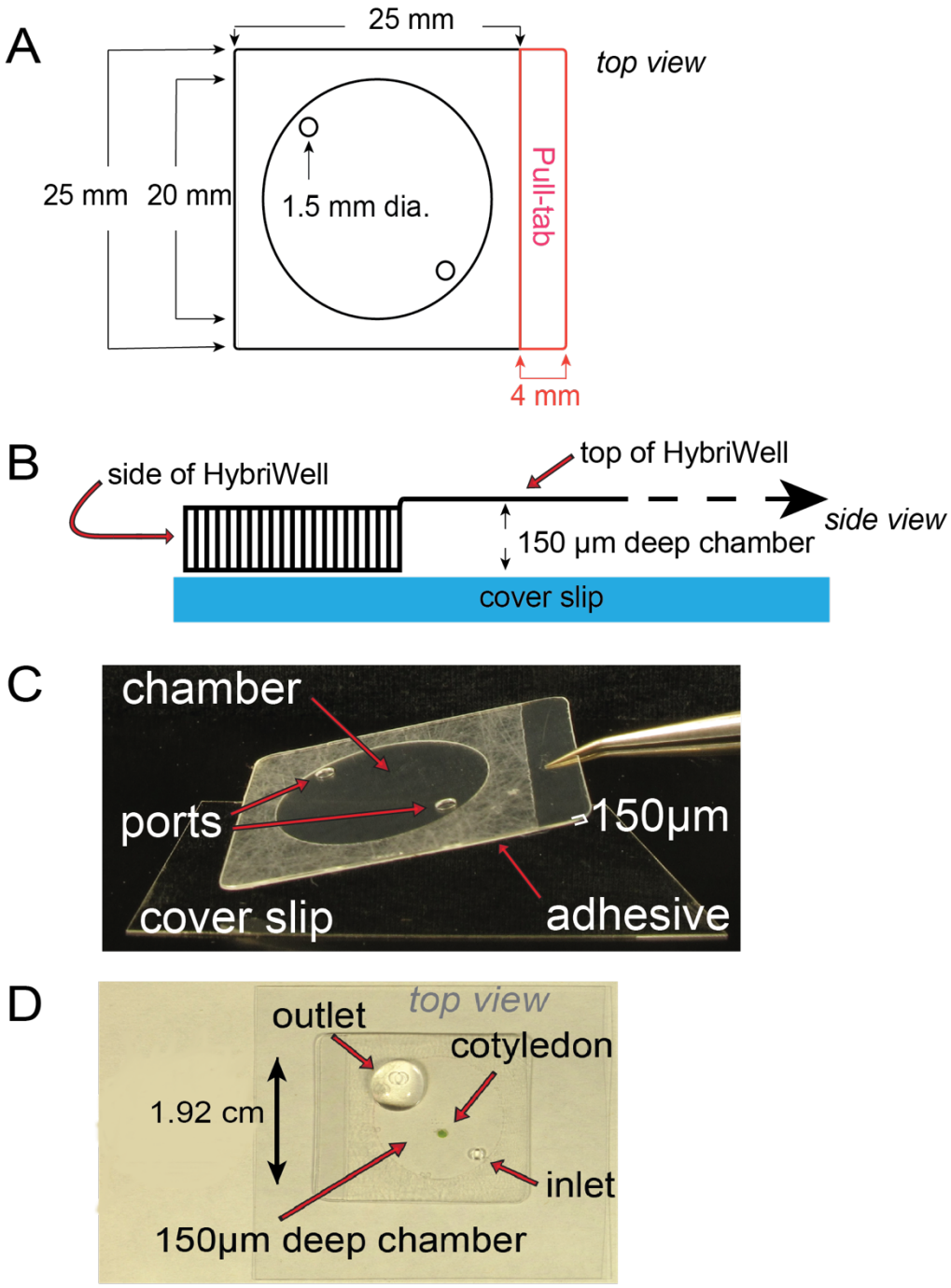

Figure 1. Overview of the HybriWell device. (A) Top view schematic of the HybriWell.This device consists of a small chamber with two ports. The bottom layer is adhesive. Red indicates the non-adhesive peel tab. (B) Side view schematic of the Hybriwell system. The HybriWell is laid on top of a cover glass, creating a sealed chamber that can be filled with water to hold a sample for imaging. The striped lines represent the adhesive outer area. (C) Image of a HybriWell about to be laid on top of a microscope cover glass. (D) Image of a HybriWell attached to a microscope slide and containing an Arabidopsis cotyledon sample. The chamber is filled with water and a large droplet is placed on the “outlet” port. The cotyledon can be imaged through the cover glass using an inverted microscope.

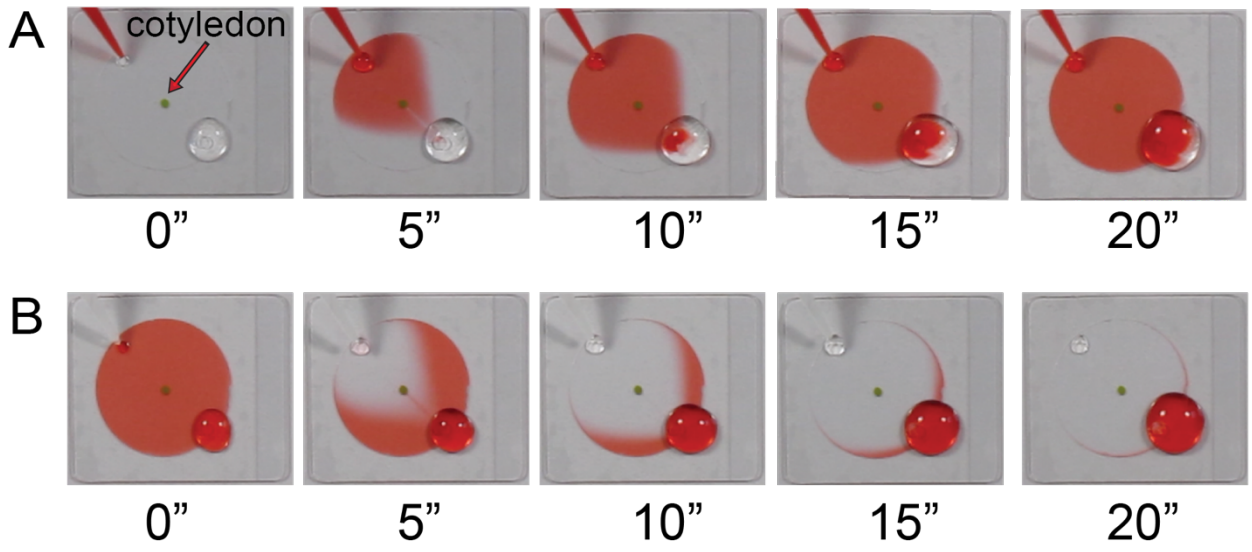

Figure. 2 Time-lapse demonstration of HybriWell fluidics. (A) 50 µl of red food coloring was added in small droplets to the ‘inlet’ port of a HybriWell mounted on a coverglass. The HybriWell contained an Arabidopsis cotyledon and was filled with clear water prior to adding the food coloring. Through the process of passive pumping, the water within the HybriWell was rapidly replaced with the red food coloring. (B) The process was repeated by adding 50 µl of water containing no food coloring.

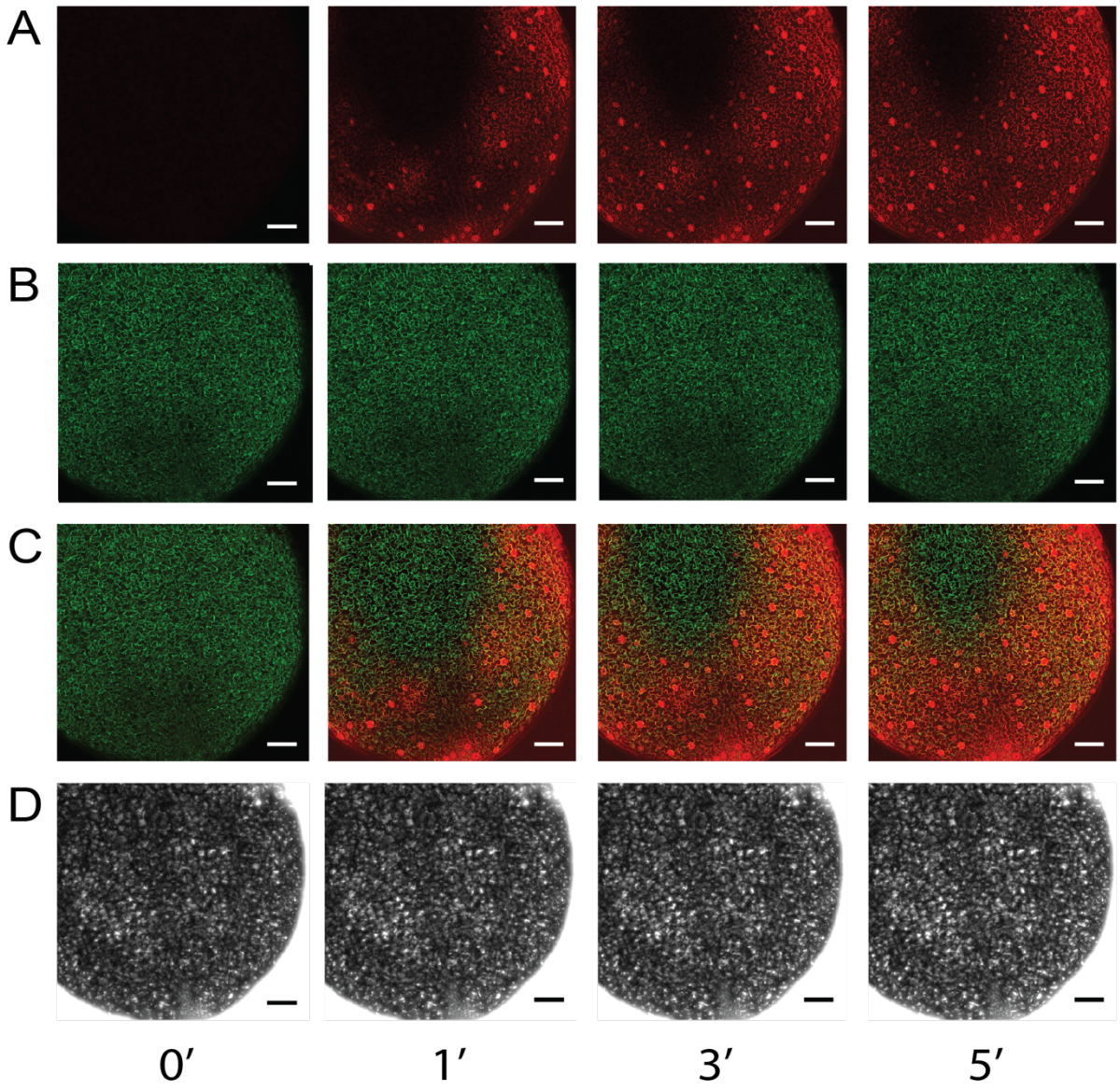

Figure 3. Propidium iodide staining of cotyledons in the Hybriwell. An Arabidopsis cotyledon expressing 35S:GFP was mounted in water in a HybriWell and treated with 50 µl of propidium iodide solution. Maximum Z-projections of confocal images collected before treatment (0') and at the indicated time points in minutes after treatment are shown. (A) Propidium iodide channel. (B) GFP channel. (C) Merged images. (D) Brightfield images. Scale bar=100 µm.

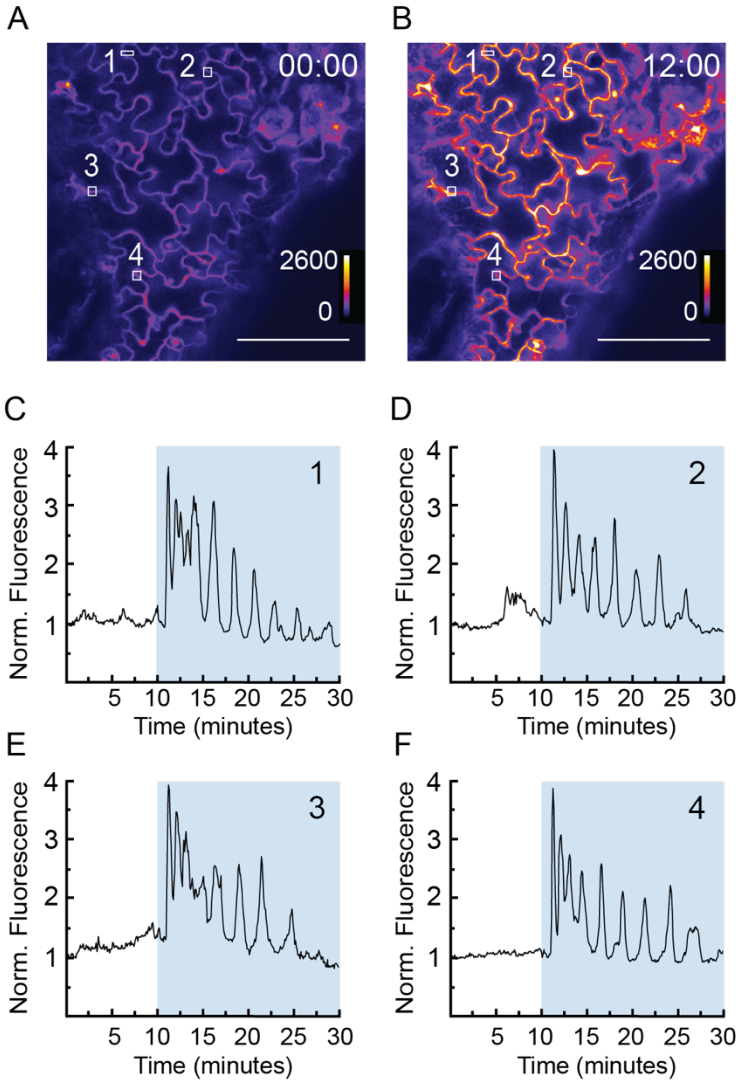

Figure 4. Calcium imaging with R-GECO1 using a HybriWell in response to flg22. An Arabidopsis true leaf expressing the intensiometric calcium indicator R-GECO1 was mounted in water in a HybriWell and imaged before and after treatment with 100 nM flg22. Images of the leaf epidermis were collected every five seconds using a confocal microscope. (A) Leaf epidermis prior to treatment. (B) Leaf epidermis 115 seconds after treatment. Fluorescence intensity of the R-GECO1 signal in arbitray units from 0 to 2600 is shown using a heat map scale. Scale bar=100 µm. White boxes indicate the Regions of Interest (ROIs) used in C-F. (C-F) Normalized R-GECO1 fluorescence for individual ROIs. Number in the upper right of each graph indicates the corresponding ROI. Blue background indicates presence of 100 nM flg22 in the HybriWell.

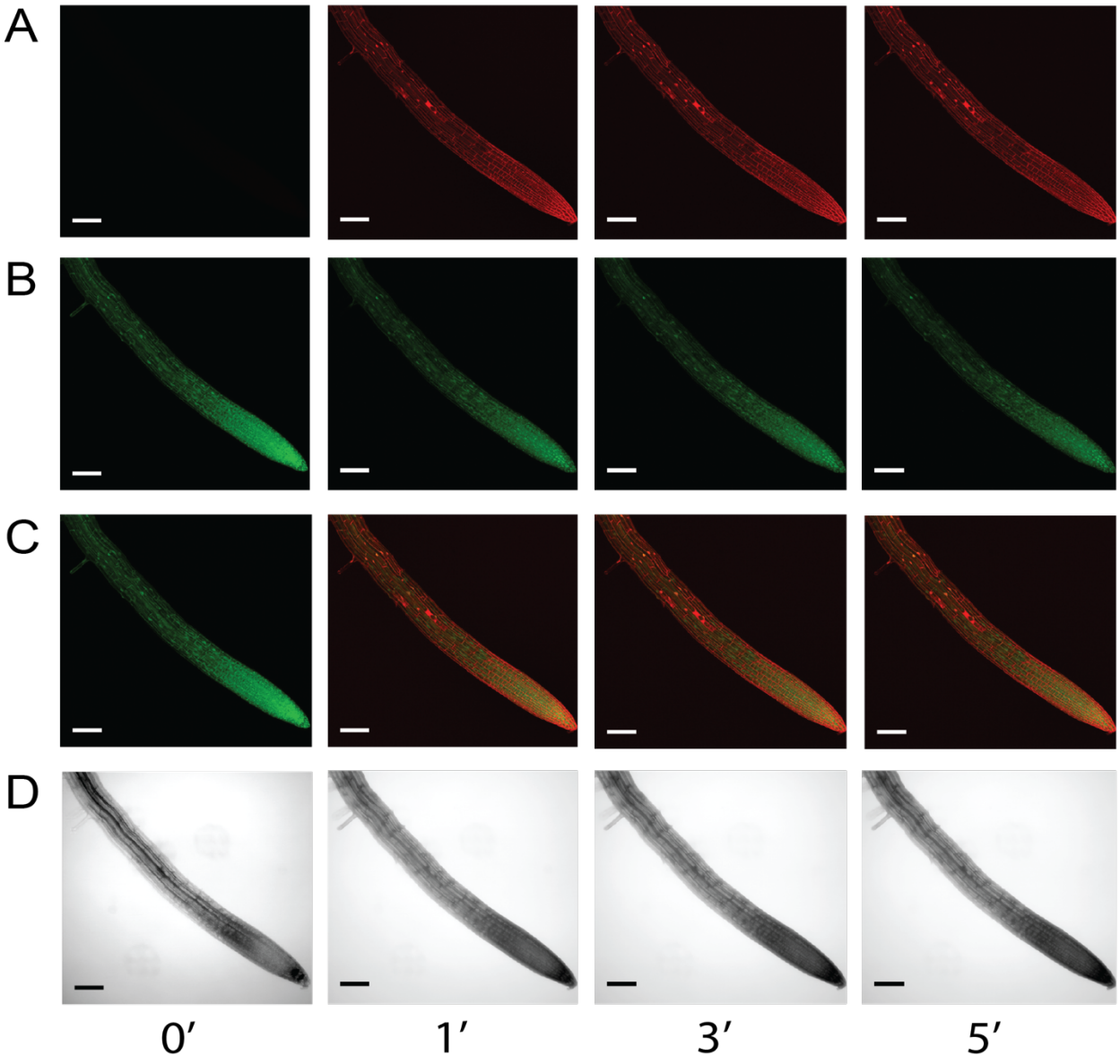

Supplemental Figure 1. Propidium iodide staining of roots in the HybriWell. Seedlings expressing 35S:GFP were placed in HybriWells, and the roots were treated with 50 µl of propidium iodide solution. Maximum Z-projections collected before treatment and every two minutes after treatment are shown. (A) Propidium iodide staining. (B) GFP fluorescence. (C) Merged images. (D) The brightfield. Scale bar=100 µm.

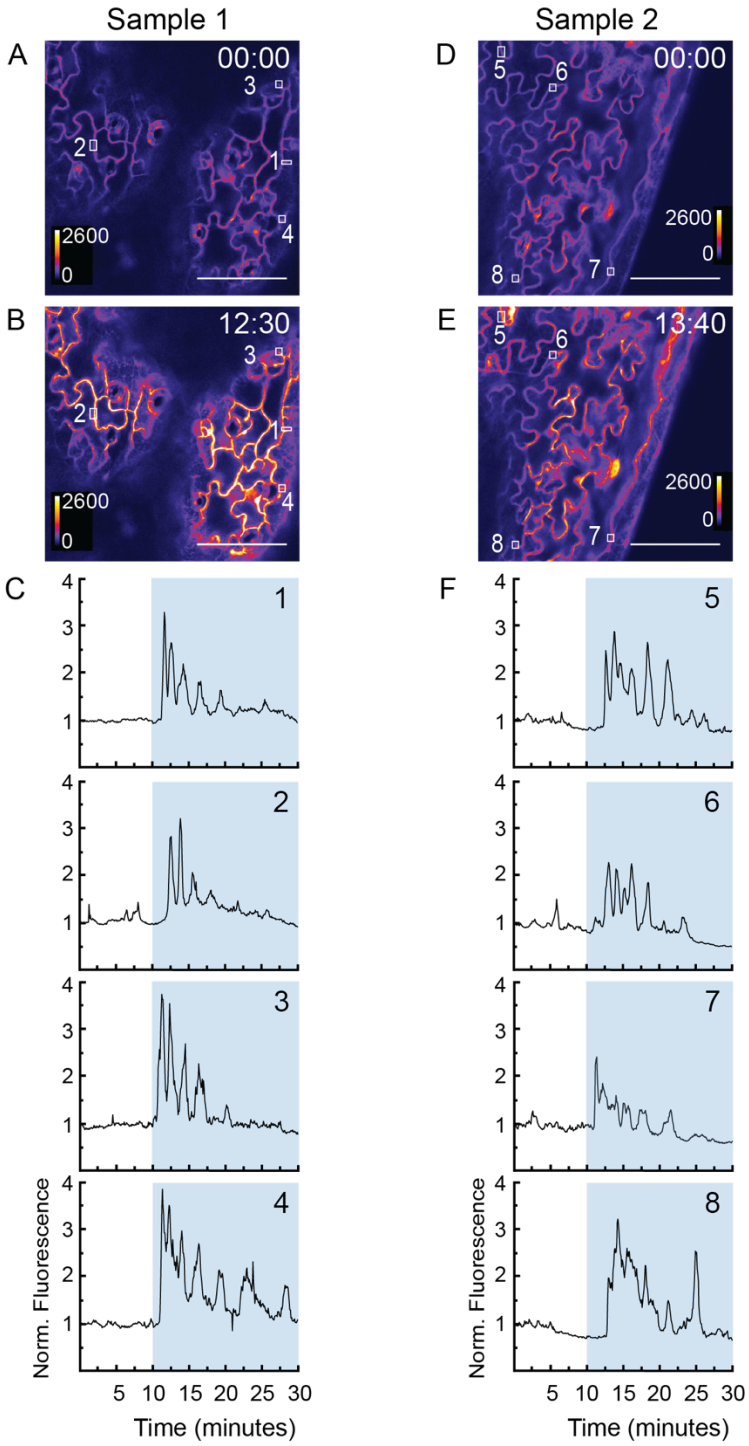

Supplemental Figure 2. Calcium imaging with R-GECO1 using a HybriWell in response to flg22. Arabidopsis true leaves expressing the intensiometric calcium indicator R-GECO1 were mounted in water in a HybriWell and imaged before and after treatment with 100 nM flg22. Images of the leaf epidermis were collected every five seconds using a confocal microscope. (A,D) Images of leaf epidermis captured prior to treatment for two independent samples. (B,E) Image of leaf epidermis captured 145 or 215 seconds after treatment, respectively. Fluorescence intensity of the R-GECO1 signal in arbitray units from 0 to 2600 is shown using a heat map scale. Scale bar=100 µm. White boxes indicate the Regions of Interest (ROIs) used to quantitate fluorescence. (C,F) Normalized R-GECO1 fluorescence for individual ROIs. Number in the upper right of each graph indicates the corresponding ROI. Blue background indicates presence of 100 nM flg22 in the HybriWell.

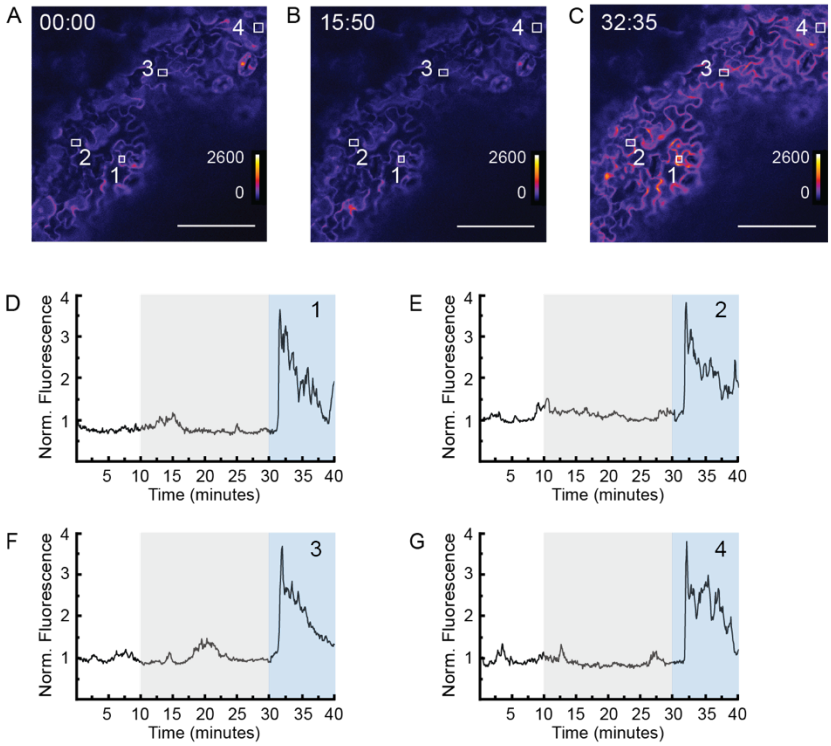

Supplemental Figure 3. Calcium imaging with R-GECO1 using a HybriWell in response to water. An Arabidopsis true leaf expressing the intensiometric calcium indicator R-GECO1 was mounted in water in a HybriWell and imaged before and after treatment with pure water, followed later by a secondary treatment of 100 nM flg22. Images of the leaf epidermis were collected every five seconds using a confocal microscope. (A) Leaf epidermis prior to treatment. (B) Leaf epidermis 345 seconds after treatment with pure water. (C) Leaf epidermis 150 seconds after treatment with 100 nM flg22. Fluorescence intensity of the R-GECO1 signal in arbitray units from 0 to 2600 is shown using a heat map scale. Scale bar=100 µm. White boxes indicate the Regions of Interest (ROIs) used to quantitate fluorescence. (D-G) Normalized R-GECO1 fluorescence for individual ROIs. Number in the upper right of each graph indicates the corresponding ROI. Gray background denotes when pure water was added to the Hybriwell. Blue background denotes when 100 nM flg22 was added.

Chapter 3: A Förster resonance energy transfer sensor for live-cell imaging of mitogen-activated protein kinase activity in Arabidopsis

My contribution: I performed and analyzed the *in vitro* FRET assays for Figure 1 and all of the SOMA *in vivo* experiments except for Figure 4D. I also wrote the Materials and Methods sections for these experiments. I created all of the Figures and Videos save for Figure 1 and Supplemental Figures 11-17.

This chapter was adapted from the following publication: Zaman, N.; Seitz, K.; Kabir, M.; George-Schreder, L.S.; Shepstone, I.; Liu, Y.; Zhang, S.; Krysan, P.J. A Förster resonance energy transfer sensor for live-cell imaging of mitogen-activated protein kinase activity in Arabidopsis. *The Plant Journal*. **2019**, *97*, 970-983.

Abstract

The catalytic activity of mitogen-activated protein kinases (MAPKs) is dynamically modified in plants. Since MAPKs have been shown to play important roles in a wide range of signaling pathways, the ability to monitor MAPK activity in living plant cells would be valuable. Here, we report the development of a genetically encoded MAPK activity sensor for use in *Arabidopsis thaliana*. The sensor is composed of yellow and blue fluorescent proteins, a phosphopeptide binding domain, a MAPK substrate domain, and a flexible linker. *In vitro* testing demonstrated that phosphorylation causes an increase in the Förster resonance energy transfer (FRET) efficiency of the sensor. The FRET efficiency can therefore serve as a readout of kinase activity. We also produced transgenic Arabidopsis lines expressing this sensor of MAPK activity (SOMA) and performed live-cell imaging experiments using detached cotyledons. Treatment with NaCl, the synthetic flagellin peptide flg22 and chitin all led to rapid gains in FRET efficiency. Control lines expressing a version of SOMA in which the phosphosite was mutated to an alanine did not show any substantial changes in FRET. The sensor was also expressed in a conditional loss-of-function double-mutant line for the Arabidopsis MAPK genes MPK3 and MPK6. These experiments demonstrated that MPK3/6 are necessary for the NaCl-induced FRET gain of the sensor, while other MAPKs are probably contributing to the chitin and flg22-induced increases in FRET. Taken together, our results suggest that SOMA is able to dynamically report MAPK activity in living plant cells.

Introduction

Live cell imaging is a powerful method for studying a variety of cellular processes in plants (Grossmann et al., 2018). Genetically encoded biosensors are critical tools for performing live-cell imaging because they allow the researcher to specifically monitor a particular biomolecule within the cell. A wide range of fluorescent biosensors have been used in plants, including those that report on the status of calcium, glucose, inorganic phosphate, zinc, ATP, hydrogen peroxide, pH, auxin, gibberellic acid and abscisic acid (Nagai et al., 2004; Deuschle et al., 2006; Zhao et al., 2011; Brunoud et al., 2012; Gjetting et al., 2012; Jones et al., 2014; Lanquar et al., 2014; Waadt et al., 2014; Hernandez-Barrera et al., 2015; Mukherjee et al., 2015; De Col et al., 2017; Rizza et al., 2017). Biosensors for measuring the activity of protein kinases have been described for use in animal cells, but to date none have been reported for plants.

The most widely used sensors of kinase activity in animal cells are based on the process of Förster resonance energy transfer (FRET) (Aoki et al., 2012; Sample et al., 2014). These sensors carry a substrate domain specific for a kinase of interest and a phosphopeptide-binding domain. When the kinase of interest is active within a cell it will phosphorylate the sensor. The phosphopeptide-binding domain then drives a conformational change that leads to a change in the ratio of fluorescence from the two fluorophores, which can be monitored in living samples using confocal microscopy. Kinase activity sensors of this type have been used to measure mitogen-activated protein kinase (MAPK) activation in animal cell cultures, *Caenorhabditis elegans*, zebrafish embryos and mice (Kamioka et al., 2012; Tomida et al., 2012; Aoki et al., 2013; Ryu et al., 2015; Sari et al., 2018).

We were interested in developing a biosensor for MAPK activity in Arabidopsis because of the central role that these kinases play in a wide range of signaling pathways. Our current understanding of MAPK function in Arabidopsis is based on extensive genetic and biochemical studies which have demonstrated roles for MAPK signaling in both stress responses and developmental regulation (Suarez-Rodriguez et al., 2010; Moustafa et al., 2014; Xu and Zhang, 2015; Liu and He, 2017; Devendrakumar et al., 2018; Komis et al., 2018; Zhang et al., 2018). Of the 20 MAPK genes present in the Arabidopsis genome, mutant phenotypes have been associated with *mpk1*, *mpk3*, *mpk4*, *mpk6*, *mpk8*, *mpk9*, *mpk10*, *mpk12*, *mpk17* and *mpk18* (Petersen et al., 2000; Bush and Krysan, 2007; Wang et al., 2007, 2008; Hord et al., 2008; Ren et al., 2008; Jammes et al., 2009; Walia et al., 2009; Galletti et al., 2011; Takahashi et al., 2011; Zeng et al., 2011; Stanko et al., 2014; Enders et al., 2017; Zhang et al., 2017; Frick and Strader, 2018). The biological processes regulated by these MAPKs include biotic and abiotic stress responses, cell division and developmental patterning.

Genetic studies typically allow one to identify a pathway or process in which a particular gene product functions but understanding the precise molecular mechanism by which it functions requires biochemical analysis. In the case of MAPK signaling, understanding the activation status of the kinase in different biological contexts has proved to be a subject of great interest to the field. The catalytic activity of a MAPK is switched on by dual phosphorylation of its conserved activation loop by an upstream MAPK kinase (MAPKK) and switched off by dephosphorylation of those residues by protein phosphatases (Suarez-Rodriguez et al., 2010). In its activated state, MAPK is able to phosphorylate a wide range of substrate molecules in a cell. Current methods for interrogating the activation status of MAPKs

in Arabidopsis involve homogenizing samples and extracting protein for *in vitro* analysis (Su et al., 2017; Sun et al., 2018). Although these methods have been very successful in documenting patterns of MAPK activation in response to a number of different biotic and abiotic stress treatments, one limitation of these studies is that they provide an average of the kinase activation across all the cells in the sample. Furthermore, it has been well documented that MAPK activity does not occur uniformly in all cell types in different mammalian signaling networks (Lahav et al., 2004; Spencer et al., 2009; Albeck et al., 2013), suggesting that Arabidopsis MAPKs may also display heterogeneity in response to a stimulus. Developing tools that allow for the observation of MAPK activation with single-cell resolution in living samples therefore has the potential to improve our understanding of how signaling is integrated across scales from cell to tissue to organism. Here, we describe the development of a genetically encoded biosensor designed to report the activity of MAPKs in *Arabidopsis thaliana*.

Results

Construction of the sensor of MAP kinase activity (SOMA)

In order to produce a genetically encoded biosensor that would report MAPK activity in Arabidopsis, we made use of a previously established MAPK activity sensor developed for use in mammalian cells (Komatsu et al., 2011). In that study, the authors evaluated a number of different fluorophore combinations and flexible linkers and identified that the combination of YPet, Turquoise GL and the 244-amino-acid version of the EV linker allowed for one of the strongest FRET gains. We took that mammalian sensor and replaced the mammalian substrate domain with DNA encoding an 80-amino-acid region surrounding threonine 64 of the

Arabidopsis MAP kinase phosphatase (MKP1) protein (Ulm et al., 2001). Threonine 64 of MKP1 has been previously shown to be phosphorylated by MAP kinase 6 (MPK6) (Park et al., 2011). The functional domains of SOMA are the YPet yellow fluorescent protein, the FHA1 phosphopeptide-binding domain of yeast RAD53, a 244-amino-acid version of the EV linker, 80 amino acids of Arabidopsis MPK1 and the Turquoise GL blue fluorescent protein (Figure 1A) (Sun et al., 1998; Nguyen and Daugherty, 2005; Goedhart et al., 2010; Komatsu et al., 2011). We also introduced a serine to aspartic acid substitution at the +3 position with respect to the phosphothreonine site in the MKP1 substrate domain of SOMA since previous work had shown that an aspartic acid at this position enhances FHA1 affinity for the phosphorylated form of the substrate (Yongkiettrakul et al., 2004; Komatsu et al., 2011).

The rationale for the design of this sensor is outlined in Figure 1B. When the sensor is in an unphosphorylated state, the FHA1 domain has low affinity for the substrate domain and the ratio of YPet to Turquoise GL fluorescent emission is consequently low in response to Turquoise GL excitation. When MAPK phosphorylates the sensor's substrate domain, the affinity of FHA1 for the substrate domain should increase substantially. Binding of FHA1 to the substrate domain then causes an increase in the ratio of YPet to Turquoise GL fluorescent emission in response to Turquoise GL excitation (Komatsu et al., 2011). Removal of the phosphate group from the sensor by a phosphatase will cause the sensor to return to a state where the ratio of YPet to Turquoise GL emission is low upon Turquoise GL excitation. The sensor therefore provides a readout of the balance between the competing activities of the kinases and phosphatases that recognize the sensor's substrate domain. In the case of SOMA, we chose a

substrate domain that has previously been shown to be phosphorylated by MPK6 in Arabidopsis (Park et al., 2011).

In order to determine if the 80-amino-acid portion of MKP1 included in SOMA could be phosphorylated by Arabidopsis MAPKs in the context of the full-length SOMA protein, we performed *in vitro* kinase assays using recombinant proteins purified from *Escherichia coli*. For these experiments, we also constructed a mutant form of the sensor, SOMA^{T679A}, in which the threonine that was expected to be phosphorylated was mutated to an alanine. We incubated these sensor constructs with Arabidopsis MPK3, MPK4, MPK6 and MPK10 that had been activated by co-incubation with constitutively active versions of Arabidopsis MAP kinase kinase 4 (MKK4) and MAP kinase kinase 5 (MKK5) (Ren et al., 2002). Phosphorylation of SOMA was detected for all of these kinases, although the intensity of the signal produced by MPK4 was weaker than that of the other kinases (Figure 1C). No phosphorylation was detected in any of the SOMA^{T679A} reactions. These results indicate that the previously characterized MKP1 phosphorylation can be recognized by MAPKs in the context of SOMA and that there are no additional MAPK phosphorylation sites in the sensor.

To determine if the phosphorylation status of SOMA affected the ratio of YPet to Turquoise GL emission, we performed *in vitro* experiments using proteins expressed in *E. coli*. We incubated SOMA and SOMA^{T679A} in the presence or absence of a constitutively active version of MPK6 (CA-MPK6), and then the fluorescence emission profile was determined with a scanning spectrofluorometer (Berriri et al., 2012). Using an excitation wavelength targeting the Turquoise GL fluorophore, we observed emission peaks corresponding to both Turquoise GL and YPet (Figure 1D, E). In the case of SOMA, co-incubation with CA-MPK6 caused a reduction

in Turquoise GL emission and an increase in YPet emission relative to SOMA alone. This result suggested that phosphorylation of the sensor caused an increase in FRET efficiency, although additional experimentation would be needed to verify that the mechanism responsible for the change in YPet to Turquoise emission is differential FRET efficiency. Supporting this conclusion, we observed that CA-MPK6 did not change the ratio of YPet to Turquoise GL emission of $SOMA^{T679A}$ upon Turquoise GL excitation. To further explore if phosphorylation of SOMA is responsible for the observed change in the ratio of YPet to Turquoise GL emission upon Turquoise GL excitation shown in Figure 1D, we performed an experiment using lambda protein phosphatase and observed that phosphatase strongly reduced the ratio of YPet to Turquoise GL emission upon Turquoise GL excitation displayed by the SOMA + CA-MPK6 reactions (Figure S1). Taken together, these results indicate that phosphorylation of threonine 679 of SOMA causes an increase in the ratio of YPet to Turquoise GL emission upon excitation of Turquoise GL *in vitro*.

***In vivo* testing of SOMA**

In order to determine if SOMA was effective *in vivo*, we generated transgenic lines expressing four different versions of SOMA as outlined in Table 1. These lines expressed SOMA or $SOMA^{T679A}$ tagged with either the SV40 nuclear localization signal (NLS) or a human immunodeficiency virus 1 (HIV-1) nuclear export signal (NES) (Kalderon et al., 1984; Wen et al., 1995). Expression was driven by the cauliflower mosaic virus 35S promoter in the case of the NES-tagged sensors and the Arabidopsis *Ubiquitin 10* (*UBQ10*) promoter in the case of the NLS-tagged sensors (Odell et al., 1985; Grefen et al., 2010). Two independent transgenic lines were

characterized for each of the four sensor constructs (Table 1). The transgenic lines expressing the SOMA constructs did not display any obvious phenotypic differences when compared with wild-type control plants (Figures S2 and S3.)

We next wanted to determine if treatments known to activate MAPK activity in Arabidopsis caused a change in the ratio of YPet to Turquoise GL emission of SOMA *in planta*. To do this we mounted 5-day-old detached cotyledons in water in a microfluidic device suitable for live-cell imaging and used confocal microscopy to measure the ratio of YPet to Turquoise GL emission in response to Turquoise GL excitation (Vang et al., 2018). This imaging chamber holds a cotyledon in a volume of about 30 µl of liquid that can be exchanged with a fresh solution in less than 1 min via microfluidic passive pumping. As a result, one can observe a sample before, during and after the application of a desired chemical treatment. Using this imaging system, a rapid gain in the ratio of YPet to Turquoise GL emission was observed with both SOMA-NLS and SOMA-NES within 2–4 min of treatment with 150 mM NaCl (Figure 2A–E, G). NaCl stress has previously been shown to activate MPK3/6 in Arabidopsis (Droillard et al., 2004; Yu et al., 2010). The ratio of YPet to Turquoise GL emission returned to pre-treatment levels 35–45 min after the initial peak. A follow-up treatment with water to induce hypo-osmotic shock or the synthetic flagellin peptide flg22 to double-stress the samples with hypo-osmotic shock plus an elicitor stimulus caused a second gain in the ratio of YPet to Turquoise GL emission. These results demonstrate that the ratio of YPet to Turquoise GL emission of SOMA rapidly changes in response to treatments known to activate MAPK activity in Arabidopsis. The observation that the ratio of YPet to Turquoise GL emission drops back to pre-treatment levels after about 35–45

min and can then be re-stimulated by a final hypo-osmotic shock indicates that the sensor remains viable for the duration of the experiment and that its changes are reversible.

No substantial changes in the ratio of YPet to Turquoise GL emission were observed in experiments using lines expressing SOMA^{T679A}-NLS and SOMA^{T679A}-NES (Figure 2F, H), indicating that the known phosphorylation site of SOMA is necessary for stress-induced changes in the ratio of YPet to Turquoise GL emission *in vivo*. In addition, treatment of SOMA-NLS and SOMA-NES lines with water as a control did not result in any substantial changes in the ratio of YPet to Turquoise GL emission (Figure S4), demonstrating that the imaging protocol did not affect the sensors. Similar results were obtained using independent transgenic lines for each of the four sensor constructs (Figure S5). We also observed that the guard cells of plants expressing SOMA-NLS did not display any change in the ratio of YPet to Turquoise GL emission when treated with NaCl, in contrast to neighboring pavement cells (Figure S6).

The NaCl-induced change in the ratio of YPet to Turquoise GL emission of SOMA is dependent on MPK3/6

We next wanted to determine if the change in the ratio of YPet to Turquoise GL emission triggered by NaCl stress in cotyledons was dependent on MAPK activity. Because MPK3 and MPK6 have been shown to be highly redundant kinases, we wanted to test SOMA in an *mpk3 mpk6* double-mutant background (Wang et al., 2007). It is also known, however, that *mpk3 mpk6* double mutants are embryo lethal (Wang et al., 2007). We therefore made use of *mpk3 mpk6* P_{mpk6}:*MPK6*^{YG}, a conditional loss-of-function *mpk3 mpk6* double-mutant line (Xu et al., 2014). This line is homozygous for T-DNA knockout mutations of *MPK3* and *MPK6*. It

also expresses MPK6^{YG}, which is a version of MPK6 that is sensitive to 1-NA-PP1, a bulky ATP analog that does not bind efficiently to the ATP-binding pockets of wild-type kinases but acts as a potent inhibitor of MPK6^{YG} (Bishop et al., 2000; Xu et al., 2014). Working with the *mpk3 mpk6* P_{mpk6}:*MPK6*^{YG} line therefore allowed us to use a chemical–genetic approach to switch off MPK3/6 activity during live-cell imaging.

We introduced SOMA-NES into the *mpk3 mpk6* P_{mpk6}: *MPK6*^{YG} line via genetic crossing and tested the effect of the 1-NA-PP1 inhibitor on NaCl-induced changes in the ratio of YPet to Turquoise GL emission. A detached cotyledon from the SOMA-NES *mpk3 mpk6* P_{mpk6}:*MPK6*^{YG} line was mounted in water in a HybriWell™ and observed using confocal microscopy. Addition of 1-NA-PP1 to the sample did not cause a substantial change in FRET efficiency. After 20 min of incubation in 1-NA-PP1, the solution in the imaging chamber was replaced with 150 mM NaCl + 10 µm 1-NA-PP1. No change in the ratio of YPet to Turquoise GL emission was observed, suggesting that MPK3/6 activity is required for the previously described NaCl-induced change in the ratio of YPet to Turquoise GL emission seen with SOMA. At the 60 min time-point, the solution in the imaging chamber was replaced with 10 µm 1-NA-PP1. The effect of this final solution change was to produce a hypo-osmotic shock to the sample while maintaining the presence of 10 µm 1-NA-PP1. With this hypo-osmotic shock, we observed a rapid gain in the ratio of YPet to Turquoise GL emission. This result suggests that a MAPK other than MPK3/6 may be responsible for this hypo-osmotic-induced change in the ratio of YPet to Turquoise GL emission. It should be noted that NaCl stress has been shown to induce the kinase activities of MP3/6 but not MPK4 (Droillard et al., 2004). By contrast, hypo-osmotic shock induces MPK3/6 and MPK4 (Droillard et al., 2004). Therefore, MPK4 is a good candidate for the

kinase driving the change in the ratio of YPet to Turquoise GL emission of SOMA caused by hypo-osmotic shock.

As a control, we performed the same experiment as described above using SOMA-NES in the wild-type Col-0 genetic background. In that case, we observed a strong increase in the ratio of YPet to Turquoise GL emission upon NaCl treatment, even in the presence of 1-NA-PP1 (Figure 3B), suggesting that the inhibitor does not affect wild-type MAPKs. When the final hypo-osmotic shock was applied to this sample, the initial NaCl-induced increase in the ratio of YPet to Turquoise GL emission had not diminished, so no additional gain was observed.

Next, we wanted to determine if 1-NA-PP1 could reverse the NaCl-induced gain in the ratio of YPet to Turquoise GL emission of the SOMA-NES *mpk3 mpk6* P_{mpk6}:$MPK6^{YG}$ line. For this experiment, an initial 150 mM NaCl treatment caused the expected increase in the ratio of YPet to Turquoise GL emission. Ten mins after that NaCl treatment, the sample was exposed to 150 mM NaCl + 10 µm 1-NA-PP1. Addition of 1-NA-PP1 caused the ratio of YPet to Turquoise GL emission to drop back to the pre-treatment level within 20 min (Figure 3C). By contrast, 1-NA-PP1 did not affect the duration of the NaCl-induced gain in the ratio of YPet to Turquoise GL emission with SOMA-NES in the wild-type Col-0 background (Figure 3D), which took about 35 min to return pre-treatment levels. Therefore, 1-NA-PP1 was able to reverse the NaCl-induced gain in the ratio of YPet to Turquoise GL emission of SOMA in the *mpk3 mpk6* P_{mpk6}:$MPK6^{YG}$ background, suggesting that MPK3/6 activity is necessary for the sustained, elevated ratio of YPet to Turquoise GL emission triggered by NaCl treatment. As before, a final hypo-osmotic/flg22 treatment produced a gain in the ratio of YPet to Turquoise GL emission at the end of the imaging period for both samples. Additional control experiments using DMSO in

place of 1-NA-PP1 confirmed that the effects we observed were due to 1-NA-PP1 rather than the DMSO solvent (Figure S7).

The response to flg22 is heterogeneous

flg22 is a synthetic peptide whose sequence is derived from the bacterial elicitor flagellin (Gómez-Gómez et al., 1999). flg22 is known to rapidly induce the activity of MPK3/4/6 via the plasma membrane-bound receptor FLS2 (Gómez-Gómez and Boller, 2000; Asai et al., 2002). We were therefore interested in characterizing the response to flg22 treatment of plants expressing SOMA. For this experiment, 5-day-old detached cotyledons were treated with 1 µm flg22 during the imaging process. In the case of SOMA-NES, we observed a heterogeneous pattern of changes in the ratio of YPet to Turquoise GL emission (Figure 4A, B). In all the pavement cells in the sample, we observed a rapid gain in the ratio of YPet to Turquoise GL emission within a few mins of flg22 treatment. In a subset of the pavement cells, the ratio of YPet to Turquoise GL emission rapidly dropped back to the pre-treatment levels within 30 min, followed by a second rapid gain in the ratio of YPet to Turquoise GL emission to produce the biphasic pattern seen in Figure 4A. In neighboring regions of the same cotyledon that is shown in Figure 4A, the initial gain in the ratio of YPet to Turquoise GL emission did not drop down to pre-treatment levels until 60 min after exposure to flg22 (Figure 4B). These results demonstrated that the ratio of YPet to Turquoise GL emission of SOMA can rapidly increase and decrease *in vivo*, and that the pattern of changes induced by flg22 treatment can vary within a single cotyledon.

In the case of SOMA-NLS, we also observed distinct patterns of the ratio of YPet to Turquoise GL emission in response to flg22 treatment. In pavement cells we saw a rapid increase in the ratio of YPet to Turquoise GL emission shortly after flg22 treatment in all samples tested. In some cases, the gain returned to pre-treatment levels within 30 min of exposure to flg22 (Figure 4C) while in other examples the gain was sustained for over 60 min (Figure 4D). In addition, we consistently observed that gain in the ratio of YPet to Turquoise GL emission displayed by SOMA-NLS in guard cells was substantially delayed when compared with pavement cells in the same sample (Figure 4D, E). In pavement cells, the flg22-induced gain begins within 4 min of flg22 exposure, while in guard cells it begins about 15 min after flg22 has been added to the sample. We did not observe any change in the ratio of YPet to Turquoise GL emission with SOMA-NES in guard cells, but this may be due to technical challenges associated with imaging the cytoplasm of guard cells with our imaging system.

Repetition of the flg22 experiments using independent transgenic lines for each sensor construct produced similar results (Figure S8). In addition, experiments performed using the SOMA-NES *mpk3 mpk6* P_{mpk6}:$MPK6^{YG}$ line indicated that 1-NA-PP1 did not affect flg22-and chitin-induced changes in the ratio of YPet to Turquoise GL emission (Figure S9). These results suggest that MAPKs in addition to MPK3/6 are able to drive the flg22-and chitin-induced changes in the ratio of YPet to Turquoise GL emission of SOMA. Since MPK4 is known to be activated by flg22 and chitin, it is a likely candidate (Ichimura et al., 2006).

Chitin induces a rapid FRET gain in guard cells

Like flg22, chitin is a pathogen-associated elicitor known to trigger rapid activation of MPK3/4/6 (Yamada et al., 2016). Using the same experimental system as described above, 5-day-old cotyledons were exposed to 40 mg ml^{-1} chitin during imaging. As with flg22, we observed a rapid gain in the ratio of YPet to Turquoise GL emission in pavement cells with SOMA-NES and SOMA-NLS (Figure 5A, B). The most pronounced difference between the response of cotyledons to chitin versus flg22 was seen in guard cells where chitin induced a gain in the ratio of YPet to Turquoise GL emission shortly after treatment, in contrast to the substantially delayed gain caused by flg22 exposure in guard cells. In addition, SOMA-NLS in guard cells often produced a strong second peak of YPet versus Turquoise GL emission intensity about 45 min after the initial treatment. Similar results were obtained with experiments performed using independent transgenic lines for each sensor construct (Figure S10).

Discussion

Reversible protein phosphorylation is a fundamental mechanism used to regulate a myriad of signal transduction pathways. Modulation of protein kinase activity therefore plays an essential role in cellular signaling. For this reason, there is considerable scientific interest in measuring the activation status of protein kinases in living systems. Established methods for monitoring the activation status of protein kinases involve first homogenizing tissues or organisms and then analyzing the kinase of interest *in vitro*. There are two major drawbacks to this approach: (1) potential heterogeneity of kinase activity within the tissue is lost due to the homogenization process and (2) the living sample must be destroyed in order to analyze it, which means that time-course experiments on a single sample cannot be performed.

Genetically encoded biosensors provide an alternative to these destructive methods for monitoring kinase activity in living cells (Aoki et al., 2012; Sample et al., 2014).

Genetically encoded biosensors for measuring MAPK activity have been developed for use in animal cells (Kamioka et al., 2012; Tomida et al., 2012; Aoki et al., 2013; Ryu et al., 2015; Sari et al., 2018). We were therefore interested in determining if one of these sensors could be adapted for use in Arabidopsis. To accomplish this, we replaced the substrate domain of an animal MAPK sensor with an 80-amino-acid portion of Arabidopsis MKP1 (Ulm et al., 2001). This substrate domain had been previously shown to contain a threonine residue (T64) that can be phosphorylated by MPK6 (Park et al., 2011). Our *in vitro* testing confirmed that this threonine can be efficiently phosphorylated by Arabidopsis MAPKs in the context of our biosensor and that this phosphorylation caused a gain of about 50% in the ratio of YPet to Turquoise GL emission, which is similar to the gain reported for kinase activity sensors used in animal cells (Komatsu et al., 2011). These experiments indicated that our sensor of MAPK activity (SOMA) is able to report the presence of activated MAPKs through an increase in the ratio of YPet to Turquoise GL emission in response to Turquoise GL excitation *in vitro*.

We were next interested in evaluating the performance of SOMA *in vivo*. The following evidence supports the idea that SOMA is able to act as a sensor of MAPK activity in living plants. To begin with, we have demonstrated that three stress treatments known to activate MAPK activity in Arabidopsis all cause rapid gains in the ratio of YPet to Turquoise GL emission of SOMA: 150 mM NaCl, 1 µm flg22 and 40 mg ml^{-1} chitin. Next, using lines expressing the phosphosite mutant $SOMA^{T679A}$, we demonstrated that these stress-induced gains in the ratio of YPet to Turquoise GL emission depend on the known MAPK phosphorylation site present in

the sensor. Finally, we tested SOMA in the *mpk3 mpk6* P_{mpk6}:$MPK6^{YG}$ genetic background, which allowed us to use a chemical–genetic approach to selectively switch off MPK3/6 activity using the 1-NA-PP1 inhibitor (Xu et al., 2014). These experiments demonstrated that MPK3/6 activity is necessary to drive the gain in the ratio of YPet to Turquoise GL emission of SOMA induced by NaCl stress. Taken together, these results show that the NaCl-induced increases in the ratio of YPet to Turquoise GL emission that we observe with SOMA require the known MPK3/6 phosphorylation site present in SOMA and the activity of MPK3/ 6. These results are consistent with a model in which SOMA acts as a reporter of MAPK activity *in vivo*.

The MAPK gene family in Arabidopsis is composed of 20 members, and it has been shown that many stress treatments activate MPK3, MPK6, MPK4 and others (Suarez-Rodriguez et al., 2010). We were therefore interested in understanding the extent to which SOMA may be reporting the activities of MAPKs in addition to MPK3/6. As discussed above, the gain in the ratio of YPet to Turquoise GL emission of SOMA caused by NaCl stress appears to be due to MPK3/6 activity. The gains in the ratio of YPet to Turquoise GL emission of SOMA caused by hypo-osmotic stress and flg22 treatment, however, are not diminished by 1-NA-PP1 when tested in the *mpk3 mpk6* P_{mpk6}:$MPK6^{YG}$ background. These results suggest that MAPKs other than MPK3/6 are able to drive changes in the ratio of YPet to Turquoise GL emission of SOMA. It is interesting to note that both hypo-osmotic shock and flg22 are known to activate MPK4 in addition to MPK3/6, and flg22 treatment also activates MPK1, MPK11 and MPK13 (Bethke et al., 2012; Nitta et al., 2014). By contrast, stress due to elevated NaCl appears to activate MPK3/ 6 but not MPK4 (Droillard et al., 2004). These results are consistent with a model in which SOMA acts as a MAPK activity reporter for MPK4 as well as MPK3/6. Further genetic testing

with additional genetic backgrounds will be needed to determine the full extent to which SOMA is able to report the activities of different MAPK isoforms. These experiments are complicated by the embryo lethality of *mpk3 mpk6* double mutants and the severe dwarf phenotype of *mpk4* single mutants (Ichimura et al., 2006; Suarez-Rodriguez et al., 2007; Wang et al., 2007).

The SOMA sensor, and similar MAPK sensors developed for use in animal cells, function by reporting the phosphorylation status of a substrate domain known to be phosphorylated by the kinase of interest. Because of this situation, it might be more accurate to think of these sensors as 'phosphorylation status reporters' since they integrate the net kinase and phosphatase activities acting on that specific phosphosite. In the case of SOMA, we have presented experimental evidence that MAPKs are able to target the sensor. It remains a possibility that other kinases may also be able to phosphorylate SOMA. Future genetic and bio-chemical studies will be needed to resolve that question.

The gain in the ratio of YPet to Turquoise GL emission displayed by kinase activity reporters such as SOMA is believed to occur due to binding of the forkhead (FHA1) domain to the phosphorylated substrate domain of the sensor (Komatsu et al., 2011; Sample et al., 2014). In order for the reporter to provide an up-to-date readout of kinase activity, it is important that phosphatases are able to efficiently dephosphorylate the sensor. Work with similar kinase sensors in animal cells has indicated that the FHA1 domain used in SOMA does not bind so tightly to phosphorylated substrate domains that it precludes efficient access by phosphatases (Komatsu et al., 2011). Our observation that the ratio of YPet to Turquoise GL emission of SOMA can rapidly drop *in vivo* after an initial stress-induced gain suggests that, like its animal cell precursor, SOMA is able to be efficiently de-phosphorylated (Figure 4A, C).

Previous work using *in vitro* methods to assay MAPK activation status has indicated that stress treatments such as NaCl, flg22 and chitin typically cause MPK3/4/6 to be transiently activated for a time period ranging from about 30 to 60 min (Droillard et al., 2004; Wan et al., 2004; Ichimura et al., 2006; Meszaros et al., 2006; Dóczi et al., 2007; Suarez-Rodriguez et al., 2007; Yu et al., 2010; Yamada et al., 2016). The patterns of changes in the ratio of YPet to Turquoise GL emission that we observed *in vivo* with SOMA are consistent with this type of transient MAPK activation. Because SOMA allows us to observe living cells in the context of intact tissue, however, we were also able to document heterogeneity at the cellular level. A common type of heterogeneity was the observation that some cells produced relatively transient peaks of the ratio of YPet to Turquoise GL emission lasting about 25 min, while other cells in the same sample maintained their elevated levels for over 60 min. In addition, we also observed that guard cells display distinct patterns of the ratio of YPet to Turquoise GL emission when compared with pavement cells in the same sample. It should be noted that one potential source of heterogeneity during this type of imaging experiment would be non-uniform exposure of the sample to the chemical treatment, such as flg22. We have previously characterized the imaging chambers used for this study, and based on that analysis we expect that the regions of the cotyledons analyzed here should have been uniformly exposed to the chemical treatments (Vang et al., 2018). Nevertheless, it is important to consider both technical and biological explanations for heterogeneous responses. If the heterogeneity is biological in origin, its biological significance is unknown at this time, but our ability to observe it highlights the potential for biosensors such as SOMA to reveal potentially new dimensions to signaling pathways that could not be observed using established *in vitro* methods.

In the present study, our objective has been to document the performance of a genetically encoded biosensor designed to report the activity of Arabidopsis MAPKs. To accomplish this we performed *in vitro* testing with *E. coli* expressed proteins and *in vivo* testing using the cotyledon epidermis as a model system. We chose the cotyledon epidermis because it provides a convenient and simple subject for confocal imaging. Because MAPK signaling has been implicated in a wide range of signaling pathways in Arabidopsis, it will be of interest to determine the extent to which SOMA can be used to study additional signaling pathways in different organ and tissue systems. While beyond the scope of the present study, such future work has the potential to reveal new aspects of MAPK signaling that can only be observed using live-cell imaging methods.

Materials and Methods

Plasmid construction

The plasmid backbones used to construct our SOMA plasmids were a kind gift of Michiyuki Matsuda and Kazuhiro Aoki. Specifically, we used the previously described AKAR3 construct (Komatsu et al., 2011) and swapped in the following functional domains using conventional restriction enzyme cloning: ECFP was replaced with Turquoise GL, the shorter linker was replaced with the 244-amino-acid EV linker and the substrate domain of AKAR3 was replaced with DNA encoding for amino acids 15–94 of the Arabidopsis MKP1 protein. We also introduced a serine to aspartic acid substitution within the MKP1 coding sequence, which corresponds to the +3 position with respect to the phosphothreonine site in the MKP1 substrate domain, as previous work has shown that an aspartic acid at this position enhances

the affinity of FHA1 for the phosphorylated form of the substrate (Yongkiettrakul et al., 2004; Komatsu et al., 2011). To make the phosphosite mutant form of SOMA, site-directed mutagenesis was then performed to change the coding sequence at the threonine 679 position of the sensor protein to alanine. The resulting SOMA and SOMA^{T679A} protein-coding sequences were then cloned into a derivative of pET-32(a)+ (Millipore Sigma, http://www.merckmillipore.com/) for expression of recombinant proteins in *E. coli*. Plasmid maps for pET-SOMA and pET-SOMA-T679A are provided in Figures S11 and S12, and the full DNA sequence for each is provided in Data S1 and S2. For targeted expression, our sensors in the nuclei of transgenic plants, the SOMA and SOMA^{T679A} protein-coding sequences, were moved into the binary vector pCAMBIA-1300 to produce pSOMA-NLS and pSOMA^{T679A}-NLS. For targeted expression in the cytoplasm of transgenic plants, the SOMA and SOMA^{T679A} protein-coding sequences were moved into a derivative of the binary vector pRI 201-AN (Takara Bio, http://www.takarabio.com/) to produce pSOMA-NES and pSOMA^{T679A}-NES. Plasmid maps for these constructs are provided in Figures S13–S16, and the full DNA sequence for each is provided in Data S3–S6. Plasmid DNA for pET-SOMA (Addgene no. 118935), pET-SOMA-T679A (Addgene no. 118936), pSOMA-NLS (Addgene no. 118937), pSOMA^{T679A}-NLS (Addgene no. 118938), pSOMA-NES (Addgene no. 118939) and pSOMA^{T679A}-NES (Addgene no. 118940) is available through Addgene (http://www.addgene.org/).

***In vitro* kinase assay**

Recombinant His-tagged MPK3, MPK4, MPK6 and MPK10 (7.5 µg each) were activated by incubation with a mixture of 0.125 µg recombinant MKK4^{DD} and 0.125 µg MKK5^{DD} as

previously described (Liu and Zhang, 2004). Activated MAPKs were then used to phosphorylate recombinant SOMA and SOMA^{T679A} proteins (1:20 enzyme: substrate weight ratio) in the kinase reaction buffer (20 mM HEPES, pH 7.5, 10 mM $MgCl_2$ and 1 mM DTT) with 25 µm ATP and [γ-32P] ATP (0.1 µCi per reaction). The reactions were stopped by the addition of SDS-loading buffer after 30 min. After resolution in a 10% SDS-polyacrylamide gel, all the proteins were visualized by Coomassie blue staining, and the phosphorylated SOMA was visualized by autoradiography.

***In vitro* FRET assay**

Recombinant SOMA, SOMA^{T679A} and CA-MPK6 were expressed in the Rosetta2 strain of *E. coli* (Millipore Sigma). CA-MPK6 is a constitutively active form of Arabidopsis MPK6 (Berriri et al., 2012). A plasmid expressing CA-MPK6 was a kind gift from Jean Colcombet. *Escherichia coli* cells expressing the recombinant proteins were treated with Bug Buster (Millipore Sigma). Then 7 µl of the SOMA cleared lysate was added to a reaction containing 25 mM 2-amino-2-(hydroxymethyl)-1,3-propanediol (TRIS)-HCl, 0.5 mM DTT, 5 mM $MgCl_2$, 0.1 mM ATP and 100 mM NaCl and water to a total volume of 200 µl. For reactions including CA-MPK6, 4 µl of the CA-MPK6 cleared lysate was also added. The reactions were then incubated at 25°C for 30–60 min and the fluorescent emission spectrum was measured using a QuantaMaster 40 Spectrofluorometer. Excitation was performed at 420 nm and the emission range analyzed was 465–545 nm. The slit size for both excitation and emission was 5 nm with a step size of 0.5 nm. For the lambda protein phosphatase (LPP) experiments, 2 µl of LPP, 20 µl of 10 mM $MgCl_2$ and 20 µl of 10x NEBuffer Pack for Protein MetalloPhosphatases

(PMP) (New England Biolabs, http://www.neb.com/) were added to the reactions after 60 min of incubation, and the reaction was further incubated at 30°C for another 15 min.

Transgenic lines

Transgenic lines expressing SOMA-NLS, SOMA^{T679A}-NLS, SOMA-NES and SOMA^{T679A}-NES were produced via the floral dip method using the GV3101 strain of *Agrobacterium tumefaciens* (Clough and Bent, 1998). Primary transformants expressing the sensor constructs were identified by screening with an epifluorescence microscope 4-day-old seedlings germinated on 1% agar (w/v) plates containing 0.5x Murashige and Skoog basal salt mixture. Seedlings showing strong fluorescence were transferred to soil and seed was collected. Two independent transgenic lines for each of the four sensor constructs were produced as shown in Table 1. Seed for the transgenic lines is available via the Arabidopsis Biological Resource Center (ABRC) (http://abrc.osu.edu/), and the ABRC stock number for each line is shown in Table 1.

Plant material and growth conditions

To prepare seedlings for confocal imaging, seeds were surface sterilized using 95% ethanol and then plated onto growth media composed of 1% agar (w/v) containing 0.5x Murashige and Skoog basal salt mixture in 130 mm square Petri dishes. The samples were incubated in the dark at 4°C for 1–3 days to stratify the seeds and then placed under constant light at 20–25°C with the plates in a vertical orientation. Cotyledons were harvested for imaging after the plates had been under light for 4–5 days.

Confocal microscopy

Detached cotyledons were prepared for imaging on the confocal microscope using the HybriWell™ method as previously described (Vang et al., 2018). Briefly, a 5-µl drop of ultrapure water was placed on a 45 mm 9× 55 mm microscope cover glass. Then, a cotyledon from a 4–5-day-old seedling was placed abaxial side down on top of the droplet. Cotyledons were gently submerged by dripping water around them with a pipette. Excess water was then removed, and a HybriWell™ (Grace Bio-Labs, http://gracebio.com/, cat. no. 611102) was gently placed on the coverslide with the cotyledon in the center to form a 150-µm deep imaging chamber with a volume of 30 µl. The dimensions of the chamber are such that the cotyledon is gently held in place by pressure from the top of the chamber, but liquid can still pass between the abaxial side of the cotyledon and the coverglass (Vang et al., 2018). Then 400 µl of ultrapure water was injected through one of the HybriWell™ ports using a pipettor to fill the 30-µl chamber with water and expel any air bubbles. A 200-µl droplet of ultrapure water was then placed on one of the ports to prevent the chamber from drying out. The HybriWells™ containing mounted seedlings were then placed in covered Petri dishes and equilibrated by incubating at 20–23°C under constant light for 6–12 h prior to imaging.

Confocal microscopy was performed using either a Zeiss LSM 510 Meta or a Zeiss LSM 780 (http://www.zeiss.com/) with a 20x objective. Samples were excited at 458 nm with 1% power for the LSM 510 and 5% power for the LSM 780. Emission was measured between 463 and 517 nm for Turquoise GL and between 534 and 570 nm for YPet. Z-stacks were collected

every 2 min with an optical slice thickness of 2.92 µm for the LSM 510 and 2 µm for the LSM 780.

Chemical treatments were added to the samples during imaging by pipetting 300 µl of solution containing the treatment onto one port of the HybriWell™. For flg22 treatment, we used a 1 µm solution of synthetic flg22 peptide (QRLSTGSRINSAKDDAAGLQIA) (PhytoTechnology Laboratories, http://phytotechlab.com/, cat. no. P6622) in water. For chitin treatment, 200 mg of chitin from shrimp shells (Sigma, http://www.sigmaaldrich.com/, cat. no. C7170–100G) was added to a 1.5 ml Eppendorf tube containing two steel pellets and ground at 25 Hz for 10 min using a Retsch MM 200 mixer mill (Retsch, http://www.retsch.com/). The pulverized chitin was then added to 5 ml of water and vortexed briefly prior to use. The ATP analog 1-NA-PP1 (MedChemExpress, http://www.medchemexpress.com/, cat. no. HY-13941) was obtained from the manufacturer as a 10 mM stock solution dissolved in dimethyl sulfoxide (DMSO).

Image analysis

Post-processing of the raw image data was performed using Fiji (Schindelin et al., 2012). First, the 'Z-projection' function was performed on an image stack using the 'Max Intensity' setting. The resulting projection was then separated into two separate images, one for the Turquoise GL emission channel and one for the YPet emission channel. The 'Subtract Background' function was performed on both images, with the 'rolling ball radius' set as the default 50 pixels. A mask was then created from the YPet channel using the 'Convert to Mask' function. The background subtracted YPet and Turquoise GL images were then converted into

32-bit images. These 32-bit images were then multiplied by the Mask file. The resulting YPet image was divided by the resulting Turquoise GL image using the 'Image Calculator' function to create to a ratio image representing the ratio of YPet to Turquoise emission. Finally, the 'Threshold' function was performed using the default values, with the 'NaN background' option enabled. The 'Fire' lookup table was then applied to the final ratio image.

To measure the ratio of YPet to Turquoise GL emission, a region of interest (ROI) was selected within the ratio image using Fiji and the average ratio value within that ROI was then measured. For time-course experiments, the change in the YPet to Turquoise GL emission ratio was normalized to the initial value of the YPet to Turquoise GL emission ratio and plotted versus time. The initial pixel intensity values for the raw image data in the YPet and Turquoise GL channels are presented for each experiment in Table S1. The ROIs used for analyzing the data presented in Figures 1–5 are shown in Figures S17–S20. Movies S1–S13 present time-course videos of the ratio image data for selected experiments.

Acknowledgements

The authors would like to thank Lauren St. George-Schreder and John Seagrist for technical assistance with this work.

References

Albeck, J. G.; Mills, G. B.; Brugge, J. S. Frequency-modulated pulses of ERK activity transmit quantitative proliferation signals. *Molecular Cell*. **2013**, *49*, 249-261.

Aoki, K.; Komatsu, N.; Hirata, E.; Kamioka, Y.; Matsuda, M. Stable expression of FRET biosensors: a new light in cancer research. *Cancer Science*. **2012**, *103*, 614-619.

Aoki, K.; Kumagai, Y.; Sakurai, A.; Komatsu, N.; Fujita, Y.; Shionyu, C.; Matsuda, M. Stochastic ERK activation induced by noise and cell-to-cell propagation regulates cell density-dependent proliferation. *Molecular Cell*. **2013**, *52*, 529-540.

Asai, T.; Tena, G.; Plotnikova, J.; Willmann, M.R.; Chiu, W.L.; Gómez-Gómez, L.; Boller, T.; Ausubel, F.M.; Sheen, J. MAP kinase signalling cascade in Arabidopsis innate immunity. *Nature*. **2002**, *415*, 977-983.

Berriri, S.; Garcia, A.V.; dit Frey, N.F.; Rozhon, W.; Pateyron, S.; Leonhardt, N.; Montillet, J.L.; Leung, J.; Hirt, H.; Colcombet, J. Constitutively active mitogen-activated protein kinase versions reveal functions of Arabidopsis MPK4 in pathogen defense signaling. *The Plant Cell*. **2012**, *24*, 4281-4293.

Bethke, G.; Pecher, P.; Eschen-Lippold, L.; Tsuda, K.; Katagiri, F.; Glazebrook, J.; Scheel, D.; Lee, J. Activation of the *Arabidopsis thaliana* mitogen-activated protein kinase MPK11 by the flagellin-derived elicitor peptide, flg22. *Molecular Plant-Microbe Interactions*. **2012**, *25*, 471-480.

Bishop, A.C.; Ubersax, J.A.; Petsch, D.T.; Matheos, D.P.; Gray, N.S.; Blethrow, J.; Shimizu, E.; Tsien, J.Z.; Schultz, P.G.; Rose, M.D.; Wood, J.L. A chemical switch for inhibitor-sensitive alleles of any protein kinase. *Nature*. **2000**, *407*, 395-401.

Brunoud, G.; Wells, D.M.; Oliva, M.; Larrieu, A.; Mirabet, V.; Burrow, A.H.; Beeckman, T.; Kepinski, S.; Traas, J.; Bennett, M.J.; Vernoux, T. A novel sensor to map auxin response and distribution at high spatio-temporal resolution. *Nature*. **2012**, *482*, 103-106.

Bush, S. M.; Krysan, P. J. Mutational evidence that the Arabidopsis MAP kinase MPK6 is involved in anther, inflorescence, and embryo development. *Journal of Experimental Botany*. **2007**, *58*, 2181-2191.

Clough, S. J.; Bent, A. F. Floral dip: a simplified method for Agrobacterium-mediated transformation of *Arabidopsis thaliana*. *The plant journal*. **1998**, *16*, 735-743.

De Col, V.; Fuchs, P.; Nietzel, T.; Elsässer, M.; Voon, C.P.; Candeo, A.; Seeliger, I.; Fricker, M.D.; Grefen, C.; Møller, I.M.; Bassi, A. ATP sensing in living plant cells reveals tissue gradients and stress dynamics of energy physiology. *Elife*. **2017**, *6*, e26770.

Deuschle, K.; Chaudhuri, B.; Okumoto, S.; Lager, I.; Lalonde, S.; Frommer, W. B. Rapid metabolism of glucose detected with FRET glucose nanosensors in epidermal cells and intact roots of Arabidopsis RNA-silencing mutants. *The Plant Cell*. **2006**, *18*, 2314-2325.

Devendrakumar, K. T.; Li, X.; Zhang, Y. MAP kinase signalling: interplays between plant PAMP- and effector-triggered immunity. *Cellular and Molecular Life Sciences*. **2018**, *75*, 2981-2989.

Dóczi, R.; Brader, G.; Pettkó-Szandtner, A.; Rajh, I.; Djamei, A.; Pitzschke, A.; Teige, M.; Hirt, H. The Arabidopsis mitogen-activated protein kinase kinase MKK3 is upstream of group C mitogen-activated protein kinases and participates in pathogen signaling. *The Plant Cell*. **2007**, *19*, 3266-3279.

Droillard, M. J.; Boudsocq, M.; Barbier-Brygoo, H.; Laurière, C. Involvement of MPK4 in osmotic stress response pathways in cell suspensions and plantlets of *Arabidopsis thaliana*: activation by hypoosmolarity and negative role in hyperosmolarity tolerance. *FEBS Letters*. **2004**, *574*, 42-48.

Enders, T. A.; Frick, E. M.; Strader, L. C. An Arabidopsis kinase cascade influences auxin-responsive cell expansion. *The Plant Journal*. **2017**, *92*, 68-81.

Frick, E. M.; Strader, L. C. Kinase MPK17 and the peroxisome division factor PMD1 influence salt-induced peroxisome proliferation. *Plant Physiology*. **2018**, *176*, 340-351.

Galletti, R.; Ferrari, S.; De Lorenzo, G. Arabidopsis MPK3 and MPK6 play different roles in basal and oligogalacturonide-or flagellin-induced resistance against *Botrytis cinerea*. *Plant Physiology*. **2011**, *157*, 804-814.

Gjetting, S. K.; Ytting, C. K.; Schulz, A.; Fuglsang, A. T. Live imaging of intra-and extracellular pH in plants using pHusion, a novel genetically encoded biosensor. *Journal of Experimental Botany*. **2012**, *63*, 3207-3218.

Goedhart, J.; Van Weeren, L.; Hink, M. A.; Vischer, N. O.; Jalink, K.; Gadella, T. W. Bright cyan fluorescent protein variants identified by fluorescence lifetime screening. *Nature Methods*. **2010**, *7*, 137-139.

Gómez-Gómez, L.; Boller, T. FLS2: an LRR receptor–like kinase involved in the perception of the bacterial elicitor flagellin in Arabidopsis. *Molecular Cell*. **2000**, *5*, 1003-1011.

Gómez-Gómez, L.; Felix, G.; Boller, T. A single locus determines sensitivity to bacterial flagellin in *Arabidopsis thaliana*. *The Plant Journal*. **1999**, *18*, 277-284.

Grefen, C.; Donald, N.; Hashimoto, K.; Kudla, J.; Schumacher, K.; Blatt, M. R. A ubiquitin-10 promoter-based vector set for fluorescent protein tagging facilitates temporal stability and native protein distribution in transient and stable expression studies. *The Plant Journal*. **2010**, *64*, 355-365.

Grossmann, G.; Krebs, M.; Maizel, A.; Stahl, Y.; Vermeer, J. E.; Ott, T. Green light for quantitative live-cell imaging in plants. *Journal of Cell Science*. **2018**, *131*.

Hernández-Barrera, A.; Velarde-Buendía, A.; Zepeda, I.; Sanchez, F.; Quinto, C.; Sánchez-Lopez, R.; Cheung, A.Y.; Wu, H.M.; Cardenas, L. Hyper, a hydrogen peroxide sensor, indicates the sensitivity of the Arabidopsis root elongation zone to aluminum treatment. *Sensors*. **2015**, *15*, 855-867.

Hord, C. L.; Sun, Y. J.; Pillitteri, L. J.; Torii, K. U.; Wang, H.; Zhang, S.; Ma, H. Regulation of Arabidopsis early anther development by the mitogen-activated protein kinases, MPK3 and MPK6, and the ERECTA and related receptor-like kinases. *Molecular Plant*. **2008**, *1*, 645-658.

Ichimura, K.; Casais, C.; Peck, S. C.; Shinozaki, K.; Shirasu, K. MEKK1 is required for MPK4 activation and regulates tissue-specific and temperature-dependent cell death in Arabidopsis. *Journal of Biological Chemistry*. **2006**, *281*, 36969-36976.

Jammes, F.; Song, C.; Shin, D.; Munemasa, S.; Takeda, K.; Gu, D.; Cho, D.; Lee, S.; Giordo, R.; Sritubtim, S.; Leonhardt, N. MAP kinases MPK9 and MPK12 are preferentially expressed in guard cells and positively regulate ROS-mediated ABA signaling. *Proceedings of the National Academy of Sciences*. **2009**, *106*, 20520-20525.

Jones, A. M.; Danielson, J. Å.; ManojKumar, S. N.; Lanquar, V.; Grossmann, G.; Frommer, W. B. Abscisic acid dynamics in roots detected with genetically encoded FRET sensors. *Elife*. **2014**, *3*, e01741.

Kalderon, D.; Richardson, W. D.; Markham, A. F.; Smith, A. E. Sequence requirements for nuclear location of simian virus 40 large-T antigen. *Nature*. **1984**, *311*, 33-38.

Kamioka, Y.; Sumiyama, K.; Mizuno, R.; Sakai, Y.; Hirata, E.; Kiyokawa, E.; Matsuda, M. Live imaging of protein kinase activities in transgenic mice expressing FRET biosensors. *Cell Structure and Function*. **2012**, 1201200102-1201200102.

Komatsu, N.; Aoki, K.; Yamada, M.; Yukinaga, H.; Fujita, Y.; Kamioka, Y.; Matsuda, M. Development of an optimized backbone of FRET biosensors for kinases and GTPases. *Molecular Biology of the Cell*. **2011**, *22*, 4647-4656.

Komis, G.; Šamajová, O.; Ovečka, M.; Šamaj, J. Cell and developmental biology of plant mitogen-activated protein kinases. *Annual Review of Plant Biology*. **2018**, *69*, 237-265.

Lahav, G.; Rosenfeld, N.; Sigal, A.; Geva-Zatorsky, N.; Levine, A. J.; Elowitz, M. B.; Alon, U. Dynamics of the p53-Mdm2 feedback loop in individual cells. *Nature Genetics*. **2004**, *36*, 147-150.

Lanquar, V.; Grossmann, G.; Vinkenborg, J. L.; Merkx, M.; Thomine, S.; Frommer, W. B. Dynamic imaging of cytosolic zinc in Arabidopsis roots combining FRET sensors and RootChip technology. *New Phytologist*. **2014**, *202*, 198-208.

Liu, Y.; He, C. A review of redox signaling and the control of MAP kinase pathway in plants. *Redox Biology*. **2017**, *11*, 192-204.

Liu, Y.; Zhang, S. Phosphorylation of 1-aminocyclopropane-1-carboxylic acid synthase by MPK6, a stress-responsive mitogen-activated protein kinase, induces ethylene biosynthesis in Arabidopsis. *The Plant Cell*. **2004**, *16*, 3386-3399.

Mészáros, T.; Helfer, A.; Hatzimasoura, E.; Magyar, Z.; Serazetdinova, L.; Rios, G.; Bardóczy, V.; Teige, M.; Koncz, C.; Peck, S.; Bögre, L. The Arabidopsis MAP kinase kinase MKK1 participates in defence responses to the bacterial elicitor flagellin. *The Plant Journal*. **2006**, *48*, 485-498.

Moustafa, K.; AbuQamar, S.; Jarrar, M.; Al-Rajab, A. J.; Trémouillaux-Guiller, J. MAPK cascades and major abiotic stresses. *Plant Cell Reports*. **2014**, *33*, 1217-1225.

Mukherjee, P.; Banerjee, S.; Wheeler, A.; Ratliff, L.A.; Irigoyen, S.; Garcia, L.R.; Lockless, S.W.; Versaw, W.K. Live imaging of inorganic phosphate in plants with cellular and subcellular resolution. *Plant Physiology*. **2015**, *167*, 628-638.

Nagai, T.; Yamada, S.; Tominaga, T.; Ichikawa, M.; Miyawaki, A. Expanded dynamic range of fluorescent indicators for Ca2+ by circularly permuted yellow fluorescent proteins. *Proceedings of the National Academy of Sciences*. **2004**, *101*, 10554-10559.

Nguyen, A. W.; Daugherty, P. S. Evolutionary optimization of fluorescent proteins for intracellular FRET. *Nature Biotechnology*. **2005**, *23*, 355-360.

Nitta, Y.; Ding, P.; Zhang, Y. Identification of additional MAP kinases activated upon PAMP treatment. *Plant Signaling Behavior*. **2014**, *9*, e976155.

Odell, J. T.; Nagy, F.; Chua, N. H. Identification of DNA sequences required for activity of the cauliflower mosaic virus 35S promoter. *Nature*. **1985**, *313*, 810-812.

Park, H.C.; Song, E.H.; Nguyen, X.C.; Lee, K.; Kim, K.E.; Kim, H.S.; Lee, S.M.; Kim, S.H.; Bae, D.W.; Yun, D.J.; Chung, W.S. Arabidopsis MAP kinase phosphatase 1 is phosphorylated and activated by its substrate AtMPK6. *Plant Cell Reports*. **2011**, *30*, 1523-1531.

Petersen, M.; Brodersen, P.; Næsted, H.; Andreasson, E.; Lindhart, U.; Johansen, B.; Nielsen, H.B.; Lacy, M.; Austin, M.J.; Parker, J.E.; Sharma, S.B. Arabidopsis MAP kinase 4 negatively regulates systemic acquired resistance. *Cell*. **2000**, *103*, 1111-1120.

Ren, D.; Yang, H.; Zhang, S. Cell death mediated by MAPK is associated with hydrogen peroxide production in Arabidopsis. *Journal of Biological Chemistry*. **2002**, *277*, 559-565.

Ren, D.; Liu, Y.; Yang, K. Y.; Han, L.; Mao, G.; Glazebrook, J.; Zhang, S. A fungal-responsive MAPK cascade regulates phytoalexin biosynthesis in Arabidopsis. *Proceedings of the National Academy of Sciences*. **2008**, *105*, 5638-5643.

Rizza, A.; Walia, A.; Lanquar, V.; Frommer, W. B.; Jones, A. M. *In vivo* gibberellin gradients visualized in rapidly elongating tissues. *Nature Plants*. **2017**, *3*, 803-813.

Ryu, H.; Chung, M.; Dobrzyński, M.; Fey, D.; Blum, Y.; Lee, S.S.; Peter, M.; Kholodenko, B.N.; Jeon, N.L.; Pertz, O. Frequency modulation of ERK activation dynamics rewires cell fate. *Molecular Systems Biology*. **2015**, *11*, 838.

Sample, V.; Mehta, S.; Zhang, J. Genetically encoded molecular probes to visualize and perturb signaling dynamics in living biological systems. *Journal of Cell Science*. **2014**, *127*, 1151-1160.

Sari, D. W. K.; Akiyama, R.; Naoki, H.; Ishijima, H.; Bessho, Y.; Matsui, T. Time-lapse observation of stepwise regression of Erk activity in zebrafish presomitic mesoderm. *Scientific reports*. **2018**, *8*, 1-10.

Schindelin, J.; Arganda-Carreras, I.; Frise, E.; Kaynig, V.; Longair, M.; Pietzsch, T.; Preibisch, S.; Rueden, C.; Saalfeld, S.; Schmid, B.; Tinevez, J.Y. Fiji: an open-source platform for biological-image analysis. *Nature Methods*. **2012**, *9*, 676-682.

Spencer, S. L.; Gaudet, S.; Albeck, J. G.; Burke, J. M.; Sorger, P. K. Non-genetic origins of cell-to-cell variability in TRAIL-induced apoptosis. *Nature*. **2009**, *459*, 428-432.

Stanko, V.; Giuliani, C.; Retzer, K.; Djamei, A.; Wahl, V.; Wurzinger, B.; Wilson, C.; Heberle-Bors, E.; Teige, M.; Kragler, F. Timing is everything: highly specific and transient expression of a MAP kinase determines auxin-induced leaf venation patterns in Arabidopsis. *Molecular Plant*. **2014**, *7*, 1637-1652.

Su, J.; Zhang, M.; Zhang, L.; Sun, T.; Liu, Y.; Lukowitz, W.; Xu, J.; Zhang, S. Regulation of stomatal immunity by interdependent functions of a pathogen-responsive MPK3/MPK6 cascade and abscisic acid. *The Plant Cell*. **2017**, *29*, 526-542.

Suarez-Rodriguez, M.C.; Petersen, M.; Mundy, J. Mitogen-activated protein kinase signaling in plants. *Annual review of Plant Biology*. **2010**, *61*, 621-649.

Suarez-Rodriguez, M.C.; Adams-Phillips, L.; Liu, Y.; Wang, H.; Su, S.H.; Jester, P.J.; Zhang, S.; Bent, A.F.; Krysan, P.J. MEKK1 is required for flg22-induced MPK4 activation in Arabidopsis plants. *Plant physiology*. **2007**, *143*, 661-669.

Sun, Z.; Hsiao, J.; Fay, D. S.; Stern, D. F. Rad53 FHA domain associated with phosphorylated Rad9 in the DNA damage checkpoint. *Science*. **1998**, *281*, 272-274.

Sun, T.; Nitta, Y.; Zhang, Q.; Wu, D.; Tian, H.; Lee, J. S.; Zhang, Y. Antagonistic interactions between two MAP kinase cascades in plant development and immune signaling. *EMBO Reports*. **2018**, *19*, e45324.

Takahashi, F.; Mizoguchi, T.; Yoshida, R.; Ichimura, K.; Shinozaki, K. Calmodulin-dependent activation of MAP kinase for ROS homeostasis in Arabidopsis. *Molecular Cell*. **2011**, *41*, 649-660.

Tomida, T.; Oda, S.; Takekawa, M.; Iino, Y.; Saito, H. The temporal pattern of stimulation determines the extent and duration of MAPK activation in a *Caenorhabditis elegans* sensory neuron. *Science Signaling*. **2012**, *5*, 76-76.

Ulm, R.; Revenkova, E.; di Sansebastiano, G. P.; Bechtold, N.; Paszkowski, J. Mitogen-activated protein kinase phosphatase is required for genotoxic stress relief in Arabidopsis. *Genes Development*. **2001**, *15*, 699-709.

Vang, S.; Seitz, K.; Krysan, P. J. A simple microfluidic device for live cell imaging of Arabidopsis cotyledons, leaves, and seedlings. *Biotechniques*. **2018**, *64*, 255-261.

Waadt, R.; Hitomi, K.; Nishimura, N.; Hitomi, C.; Adams, S. R.; Getzoff, E. D.; Schroeder, J. I. FRET-based reporters for the direct visualization of abscisic acid concentration changes and distribution in Arabidopsis. *Elife*. **2014**, *3*, e01739.

Walia, A.; Lee, J. S.; Wasteneys, G.; Ellis, B. Arabidopsis mitogen-activated protein kinase MPK18 mediates cortical microtubule functions in plant cells. *The Plant Journal*. **2009**, *59*, 565-575.

Wan, J.; Zhang, S.; Stacey, G. Activation of a mitogen-activated protein kinase pathway in Arabidopsis by chitin. *Molecular Plant Pathology*. **2004**, *5*, 125-135.

Wang, H.; Ngwenyama, N.; Liu, Y.; Walker, J. C.; Zhang, S. Stomatal development and patterning are regulated by environmentally responsive mitogen-activated protein kinases in Arabidopsis. *The Plant Cell*. **2007**, *19*, 63-73.

Wang, H.; Liu, Y.; Bruffett, K.; Lee, J.; Hause, G.; Walker, J. C.; Zhang, S. Haplo-insufficiency of MPK3 in MPK6 mutant background uncovers a novel function of these two MAPKs in Arabidopsis ovule development. *The Plant Cell*. **2008** *20*, 602-613.

Wen, W.; Meinkotht, J. L.; Tsien, R. Y.; Taylor, S. S. Identification of a signal for rapid export of proteins from the nucleus. *Cell*. **1995**, *82*, 463-473.

Xu, J.; Zhang, S. Mitogen-activated protein kinase cascades in signaling plant growth and development. *Trends in Plant Science*. **2015**, *20*, 56-64.

Xu, J.; Xie, J.; Yan, C.; Zou, X.; Ren, D.; Zhang, S. A chemical genetic approach demonstrates that MPK 3/MPK 6 activation and NADPH oxidase-mediated oxidative burst are two independent signaling events in plant immunity. *The Plant Journal*. **2014**, *77*, 222-234.

Yamada, K.; Yamaguchi, K.; Shirakawa, T.; Nakagami, H.; Mine, A.; Ishikawa, K.; Fujiwara, M.; Narusaka, M.; Narusaka, Y.; Ichimura, K.; Kobayashi, Y. The Arabidopsis CERK 1-associated kinase PBL 27 connects chitin perception to MAPK activation. *The EMBO Journal*. **2016**, *35*, 2468-2483.

Yongkiettrakul, S.; Byeon, I. J. L.; Tsai, M. D. The ligand specificity of yeast Rad53 FHA domains at the+ 3 position is determined by nonconserved residues. *Biochemistry*. **2004**, *43*, 3862-3869.

Yu, L.; Nie, J.; Cao, C.; Jin, Y.; Yan, M.; Wang, F.; Liu, J.; Xiao, Y.; Liang, Y.; Zhang, W. Phosphatidic acid mediates salt stress response by regulation of MPK6 in Arabidopsis thaliana. *New Phytologist*. **2010**, *188*, 762-773.

Zeng, Q.; Chen, J. G.; Ellis, B. E. AtMPK4 is required for male-specific meiotic cytokinesis in Arabidopsis. *The Plant Journal*. **2011**, *67*, 895-906.

Zhang, M.; Wu, H.; Su, J.; Wang, H.; Zhu, Q.; Liu, Y.; Xu, J.; Lukowitz, W.; Zhang, S. Maternal control of embryogenesis by MPK6 and its upstream MKK4/MKK5 in Arabidopsis. *The Plant Journal*. **2017**, *92*, 1005-1019.

Zhang, M.; Su, J.; Zhang, Y.; Xu, J.; Zhang, S. Conveying endogenous and exogenous signals: MAPK cascades in plant growth and defense. *Current opinion in Plant Biology*. **2018**, *45*, 1-10.

Zhao, Y.; Araki, S.; Wu, J.; Teramoto, T.; Chang, Y.F.; Nakano, M.; Abdelfattah, A.S.; Fujiwara, M.; Ishihara, T.; Nagai, T.; Campbell, R.E. An expanded palette of genetically encoded Ca2+ indicators. *Science*. **2011**, *333*, 1888-1891.

Table 1. Transgenic lines produced for this study

Line Name	Plasmid	Promoter	Localization	Background
SOMA-NLS-1	pSOMA-NLS	*UBQ10*	nucleus	Col-0
SOMA-NLS-2	"	"	"	"
SOMA-NES-1	pSOMA-NES	CaMV 35S	cytoplasm	Col-0
SOMA-NES-2	"	"	"	"
SOMA^{T679A}-NLS-1	pSOMA^{T679A}-NLS	*UBQ10*	nucleus	Col-0
SOMA^{T679A}-NLS-2	"	"	"	"
SOMA^{T679A}-NES-1	pSOMA^{T679A}-NES	CaMV 35S	cytoplasm	Col-0
SOMA^{T679A}-NES-2	"	"	"	"
MPK6^{YG} SOMA-NES	pSOMA-NES	CaMV 35S	cytoplasm	*mpk3 mpk6* P_{mpk6}:*MPK6*^{YG}

Localization: Indicates the subcellular localization of the sensor protein

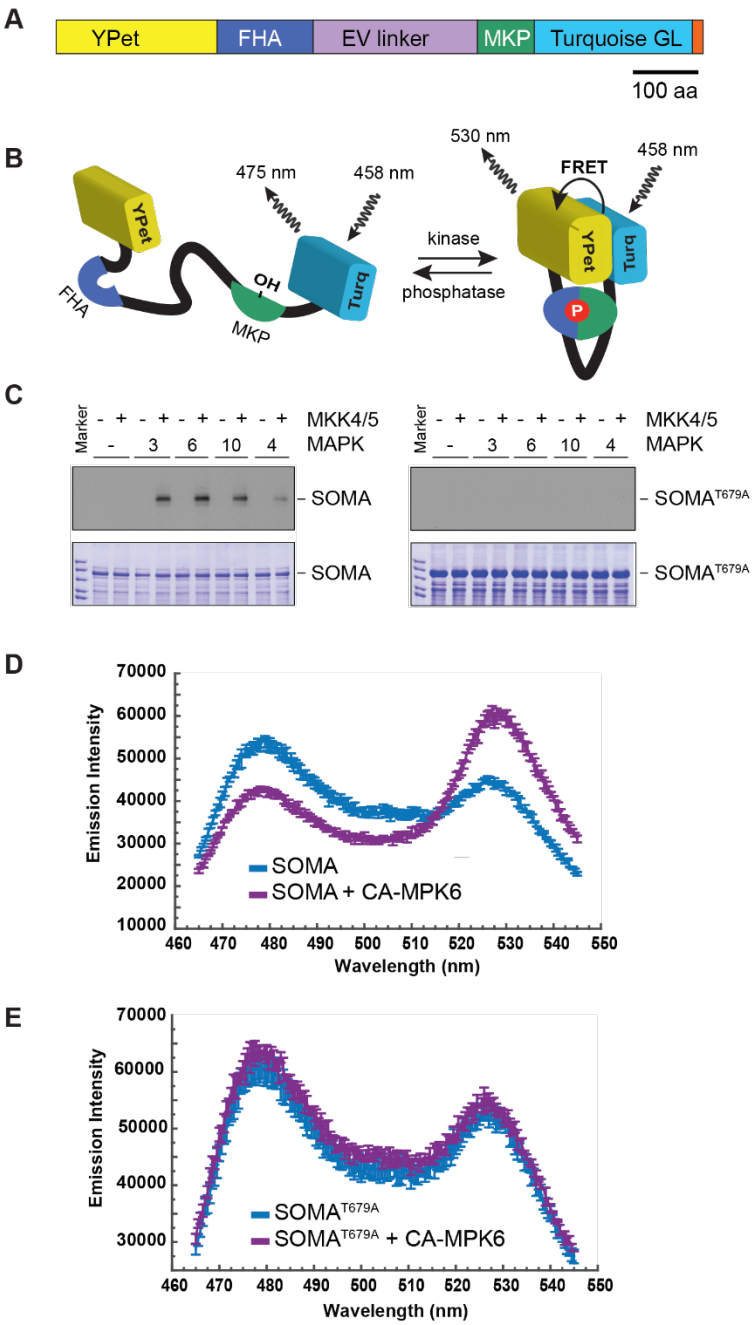

Figure 1. Structure and *in vitro* testing of the Sensor Of Mitogen-Activated Protein Kinase (MAPK) Activity (SOMA). (a) Domain structure of the SOMA protein. YPet is a yellow fluorescent protein, FHA is the FHA1 phosphopeptide-binding domain of yeast RAD53, EV linker is a flexible linker domain, MPK is an 80-amino-acid segment of the Arabidopsis MKP1 protein containing a MPK6 phosphorylation site, and Turquoise GL is a blue fluorescent protein. The small segment at the extreme C-terminus of the diagram indicates the location of the nuclear localization or nuclear exclusion signal. aa, amino acid. (b) Phosphorylation of SOMA within the MKP1 domain is expected to produce a conformation shift that increases Förster resonance energy transfer (FRET) efficiency due to the enhanced affinity of the FHA1 domain for the phosphorylated form of the substrate domain. Removal of that phosphate by a phosphatase is expected to cause SOMA to revert to a conformation with lower FRET efficiency.(c) In vitro kinase assays performed using proteins extracted from Escherichia coli. SOMA and SOMAT679A as substrates were incubated in the presence of the indicated Arabidopsis MAPK protein with (+) and without (−) constitutively active Arabidopsis MKK4 and MKK5. Reaction products were separated on gels and the incorporation of 32P into the substrates was evaluated via autoradiography (upper panels). Lower panels show the loading controls stained with Coomassie brilliant blue. (d), (e) In vitro FRET assays using E. coli expressed SOMA and SOMAT679A performed in the presence or absence of E. coli expressed constitutively active MPK6 (CA-MPK6). The emission spectra of SOMA and SOMAT679A produced by excitation of the Turquoise GL domain with 435 nm light is shown.

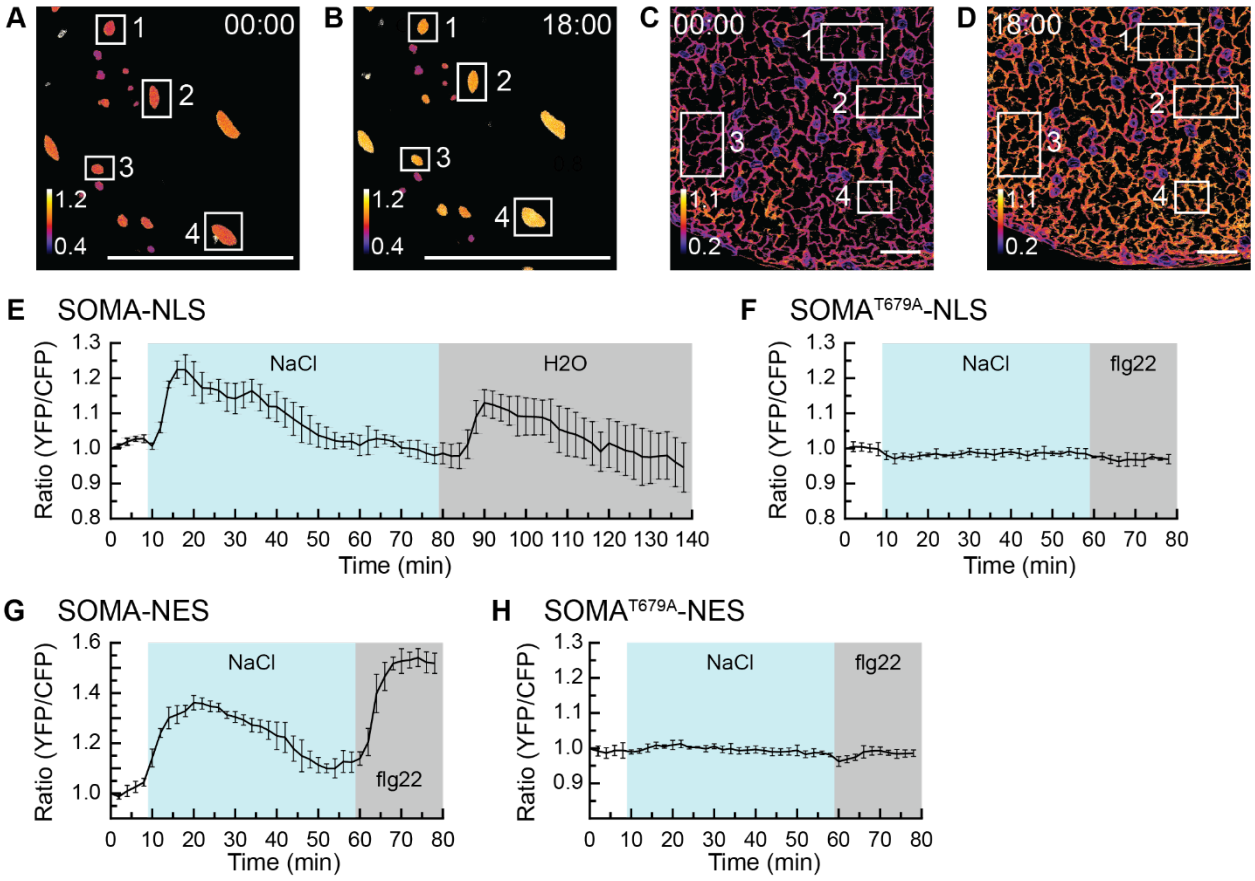

Figure 2. The *in vivo* response of Sensor Of Mitogen-Activated Protein Kinase (MAPK) Activity (SOMA) to NaCl stress. (a)–(d) Processed confocal images of the cotyledon epidermis from the SOMA-NLS-1 (a,b) and SOMA-NES-1 (c,d) transgenic lines depicting the ratio of YPet to Turquoise GL emission produced by exciting Turquoise GL. The calibration bar in the lower left indicates the numerical scale corresponding to the heat map. The scale bar on the bottom indicates 100 µm. Time stamps indicate when the image was collected in minutes:seconds. Images at time 00:00 were collected before treatment, while those at time point 18:00 were collected 12 min after treatment with 150 mM NaCl. Numbered rectangles indicate the regions of interest (ROIs) used to measure YPet and Turquoise GL emission. (e), (f) The average ratio of YPet to Turquoise GL emission produced by exciting Turquoise GL was determined using the ROIs shown in (a–d), normalized to the starting value for each ROI, and plotted versus time. The shaded background on each graph indicates when the sample was exposed to a given treatment. During the first 10 min of each experiment the samples were incubated in pure water. 'NaCl' indicates 150 mM NaCl, 'H2O' indicates pure water, and 'flg22' indicates that 1 µm flg22 was present in the imaging chamber during the shaded time period. Error bars indicate standard deviation. 'Ratio (YFP/CFP)' indicates the normalized value of YPet emission divided by Turquoise GL emission after excitation of Turquoise GL with 458 nm light. (g), (h) Transgenic lines SOMAT679A-NLS-1 and SOMAT679A-NES-1 were analyzed as above using the ROIs indicated in Figure S17. Videos are available as Movies S1–S4. These experiments were repeated at least five times with similar results.

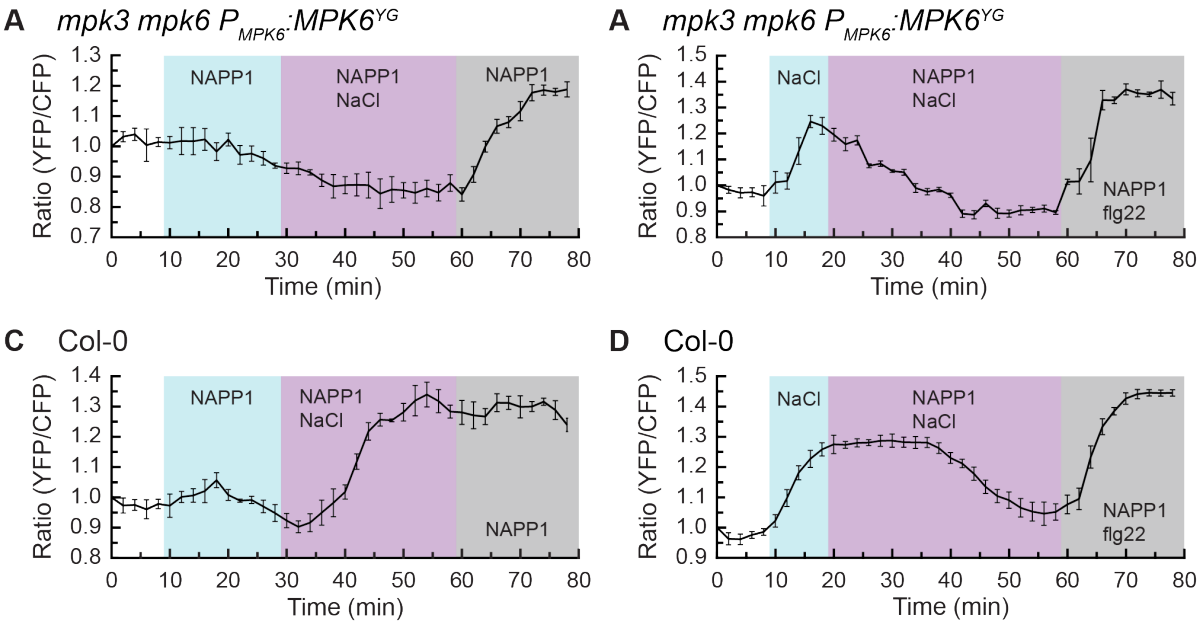

Figure 3. MPK6 activity is needed for the NaCl-induced increase in the ratio of YPet to Turquoise GL emission of Sensor Of Mitogen-Activated Protein Kinase (MAPK) Activity (SOMA). The SOMA-NES in the cotyledon epidermis was analyzed in wild-type Col-0 and mpk3 mpk6 Pmpk6:MPK6YG genetic backgrounds. Graphs depict the average ratio of YPet to Turquoise GL emission produced by exciting Turquoise GL using the regions of interest shown in Figure S18. The shaded background on each graph indicates when the sample was exposed to a given treatment. During the first 10 min of each experiment the samples were incubated in pure water. '1-NA-PP1' indicates 10 µm 1-NA-PP1, '1-NA-PP1 NaCl' indicates 10 µm 1-NA-PP1 + 150 mM NaCl, and '1-NA-PP1 flg22' indicates 10 µm 1-NA-PP1 + 1 µm flg22 was present in the imaging chamber during the shaded time period. Error bars indicate standard deviation. 'Ratio (YFP/CFP)' indicates the normalized value of YPet emission divided by Turquoise GL emission after excitation of Turquoise GL with 458 nm light. Videos are available as Movies S5–S8. 1-NA-PP1 is an ATP analog. These experiments were repeated at least four times with similar results.

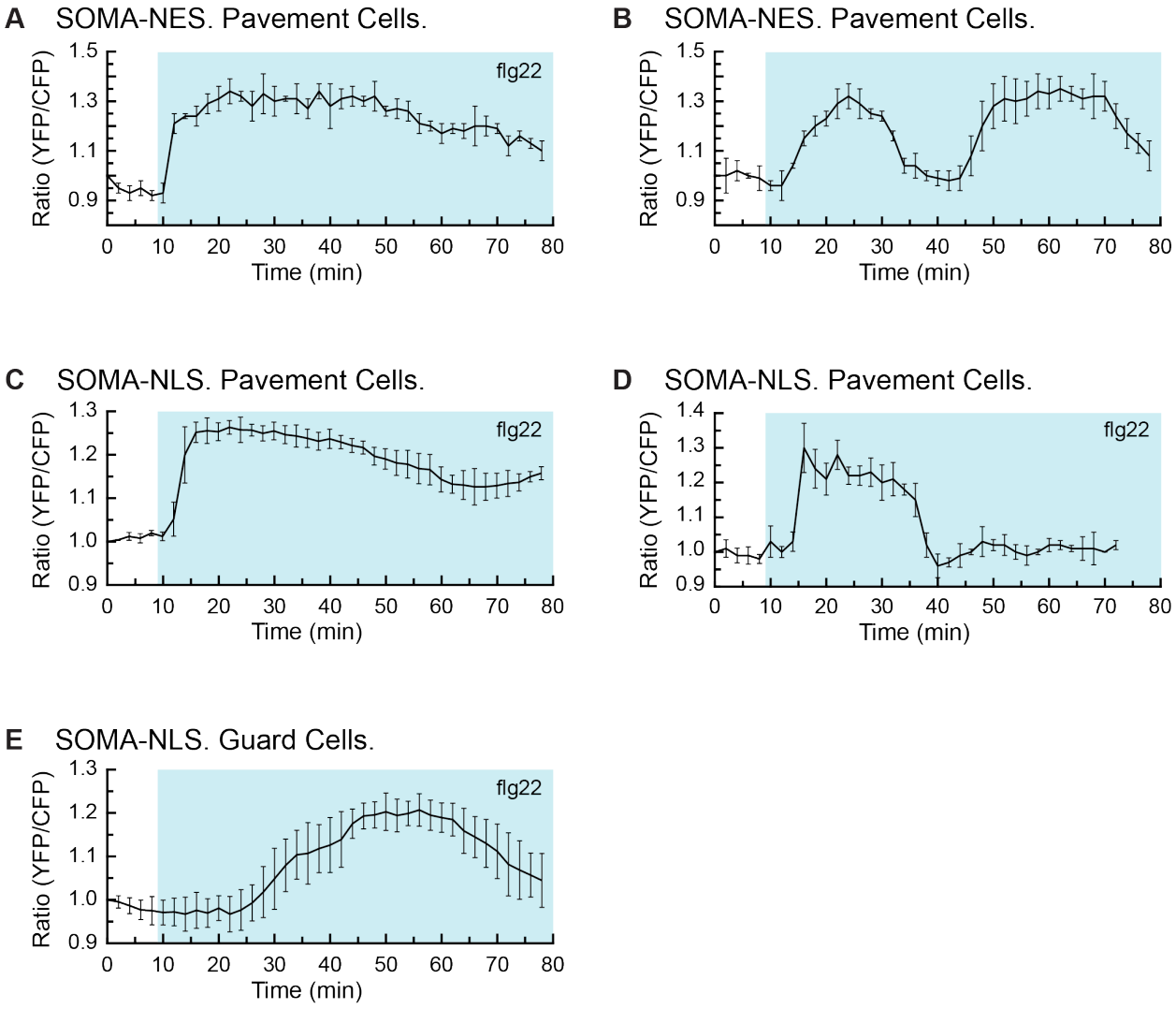

Figure 4. The response of Sensor Of Mitogen-Activated Protein Kinase (MAPK) Activity (SOMA) to flg22 is heterogeneous. The response of the SOMA-NES-1 and SOMA-NLS-1 transgenic lines to flg22 treatment was evaluated by analyzing cotyledon epidermal cells. Graphs depict the average ratio of YPet to Turquoise GL emission produced by exciting Turquoise GL using the regions of interest shown in Figure S19. The shaded background on each graph indicates when the sample was exposed to a given treatment. During the first 10 min of each experiment the samples were incubated in pure water. 'flg22' indicates that 1 µm flg22 was present in the imaging chamber during the shaded time period. Error bars indicate standard deviation. 'Ratio (YFP/CFP)' indicates the normalized value of YPet emission divided by Turquoise GL emission after excitation of Turquoise GL with 458 nm light. Videos are available as Movies S9–S11. These experiments were repeated at least five times with similar results.

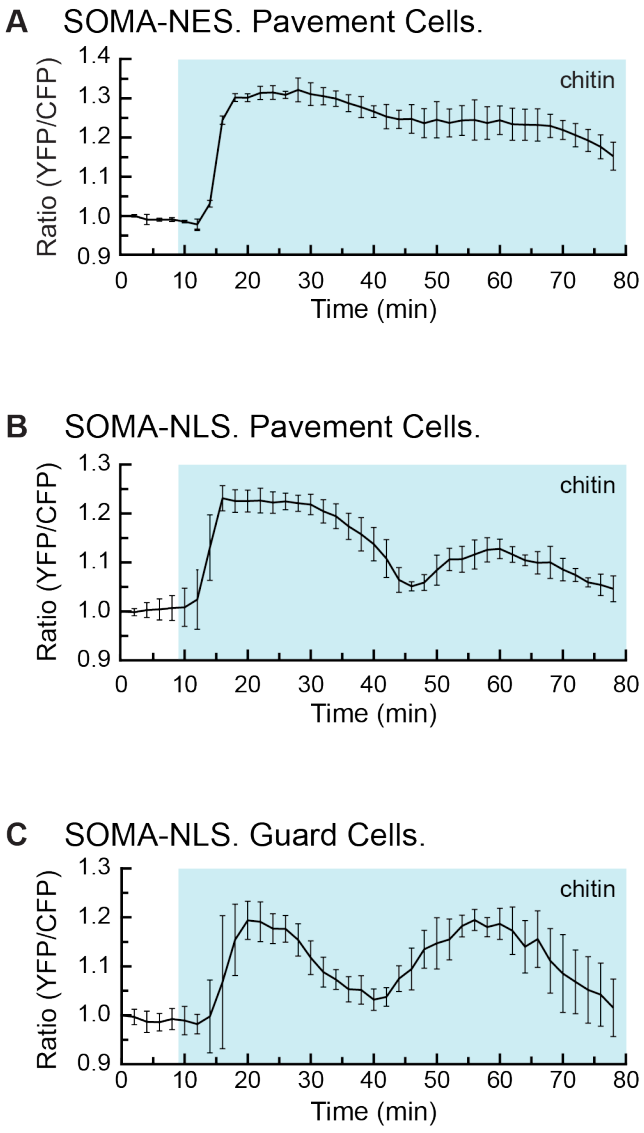

Figure 5. Chitin induces a rapid increase in the ratio of YPet to Turquoise GL emission in guard cells. The response of the SOMA-NES-1 and SOMA-NLS-1 transgenic lines to chitin treatment was evaluated by analyzing cotyledon epidermal cells. Graphs depict the average ratio of YPet to Turquoise GL emission produced by exciting Turquoise GL using the regions of interest shown in Figure S20. The shaded background on each graph indicates when the sample was exposed to a given treatment. During the first 10 min of each experiment the samples were incubated in pure water. 'chitin' indicates that 40 mg ml−1 chitin was present in the imaging chamber during the shaded time period. Error bars indicate standard deviation. 'Ratio (YFP/CFP)' indicates the normalized value of YPet emission divided by Turquoise GL emission after excitation of Turquoise GL with 458 nm light. Videos are available as Movies S12 and S13. These experiments were repeated at least five times with similar results.

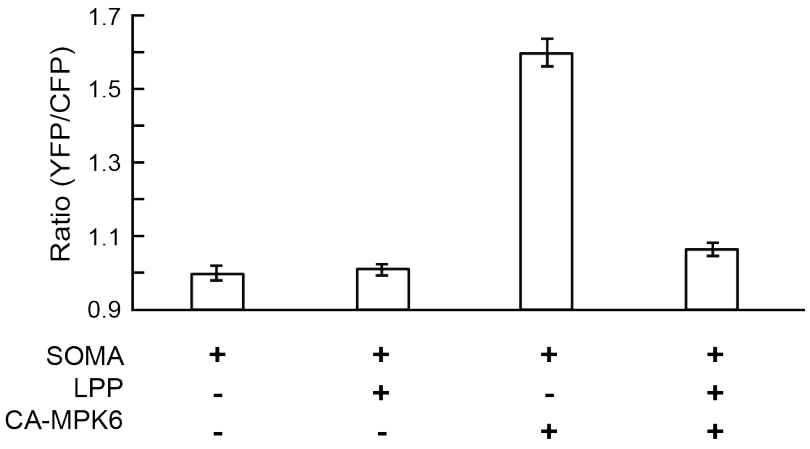

Fig. S1. *In vitro* FRET assay with lambda protein phosphatase.
In vitro FRET assays were performed using SOMA protein and constitutively active MPK6 (CA-MPK6) expressed in *E. coli*. The emission spectra of SOMA produced by excitation of the Turquoise GL domain with 435 nm light was collected using a scanning spectrofluorimeter and the peak values for YPet and Turquoise GL emission were recorded and the ratio of YPet to Turquoise GL emission was calculated. The components present in a given reaction are indicated with "+". "LPP" indicates lambda protein phosphatase. "Ratio (YFP/CFP) indicates the peak YPet emission divided by peak Turquoise GL emission. These values are normalized to the reaction containing only SOMA protein. Error bars indicate standard deviation of three independent samples.

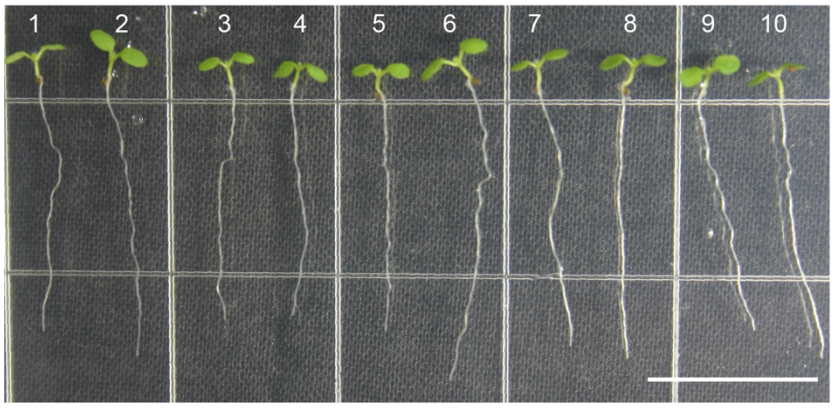

Fig. S2. Seedling phenotypes of SOMA transgenic lines.
Representative 7-day-old seedlings grown on vertically oriented agar plates under continuous light. Seedling genotypes are as follows: (1) Col-0, (2) SOMA-NLS-1, (3) SOMA-NLS-2, (4) SOMA-NES-1, (5) SOMA-NES-2, (6) SOMA-T679A-NLS-1, (7) SOMA-T679A-NLS-2, (8) SOMA-T679A-NES-1, (9) SOMA-T679A-NES-2, (10) MPK6-YG SOMA-NES. Scale bar is 1 cm.

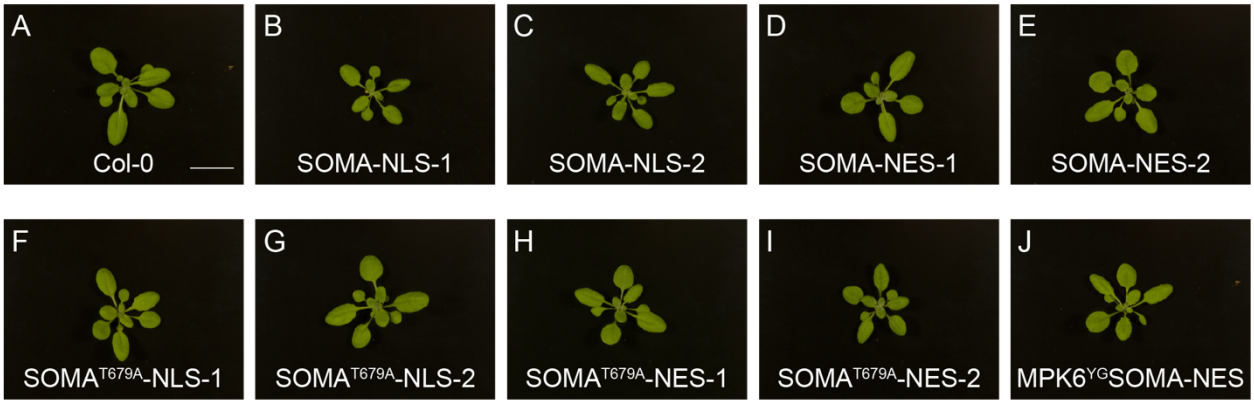

Fig. S3. Rosette phenotypes of SOMA transgenic lines.
Representative 26-day-old plants grown in soil. Genotype is indicated in each figure. Scale bar equals 2 cm.

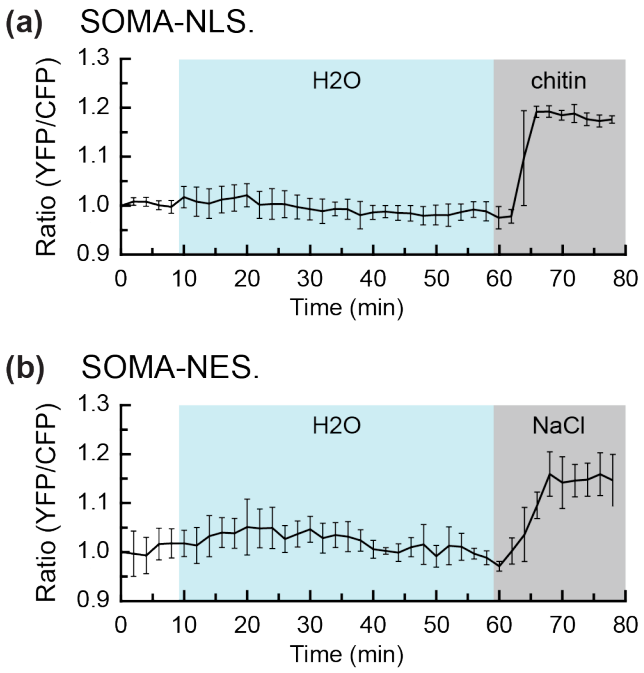

Fig. S4. Control treatment with only water for SOMA-NLS and SOMA-NES. The response of the SOMA-NES-1 and SOMA-NLS-1 transgenic lines to water treatment was evaluated by analyzing cotyledon epidermal pavement cells. Graphs depict the average ratio of YPet to Turquoise GL emission produced by exciting Turquoise GL. The shaded background on each graph indicates when the sample was exposed to a given treatment. During the first ten minutes of each experiment the samples were incubated in pure water. "H2O" indicates when a fresh volume of water was introduced into the imaging chamber. "chitin" indicates 40 mg/ml chitin and "NaCl" indicates 150 mM NaCl were present in the imaging chamber during the shaded time period. Error bars indicate standard deviation. "Ratio (YFP/CFP)" indicates the normalized value of YPet emission divided by Turquoise GL emission.

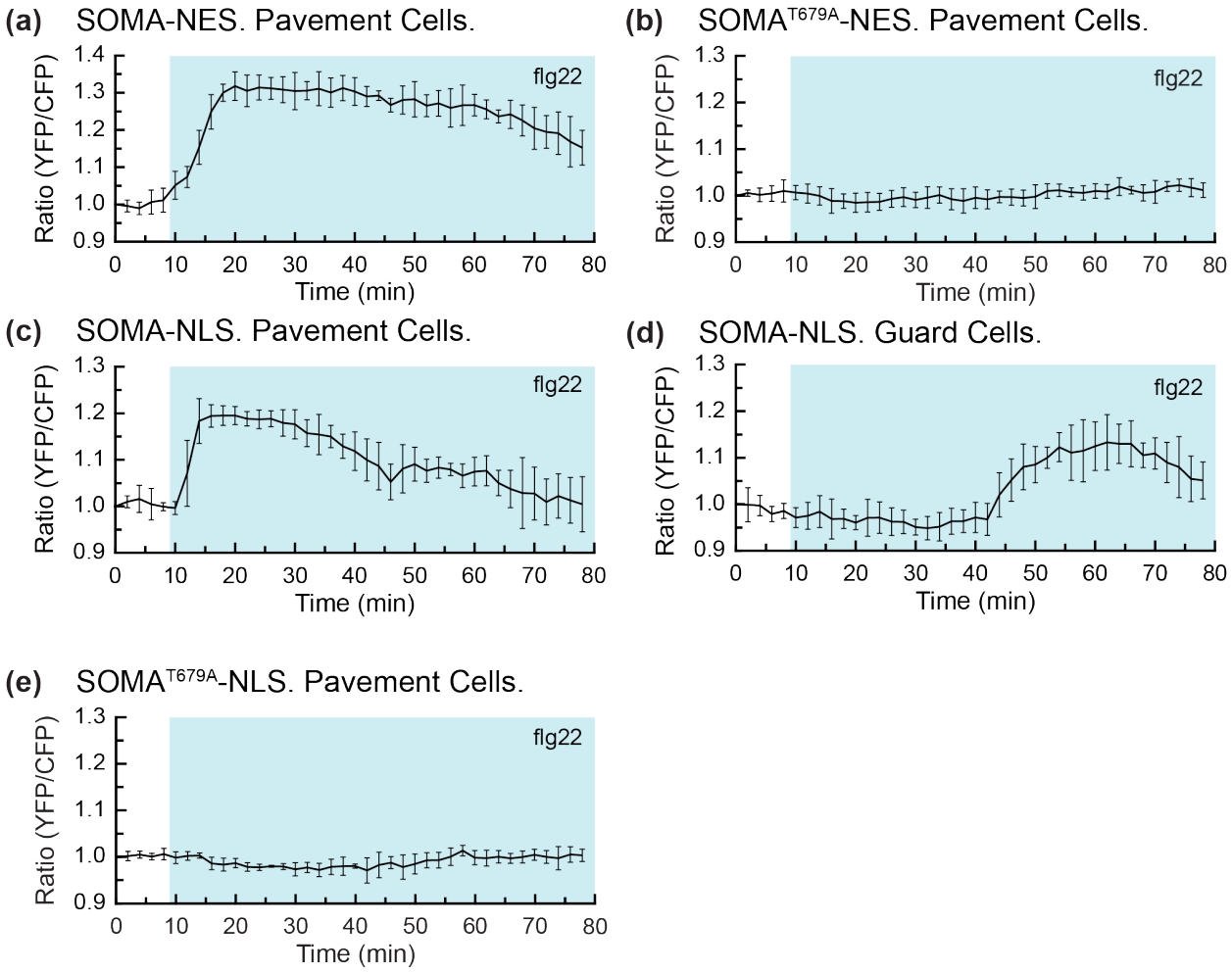

Fig. S5. flg22 treatment of SOMA-NLS-2, SOMA-NES-2, SOMA^{T679A}-NLS-2, and SOMA^{T679A}-NES-2.

The effect of flg22 treatment on the indicated lines was evaluated by analyzing cotyledon epidermal cells. Graphs depict the average ratio of YPet to Turquoise GL emission produced by exciting Turquoise GL. The shaded background on each graph indicates when the sample was exposed to a given treatment. During the first ten minutes of each experiment the samples were incubated in pure water. "flg22" indicates that 1 μM flg22 was present in the imaging chamber during the shaded time period. Error bars indicate standard deviation. "Ratio (YFP/CFP)" indicates the normalized value of YPet emission divided by Turquoise GL emission.

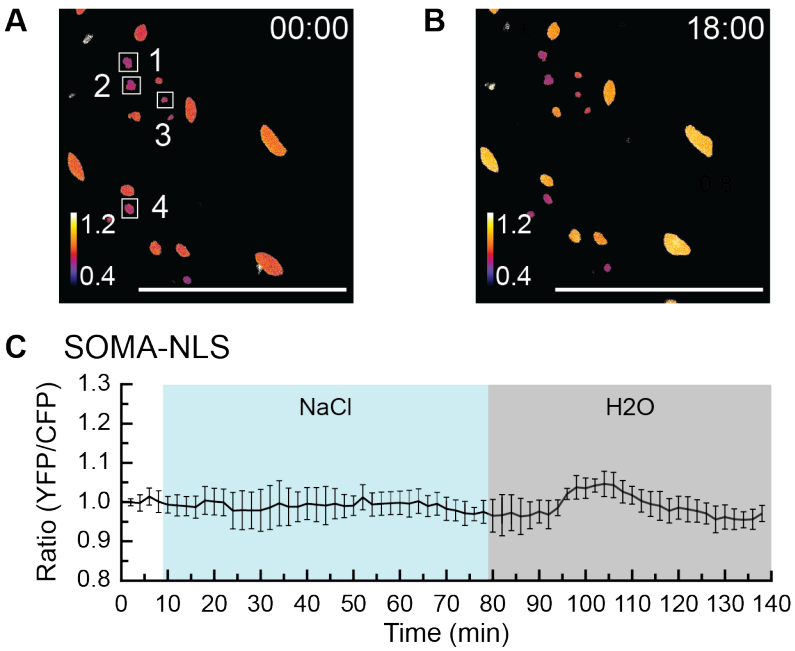

Fig. S6. The *in vivo* response of guard cells expressing SOMA-NLS-1 to NaCl stress.

(a-b) Processed confocal images of the cotyledon epidermis from the SOMA-NLS-1 transgenic line. Image depicts the ratio of YPet to Turquoise GLC emission produced by exciting Turquoise GL. The calibration bar in the lower left indicates the numerical scale corresponding to the heat map. Scale bar indicates 100 μM. Time stamps are in minutes:seconds. Regions of Interest (ROI) measured is indicated by numbered white rectangles. (a) SOMA-NLS-1 collected at time 00:00. No treatment has been administered. (b) SOMA-NLS-1 collected at time point 18:00. (c) Graph depicts the average ratio of YPet to Turquoise GL emission using the ROIs shown in panels (a-b). The shaded background indicates when the sample was exposed to a given treatment. During the first ten minutes of each experiment the sample are incubated in pure water. “NaCl’ indicates 150 mM NaCl, “H20” indicates pure water. Error bars indicate standard deviation. “Ratio (YFP/CFP)” indicates the normalized value of YPet emission divided by Turquoise GL emission produced by exciting Turquoise GL. Video is available as Movie S1.

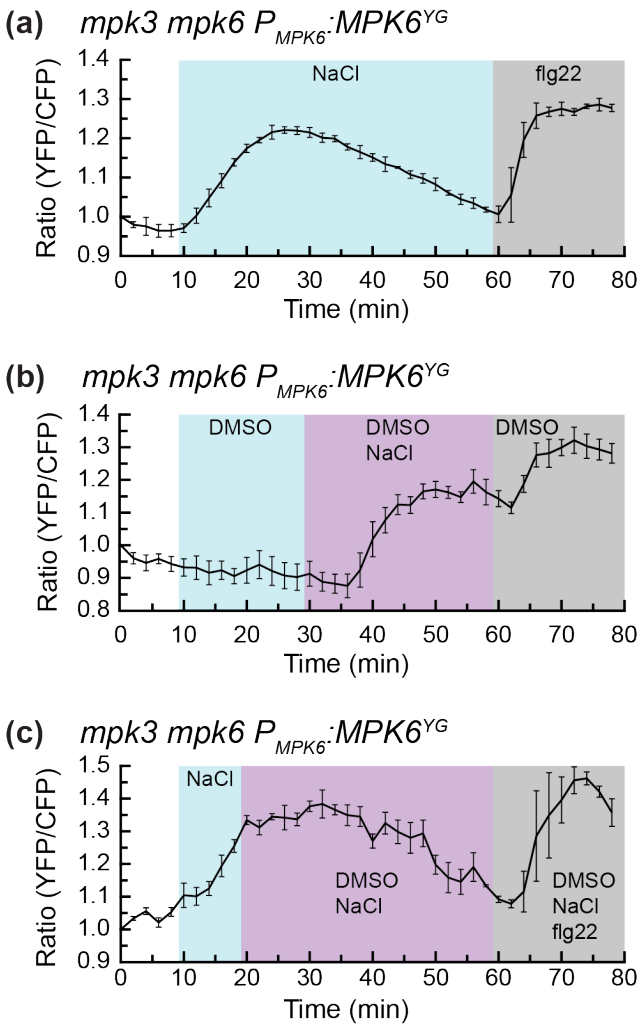

Fig. S7. DMSO controls for SOMA-NES in *mpk3 mpk6 P_{mpk6}:MPK6^{YG}*.
The response of the SOMA-NES to DMSO treatment in the *mpk3 mpk6 P_{mpk6}:MPK6^{YG}* genetic background was evaluated by analyzing cotyledon epidermal pavement cells. Graphs depict the average ratio of YPet to Turquoise GL emission produced by exciting Turquoise GL. The shaded background on each graph indicates when the sample was exposed to a given treatment. During the first ten minutes of each experiment the samples were incubated in pure water. "NaCl" indicates 150 mM NaCl, "DMSO" indicates 0.1% DMSO, "DMSO NaCl" indicates 0.1% DMSO + 150 mM NaCl, and "flg22" indicates 1 μM flg22, and "DMSO NaCl flg22" indicates 0.1% DMSO + 150 mM NaCl + 1 μM flg22 was present in the imaging chamber during the shaded time period. Error bars indicate standard deviation. "Ratio (YFP/CFP)" indicates the normalized value of YPet emission divided by Turquoise GL emission.

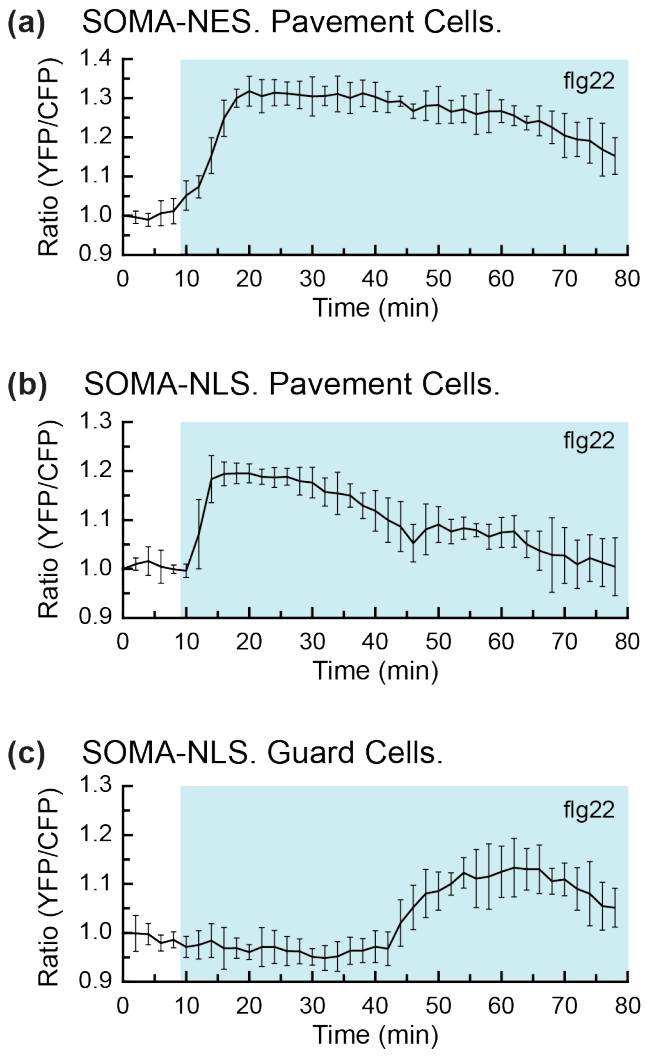

Fig. S8. flg22 treatment of SOMA-NLS-2, SOMA-NES-2, SOMA^{T679A}-NLS-2, and SOMA^{T679}A-NES-2.

The effect of flg22 treatment on the indicated lines was evaluated by analyzing cotyledon epidermal cells. Graphs depict the average ratio of YPet to Turquoise GL emission produced by exciting Turquoise GL. The shaded background on each graph indicates when the sample was exposed to a given treatment. During the first ten minutes of each experiment the samples were incubated in pure water. “flg22” indicates that 1 μM flg22 was present in the imaging chamber during the shaded time period. Error bars indicate standard deviation. “Ratio (YFP/CFP)” indicates the normalized value of YPet emission divided by Turquoise GL emission.

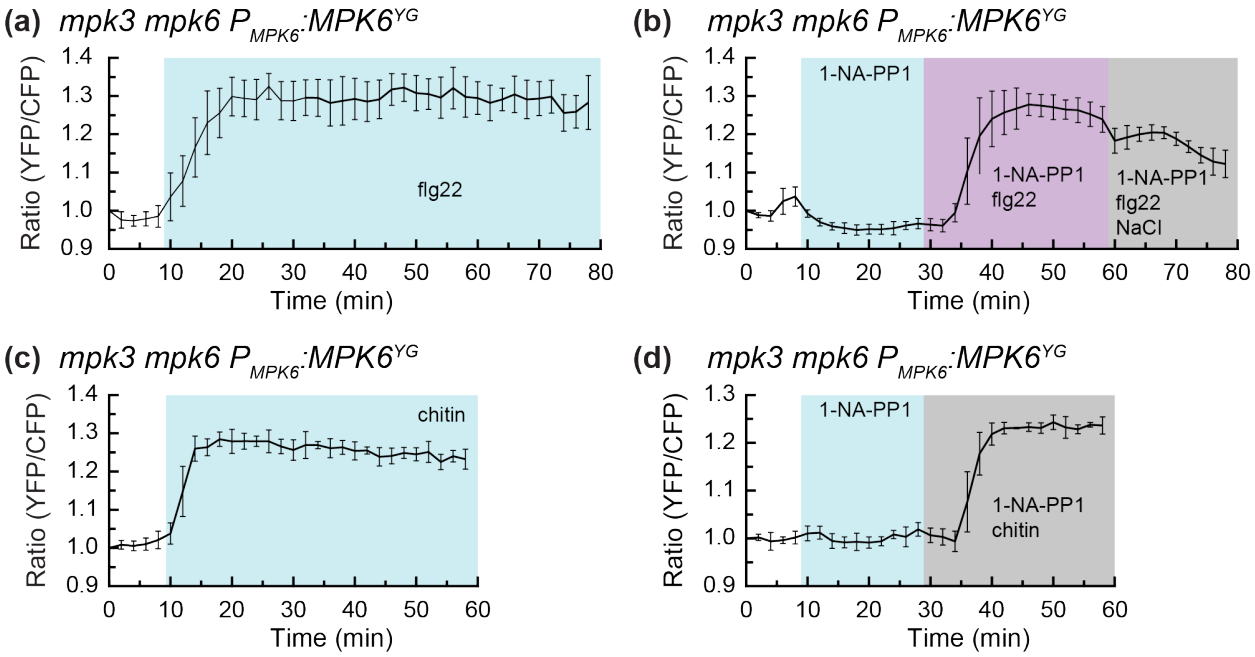

Fig. S9. flg22 and chitin treatment of SOMA-NES in *mpk3 mpk6 P_{mpk6}:MPK6^{YG}*. The effect of 1-NA-PP1 on the response of the SOMA-NES to flg22 and chitin treatment in the *mpk3 mpk6 P_{mpk6}:MPK6^{YG}* genetic background was evaluated by analyzing cotyledon epidermal pavement cells. Graphs depict the average ratio of YPet to Turquoise GL emission produced by exciting Turquoise GL. The shaded background on each graph indicates when the sample was exposed to a given treatment. During the first ten minutes of each experiment the samples were incubated in pure water. "flg22" indicates 1 μM flg22, "chitin" indicates 40 mg/ml chitin, "1-NA-PP1" indicates 10 μM 1-NA-PP1, "1-NA-PP1 flg22" indicates 10 μM 1-NA-PP1 + 1 μM flg22, "1-NA-PP1 chitin" indicates 10 μM 1-NA-PP1 + 40 mg/ml chitin, and "1-NA-PP1 flg22 NaCl" indicates 10 μM 1-NA-PP1 + 1 μM flg22 + 150 mM NaCl were present in the imaging chamber during the shaded time period. Error bars indicate standard deviation. "Ratio (YFP/CFP)" indicates the normalized value of YPet emission divided by Turquoise GL emission.

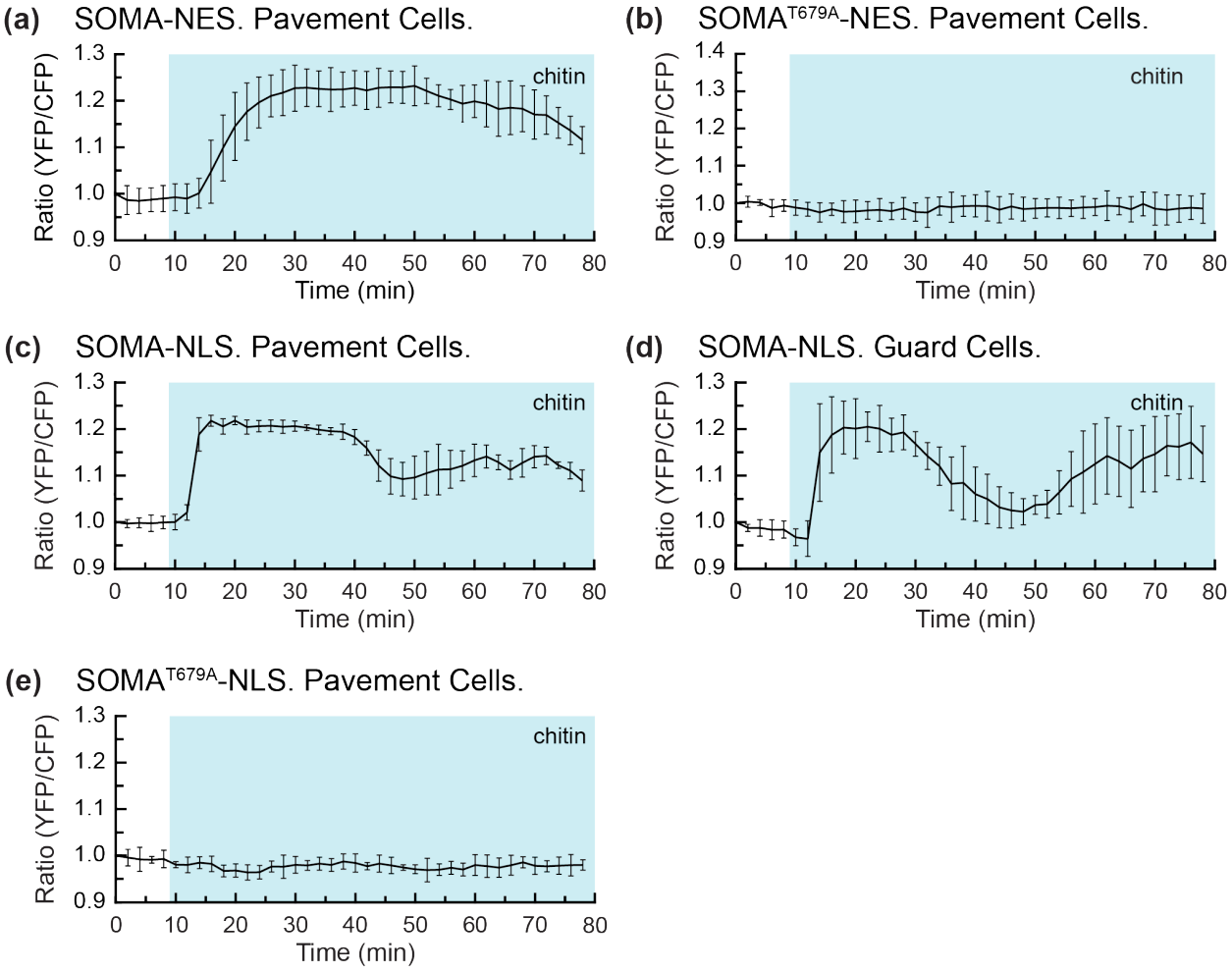

Fig. S10. Chitin treatment of SOMA-NLS-2, SOMA-NES-2, SOMA^{T679A}-NLS-2, and SOMA^{T679}A-NES-2.

The effect of chitin treatment on the indicated lines was evaluated by analyzing cotyledon epidermal cells. Graphs depict the average ratio of YPet to Turquoise GL emission produced by exciting Turquoise GL. The shaded background on each graph indicates when the sample was exposed to a given treatment. During the first ten minutes of each experiment the samples were incubated in pure water. “chitin” indicates that 40 mg/ml chitin was present in the imaging chamber during the shaded time period. Error bars indicate standard deviation. “Ratio (YFP/CFP)” indicates the normalized value of YPet emission divided by Turquoise GL emission.

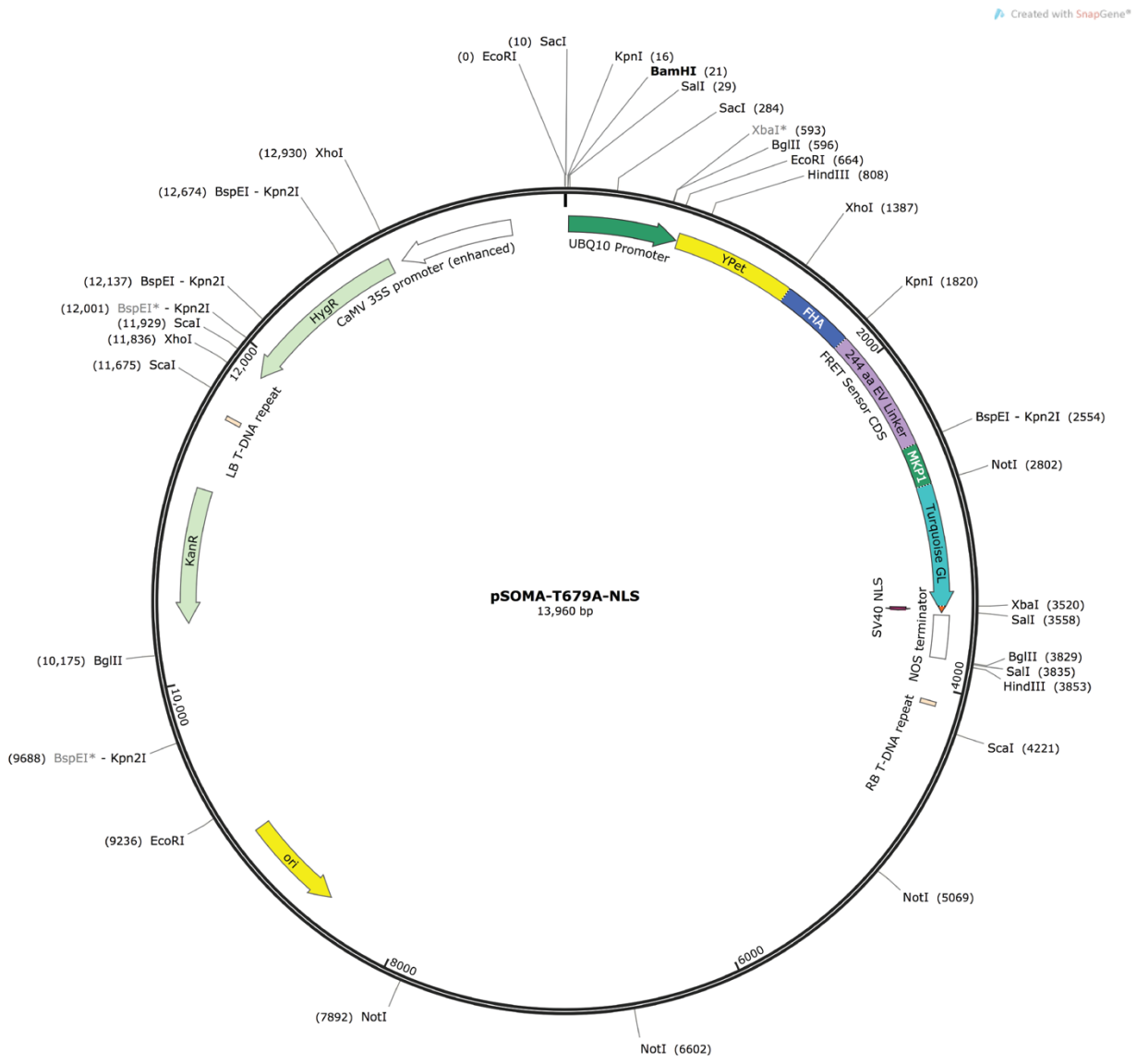

Fig. S11. Plasmid map for pET-SOMA.

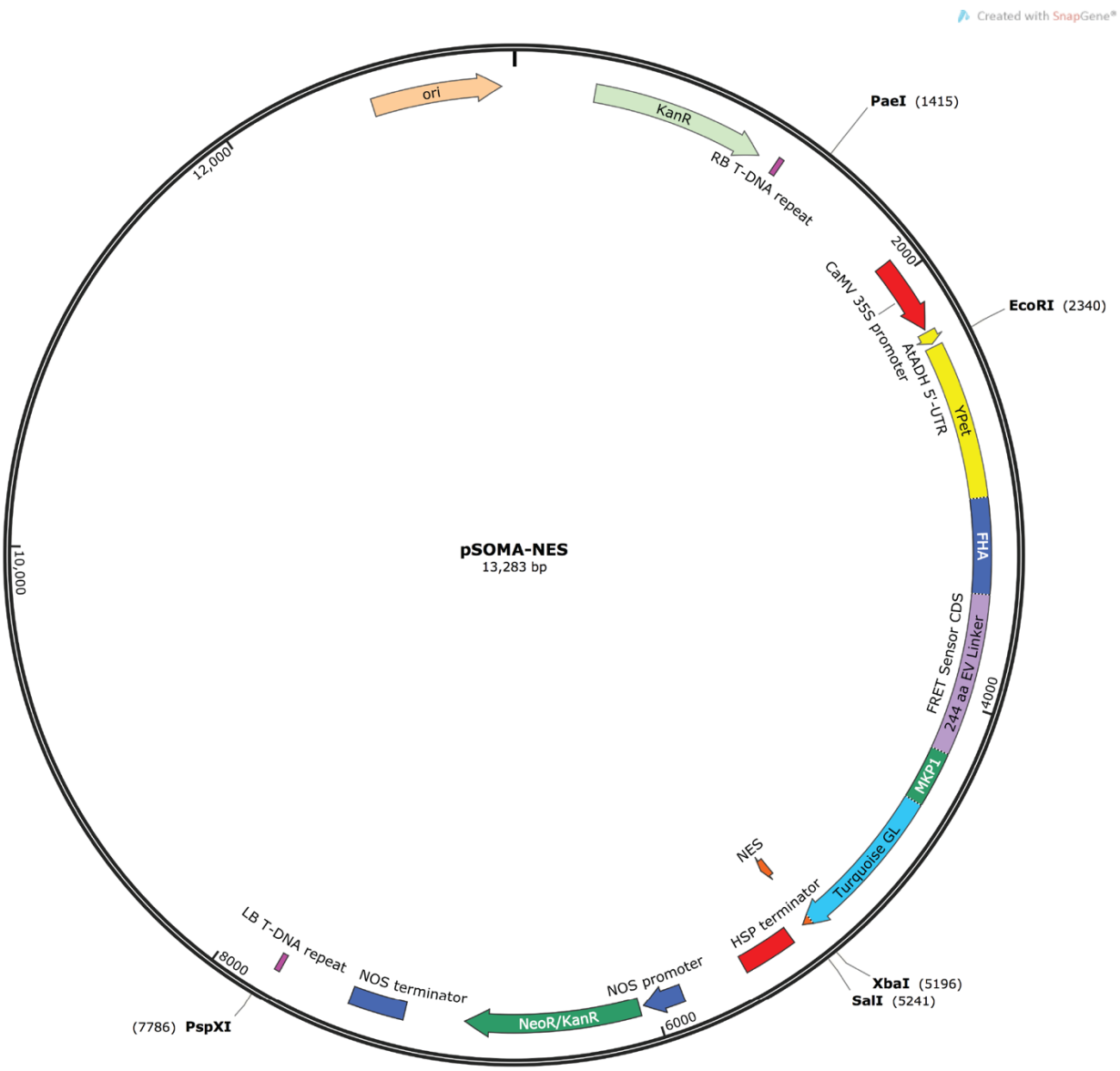

Fig. S12. Plasmid map for pET-SOMA-T679A.

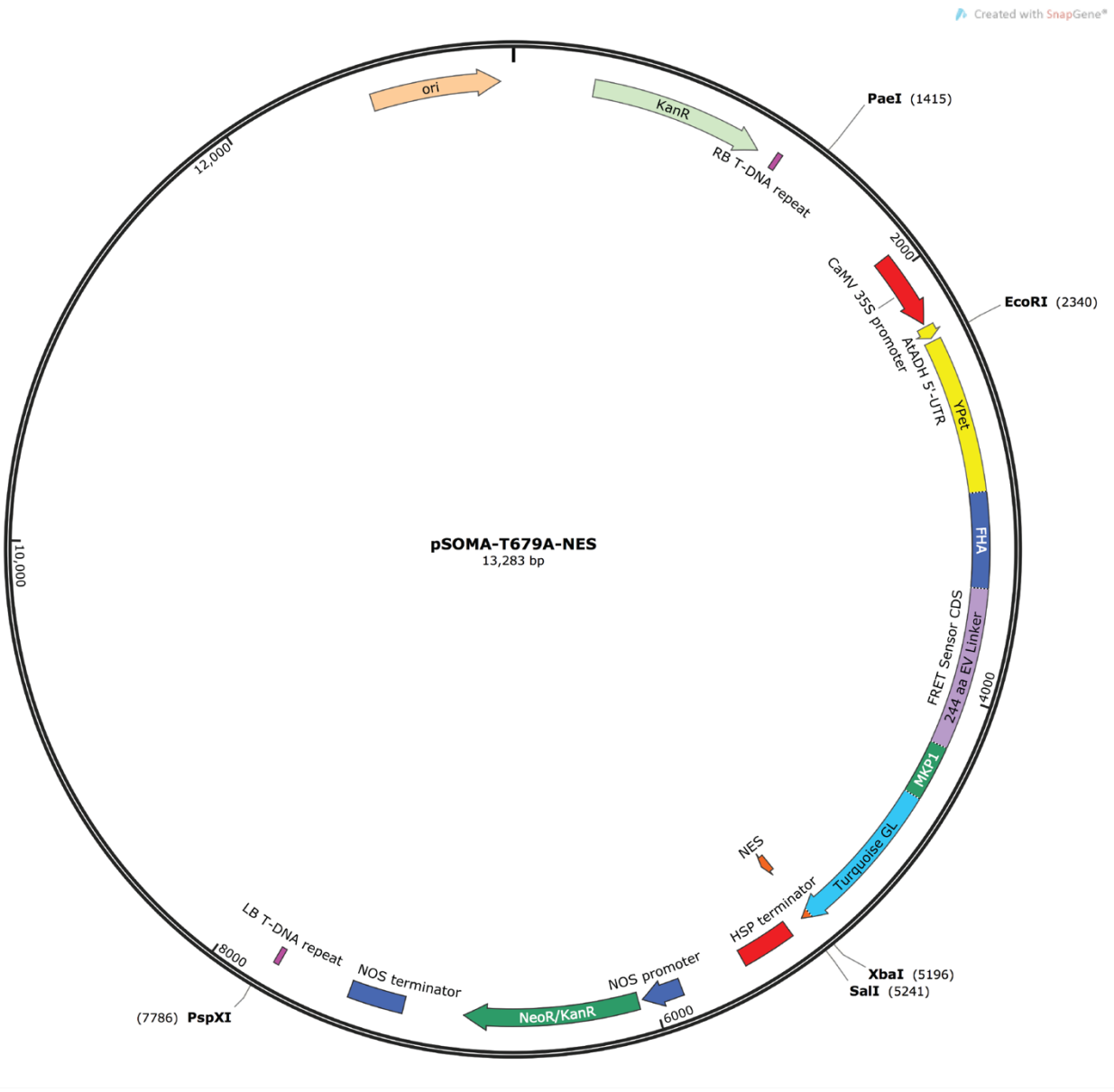

Fig. S13. Plasmid map for pSOMA-NLS.

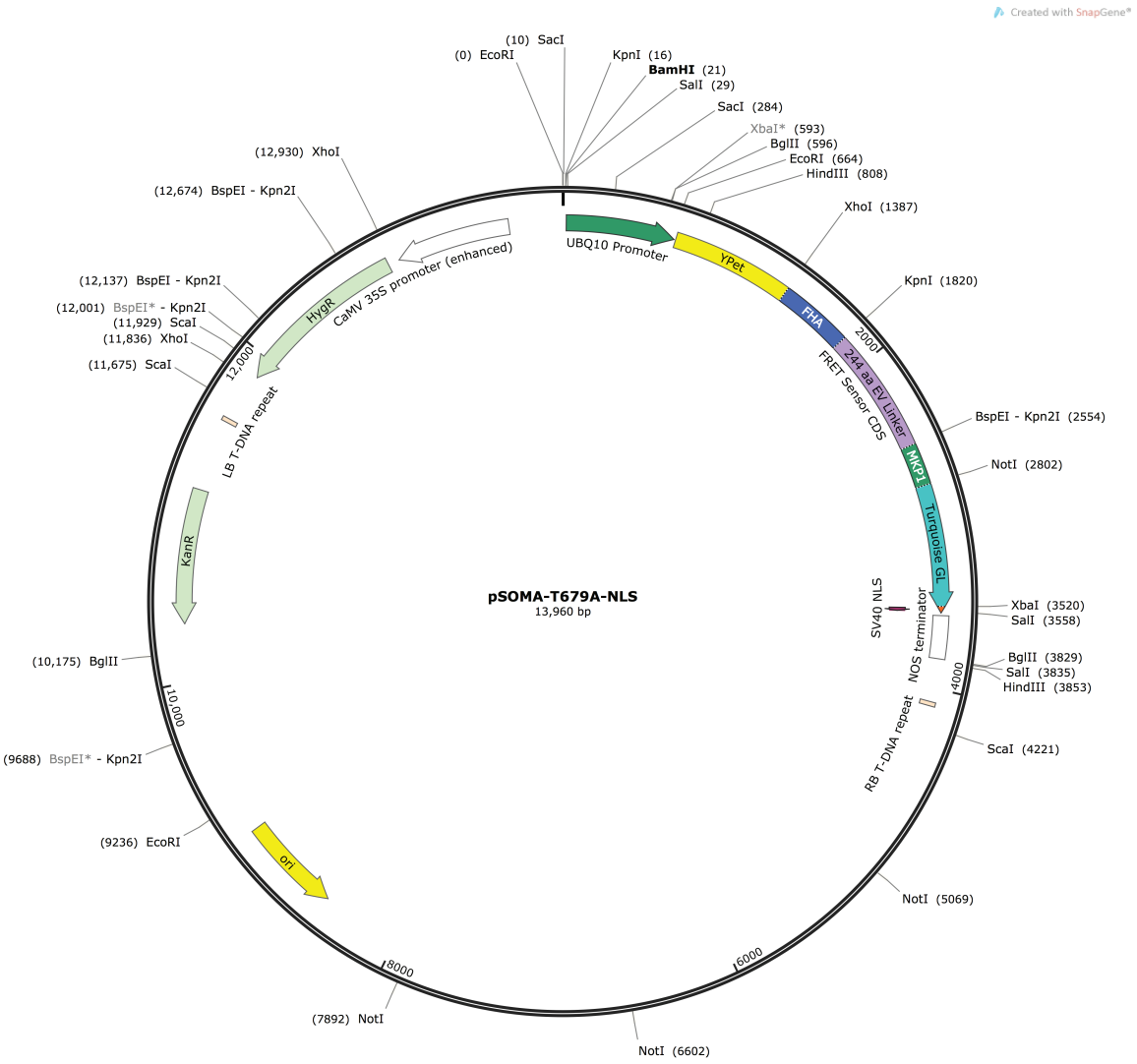

Fig. S14. Plasmid map for pSOMA-T679A-NLS.

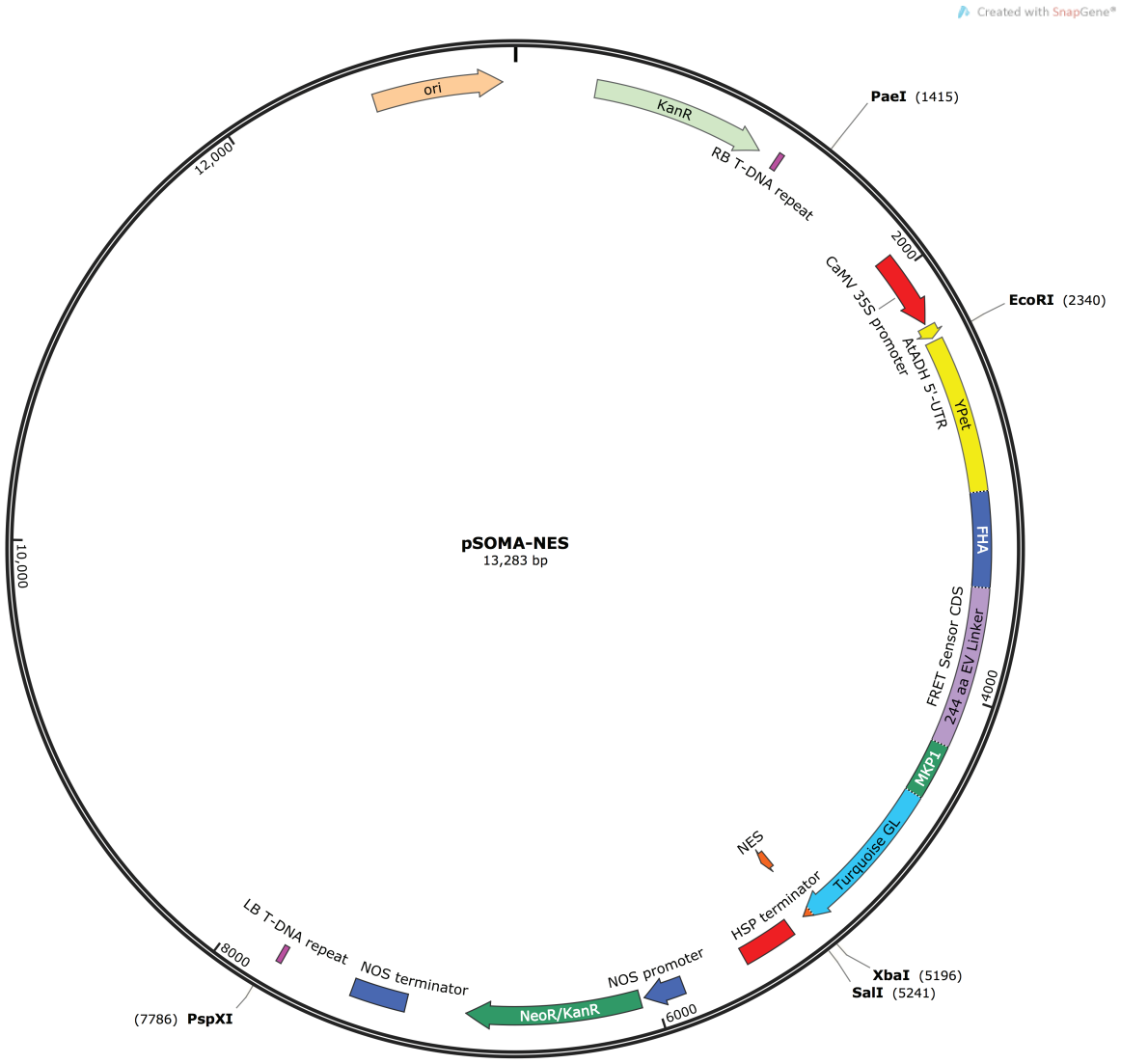

Fig. S15. Plasmid map for pSOMA-NES.

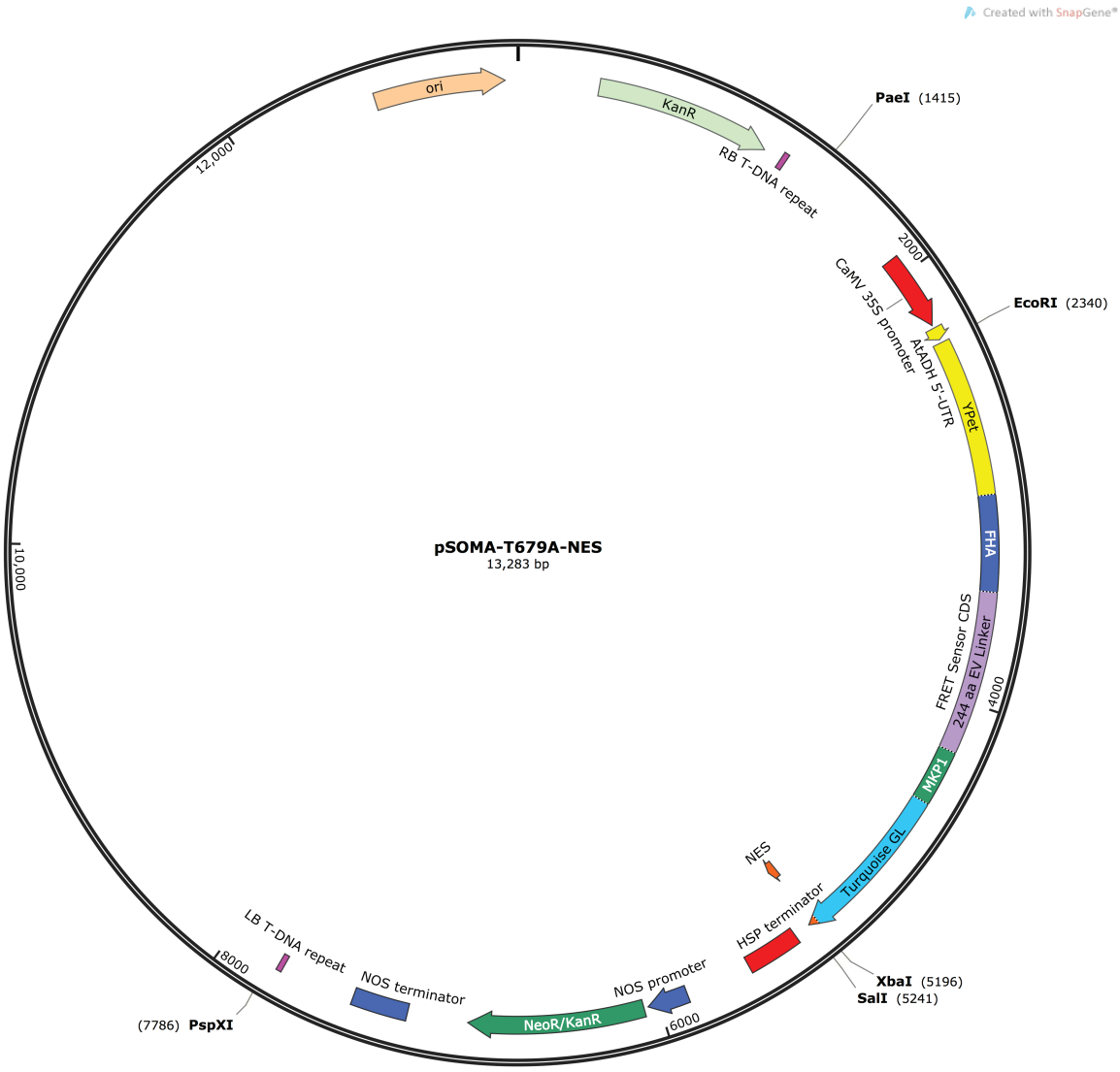

Fig. S16. Plasmid map for pSOMA-T679A-NES.

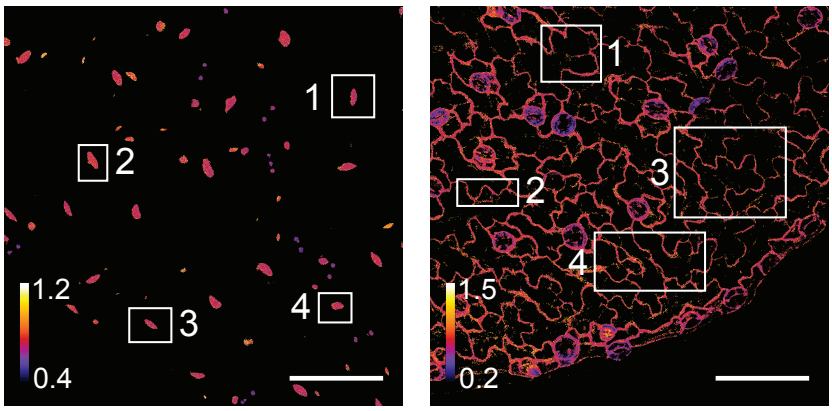

ROIs for Fig. 2G ROIs for Fig. 2H

Fig. S17. ROIs for Figure 2.
The ROIs used to collect YPet and Turquoise GL emission intenstify values are indicated by white rectangles.

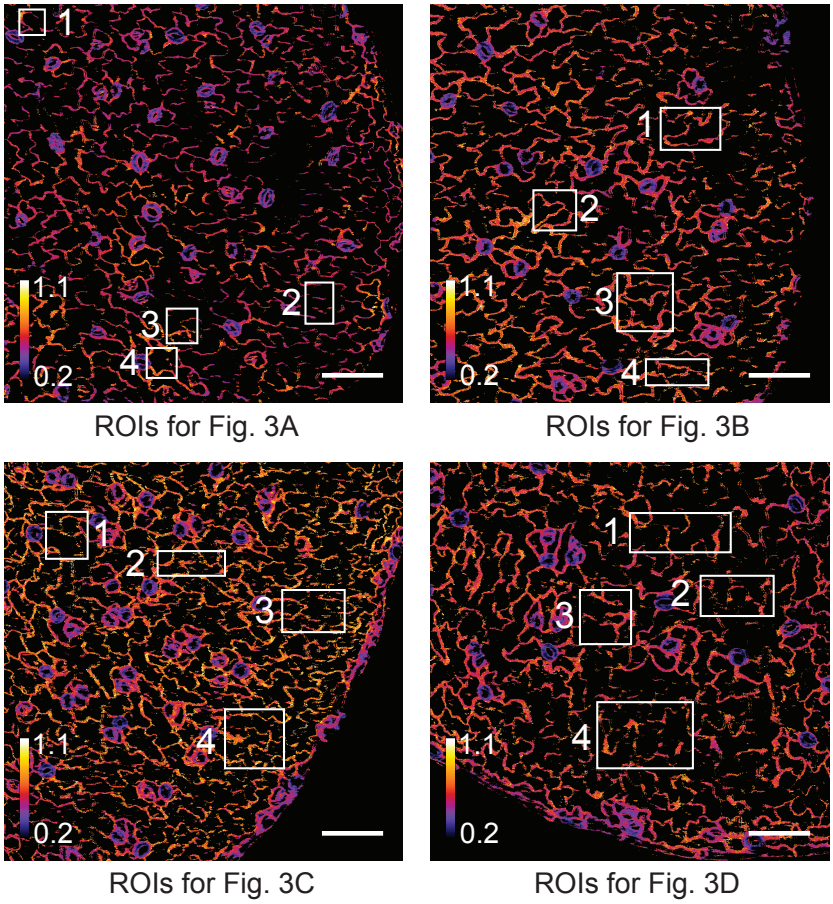

Fig. S18. ROIs for Figure 3.
The ROIs used to collect YPet and Turquoise GL emission intenstify values are indicated by white rectangles.

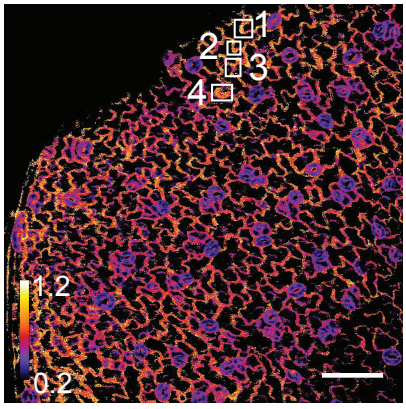

ROIs for Fig. 4A

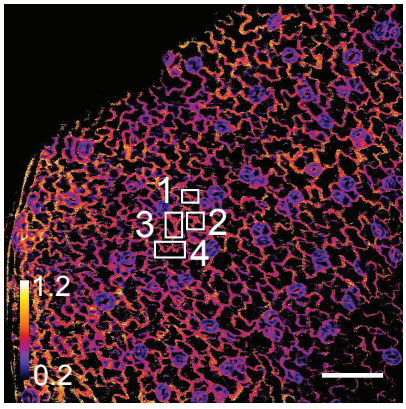

ROIs for Fig. 4B

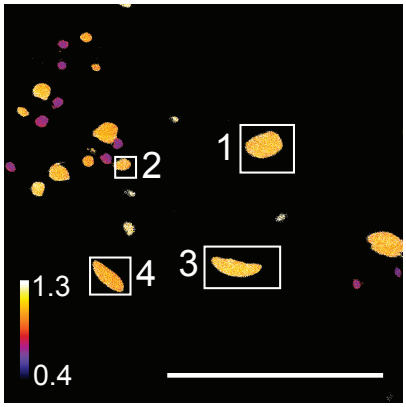

ROIs for Fig. 4C

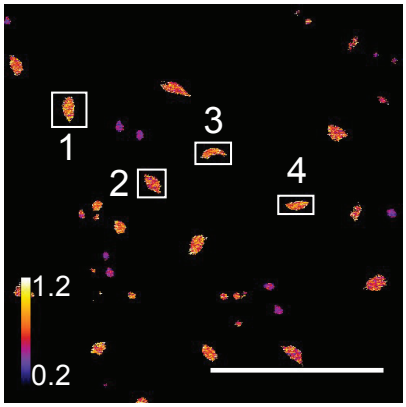

ROIs for Fig. 4D

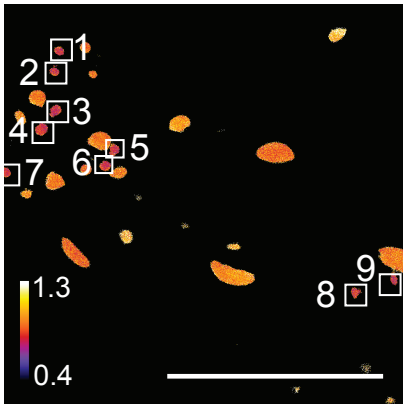

ROIs for Fig. 4E

Fig. S19. ROIs for Figure 4.
The ROIs used to collect YPet and Turquoise GL emission intenstify values are indicated by white rectangles.

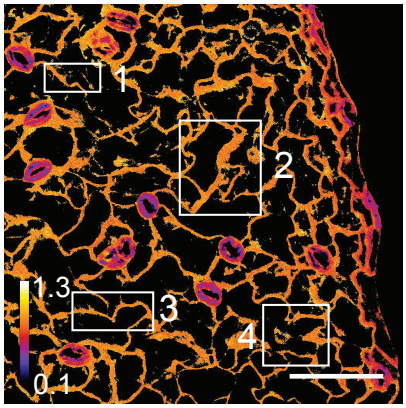

ROIs for Fig. 5A

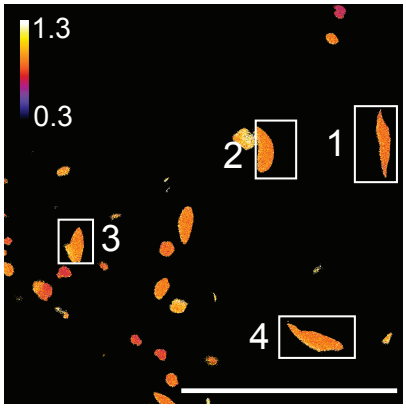

ROIs for Fig. 5B

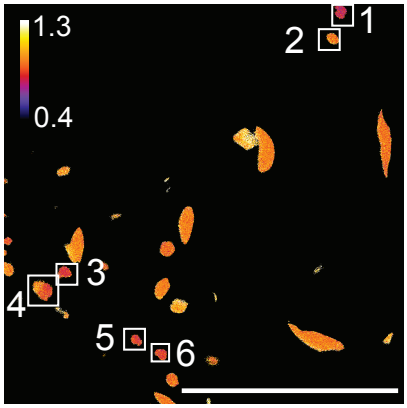

ROIs for Fig. 5C

Fig. S20. ROIs for Figure 5.
The ROIs used to collect YPet and Turquoise GL emission intenstify values are indicated by white rectangles.

Chapter 4: Expanding the Toolkit of Fluorescent Biosensors for Studying Mitogen Activated Protein Kinases in Plants

My contribution: I performed and analyzed all of the experiments within this paper. I made all of the Figures and Videos and co-authored the manuscript.

This chapter was adapted from the following publication: Seitz, K., & Krysan, P. J. Expanding the Toolkit of Fluorescent Biosensors for Studying Mitogen Activated Protein Kinases in Plants. *International Journal of Molecular Sciences*. **2020**, *21*, 5350.

Abstract

Mitogen-activated protein kinases (MAPKs) are key regulators of numerous biological processes in plants. To better understand the mechanisms by which these kinases function, high resolution measurement of MAPK activation kinetics in different biological contexts would be beneficial. One method to measure MAPK activation in plants is via fluorescence-based genetically encoded biosensors, which can provide real-time readouts of the temporal and spatial dynamics of kinase activation in living tissue. While fluorescent biosensors have been widely used to study MAPK dynamics in animal cells, there is currently only one MAPK biosensor that has been described for use in plants. To facilitate creation of additional plant-specific MAPK fluorescent biosensors, we report the development of two new tools: an *in vitro* assay for efficiently characterizing MAPK docking domains and a translocation-based kinase biosensor for use in plants. The implementation of these two methods has allowed us to expand the available pool of plant MAPK biosensors, while also providing a means to generate more specific and selective MAPK biosensors in the future. Biosensors developed using these methods have the potential to enhance our understanding of the roles MAPKs play in diverse plant signaling networks affecting growth, development, and stress response.

Introduction

Conserved across all eukaryotes (Kültz, 1998), Mitogen-activated Protein Kinases (MAPKs) have been shown to play critical roles in a wide array of biological processes. Within the plant model system *Arabidopsis thaliana*, MAPKs have been implicated in many aspects of plant life, including cell division (Müller et al., 2010; Xu & Zhang, 2015), abiotic stress responses (Mizoguchi et al., 1996; Ichimura et al., 2000; Droillard et al., 2002; Ahlfors et al., 2004; Droillard et al., 2004; Teige et al., 2004), biotic stress responses (Felix et al., 1999; Gómez-Gómez & Boller, 2000; Petersen et al., 2001; Frye et al., 2001; Asai et al., 2002; Miya et al., 2007; Rasmussen et al., 2012; Meng et al., 2013), developmental patterning (Shinkai et al., 2002; Wang et al., 2008; López-Bucio et al., 2014), stomatal closure (Liu et al., 2010; Lee et al., 2016), and many other pathways (Jonak et al., 2002; Rodriguez et al., 2010; Krysan & Colcombet, 2018). While biochemical methods to measure MAPK signaling have provided valuable insight into MAPK function within these pathways, these methods generally report the average MAPK activity within a population of cells and cannot provide cell-level resolution of the spatiotemporal dynamics these kinases display in different biological contexts.

One approach that can allow one to measure MAPK activation with greater resolution involves the use of fluorescence-based genetically encoded biosensors (Harvey et al., 2008; Oldach & Zhang, 2014). Fluorescent biosensors provide an easily quantifiable, real-time readout of a targeted parameter in living cells, elucidating the roles of different biomolecules in the complex dynamics that underlie cellular networks (Greenwald et al., 2018). A variety of fluorescent biosensors have been developed to shed light on the mechanisms by which MAPKs function and are regulated in animal cells (Oldach & Zhang, 2014), the most common of which

are Förster Resonance Energy Transfer (FRET) biosensors (Harvey et al., 2008; Sato et al., 2002; Fosbrink et al., 2010; Kamioka et al., 2012; Aoki et al., 2012; 2013; Sample et al., 2014; Tomida et al., 2015; Sari et al., 2018).

A FRET biosensor that measures MAPK activity is a single polypeptide that contains two fluorophore domains that are able to engage in FRET, a phosphoamino acid binding domain, a linker region, and a substrate domain. The substrate domain itself contains two important functional elements: a MAPK docking domain and a phosphoacceptor site. In the absence of active MAPK, the FRET biosensor is expected to exist in a non-phosphorylated state. In this condition, the phosphoamino acid binding domain has low affinity for interaction with the phosphoacceptor domain. If active MAPK is present, however, then the FRET biosensor is expected to become phosphorylated at the phosphoacceptor site. A conformational shift driven by binding of the phosphoamino acid binding domain to the phosphorylated substrate domain occurs, resulting in an increase in FRET efficiency. This change in FRET can be measured in real-time in living tissue using confocal microscopy, with the change in FRET serving as a readout of MAPK activation *in vivo*. Because of the high resolution with which confocal microscopes can image living tissue, changes in MAPK activity can be observed with single-cell resolution. Changes in FRET produced by these biosensors in response to phosphorylation can also be measured *in vitro* using an instrument such as a spectrofluorometer. By implementing these MAPK FRET biosensors within animal systems, researchers have mapped aspects of MAPK activity such as the duration or amplitude of activation (Zhang & Allen, 2007), heterogeneity of response at the cell population level (Kumagai et al., 2015; Durandau et al., 2015) or the subcellular level (Sato et al., 2007), and fluctuations in activity such as oscillations (Tomida et

al., 2015; Ryu et al., 2018), greatly enriching comprehension of MAPK spatiotemporal dynamics within these cells (Van et al., 2013; Lin et al., 2019).

The first plant MAPK fluorescent biosensor, the FRET-based Sensor Of MAPK in Arabidopsis (SOMA) was recently described (Zaman et al., 2019). SOMA has been shown to report the activities of the Arabidopsis MAPKs MPK3 and MPK6, and it is also likely to report the activities of additional MAPK isoforms in Arabidopsis such as MPK4 (Zaman et al., 2019). As the Arabidopsis genome encodes 20 MAPK isoforms, there remains a need for additional plant MAPK biosensors that report the activities of different MAPK isoforms. It would also be of great value to have biosensors with the specificity to report the activity of a single MAPK isoform. For these reasons, the plant MAPK research community would benefit from the ability to efficiently develop new plant MAPK biosensors. However, development of a new FRET biosensor tends to require a considerable amount of time as no universal design rules exist to guide the optimization process (Zhang et al., 2002; Aye-Han et al., 2009; Ibraheem & Campbell, 2010; Komatsu et al., 2011; Morris, 2012; Lindenburg et al., 2014). For this reason, we felt that it would be valuable to establish a set of tools that would streamline the process of developing new plant MAPK biosensors.

For a MAPK FRET biosensor to be useful, all of the functional domains that comprise that biosensor must work together to produce a protein that undergoes an appropriate conformational shift in response to phosphorylation. One of the most important determinants of that conformational shift is the interaction between the phosphoamino acid binding domain and the phosphorylated phosphoacceptor site. When designing FRET biosensors for a specific MAPK isoform, the standard approach involves testing a number of candidate substrate

domains that contain both a phosphoacceptor site and a docking domain that facilitates association of the substrate with the target MAPK (Harvey et al., 2008; Ibraheem & Campbell, 2010; Komatsu et al., 2011; Morris, 2012). By doing so, one hopes to find a substrate domain that can not only be efficiently phosphorylated by the MAPK, but that also has the ability to efficiently interact with the phosphoamino acid binding domain of the FRET biosensor. Unfortunately, this approach requires screening candidate sequences for their ability to simultaneously meet two functional criteria: (1) the ability to be efficiently phosphorylated and (2) the ability to effectively interact with the phosphoamino acid binding domain. Reducing the complexity of this process so that new sequences are screened using only a single functional criterion would make it possible to more efficiently develop new plant MAPK biosensors. The approach we took to accomplish this goal was to re-purpose a previously optimized mammalian MAPK FRET biosensor to serve as a plant MAPK docking domain trap.

The plant MAPK docking domain trap that we developed allowed us to screen for plant amino acid sequences that facilitate efficient phosphorylation of a mammalian MAPK phosphoacceptor site. Because the two fluorophores, the linker, the phosphoacceptor site, and the phosphoamino acid binding domain of this plant MAPK docking domain trap have been pre-optimized to produce a strong FRET change in response to phosphorylation, the only functional contribution required from the plant sequences was the ability to facilitate binding of the MAPK to the biosensor. In the present study we report how this plant MAPK docking domain trap can be deployed using an *in vitro* assay to efficiently screen for new plant MAPK docking domains.

In order to diversify the variety of tools available to plant scientists for studying MAPK activity *in vivo*, we sought to determine if an alternative to FRET-based biosensors could be

established for use in plants. To accomplish this, we turned to a biosensor variant used to study kinase activation in animal cells called a translocation biosensor (Regot et al., 2014]. This type of biosensor possesses both a Nuclear Localization Signal (NLS) module and a Nuclear Exclusion Signal (NES) module, with several phosphorylation sites scattered throughout (Regot et al., 2014). The phosphorylation status of these sites impacts the activities of these localization signals, directing the biosensor to either localize or be excluded from the nuclei of cells in a phosphorylation-dependent manner. By attaching a docking domain targeted by a kinase of interest to this type of biosensor, the nucleocytoplasmic shuttling of the sensor can serve as a visual indicator of kinase activity (Regot et al., 2014). Translocation biosensors offer several potential benefits in comparison to FRET-based biosensors and have proven to be powerful tools for documenting kinase spatiotemporal dynamics in different animal models (Regot et al., 2014; Sparta et al., 2015; de la Cova et al., 2017; Mayr et al., 2018; Kim et al., 2019).

In the present study we demonstrate that the translocation biosensor strategy described above is applicable to plants by showing that the nuclear localization activity of the bNLS/NES domain can be modulated by phosphomimetic mutations. We also demonstrate that inclusion of a plant MAPK docking domain in the translocation biosensor construct produces a protein that shifts from nuclear to cytoplasmic localization in response to treatments known to elicit MAPK activation in plants. Taken together, these results suggest that the kinase translocation biosensor approach developed for studying animal cell MAPK activation can also be effectively deployed for studying plant MAPKs.

The design of these translocation biosensors is such that the only functional element that needs to be added to the biosensor backbone to produce the functional biosensor is a

docking domain specific for the kinase of interest. When paired with the docking domain trap described earlier, this combination of tools produces a compact toolkit for efficiently generating new plant MAPK biosensors. The docking domain trap can be used to rapidly screen *in vitro* for amino acid sequences that specifically interact with chosen plant MAPK isoforms. Once those docking domains have been characterized *in vitro*, they can be deployed *in vivo* either in the context of the FRET biosensor backbone or transferred to the translocation biosensor backbone. Application of these tools should allow for enhanced exploration of the role of MAPK activation kinetics in many aspects of plant biology.

Results

Developing a FRET-based plant MAPK docking domain trap

In order to establish a pipeline for efficiently developing new plant MAPK fluorescent biosensors, we first set out to establish an *in vitro* assay for efficiently identifying new plant MAPK docking domains. To do so, the approach that we took was to develop a vector that would serve as a plant MAPK docking domain trap. We produced this trap by re-purposing an established MAPK FRET biosensor called EKAREV (Harvey et al., 2008; Komatsu et al., 2011) that had been proven effective for reporting MAPK activity in animal cells. The important functional domains of EKAREV are the YPet yellow fluorescent protein domain (Nguyen et al., 2005), the Turquoise GL cyan fluorescent protein domain (Goedhart et al., 2010), the EV linker (Komatsu et al., 2011), the forkhead (FHA1) phosphoamino acid binding domain (Hofmann & Bucher, 1995; Sun et al., 1998), a 14 amino acid phosphoacceptor domain from the mammalian Cdc25C protein (Gonzalez, et al., 1991), and a docking domain recognized by the human extracellular

signal-regulated kinases (ERKs) (Jacobs et al., 1999) (Figure 1A), which are a type of MAPK. A cartoon schematic of EKAREV in action is shown in Figure 1(B). As the EKAREV biosensor does not contain a plant-specific MAPK docking domain, we postulated that it may not be efficiently phosphorylated by plant MAPKs. If so, this FRET biosensor had the potential to serve as a plant MAPK docking domain trap. To test this hypothesis, we used an *in vitro* assay that we previously developed for evaluating candidate plant MAPK FRET biosensors (Zaman et al., 2019).

For this *in vitro* assay, biosensor protein and constitutively active versions of the Arabidopsis MAPKs MPK4 and MPK6 (CA-MPK4 and CA-MPK6) are expressed as recombinant proteins using *E. coli* [44, 62]. Recombinant biosensor protein is then incubated together with constitutively active kinase and adenosine triphosphate (ATP), and the reactions are subsequently analyzed using a scanning spectrofluorometer to measure the fluorescent emission generated by illumination of the samples at a wavelength that excites the mTurquoise-GL FRET donor. When EKAREV was incubated in the presence of CA-MPK6, we observed a ca. 9% increase in FRET efficiency when compared to the control reaction that did not contain kinase (Figure 1C, Table 1). This FRET gain was substantially lower than the ca. 68% increase in FRET that CA-MPK6 induced in our previously described Arabidopsis MAPK biosensor SOMA (Figure 1D, Table 1). These results suggested that CA-MPK6 may have only a limited capacity to phosphorylate EKAREV. Next, we repeated the above experiment using CA-MPK4 and found that this kinase caused no FRET gain for EKAREV (Figure 1E). In the control reaction, we observed that CA-MPK4 induced a ca. 27% increase in the FRET efficiency of SOMA (Figure 1F).

Testing the plant MAPK docking domain trap

We hypothesized that the low FRET gain induced in EKAREV by CA-MPK6 and the lack of a FRET gain caused by CA-MPK4 could be explained by at least two different mechanisms. First, the mammalian phosphoacceptor domain present in EKAREV may not be able to be efficiently targeted by CA-MPK4/6. Alternatively, the mammalian MAPK docking domain present in EKAREV may not efficiently recruit CA-MPK4/6 to bind to the biosensor. To explore these two possibilities, we inserted DNA sequence that encoded a known Arabidopsis MAPK docking domain into the EKAREV vector.

For this experiment we used a region of the coding sequence from the Arabidopsis BREAKING OF ASYMMETRY IN THE STOMATAL LINEAGE (BASL) gene (Dong et al., 2009). The BASL protein has been previously characterized as a MPK3/6 substrate, and several plant MAPK docking domains have been mapped on its structure (Zhang et al., 2015; 2016). We used a section of the BASL gene encoding 39 amino acids that contained the D1 docking domain and inserted it into the EKAREV plasmid, resulting in EKAREV-BASL (Figure 2A-B). Incubating EKAREV-BASL with CA-MPK6 resulted in a ca. 115% gain in FRET while CA-MPK4 induced a ca. 85% gain (Figure 2C, Table 1). Our observation that EKAREV-BASL exhibited substantially higher MAPK-induced FRET increases than EKAREV is consistent with the hypothesis that adding a suitable Arabidopsis MAPK docking domain to EKAREV is sufficient to allow the biosensor to be efficiently phosphorylated by plant MAPKs.

To determine if the mammalian phosphoacceptor domain present in EKAREV was being targeted by CA-MPK4/6, we mutagenized the threonine residue in EKAREV-BASL thought to behave as the phosphorylation site into an alanine (Harvey et al., 2008; Komatsu et al., 2011;

Gonzalez et al., 1991. The resulting mutant version of the biosensor, EKAREV^{T48A}-BASL, showed no increase in FRET efficiency when incubated with either CA-MPK4 or CA-MPK6 (Figure 2D, Table 1), similar to the results observed when the phosphorylation site of SOMA was mutagenized to an alanine (Supplemental Figure 1, Table 1) (Zaman et al., 2019; Schweighofer et al., 2007, Park et al., 2011). These results demonstrate that the MAPK-induced FRET gain observed with EKAREV-BASL is dependent on the threonine present within the EKAREV phosphoacceptor domain and suggest that the increase in FRET efficiency is likely caused by phosphorylation of that threonine by CA-MPK4/6. The results described above suggested that EKAREV has the potential to serve as a plant MAPK docking domain trap. To further test this hypothesis, we cloned DNA sequence encoding another previously characterized plant MAPK docking domain into the EKAREV vector. We used a region of the Arabidopsis PP2C-type phosphatase AP2C1, which is a characterized MPK6 substrate that contains verified MAPK docking domains (Umbrasaite et al., 2010; Shubchynskyy et al., 2017). When a region of the *AP2C1* gene encoding one such docking domain was added to the EKAREV backbone (Figure 2A and 2B), the resulting biosensor, EKAREV-AP2C1, exhibited an increase in FRET efficiency of ca. 150% in response to CA-MPK6 and an increase of ca. 140% in response to CA-MPK4 (Figure 2E, Table 1). Mutagenizing the predicted phosphorylation site within the EKAREV phosphoacceptor domain eliminated this effect (Figure 2F, Table 1). Therefore, incorporating a different plant MAPK docking domain into EKAREV also produced a biosensor able to report MAPK-induced FRET increases when treated with plant MAPKs. Taken together with the results obtained with EKAREV-BASL, these results indicate that EKAREV is able to function as a plant MAPK docking domain trap.

By establishing EKAREV as a plant MAPK docking domain trap, we have developed a tool for functionally assessing candidate Arabidopsis MAPK docking domains. It should also be noted that the EKAREV-docking domain constructs that we produced are also functional FRET-based biosensors which can be directly moved into plants for evaluation of their potential to serve as *in vivo* biosensors for MAPK activity in living plant tissue. In addition, the plant MAPK docking domains identified using this *in vitro* assay likely possess some degree of modularity such that they could potentially be incorporated into other types of fluorescent biosensors, as described below.

Developing a translocation-based biosensor for use in Arabidopsis

One alternative to FRET-based biosensors for studying MAPK activity *in vivo* are translocation biosensors, or Kinase Translocation Reporters (KTRs) (Regot et al., 2014). KTRs are distinct from FRET-based kinase biosensors in that the subcellular localization of the fluorescent signal is the main readout of kinase activity. KTRs possess a bipartite nuclear localization signal (bNLS)/nuclear exclusion signal (NES) module, with several phospho-sites scattered through the bNLS sequence. In an unphosphorylated state, the activity of the bNLS is dominant, resulting in the biosensor localizing to the nucleus of the cell. However, upon phosphorylation, the activity of the bNLS is repressed and the activity of the NES is enhanced, causing the biosensor to be excluded from the nucleus and accumulate in the cytoplasm. If a docking domain is added to the KTR that allows the biosensor to be phosphorylated by a kinase of interest, the subcellular localization of the resulting biosensor reflects the activation state of the chosen kinase.

Although relatively recently established, KTRs offer several potential advantages in comparison to FRET biosensors, such as a wider dynamic range and seemingly more accurate reporting of the downregulation of kinase activity (Regot et al., 2014; de la Cova et al., 2017). Although KTRs have been successfully implemented in mammalian cells, *C. elegans,* and zebrafish (Regot et al., 2014; Sparta et al., 2015; de la Cova et al., 2017; Mayr et al., 2018; Kim et al., 2019), their use has not yet been reported in plants. In order to expand the set of fluorescent reporters available for studying MAPK activation in plants, we were therefore interested in determining if the KTR principle could be applied to Arabidopsis.

To create a translocation biosensor for reporting MAPK activity in plants, we began with the nuclear Kinase Translocation Reporter (nKTR) developed for imaging MAPK activity in *C. elegans* (de la Cova et al., 2017). nKTR contains a 44 amino acid docking domain derived from the mammalian Ets-like protein 1 (Elk1) (Hipskind et al., 1991; Dalton et al., 1993), a bNLS containing two phospho-sites sites (S55 and S62), a NES, a FQFP motif (Jacobs et al., 1999), and the green fluorophore mClover (Lam et al., 2012). The subcellular localization of the nKTR protein when expressed in *C. elegans* is driven by the equilibrium between the competing activities of the bNLS and NES domains, with the phosphorylation status of the bNLS capable of shifting the balance between nuclear localization and nuclear exclusion. Unphosphorylated nKTR was shown to localize to the nuclei of *C. elegans* germline cells while phosphorylated nKTR was excluded from the nucleus (de la Cova et al., 2017).

In order to create a plant-based KTR, we synthesized a vector based on nKTR, with the following modifications: (1) the region encoding the Elk1 docking domain was removed, (2) the coding sequence for the mClover fluorophore was replaced with coding sequence for

mNeonGreen (Shaner et al., 2013), and (3) the entire coding sequence of the construct was codon optimized for expression in plants. We assigned the name Kinase Localization Reporter (KLR) to this plant-focused reporter to distinguish it from the KTRs used in animal cells. This KLR construct does not contain any MAPK docking domains (Figure 3A). Based on the behavior of nKTR, unphosphorylated KLR was expected to localize to the nucleus. Upon phosphorylation, KLR would be expected to shift its localization to the cytoplasm, while dephosphorylation should cause it to return to the nucleus (Figure 3B). Quantifying the intensity of mNeonGreen fluorescence within the nucleus versus cytoplasm should thereby serve as a measure of kinase activity in the Arabidopsis cells in which the KLR biosensor is expressed.

The design of the nKTR biosensor construct used in *C. elegans* also contained coding sequence for the spectrally-distinct mCherry fluorophore linked to histone 2B (H2B) sequence. The mCherry-H2B portion of the nKTR construct provided an internal control for quantifying nuclear fluorescence (de la Cova et al., 2017). The protein coding sequences for nKTR and mCherry-H2B were joined by a self-cleaving peptide from *Thosea asigna* virus 2A (T2A) (Halpin et al., 1999; Ahier & Jarriault, 2014), an element which induces ribosomal pausing during translation. Inclusion of this T2A peptide causes the single mRNA transcript generated by the nKTR vector to produce nKTR and mCherry-H2B as separate polypeptides. This arrangement allows the two proteins to be produced in equimolar quantities, while permitting each to localize independently within the cell. When nKTR was expressed in *C. elegans*, mCherry-H2B was found to be constitutively present in the nucleus, while the localization of nKTR was determined by the phosphorylation status of the reporter (de la Cova et al., 2017).

We chose to emulate the dual-fluorophore approach described above for our KLR construct. The final vector that we produced for the KLR reporter encoded a single messenger RNA containing the following components: the KLR reporter, the T2A self-cleaving peptide, and a mRuby3 red fluorophore (Bajar et al., 2016) linked to an NLS derived from simian virus 40 (SV40 NLS) (Kalderon et al., 1984). If the resulting KLR reporter construct performs as expected, mRuby3 will be constitutively localized to the nuclei of plant cells due to the SV40 NLS, while the localization of the mNeonGreen-tagged KLR reporter should shift between the nucleus and the cytoplasm depending on the phosphorylation status of the reporter (Figure 3B).

Upon creation of our KLR construct, the first step in our validation process was to determine if the KLR reporter could localize to or be excluded from plant cell nuclei in a phosphorylation-dependent manner. To investigate this, the serine phosphorylation sites in the bNLS domain of KLR were mutagenized to either the non-phosphorylatable alanine, creating a "phospho-dead" variant (KLR^{AA}), or the negatively-charged glutamic acid, resulting in a "phosphomimetic" construct (KLR^{EE}). As KLR^{AA} mimicked a fully "unphosphorylated" biosensor, we expected it to localize mainly to the nucleus. In contrast, the fully "phosphorylated" KLR^{EE} was expected to localize mainly to the cytoplasm. Stable transgenic lines expressing KLR, KLR^{AA}, or KLR^{EE} were produced and imaged using confocal microscopy. The fluorescence emission intensities of the mNeonGreen and mRuby3 fluorophores were captured for these samples. As described above, mNeonGreen fluorescence is derived from the KLR reporter, while mRuby3 red fluorescence serves as a nuclear marker in these experiments (Figure 3C). In most plant cells, the vacuole occupies much of the volume, compressing the cytoplasm and making quantification of cytoplasmic fluorescent signal difficult. As such, we choose to image the root

tips of seedlings expressing the KLR constructs, due to their relatively smaller vacuoles and the consequent ease of measuring cytoplasmic versus nuclear fluorescence.

Strong nuclear mNeonGreen fluorescence was observed in root cells that expressed either KLR or KLR^{AA} (Figure 3C). In contrast, roots cells expressing KLR^{EE} had much lower mNeonGreen fluorescence in the nuclei, and higher mNeonGreen fluorescence in the cytoplasm (Figure 3C). The localization of KLR and KLR^{AA} appeared to be mainly nuclear, while that of KLR^{EE} was mainly cytoplasmic. When the ratio of cytoplasmic to nuclear mNeonGreen fluorescence intensity was calculated, it was significantly higher for KLR^{EE} than either KLR ($p<.001$, two-tailed t-test) or KLR^{AA} ($p<.001$, two-tailed t-test) (Figure 3D), indicating that cells expressing KLR^{EE} have more mNeonGreen fluorescence in the cytoplasm than those expressing KLR or KLR^{AA}. These results are consistent with our expectation that the non-phosphorylatable KLR^{AA} would localize mainly to the nuclei, while phosphomimetic KLR^{EE} would localize mainly to the cytoplasm.

Addition of a plant MAPK docking domain to KLR facilitates subcellular localization shifts in response to chitin

The experiments described above using the KLR^{EE} construct containing phosphomimetic mutations suggested that the KLR reporter may have the potential to report kinase activity in plant cells. The KLR reporter, however, does not contain any kinase docking domain. In order to test KLR's potential as plant MAPK reporter, it was therefore first necessary to add a plant MAPK docking domain to the KLR construct. For this experiment, we incorporated the MKP1 substrate domain from our previously described plant MAPK FRET biosensor SOMA (Zaman et

al., 2019; Ulm et al., 2001) into KLR, creating KLR-MKP1 (Figure 3A). Since SOMA is able to report MAPK activity in living plant tissue, we reasoned that the MKP1 substrate domain must possess a functional plant MAPK docking domain. To minimize potentially confounding effects of the phosphosite present in this MKP1 substrate domain (Zaman et al., 2019; Schweighofer et al., 2007; Umbrasaite et al., 2010) we mutated that phosphorylation site to alanine so that the only phosphorylation sites present on the KLR-MKP1 construct were those present in the bNLS domain.

Arabidopsis lines stably expressing KLR-MKP1 were created and seedlings of these lines were placed in imaging chambers that allowed us to apply chemical treatments to the samples during imaging (Vang et al., 2018). In order to determine if KLR-MKP1 had the potential to report *in vivo* changes in MAPK activation, we subjected the seedlings to treatment with an aqueous suspension of chitin, which is known to elicit the rapid activation of MPK3/6 in Arabidopsis (Miya et al., 2007; Wan et al., 2004; Yamada et al., 2016). Root tip cells of these seedlings were imaged using confocal microscopy to measure mNeonGreen and mRuby3 fluorescence. For each experiment, the first image was taken prior to chitin treatment while the seedling was resting in pure water. After this image was taken, the water within the imaging chamber was replaced with an aqueous suspension of chitin, and two additional images were collected at time points 12 min and 52 min following chitin treatment.

When the three time points of the mNeonGreen channel were examined, we observed weaker nuclear fluorescence and stronger cytoplasmic fluorescence at the 12 min time point in comparison to the 0 min and 52 min time points. In contrast, there were no substantial differences between the three time points for the mRuby3 channel (Figure 3E). When the

fluorescent emission intensity was quantified, the nuclear mNeonGreen signal at the 12 min mark had decreased by ca. 60% when compared to the 0 min time point, while the cytoplasmic mNeonGreen fluorescent intensity had increased by ca. 61% (Figure 3G). In contrast, the difference in nuclear and cytoplasmic mNeonGreen fluorescent intensities at the 52 min time point to those of the 0 min time point were ca. 0% and ca. 5%, respectively (Figure 3G). This data is consistent with a model in which the KLR-MKP1 reporter transiently leaves the nucleus for the cytoplasm in response to chitin treatment.

As a control, we also tested the response to chitin of the KLR reporter lacking a MAPK docking domain. In these experiments, chitin treatment had no effect on the nuclear localization of KLR (Supplemental Figure 2 A-C). This result is consistent with the hypothesis that a MAPK docking domain is required for KLR to change its subcellular localization in response to treatments know to activate MAPK activity in Arabidopsis.

Based on these results, the addition of the MKP1 substrate domain to KLR resulted in a reporter that appears to have changed localization in response to chitin treatment in Arabidopsis seedlings. To determine if this apparent change in localization was dependent on the bNLS phosphorylation sites present in KLR, the phosphosites were mutagenized to non-phosphorylatable alanine residues, resulting in a “phosphodead” KLR^{AA}-MKP1 reporter. When seedlings expressing KLR^{AA}-MKP1 were treated with chitin, no substantial changes in either mNeonGreen or mRuby3 fluorescent signal were observed (Figure 3F, 3H). These results are consistent with a model in which the nucleocytoplasmic shuttling of KLR-MKP1 is regulated by its phosphorylation sites, likely through their phosphorylation.

KLR-MKP1 exhibited shifts in localization in Arabidopsis cotyledons in response to different chemical treatments known to trigger MAPK activation

To further explore the potential of KLR-MKP1 as a MAPK biosensor, we tested the behavior of KLR-MKP1 under experimental conditions that had been previously used to characterize the Arabidopsis MAPK FRET biosensor SOMA (Zaman et al., 2019). Arabidopsis cotyledons expressing KLR-MKP1 were imaged every 2 min, with chitin added between the 8 min and 10 min time points (Figure 4A). As cytoplasmic mNeonGreen fluorescence was difficult to quantify in this tissue type, fluorescent emission intensity was measured solely in the nuclei of cells. In response to chitin, the nuclear mNeonGreen signal of KLR-MKP1 dropped ca. 60% before returning to pre-treatment levels at the 52 min time point, while nuclear mRuby3 exhibited no such change (Supplemental Figure 3A).

As we were unable to accurately quantify cytoplasmic mNeonGreen signal, we normalized the data by dividing the nuclear mRuby3 fluorescence intensity by the nuclear mNeonGreen fluorescent intensity (Figure 4E), following the convention established by the developers of the nKTR reporter [53]. Normalizing the data in this way produces numerical results in which an increase in kinase activity is expected to result in an increase in the nuclear mRuby3/mNeonGreen ratio. When this approach was employed, the resulting ratio of nuclear mRuby3/mNeonGreen fluorescence intensity rapidly increases upon exposure to chitin, reaching a peak gain of ca. 180% before returning to basal levels 42 min after chitin was added. The increase in this ratio is driven by dramatic reductions in the nuclear mNeonGreen signal, while the nuclear mRuby3 signal does not undergo large changes (Supplementary Figure 3A).

We also repeated this experiment using the non-phosphorylatable KLR^{AA}-MKP1 as a control. When cotyledons expressing KLR^{AA}-MKP1 were treated with chitin (Figure 4B), there was no increase in the mRuby3/mNeonGreen ratio (Figure 4F), and the nuclear mNeonGreen fluorescence signal did not display any dramatic changes (Supplementary Figure 3B). The observation that KLR^{AA}-MKP1 does not change localization in response to chitin treatment is consistent with our hypothesis that phosphorylation of the bNLS is responsible for the changes in nuclear fluorescence observed with KLR-MKP1. As additional controls, cotyledons expressing either construct were also treated with pure water rather than the aqueous chitin solution, (Figure 4C-D, G-H, Supplementary Figure 3C-D) or imaged with no additional manipulation (Supplementary Figure 4A-F). No substantial responses were observed for these experiments, demonstrating that the imaging protocol was not responsible for the changes in nuclear mNeonGreen fluorescence observed when cotyledons expressing KLR-MKP1 were exposed to chitin.

We next wanted to determine if KLR-MKP1 localization could be affected by additional chemical treatments know to activate MAPKs. Cotyledons expressing KLR-MKP1 were treated with either the synthetic flagellin peptide flg22 (Figure 5A, C, Supplementary Figure 5A) or NaCl (Figure 5B, D, Supplementary Figure 5B). Both treatments have been previously demonstrated to trigger MAPK activation [8, 10, 11, 14, 82-86] and had also induced an increase in FRET efficiency for the plant MAPK FRET biosensor SOMA [44]. When cotyledons expressing KLR-MKP1 were exposed to a 1 µM solution of flg22, an initial increase in the nuclear mRuby3/mNeonGreen ratio of ca. 190% was observed, which lasted a for 46 min (Figure 5C). This first peak was followed by a weaker second increase approximately 47 min after flg22 was

added. When 150 mM NaCl was the treatment, the increase in nuclear mRuby3/mNeonGreen ratio was smaller, with a gain of ca. 92% and more transient, lasting for only 26 min (Figure 5D). The observation that KLR-MKP1 displays different responses to chitin, flg22, and NaCl treatments raises the possibility that this type of biosensor can offer insights into the mechanisms by which these external stimuli can lead to differential activation of response pathway(s).

Incorporating the AP2C1 docking domain into KLR produces a biosensor that changes localization in response to chitin

The work described above with KLR-MKP1 suggested that KLR has the potential to serve as a kinase activity reporter in Arabidopsis provided that a MAPK docking domain is added to the construct. To further test this hypothesis, we wanted to determine if adding a different MAPK docking domain to KLR would produce a biosensor able to respond to chitin treatment. For this experiment, we chose the AP2C1 docking domain that we characterized using the *in vitro* docking domain trap described above in section 2.2. We chose this docking domain because it had driven the highest MAPK-induced increase in FRET efficiency in the *in vitro* assay. The KLR construct that we produced by adding the AP2C1 docking domain was named KLR-AP2C1. A "phosphodead" variant of this biosensor was also created by mutagenizing the bNLS phosphorylation sites into alanine to produce KLR^{AA}-AP2C1.

Cotyledons from stable transgenic lines expressing either KLR-AP2C1 or KLR^{AA}-AP2C1 were treated with chitin, pure water, or received no treatment (Figure 6A-H, Supplemental Figure 6A-D, Supplemental Figure 7A-F). The addition of chitin to cotyledons expressing KLR-

AP2C1 triggered a ca. 193% increase in the nuclear mRuby3/mNeonGreen ratio over 32 min (Figure 6B), corresponding to a ca. 42% drop in nuclear mNeonGreen signal over the same period of time (Supplemental Figure 6E). As expected, pure water and no treatment did not induce a gain in the nuclear mRuby3/mNeonGreen ratio nor a drop in nuclear mNeonGreen signal. These results demonstrated that a MAPK docking domain identified by the *in vitro* docking domain trap could be added to the KLR construct to produce a biosensor capable of exhibiting a shift in subcellular localization in response to a chemical elicitor known to induce MAPK activity.

Discussion

MAPKs play an essential role in mediating numerous cellular processes. In many signaling networks, activation of MAPKs is necessary to translate external stimuli into a specific biological response. To better understand the mechanisms by which MAPKs operate, quantification of their spatiotemporal dynamics would be advantageous. Genetically encoded biosensors serve as potential tools for capturing these kinetics, offering several advantages over biochemical methods for studying kinase activation. In animal models, fluorescent biosensors targeted to MAPKs have been widely used, while application of these tools to the field of plant MAPK research has lagged behind. To facilitate further adoption of MAPK fluorescent biosensors for plant research, we have established an experimental pipeline that utilizes both *in vitro* and *in vivo* components to efficiently streamline the process of developing new fluorescent biosensors for studying MAPKs in plants.

The first part of this paper describes an *in vitro* FRET-based assay for evaluating plant MAPK docking domains. This "docking domain trap" was developed by repurposing a FRET-based biosensor developed for studying the activation of MAPKs in animal cells called EKAREV (Komatsu et al., 2011). EKAREV possesses a phosphoamino acid binding domain, phosphoacceptor domain, two fluorophores, and a linker that have all been shown to work effectively together to serve as a kinase activity biosensor. For application in plants, the only functional element missing from this construct is a MAPK docking domain that interacts effectively with plant MAPKs. Indeed, inserting known plant MAPK docking domains from the Arabidopsis proteins BASL or AP2C1 into the EKAREV backbone resulted in biosensors that underwent a 10-fold increase in their FRET efficiency when treated with constitutively active versions of the Arabidopsis MAPKs MPK4 or MPK6 when compared to the EKAREV backbone alone (Berriri et al., 2012). Furthermore, mutagenizing the phosphorylation site within the EKAREV phosphoacceptor for either construct abolished this increase in FRET, suggesting that the CA-MAPK isoforms induce an increase in FRET efficiency in a phosphorylation-dependent manner.

One of the potential applications of this plant MAPK docking domain trap would be the development of fluorescent biosensors that specifically report the activation of a single MAPK isoform. A systematic approach to accomplishing this goal would be to screen a large panel of candidate docking domains *in vitro* using the EKAREV plant MAPK docking domain trap to find candidate sequences that show promising activity profiles in response to a panel of constitutively active MAPK variants that can be effectively expressed as recombinant proteins. Site directed mutagenesis or molecular evolution could then be employed to further refine

these candidate sequences to ultimately produce a docking domain that possesses input specificity towards a MAPK isoform of interest. These docking domains could then be deployed *in vivo* as either FRET biosensors using the EKAREV backbone or as translocation biosensors using the approach described below. If such isoform-specific reporters can be developed, they should allow researchers to more precisely investigate issues related to specificity and cross-talk in plant signaling pathways.

In addition to the docking domain trap described above, the other main focus of our study was to expand the types of fluorescent kinase biosensors currently available to plant researchers. For this work we focused on translocation biosensors, which are a type of kinase reporter that changes its subcellular localization in response to phosphorylation of a bNLS/NES module present within the biosensor (Regot et al., 2014). Starting with the nKTR reporter developed for measuring kinase activity in *C. elegans* (de la Cova et al., 2017), we removed the 44 amino acid Elk1 docking domain and optimized the coding sequence for expression in plants, naming the resulting construct KLR for Kinase Localization Reporter. To investigate whether KLR localization was influenced by the phosphorylation status of the bNLS/NES domain, we created a “phosphodead” KLR^{AA} variant and a “phosphomimetic” KLR^{EE} variant in which the two phosphorylation sites were mutated to either alanine or glutamic acid residues. KLR^{AA} was localized largely in the nucleus, while the phosphomimetic KLR^{EE} was localized largely in the cytoplasm. These results suggested that the phosphorylation-responsive bNLS/NES developed for animal cells was functional in plant cells. Follow-up experiments in which we added plant MAPK docking domains to our KLR construct provided further evidence that KLR has the capacity to serve as a kinase reporter in plants. Specifically, we observed that KLR variants with

plant MAPK docking domains showed transient reductions in nuclear fluorescence emission intensity when plant tissue expressing these reporters was exposed to chitin, flg22, or NaCl, which are treatments known to activate MAP kinases in plants.

Our observation that the nuclear fluorescence intensities of KLR-MKP1 and KLR-AP2C1 undergo transient reductions in response to stress treatments known to activate MAPKs is consistent with the hypothesis that these biosensors are reporting the activity of MAPKs *in vivo*. Further experimentation will be needed, however, to prove this hypothesis. Our observation that the phosphorylation sites within the bNLS/NES of KLR are necessary for the stress-induced changes in nuclear fluorescence intensity is consistent with the idea that phosphorylation of the NLS/NES by a kinase is responsible for the changes in fluorescent signal observed. In order to prove that a MAPK is responsible for this *in vivo* phosphorylation, it will be necessary to generate transgenic lines that express the KLR-MKP1 or KLR-AP2C1 reporter in a genetic background carrying null mutants of one or more Arabidopsis MAPKs. Because many MAPK substrates in Arabidopsis are able to be phosphorylated by multiple MAPK isoforms (Krysan & Colcombet, 2018), it may be necessary to work with mutant lines that have more than one member of the MAPK gene family knocked out. This approach is complicated by the fact that MPK3/6, the two MAPKs known to interact with MKP1 and AP2C1, are a synthetic lethal gene pair (Wang et al., 2007). In our previous work with the plant MAPK FRET biosensor SOMA, we demonstrated how the use of an analog-sensitive variant of MPK6 expressed in a *mpk3/6* null background can enable one to use a chemical inhibitor to specifically switch off MPK6 activity (Zaman et al., 2019; Bishop et al., 2000; Xu et al., 2014). Using that approach, we were able to demonstrate that the SOMA biosensor was reporting MPK6 activation in response to NaCl

treatment. A similar approach could be taken to directly test if KLR-MKP1 or KLR-AP2C1 are acting as MAPK biosensors in Arabidopsis.

In this study we have described an experimental pipeline for building new FRET and translocation biosensors as complimentary tools to study MAPK signaling in Arabidopsis. The first component of this pipeline is an *in vitro* FRET-based assay for identifying and assessing the specificity of plant MAPK docking domains. Docking domains that perform well in this *in vitro* assay can remain within the EKAREV construct to be directly used as MAPK FRET biosensors in plants or swapped into the KLR translocation biosensor construct for use *in vivo*. It is our hope that this pipeline will allow the diversity of plant MAPK fluorescent biosensors to continue to grow and broaden, providing the research community with additional tools to further document and explore the role MAPKs play in the regulation of signaling pathways in plants.

Materials and Methods

Plasmid construction

EKAREV was a kind gift from Michiyuki Matsuda and Kazuhiro Aoki. Specifically, we used the previously described SOMA construct (Zaman et al., 2019) and replaced the substrate domain encoding amino acid residues 15-94 of the Arabidopsis MKP1 protein with the 18 amino acids that make up the optimized substrate sequence in the EKAREV construct, including the FQFP kinase docking domain, (Komatsu et al., 2011) using restriction enzyme cloning. To create EKAREV-BASL, a region encoding amino acid residues 51-89 of the Arabidopsis BASL protein was added to the EKAREV construct. Additionally, the serine at position 72 of the BASL protein was mutagenized to an alanine. To create EKAREV-AP2C1, a region encoding amino acid residues

92-124 of the Arabidopsis AP2C1 protein was added to the EKAREV construct. To create the phosphorylation site mutant forms of the above EKAREV variants, site-directed mutagenesis was performed to change the coding sequence at the threonine phosphorylation site of the sensor protein to alanine. The resulting protein-coding sequences were then cloned into a derivative of Pet-32(a)+ (Millipore Sigma, http://www.merckmillipore.com/) for expression of recombinant proteins in *E. coli*. Plasmid maps and DNA sequence for pET-EKAREV, pET-EKAREV-BASL, pET-EKAREV^{T48A}-BASL, pET-EKAREV-AP2C1 and pET-EKAREV^{T48A}-AP2C1 are provided in Data Files S1-S5 and Supplemental Figures S8-S12. The full plasmid maps for the pKLR expression vector and its derivatives pKLR^{AA}, pKLR^{EE}, pKLR-AP2C1, pKLR^{AA}-AP2C1, pKLR-MKP1, and pKLR^{AA}-MKP1 are provided in Data Files S6-S12 and Supplemental Figures S13-S19.

***In vitro* FRET assay**

The *in vitro* FRET assay was performed as previously described (Zaman et al., 2019). Recombinant EKAREV, SOMA, EKAREV-BASL, EKAREV^{T48A}-BASL, SOMA^{T679A}, EKAREV-AP2C1, EKAREV^{T48A}-AP2C1, CA-MPK6 and CA-MPK4 were expressed in the Rosetta2 strain of *E. coli* (Millipore Sigma). CA-MPK6 and CA-MPK4 are constitutively active forms of Arabidopsis MPK6 and MPK4, respectively Berriri et al., 2012). Plasmids expressing CA-MPK6 or CA-MKP4 were kind gifts from Jean Colcombet. To perform the assay, Rosetta2 *E. coli* cells were grown overnight in 1 ml Lysogeny broth (LB) with the appropriate antibiotics at 25°C at 276 revolutions per min (RPM). The next day, 200 µl of each culture was added to fresh tubes of 1 ml LB containing the appropriate antibiotics and 0.1 mM Isopropyl ß-D-1-thiogalactopyranoside (IPTG) (Sigma-Aldrich), before growing overnight at 25°C at 276 RPM. The next day, the 1.2 ml

cultures were spun down, supernatant removed, and the tubes were incubated at -20°C for at least 30 min. Tubes were then returned to room temperature and the cell pellets was treated with 200 µl Bug Buster reagent (Millipore Sigma) for the *E. coli* expressing biosensor proteins or 100 µl Bug Buster for the *E. coli* expressing CA-MPK6 or CA-MPK4. Samples were then centrifuged at 4°C at 13,000 RPM in a microcentrifuge and the cleared lysate was transferred to new tubes. 7 µl of the cleared lysate containing recombinant biosensor protein was added to a reaction containing 25 mM 2-amino-2-(hydroxymethyl)-1,3-propanediol (TRIS)-HCl, 0.5 mM DTT, 5 mM MgCl2, 0.1 mM ATP, 100 mM NaCl and water to a total volume of 200 µl. For reactions including CA-MPK6 or CA-MPK4, 4 µl of the appropriate CA-MAPK cleared lysate was also added. The reactions were then incubated at room temperature for 30–60 min and the fluorescent emission spectrum was measured using a QuantaMaster 40 Spectrofluorometer. Excitation was performed at 420 nm, and the emission range analyzed was 465–545 nm. The slit size for both excitation and emission was 5 nm with a step size of 0.5 nm and integration of 0.1 nm. All experiments were performed with at least three technical reps.

Transgenic lines

Transgenic lines expressing KLR, KLR^{AA}, KLR^{EE}, KLR-MKP1, KLR^{AA}-MKP1, KLR-AP2C1, and KLR^{AA}-AP2C1 were produced via the floral dip method using the GV3101 strain of *Agrobacterium tumefaciens* (Clough & Bent, 1998). Primary transformants expressing the biosensor constructs were identified by screening seedlings with an epifluorescence microscope. These seedlings were 4-day-old seedlings germinated on 1% agar (w/v) plates containing 0.5x Murashige and Skoog basal salt mixture. Seedlings exhibiting strong

fluorescence were transferred to soil and seed was collected. Seed for the transgenic lines is available via the Arabidopsis Biological Resource Center (ABRC) (http://abrc.osu.edu/).

Plant material and growth conditions

To prepare seedlings for confocal imaging, seeds were surface sterilized using 95% ethanol and then plated onto growth media composed of 1% agar (w/v) containing 0.5x Murashige and Skoog basal salt mixture in 130 mm square Petri dishes. The samples were incubated in the dark at 4°C for 2 days to stratify the seeds and then placed under constant light at 20–25°C with the plates in a vertical orientation. Seedlings were collected for imaging after the plates had been under light for 3-4 days. Cotyledons were collected for imaging after the plates had been under light for 4–5 days.

Confocal microscopy

Whole seedlings or detached cotyledons were prepared for imaging on the confocal microscope using the previously described HybriWell™ method (Vang et al., 2018). Briefly, a 5 µl drop of ultrapure water was placed on a 45 mm x 55 mm microscope cover glass. Then, the sample was placed on top of the droplet (cotyledons were place abaxial side down). The sample was gently submerged by dripping water around it with a pipette. Excess water was then removed, and a HybriWell™ (Grace Bio-Labs, http://gracebio.com/, cat. no. 611102) was gently placed on the cover slide with the sample centered to form a 150 µm deep imaging chamber with a volume of 30 µl. The dimensions of the chamber are such that the sample is gently held in place by pressure from the top of the chamber, but liquid can still pass between the sample

and the cover glass (Vang et al., 2018). Then, 400 µl of ultrapure water was injected through one of the HybriWell™ ports using a pipettor to fill the 30 µl chamber with water and expel any air bubbles. A 200 µl droplet of ultrapure water was then placed on one of the ports to prevent the chamber from drying out. The HybriWells™ were then placed in covered Petri dishes and equilibrated by incubating at 20–23°C under constant light for 12-16 hours prior to imaging.

Confocal microscopy was performed using a Zeiss LSM 780 (http://www.zeiss.com/) with a 40x objective for root tips or a 20x objective for cotyledons. mNeonGreen was excited at 458 nm at 2% power and mRuby3 was excited at 561 nm at 2.5% power. Emission was measured between 489 nm and 544 nm for mNeonGreen and between 579 nm and 632 nm for mRuby3. Z-stacks were collected every 2 min with an optical slice thickness of 2 µm.

Chemical treatments were added to the samples during imaging by pipetting 200 µl of solution containing the treatment onto one port of the HybriWell™. For chitin treatment, 200 mg of chitin from shrimp shells (Sigma, http://www.sigmaaldrich.com/, cat. no. C7170–100G) was added to a 1.5 ml Eppendorf tube containing two steel pellets and ground at 25 Hz for 10 min using a Retsch MM 200 mixer mill (Retsch, http://www.retsch.com/). The pulverized chitin was then added to 5 ml of pure water and vortexed briefly prior to use for a working concentration of 40 mg/ml. For flg22 treatment, a 1 µM solution of synthetic flg22 peptide (QRLSTGSRINSAKDDAAGLQIA) (PhytoTechnology Laboratories, http://phytotechlab.com/, cat. no. P6622) in 5 ml pure water was used.

Image analysis

Post-processing of the raw image data was performed using Fiji (Schindelin et al., 2012). Image sets were concatenated before the 'Z-projection' function was performed on an image stack using the 'Max Intensity' setting. To quantify the emission channels individually, the 'Subtract Background' function was performed, with the 'rolling ball radius' set at the default 50 pixels. The resulting image stack was then converted to 32-bit, and the 'Threshold' function was performed with the default values by selecting 'Apply' and enabling the 'Set to NaN' option. To create a merged image, the channels were split and then merged back together. Movies S11, S13, S14, S15, S16, S19-S26, S29 and S30 present time-course videos of the merged image data for select experiments.

To create a ratio image, the Z-projection was divided into separate mNeonGreen and mRuby3 emission channels. The 'Subtract Background' function was performed on both images, with the 'rolling ball radius' set as the default 50 pixels. A mask was then created from the mRuby3 channel using the 'Convert to Mask' function. The background subtracted mRuby3 and mNeonGreen images were then converted into 32-bit images. These 32-bit images were then multiplied by the Mask file. The resulting mRuby3 image was divided by the resulting mNeonGreen image using the 'Image Calculator' function to create a ratio image representing the ratio of mRuby3 to mNeonGreen emission. Finally, the 'Threshold' function was performed using the default values, with the 'NaN background' option enabled. The 'Fire' lookup table was then applied to the final ratio image. To measure the ratio of mRuby3 to mNeonGreen emission, a region of interest (ROI) containing a nucleus was manually selected using Fiji and then average intensity was measured. For time-course experiments, the change in the mRuby3 to mNeonGreen emission ratio was normalized to the initial value of the mRuby3/mNeonGreen

emission ratio and plotted versus time. Movies S1-S10, S12, S17, S18, S27, and S28 present time-course videos of the ratio image data for selected experiments.

Acknowledgements

The authors wish to thank Michiyuki Matsuda and Kazuhiro Aoki for generously sharing their FRET sensor constructs. This work was supported by the National Science Foundation (NSF MCB-1137950). The authors wish to thank John Seagrist for technical assistance with this project.

References

Ahier, A.; Jarriault, S. Simultaneous expression of multiple proteins under a single promoter in *Caenorhabditis elegans* via a versatile 2A-based toolkit. *Genetics*. **2014**, *196*, 605-613.

Ahlfors, R.; Macioszek, V.; Rudd, J.; Brosché, M.; Schlichting, R.; Scheel, D.; Kangasjärvi, J. Stress hormone-independent activation and nuclear translocation of mitogen-activated protein kinases in *Arabidopsis thaliana* during ozone exposure. *The Plant Journal*. **2004**, *40*, 512-522.

Aoki, K.; Komatsu, N.; Hirata, E.; Kamioka, Y.; Matsuda, M. Stable expression of FRET biosensors: a new light in cancer research. *Cancer Science*. **2012**, *103*, 614-619.

Aoki, K.; Kumagai, Y.; Sakurai, A.; Komatsu, N.; Fujita, Y.; Shionyu, C.; Matsuda, M. Stochastic ERK activation induced by noise and cell-to-cell propagation regulates cell density-dependent proliferation. *Molecular Cell*. **2013**, *52*, 529-540.

Asai, T.; Tena, G.; Plotnikova, J.; Willmann, M.R.; Chiu, W.L.; Gomez-Gomez, L.; Boller, T.; Ausubel, F.M.; Sheen, J. MAP kinase signaling cascade in Arabidopsis innate immunity. *Nature*. **2002**, *415*, 977-983.

Aye-Han, N. N.; Ni, Q.; Zhang, J. Fluorescent biosensors for real-time tracking of post-translational modification dynamics. *Current Opinion in Chemical Biology*. **2009**, *13*, 392-397.

Bajar, B.T.; Wang, E.S.; Lam, A.J.; Kim, B.B.; Jacobs, C.L.; Howe, E.S.; Davidson, M.W.; Lin, M.Z.; Chu, J. Improving brightness and photostability of green and red fluorescent proteins for live cell imaging and FRET reporting. *Scientific Reports*. **2016**, *6*, 1-12.

Berriri, S.; Garcia, A.V.; dit Frey, N.F.; Rozhon, W.; Pateyron, S.; Leonhardt, N.; Montillet, J.L.; Leung, J.; Hirt, H.; Colcombet, J. Constitutively active mitogen-activated protein kinase versions reveal functions of Arabidopsis MPK4 in pathogen defense signaling. *The Plant Cell*. **2012**, *24*, 4281-4293.

Bishop, A.C.; Ubersax, J.A.; Petsch, D.T.; Matheos, D.P.; Gray, N.S.; Blethrow, J.; Shimizu, E.; Tsien, J.Z.; Schultz, P.G.; Rose, M.D.; Wood, J.L. A chemical switch for inhibitor-sensitive alleles of any protein kinase. *Nature*. **2000**, *407*, 395-401.

Clough, S. J.; Bent, A. F. Floral dip: a simplified method for Agrobacterium-mediated transformation of *Arabidopsis thaliana*. *The Plant Journal*. **1998**, *16*, 735-743.

Dalton, S.; Marais, R.; Wynne, J.; Treisman, R. Isolation and characterization of SRF accessory proteins. *Philosophical Transactions of the Royal Society of London. Series B: Biological Sciences*. **1993**, *340*, 325-332.

de la Cova, C.; Townley, R.; Regot, S.; Greenwald, I. A real-time biosensor for ERK activity reveals signaling dynamics during *C. elegans* cell fate specification. *Developmental Cell*. **2017**, *42*, 542-553.

Dóczi, R.; Brader, G.; Pettkó-Szandtner, A.; Rajh, I.; Djamei, A.; Pitzschke, A.; Teige, M.; Hirt, H. The Arabidopsis mitogen-activated protein kinase kinase MKK3 is upstream of group C mitogen-activated protein kinases and participates in pathogen signaling. *The Plant Cell*. **2007**, *19*, 3266-3279.

Dong, J.; MacAlister, C. A.; Bergmann, D. C. BASL controls asymmetric cell division in Arabidopsis. *Cell*. **2009**. *137*, 1320-1330.

Droillard, M. J.; Boudsocq, M.; Barbier-Brygoo, H.; Laurière, C. Different protein kinase families are activated by osmotic stresses in *Arabidopsis thaliana* cell suspensions: involvement of the MAP kinases AtMPK3 and AtMPK6. *FEBS Letters*. **2002**, *527*, 43-50.

Droillard, M. J.; Boudsocq, M.; Barbier-Brygoo, H.; Laurière, C. Involvement of MPK4 in osmotic stress response pathways in cell suspensions and plantlets of *Arabidopsis thaliana*: activation by hypoosmolarity and negative role in hyperosmolarity tolerance. *FEBS Letters*. **2004**, *574*, 42-48.

Durandau, E.; Aymoz, D.; Pelet, S. Dynamic single cell measurements of kinase activity by synthetic kinase activity relocation biosensors. *BMC Biology*. **2015**, *13*, 55.

Felix, G.; Duran, J. D.; Volko, S.; Boller, T. Plants have a sensitive perception system for the most conserved domain of bacterial flagellin. *The Plant Journal*. **1999**, *18*, 265-276.

Fosbrink, M.; Aye-Han, N. N.; Cheong, R.; Levchenko, A.; Zhang, J. Visualization of JNK activity dynamics with a genetically encoded fluorescent biosensor. *Proceedings of the National Academy of Sciences*. **2010**, *107*, 5459-5464.

Frye, C. A.; Tang, D.; Innes, R. W. Negative regulation of defense responses in plants by a conserved MAPKK kinase. *Proceedings of the National Academy of Sciences*. **2001**, *98*, 373-378.

Goedhart, J.; Van Weeren, L.; Hink, M. A.; Vischer, N. O.; Jalink, K.; Gadella Jr, T. W. Bright cyan fluorescent protein variants identified by fluorescence lifetime screening. *Nature Methods*. **2010**, *7*, 137.

Gómez-Gómez, L.; Boller, T. FLS2: an LRR receptor–like kinase involved in the perception of the bacterial elicitor flagellin in Arabidopsis. *Molecular Cell*. **2000**, *5*, 1003-1011.

Gonzalez, F. A.; Raden, D. L.; Davis, R. J. Identification of substrate recognition determinants for human ERK1 and ERK2 protein kinases. *Journal of Biological Chemistry*. **1991**, *266*, 22159-22163.

Greenwald, E. C.; Mehta, S.; Zhang, J. Genetically encoded fluorescent biosensors illuminate the spatiotemporal regulation of signaling networks. *Chemical Reviews*. **2018**, *118*, 11707-11794.

Halpin, C.; Cooke, S. E.; Barakate, A.; Amrani, A. E.; Ryan, M. D. Self-processing 2A-polyproteins–a system for co-ordinate expression of multiple proteins in transgenic plants. *The Plant Journal*. **1999**, *17*, 453-459.

Harvey, C. D.; Ehrhardt, A. G.; Cellurale, C.; Zhong, H.; Yasuda, R.; Davis, R. J.; Svoboda, K. A genetically encoded fluorescent biosensor of ERK activity. *Proceedings of the National Academy of Sciences*. **2008**, *105*, 19264-19269.

Hipskind, R. A.; Roa, V. N.; Muller, C. G. F.; Raddy, E. S. P.; Nordheim, A. Ets-related protein Elk-1 is homologous to the c-fos regulatory factor p62TCF. *Nature*. **1991**, *354*, 531-534.

Hofmann, K.; Bucher, P. The FHA domain: a putative nuclear signaling domain found in protein kinases and transcription factors. *Trends in Biochemical Sciences*. **1995**, *20*, 347-349.

Ibraheem, A.; Campbell, R. E. Designs and applications of fluorescent protein-based biosensors. *Current Opinion in Chemical Biology*. **2010**, *14*, 30-36.

Ichimura, K.; Casais, C.; Peck, S. C.; Shinozaki, K.; Shirasu, K. MEKK1 is required for MPK4 activation and regulates tissue-specific and temperature-dependent cell death in Arabidopsis. *Journal of Biological Chemistry*. **2006**, *281*, 36969-36976.

Ichimura, K.; Mizoguchi, T.; Yoshida, R.; Yuasa, T.; Shinozaki, K. Various abiotic stresses rapidly activate Arabidopsis MAP kinases ATMPK4 and ATMPK6. *The Plant Journal*. **2000**, *24*, 655-665.

Jacobs, D.; Glossip, D.; Xing, H.; Muslin, A. J.; Kornfeld, K. Multiple docking sites on substrate proteins form a modular system that mediates recognition by ERK MAP kinase. *Genes Development*. **1999**, *13*, 163-175.

Jonak, C.; Ökrész, L.; Bögre, L.; Hirt, H. Complexity, cross talk and integration of plant MAP kinase signaling. *Current Opinion in Plant Biology*. **2002**, *5*, 415-424.

Kalderon, D. Roberts BL, Richardson WD, Smith AE. A short amino acid sequence able to specify nuclear location. *Cell*. **1984**, *39*, 499-509.

Kamioka, Y.; Sumiyama, K.; Mizuno, R.; Sakai, Y.; Hirata, E.; Kiyokawa, E.; Matsuda, M. Live imaging of protein kinase activities in transgenic mice expressing FRET biosensors. *Cell Structure and Function*. **2012**, 1201200102-1201200102.

Kim, J.; Lee, S.; Jung, K.; Oh, W.C.; Kim, N.; Son, S.; Jo, Y.; Kwon, H.B.; Do Heo, W. Intensiometric biosensors visualize the activity of multiple small GTPases *in vivo*. *Nature Communications*. **2019**, *10*, 1-11.

Komatsu, N.; Aoki, K.; Yamada, M.; Yukinaga, H.; Fujita, Y.; Kamioka, Y.; Matsuda, M. Development of an optimized backbone of FRET biosensors for kinases and GTPases. *Molecular Biology of the Cell*. **2011**, *22*, 4647-4656.

Krysan, P. J.; Colcombet, J. Cellular complexity in MAPK signaling in plants: Questions and emerging tools to answer them. *Frontiers in Plant Science*. **2018**, *9*, 1674.

Kültz, D. Phylogenetic and functional classification of mitogen-and stress-activated protein kinases. *Journal of Molecular Evolution*. **1998**, *46*, 571-88.

Kumagai, Y.; Naoki, H.; Nakasyo, E.; Kamioka, Y.; Kiyokawa, E.; Matsuda, M. Heterogeneity in ERK activity as visualized by *in vivo* FRET imaging of mammary tumor cells developed in MMTV-Neu mice. *Oncogene*. **2015**, *34*, 1051-1057.

Lam, A.J.; St-Pierre, F.; Gong, Y.; Marshall, J.D.; Cranfill, P.J.; Baird, M.A.; McKeown, M.R.; Wiedenmann, J.; Davidson, M.W.; Schnitzer, M.J.; Tsien, R.Y. Improving FRET dynamic range with bright green and red fluorescent proteins. *Nature Methods*. **2012**, *9*, 1005-1012.

Lee, Y.; Kim, Y. J.; Kim, M. H.; Kwak, J. M. MAPK cascades in guard cell signal transduction. *Frontiers in Plant Science*. **2016**, *7*, 80.

Lin, W.; Mehta, S.; Zhang, J. Genetically encoded fluorescent biosensors illuminate kinase signaling in cancer. *Journal of Biological Chemistry*. **2019**, *294*, 14814-14822.

Lindenburg, L.; Merkx, M. Engineering genetically encoded FRET biosensors. *Sensors*. **2014**, *14*, 11691-11713.

Liu, Y. K.; Liu, Y. B.; Zhang, M. Y.; Li, D. Q. Stomatal development and movement: the roles of MAPK signaling. *Plant Signaling Behavior*. **2010**, *5*, 1176-1180.

López-Bucio, J.S.; Dubrovsky, J.G.; Raya-González, J.; Ugartechea-Chirino, Y.; López-Bucio, J.; de Luna-Valdez, L.A.; Ramos-Vega, M.; León, P.; Guevara-García, A.A. *Arabidopsis thaliana* mitogen-activated protein kinase 6 is involved in seed formation and modulation of primary and lateral root development. *Journal of Experimental Botany*. **2014**, *65*, 169-183.

Mayr, V.; Sturtzel, C.; Stadler, M.; Grissenberger, S.; Distel, M. Fast dynamic *in vivo* monitoring of Erk activity at single cell resolution in DREKA zebrafish. *Frontiers in Cell and Developmental Biology*. **2018**, *6*, 111.

Meng, X.; Zhang, S. MAPK cascades in plant disease resistance signaling. *Annual Review of Phytopathology*. **2013**, *51*, 245-266.

Mészáros, T.; Helfer, A.; Hatzimasoura, E.; Magyar, Z.; Serazetdinova, L.; Rios, G.; Bardóczy, V.; Teige, M.; Koncz, C.; Peck, S.; Bögre, L. The Arabidopsis MAP kinase kinase MKK1 participates in defence responses to the bacterial elicitor flagellin. *The Plant Journal*. **2006**, *48*, 485-498.

Miya, A.; Albert, P.; Shinya, T.; Desaki, Y.; Ichimura, K.; Shirasu, K.; Narusaka, Y.; Kawakami, N.; Kaku, H.; Shibuya, N. CERK1, a LysM receptor kinase, is essential for chitin elicitor signaling in Arabidopsis. *Proceedings of the National Academy of Sciences*. **2007**, *104*, 19613-19618.

Mizoguchi, T.; Irie, K.; Hirayama, T.; Hayashida, N.; Yamaguchi-Shinozaki, K.; Matsumoto, K.; Shinozaki, K. A gene encoding a mitogen-activated protein kinase kinase kinase is induced simultaneously with genes for a mitogen-activated protein kinase and an S6 ribosomal protein kinase by touch, cold, and water stress in *Arabidopsis thaliana*. *Proceedings of the National Academy of Sciences*. **1996**, *93*, 765-769.

Morris, M. C. Fluorescence-based biosensors: from concepts to applications. **2012**, Academic Press.

Müller, J.; Beck, M.; Mettbach, U.; Komis, G.; Hause, G.; Menzel, D.; Šamaj, J. Arabidopsis MPK6 is involved in cell division plane control during early root development, and localizes to the pre-prophase band, phragmoplast, trans-Golgi network and plasma membrane. *The Plant Journal*. **2010**, *61*, 234-248.

Nguyen, A. W.; Daugherty, P. S. Evolutionary optimization of fluorescent proteins for intracellular FRET. *Nature Biotechnology*. **2005**, *23*, 355-360.

Oldach, L.; Zhang, J. Genetically encoded fluorescent biosensors for live-cell visualization of protein phosphorylation. *Chemistry Biology*. **2014**, *21*, 186-197.

Park, H.C.; Song, E.H.; Nguyen, X.C.; Lee, K.; Kim, K.E.; Kim, H.S.; Lee, S.M.; Kim, S.H.; Bae, D.W.; Yun, D.J.; Chung, W.S. Arabidopsis MAP kinase phosphatase 1 is phosphorylated and activated by its substrate AtMPK6. *Plant Cell Reports*. **2011**, *30*, 1523-1531.

Petersen, M.; Brodersen, P.; Næsted, H.; Andreasson, E.; Lindhart, U.; Johansen, B.; Nielsen, H.B.; Lacy, M.; Austin, M.J.; Parker, J.E.; Sharma, S.B. Arabidopsis MAP kinase 4 negatively regulates systemic acquired resistance. *Cell*. **2000**, *103*, 1111-1120.

Rasmussen, M. W.; Roux, M.; Petersen, M.; Mundy, J. MAP kinase cascades in Arabidopsis innate immunity. *Frontiers in Plant Science*. **2012**, *3*, 169.

Regot, S.; Hughey, J. J.; Bajar, B. T.; Carrasco, S.; Covert, M. W. High-sensitivity measurements of multiple kinase activities in live single cells. *Cell*. **2014**, *157*, 1724-1734.

Ryu, H.; Chung, M.; Song, J.; Lee, S. S.; Pertz, O.; Jeon, N. L. Integrated platform for monitoring single-cell MAPK kinetics in computer-controlled temporal stimulations. *Scientific Reports*. **2018**, *8*, 1-7.

Sample, V.; Mehta, S.; Zhang, J. Genetically encoded molecular probes to visualize and perturb signaling dynamics in living biological systems. *J Cell Sci*. **2014**, *127*, 1151-1160.

Sari, D. W. K.; Akiyama, R.; Naoki, H.; Ishijima, H.; Bessho, Y.; Matsui, T. Time-lapse observation of stepwise regression of Erk activity in zebrafish presomitic mesoderm. *Scientific Reports*. **2018**, *8*, 1-10.

Sato, M.; Kawai, Y.; Umezawa, Y. Genetically encoded fluorescent indicators to visualize protein phosphorylation by extracellular signal-regulated kinase in single living cells. *Analytical Chemistry*. **2007**, *79*, 2570-2575.

Sato, M.; Ozawa, T.; Inukai, K.; Asano, T.; Umezawa, Y. Fluorescent indicators for imaging protein phosphorylation in single living cells. *Nature Biotechnology*. **2002**, *20*, 287-294.

Schindelin, J.; Arganda-Carreras, I.; Frise, E.; Kaynig, V.; Longair, M.; Pietzsch, T.; Preibisch, S.; Rueden, C.; Saalfeld, S.; Schmid, B.; Tinevez, J.Y. Fiji: an open-source platform for biological-image analysis. *Nature Methods*. **2012**, *9*, 676-682.

Schweighofer, A.; Kazanaviciute, V.; Scheikl, E.; Teige, M.; Dóczi, R.; Hirt, H.; Schwanninger, M.; Kant, M.; Schuurink, R.; Mauch, F.; Buchala, A. The PP2C-type phosphatase AP2C1, which negatively regulates MPK4 and MPK6, modulates innate immunity, jasmonic acid, and ethylene levels in Arabidopsis. *The Plant Cell*. **2007**, *19*, 2213-2224.

Shaner, N.C.; Lambert, G.G.; Chammas, A.; Ni, Y.; Cranfill, P.J.; Baird, M.A.; Sell, B.R.; Allen, J.R.; Day, R.N.; Israelsson, M.; Davidson, M.W. A bright monomeric green fluorescent protein derived from *Branchiostoma lanceolatum*. *Nature Methods*. **2013**, *10*, 407-409.

Shinkai, Y.; Satoh, H.; Takeda, N.; Fukuda, M.; Chiba, E.; Kato, T.; Kuramochi, T.; Araki, Y. A testicular germ cell-associated serine-threonine kinase, MAK, is dispensable for sperm formation. *Molecular and Cellular Biology*. **2002**, *22*, 3276-3280.

Shubchynskyy, V.; Boniecka, J.; Schweighofer, A.; Simulis, J.; Kvederaviciute, K.; Stumpe, M.; Mauch, F.; Balazadeh, S.; Mueller-Roeber, B.; Boutrot, F.; Zipfel, C. Protein phosphatase AP2C1 negatively regulates basal resistance and defense responses to *Pseudomonas syringae*. *Journal of Experimental Botany*. **2017**, *68*, 1169-1183.

Sparta, B.; Pargett, M.; Minguet, M.; Distor, K.; Bell, G.; Albeck, J. G. Receptor level mechanisms are required for epidermal growth factor (EGF)-stimulated extracellular signal-regulated kinase (ERK) activity pulses. *Journal of Biological Chemistry*. **2015**, *290*, 24784-24792.

Suarez-Rodriguez, M.C.; Adams-Phillips, L.; Liu, Y.; Wang, H.; Su, S.H.; Jester, P.J.; Zhang, S.; Bent, A.F.; Krysan, P.J. MEKK1 is required for flg22-induced MPK4 activation in Arabidopsis plants. *Plant Physiology*. **2007**, *143*, 661-669.

Suarez-Rodriguez, M. C.; Petersen, M.; Mundy, J. Mitogen-activated protein kinase signaling in plants. *Annual Review of Plant Biology*. **2010**, *61*, 621-649.

Sun, Z.; Hsiao, J.; Fay, D. S.; Stern, D. F. Rad53 FHA domain associated with phosphorylated Rad9 in the DNA damage checkpoint. *Science*. **1998**, *281*, 272-274.

Teige, M.; Scheikl, E.; Eulgem, T.; Dóczi, R.; Ichimura, K.; Shinozaki, K.; Dangl, J.L.; Hirt, H. The MKK2 pathway mediates cold and salt stress signaling in Arabidopsis. *Molecular Cell*. **2004**, *15*, 141-152.

Tomida, T.; Takekawa, M.; Saito, H. Oscillation of p38 activity controls efficient pro-inflammatory gene expression. *Nature Communications*. **2015**, *6*, 1-9.

Ulm, R.; Revenkova, E.; di Sansebastiano, G. P.; Bechtold, N.; Paszkowski, J. Mitogen-activated protein kinase phosphatase is required for genotoxic stress relief in Arabidopsis. Genes Development. **2001**, 15, 699-709.

Umbrasaite, J.; Schweighofer, A.; Kazanaviciute, V.; Magyar, Z.; Ayatollahi, Z.; Unterwurzacher, V.; Choopayak, C.; Boniecka, J.; Murray, J.A.; Bogre, L.; Meskiene, I. MAPK phosphatase AP2C3 induces ectopic proliferation of epidermal cells leading to stomata development in Arabidopsis. *PloS One*. **2010**, *5*, 15357.

Van, T. N. N.; Morris, M. C. Fluorescent biosensors of protein kinases: from basics to biomedical applications. *In Progress in Molecular Biology and Translational Science.* **2013**, *113*, 217-274. Academic Press.

Vang, S.; Seitz, K.; Krysan, P. J. A simple microfluidic device for live cell imaging of Arabidopsis cotyledons, leaves, and seedlings. *Biotechniques*. **2018**, *64*, 255-261.

Wan, J.; Zhang, S.; Stacey, G. Activation of a mitogen-activated protein kinase pathway in Arabidopsis by chitin. *Molecular Plant Pathology*. **2004**, *5*, 125-135.

Wang, H.; Liu, Y.; Bruffett, K.; Lee, J.; Hause, G.; Walker, J. C.; Zhang, S. Haplo-insufficiency of MPK3 in MPK6 mutant background uncovers a novel function of these two MAPKs in Arabidopsis ovule development. *The Plant Cell*. **2008,** *20*, 602-613.

Wang, H.; Ngwenyama, N.; Liu, Y.; Walker, J. C.; Zhang, S. Stomatal development and patterning are regulated by environmentally responsive mitogen-activated protein kinases in Arabidopsis. *The Plant Cell*. **2007**, *19*, 63-73.

Xu, J.; Xie, J.; Yan, C.; Zou, X.; Ren, D.; Zhang, S. A chemical genetic approach demonstrates that MPK 3/MPK 6 activation and NADPH oxidase-mediated oxidative burst are two independent signaling events in plant immunity. *The Plant Journal*. **2014**, *77*, 222-234.

Xu, J.; Zhang, S. Mitogen-activated protein kinase cascades in signaling plant growth and development. *Trends in Plant Science*. **2015**, *20*, 56-64.

Yamada, K.; Yamaguchi, K.; Shirakawa, T.; Nakagami, H.; Mine, A.; Ishikawa, K.; Fujiwara, M.; Narusaka, M.; Narusaka, Y.; Ichimura, K.; Kobayashi, Y. The Arabidopsis CERK 1-associated kinase PBL 27 connects chitin perception to MAPK activation. *The EMBO Journal*. **2016**, *35*, 2468-2483.

Yu, L.; Nie, J.; Cao, C.; Jin, Y.; Yan, M.; Wang, F.; Liu, J.; Xiao, Y.; Liang, Y.; Zhang, W. Phosphatidic acid mediates salt stress response by regulation of MPK6 in *Arabidopsis thaliana*. *New Phytologist*. **2010**, *188*, 762-773.

Zaman, N.; Seitz, K.; Kabir, M.; George-Schreder, L.S.; Shepstone, I.; Liu, Y.; Zhang, S.; Krysan, P.J. A Förster resonance energy transfer sensor for live-cell imaging of mitogen-activated protein kinase activity in Arabidopsis. *The Plant Journal*. **2019**, *97*, 970-983.

Zhang, J.; Allen, M. D. FRET-based biosensors for protein kinases: illuminating the kinome. *Molecular BioSystems*. **2007**, *3*, 759-765.

Zhang, J.; Campbell, R. E.; Ting, A. Y.; Tsien, R. Y. Creating new fluorescent probes for cell biology. *Nature Reviews Molecular Cell Biology*. **2002**, *3*, 906-918.

Zhang, Y.; Guo, X.; Dong, J. Phosphorylation of the polarity protein BASL differentiates asymmetric cell fate through MAPKs and SPCH. *Current Biology*. **2016**, *26*, 2957-2965.

Zhang, Y.; Wang, P.; Shao, W.; Zhu, J. K.; Dong, J. The BASL polarity protein controls a MAPK signaling feedback loop in asymmetric cell division. *Developmental Cell*. **2015**, *33*, 136-149.

Table 1. In vitro FRET of EKAREV and SOMA variants. Rows indicate specific biosensor variants. 'No Kinase' indicates no kinase was added to the extract containing the biosensor protein when fluorescent emission intensity was measured. 'CA-MPK6' indicates constitutively active MPK6 was present. 'CA-MPK4' indicates constitutively active MPK4 was present. 'Turq' is the average value of the three highest sequential data points for the Turquoise GL emission peak. 'YPet' is the average value of the three highest sequential data points for the YPet emission peak. 'YPet/Turq' is YPet divided by Turq. 'ΔFRET' was calculated by dividing the YPet/Turq ratio with No Kinase by either the YPet/Turq ratio plus CA-MPK6 or CA-MPK4.

	No Kinase			CA-MPK6				CA-MPK4			
	Turq	YPet	YPet/Turq	Turq	YPet	YPet/Turq	Δ FRET	Turq	YPet	YPet/Turq	Δ FRET
EKAREV	102547	76365	0.74	106420	86561	0.81	9%	111014	82988	0.75	0%
SOMA	77325	69725	0.90	63494	96300	1.52	68%	73668	84687	1.15	27%
EKAREV-BASL	81070	58495	0.72	56506	87706	1.55	115%	62386	83222	1.33	85%
EKAREV^{T48A}-BASL	75400	55327	0.73	84693	60990	0.72	-2%	83782	59807	0.71	-3%
SOMA^{T679A}	65166	60931	0.94	71900	65530	0.91	-3%	67915	62828	0.93	-1%
EKAREV-AP2C1	89861	66267	0.74	55116	101647	1.84	150%	55971	99090	1.77	140%
EKAREV^{T48A}-AP2C1	87272	66980	0.77	97788	74682	0.76	0%	95430	73391	0.77	0%

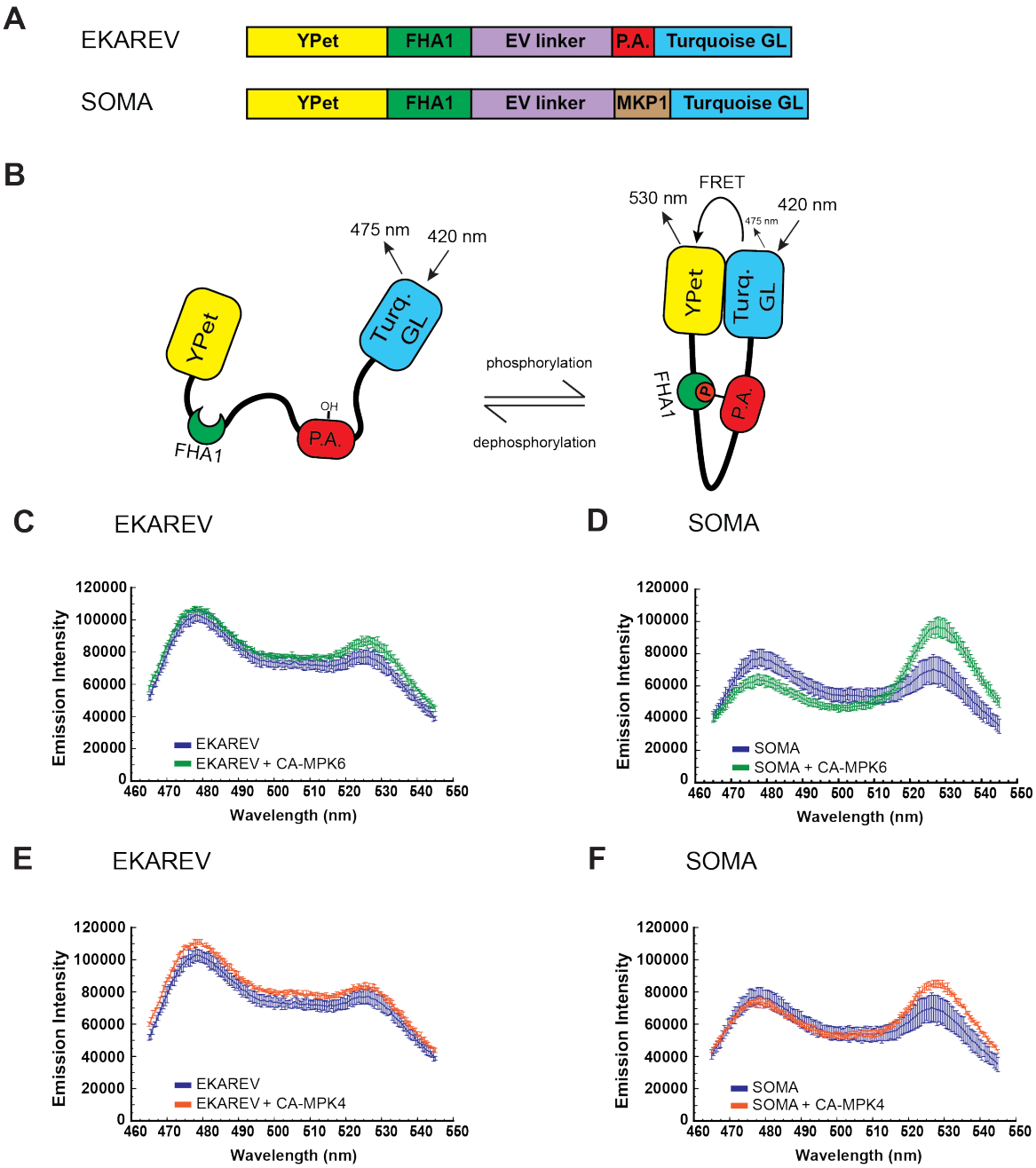

Figure 1. Development of the plant MAPK docking domain trap. (A) Domain structure of EKAREV and SOMA. YPet is a yellow fluorescent protein, FHA is the FHA1 phosphopeptide binding domain of yeast RAD53, EV linker is a flexible linker domain, P.A. is the phosphoacceptor region of the mammalian CdC25C protein, MKP1 is an 80 amino acid region of the Arabidopsis MKP1 protein and Turquoise GL is a blue fluorescent protein. Maps are not to scale. (B) Cartoon schematic of the EKAREV biosensor. Phosphorylation of EKAREV within the phosphoacceptor domain is expected to produce a conformation shift that increases Förster resonance energy transfer (FRET) efficiency between the Turquoise GL and YPet fluorophores due to the enhanced affinity of the FHA1 domain for the phosphorylated form of the phosphoacceptor domain. Removal of the phosphate is expected to cause EKAREV to revert to a conformation with lower FRET efficiency. (C-F) Data from in vitro FRET assays using EKAREV (C), (E) or SOMA (D), (F) in the presence or absence of constitutively active MPK6 (CA-MPK6) (C-D) or MPK4 (CA-MPK4) (E-F). The emission spectra of the biosensors in response to excitation with 420 nm light is shown. Three technical replications were performed for each experiment, and the values plotted are the means for those three trials with the error bars indicating standard deviation. Absence of a CA-MAPK is represented in blue. Presence of CA-MPK6 is represented in green. Presence of CA-MPK4 is represented in orange. Emission Intensity units are arbitrary "counts per second".

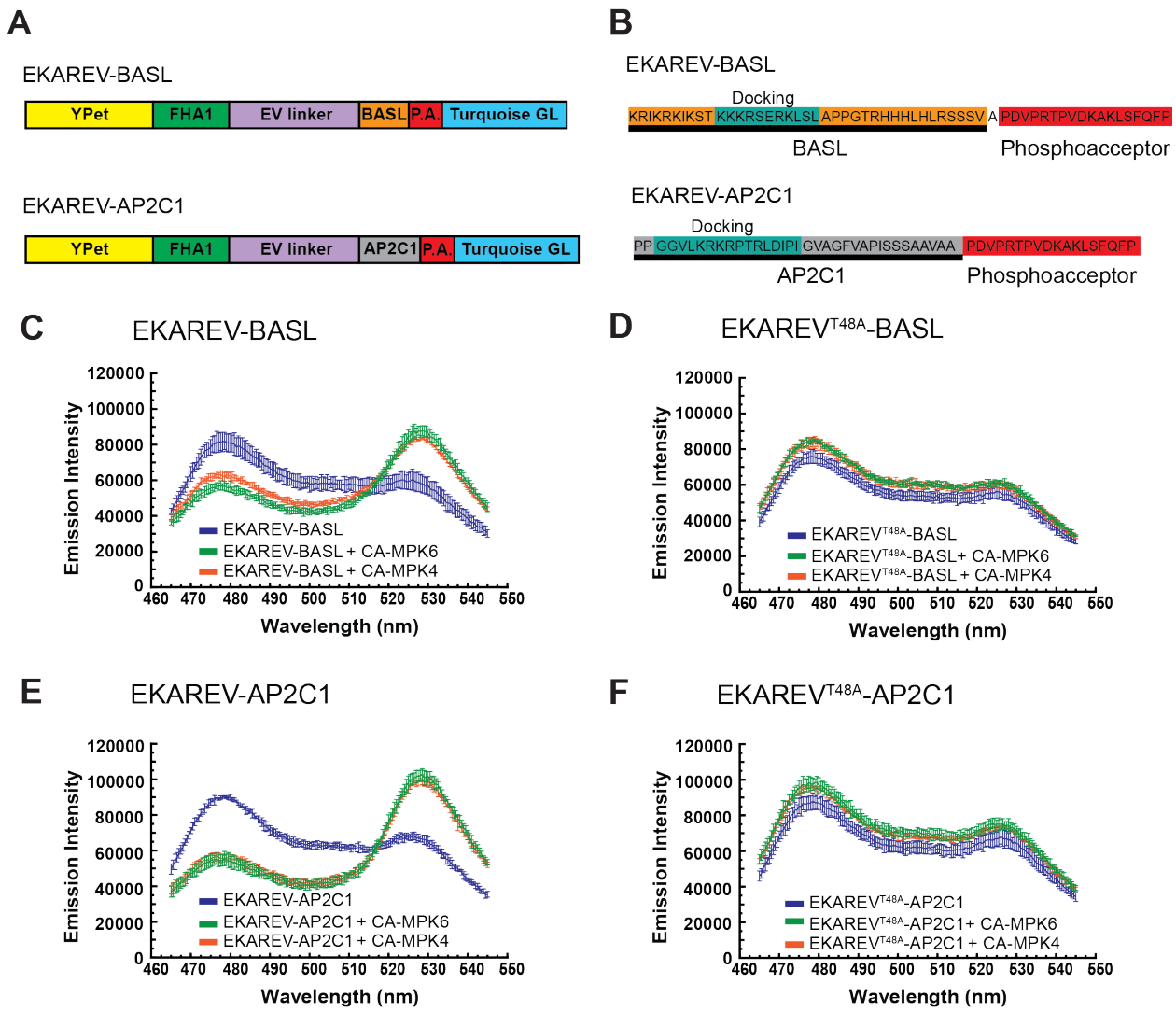

Figure 2. Inserting plant MAPK docking domains into EKAREV allows for large MAPK-induced increases in FRET. (A) Domain structure of EKAREV-BASL and EKAREV-AP2C1. YPet is a yellow fluorescent protein, FHA is the FHA1 phosphopeptide binding domain of yeast RAD53, EV linker is a flexible linker domain, P.A. is the phosphoacceptor region of the mammalian CdC25C protein, BASL is a 39 aa region of the plant BASL protein that contains a plant MAPK docking domain. AP2C1 is a 35 aa region of the AP2C1 protein that contains a plant MAPK docking domain. Maps are not to scale. (B) Protein sequence for the docking domain and phosphoacceptor regions of each biosensor. Sequence from the BASL protein is highlighted in orange, sequence from the AP2C1 protein is highlighted in grey, and the EKAREV phosphoacceptor domain is highlighted in red. The docking domains are highlighted in blue-green. (C-F), Data from in vitro FRET assays using EKAREV-BASL (C), EKAREVT48A-BASL (D), EKAREV-AP2C1 (E) or EKAREVT48A-AP2C1 (F) in the presence or absence of constitutively active MPK6 (CA-MPK6) or MPK4 (CA-MPK4). The emission spectra in response to excitation at 435 nm is shown. The values plotted are the means of three technical replicates of each experiment, with the error bars indicating standard deviation. Emission Intensity units are arbitrary “counts per second”.

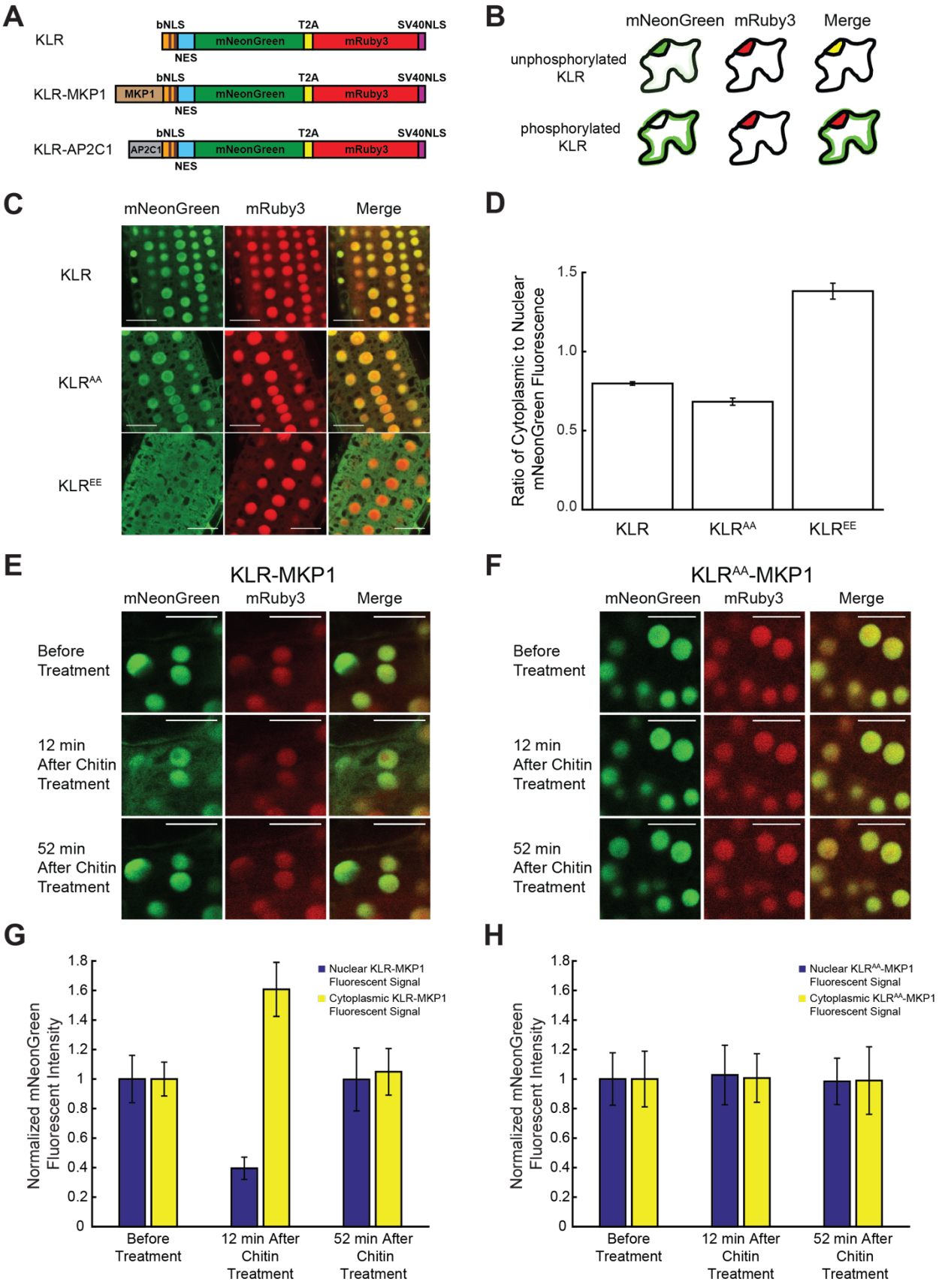
A
KLR
bNLS
T2A
SV40NLS
mNeonGreen
mRuby3
NES
KLR-MKP1
MKP1
KLR-AP2C1
AP2C1
B
mNeonGreen
mRuby3
Merge
unphosphorylated KLR
phosphorylated KLR
C
mNeonGreen
mRuby3
Merge
KLR
KLR^AA
KLR^EE
D
Ratio of Cytoplasmic to Nuclear mNeonGreen Fluorescence
1.5
1.0
0.5
0.0
KLR
KLR^AA
KLR^EE
E
KLR-MKP1
mNeonGreen
mRuby3
Merge
Before Treatment
12 min After Chitin Treatment
52 min After Chitin Treatment
F
KLR^AA-MKP1
mNeonGreen
mRuby3
Merge
Before Treatment
12 min After Chitin Treatment
52 min After Chitin Treatment
G
Normalized mNeonGreen Fluorescent Intensity
1.8
1.6
1.4
1.2
1
0.8
0.6
0.4
0.2
0
Nuclear KLR-MKP1 Fluorescent Signal
Cytoplasmic KLR-MKP1 Fluorescent Signal
Before Treatment
12 min After Chitin Treatment
52 min After Chitin Treatment
H
Normalized mNeonGreen Fluorescent Intensity
Nuclear KLR^AA-MKP1 Fluorescent Signal
Cytoplasmic KLR^AA-MKP1 Fluorescent Signal
Before Treatment
12 min After Chitin Treatment
52 min After Chitin Treatment

Figure 3. Functional Characterization of the KLR kinase translocation reporter in Arabidopsis root cells. (A) Domain structure of KLR, KLR-MKP1 and KLR-AP2C1. bNLS is a bipartite modified Nuclear Localization Signal derived from mouse C-Jun protein. The two phospho-acceptor sites (S63 and S73) are indicated by brown lines. NES is a consensus Nuclear Exclusion Signal. mNeonGreen is a green fluorescent protein. T2A refers to the “self-cleaving” Thosea asigna virus 2A peptide. mRuby3 is a red fluorescent protein. SV40NLS is an NLS derived from simian virus 40 (SV40). Maps are not to scale (B) Cartoon of predicted KLR and mRuby3 localization. Unphosphorylated KLR is expected to localize to the nucleus, while phosphorylated KLR should be excluded from the nucleus. The nuclear marker mRuby3 is expected to constitutively localize to the nucleus. (C) mNeonGreen and mRuby3 emission in root tips of Arabidopsis seedlings expressing either KLR, KLRAA, or KLREE was imaged using confocal microscopy and emission intensity was plotted in (D). Values plotted in (D) are the average cytoplasmic mNeonGreen emission divided by the average mNeonGreen nuclear emission. Scale bar= 20 μm. (E-F) Root tips of Arabidopsis seedlings expressing ether KLR-MKP1 (E) or KLRAA-MKP1 (F) were treated with 40 mg/ml chitin, and the mNeonGreen and mRuby3 emission channels were imaged using confocal microscopy at the indicated timepoints and emission intensity was plotted in (G-H). The emission intensity values in (G-H) were normalized to the corresponding “before treatment” values. The quantitative data shown in (D,G,H) was obtained by measuring emission intensity in 8 nuclear and 8 cytoplasmic regions of interest in each of 12 cells for each sample type. Error bars indicate standard deviation. Scale bar= 10 μm.

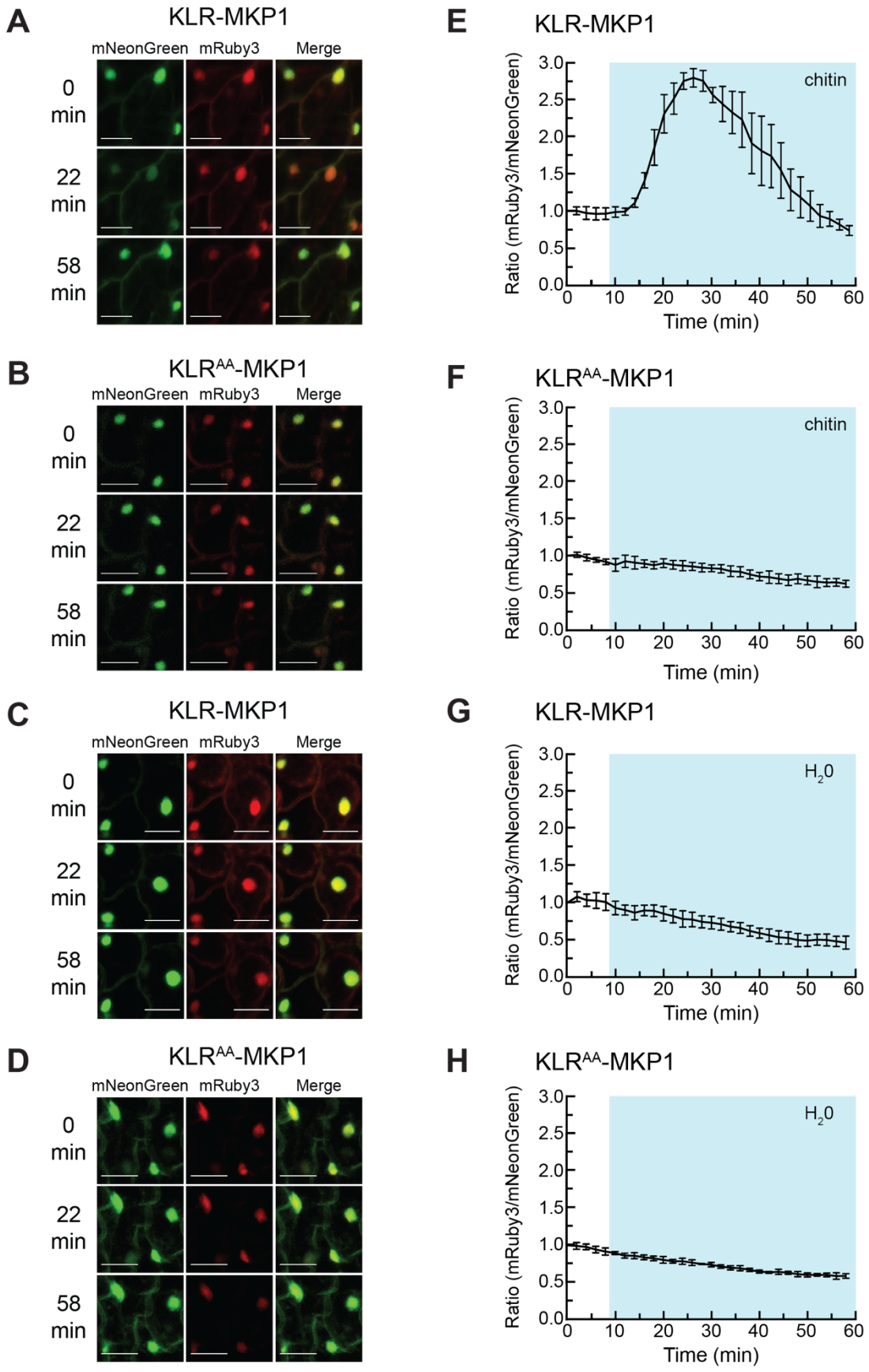
A
KLR-MKP1
mNeonGreen
mRuby3
Merge
0 min
22 min
58 min
B
KLR^AA-MKP1
C
KLR-MKP1
D
KLR^AA-MKP1
E
KLR-MKP1
chitin
Ratio (mRuby3/mNeonGreen)
Time (min)
F
KLR^AA-MKP1
G
KLR-MKP1
H2O
H
KLR^AA-MKP1

Figure 4. Chitin causes a transient reduction in nuclear mNeonGreen fluorescence of KLR-MKP1. (A-D) Arabidopsis cotyledons expressing KLR-MKP1 or KLRAA-MKP1 were treated with chitin (A-B) or water (C-D) and imaged every two min using confocal microscopy. The mNeonGreen, mRuby3, and merged channels for the 0 min 22 min and 58 min time points are shown for each experiment. (E-H) Quantification of the nuclear fluorescent emission for the experiments shown in (A-D). Each data point represents the ratio of the average mNeonGreen and mRuby3 emission intensities within four regions of interest (ROIs) corresponding to cell nuclei. The data was normalized by dividing each value in the time-course by the 0 min value. The shaded background on each graph indicates when the sample was exposed to a given treatment. During the first 10 min of each experiment the samples were incubated in pure water. Error bars indicate standard deviation. Scale bar= 20 μm. Videos are available as Movies S1-S4.

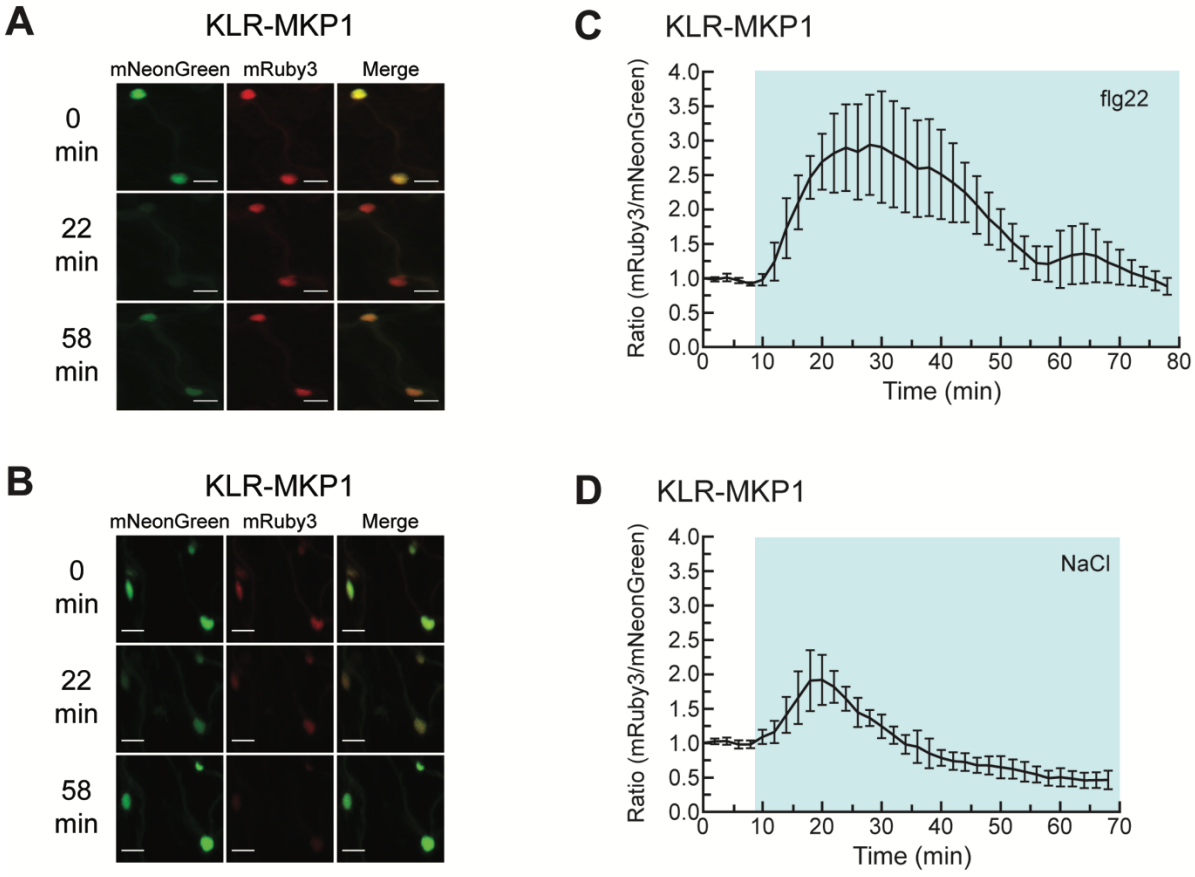

Figure 5. Flg22 and NaCl cause a transient reduction in nuclear mNeonGreen fluorescence of KLR-MKP1. (A-B) Arabidopsis cotyledons expressing KLR-MKP1 were treated with 1µ M of flg22 (A) or 150 mM NaCl (B) and imaged every two min using confocal microscopy. The mNeonGreen, mRuby3, and Merged channels for the 0 min, 22 min and 58 min time points are shown for each experiment. (C-D) Quantification of the nuclear fluorescent emission for the experiments shown in (A-B). Each data point represents the ratio of the average mNeonGreen and mRuby3 emission intensities within four regions of interest (ROIs) corresponding to cell nuclei. The data was normalized by dividing each value in the time-course by the 0 min value. The shaded background on each graph indicates when the sample was exposed to a given treatment. During the first 10 min of each experiment the samples were incubated in pure water. Error bars indicate standard deviation. Scale bar = 20 µm. Videos are available as Movies S5 and S6.

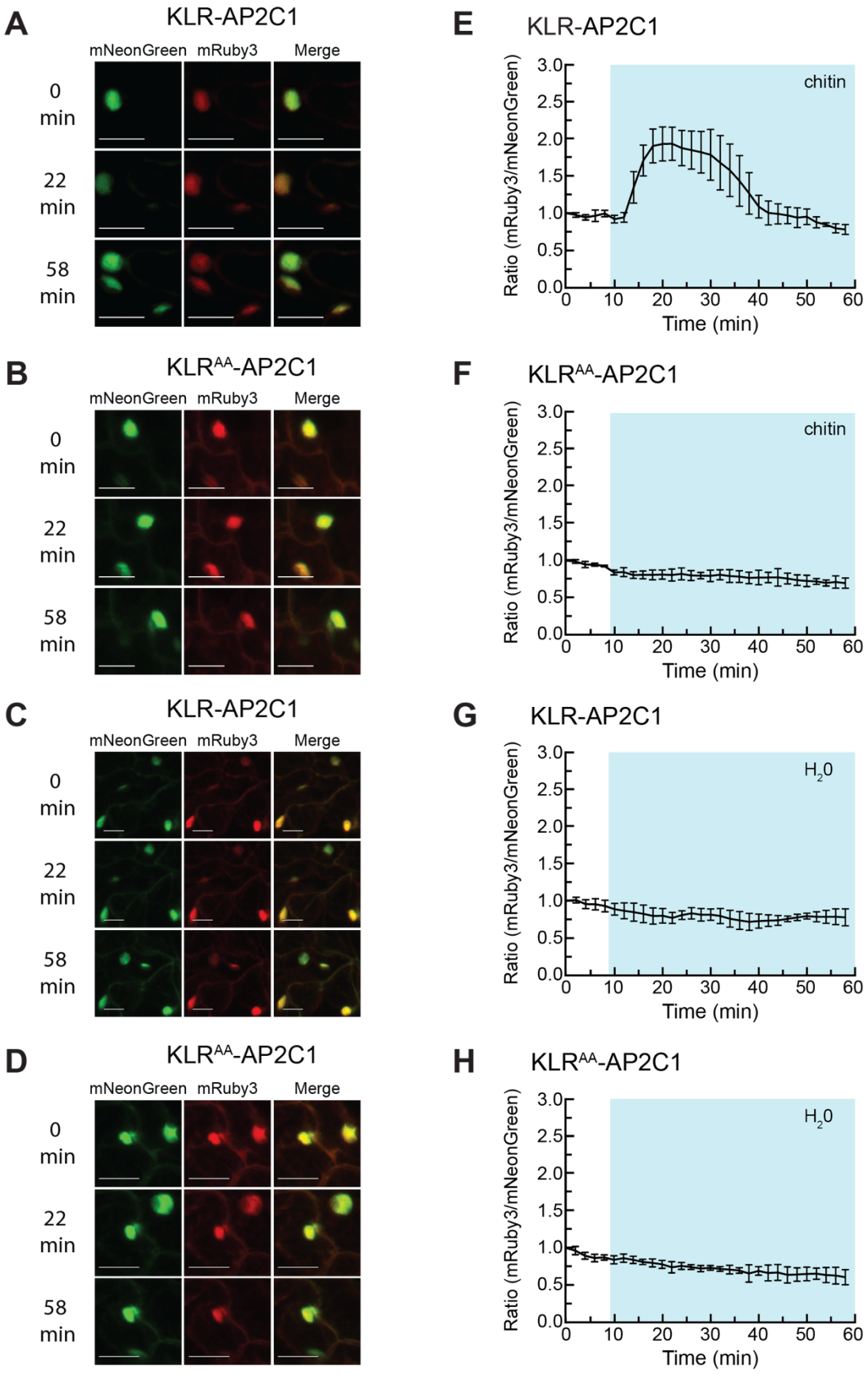
A
KLR-AP2C1
mNeonGreen mRuby3 Merge
0 min
22 min
58 min
B
KLR^AA-AP2C1
mNeonGreen mRuby3 Merge
0 min
22 min
58 min
C
KLR-AP2C1
mNeonGreen mRuby3 Merge
0 min
22 min
58 min
D
KLR^AA-AP2C1
mNeonGreen mRuby3 Merge
0 min
22 min
58 min
E
KLR-AP2C1
chitin
Ratio (mRuby3/mNeonGreen)
Time (min)
F
KLR^AA-AP2C1
chitin
Ratio (mRuby3/mNeonGreen)
Time (min)
G
KLR-AP2C1
H2O
Ratio (mRuby3/mNeonGreen)
Time (min)
H
KLR^AA-AP2C1
H2O
Ratio (mRuby3/mNeonGreen)
Time (min)

Figure 6. KLR-AP2C1 exhibits a transient reduction in nuclear mNeonGreen fluorescence in response to chitin treatment. (A-D) Arabidopsis cotyledons expressing KLR-AP2C1 or KLRAA-AP2C1 were treated with 40 mg/ml chitin (A-B) or 200 µl water (C-D) and imaged every two min using confocal microscopy. The mNeonGreen, mRuby3, and merged channels for the 0 min, 22 min and 58 min time points are shown for each experiment. (E-H) Quantification of the nuclear fluorescent emission for the experiments shown in (A-D). Each data point represents the ratio of the average mNeonGreen and mRuby3 emission intensities within four regions of interest (ROIs) corresponding to cell nuclei. The data was normalized by dividing each value in the time-course by the 0 min value. The shaded background on each graph indicates when the sample was exposed to a given treatment. During the first 10 min of each experiment the samples were incubated in pure water. Error bars indicate standard deviation. Scale bar= 20 µm. Videos are available as Movies S7-S10.

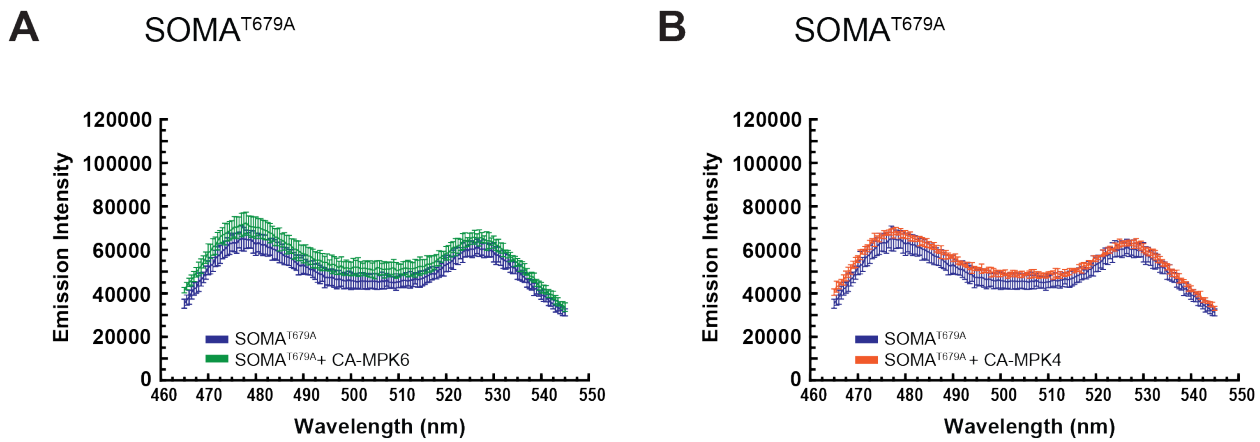

Figure S1. SOMAT679A does not exhibit an increase in FRET efficiency in response to either CA-MPK6 or CA-MPK4. (A-B) Data from in vitro FRET assays measuring the emission spectrum of SOMAT679A in response to excitation with 435 nm light in the presence or absence of constitutively active MPK6 (CA-MPK6) (A) or MPK4 (CA-MPK4) (B). Three technical replications were performed for each experiment. Absence of a CA-MAPK is represented in blue. Presence of CA-MPK6 is represented in green. Presence of CA-MPK4 is represented in orange. Emission Intensity units are arbitrary “counts per second”. Error bars indicate standard deviation.

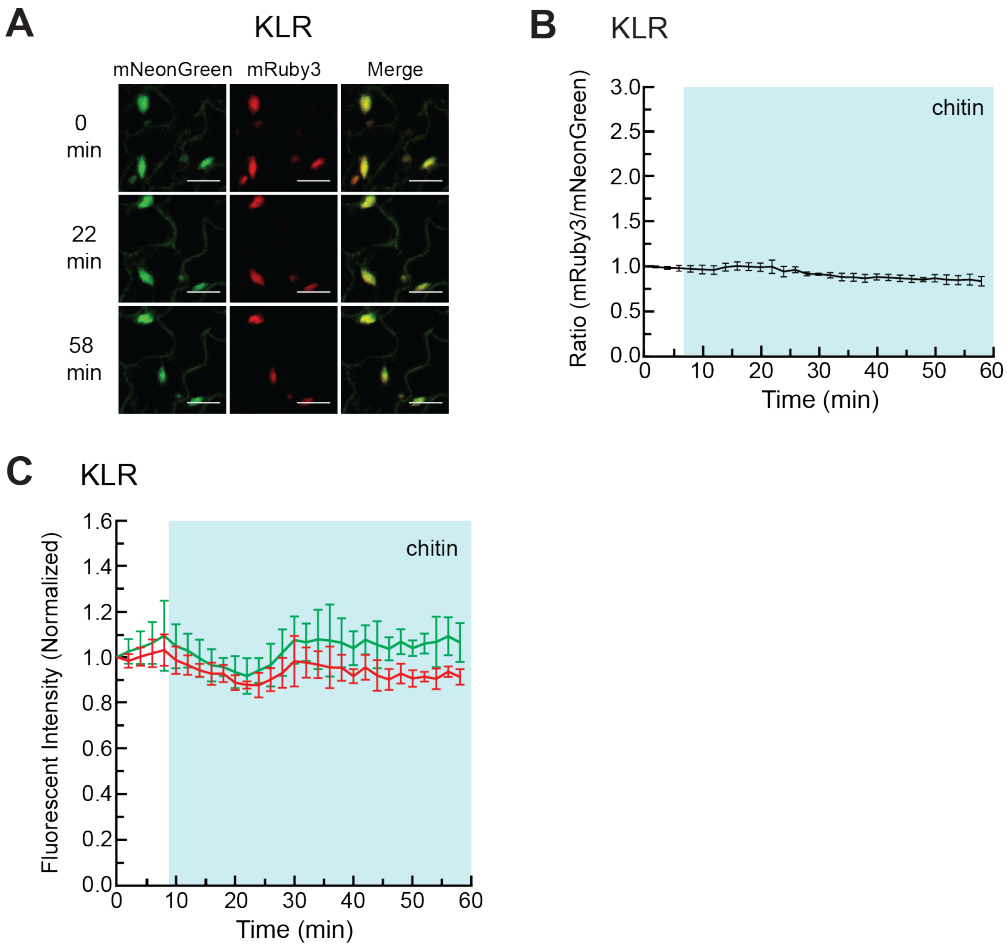

Supplementary Figure 2. KLR without a plant docking domain does not exhibit a transient reduction in nuclear mNeonGreen fluorescence in response to chitin. (A) Arabidopsis cotyledons expressing KLR (which lacks a plant MAPK docking domain) were treated with 40 mg/ml of chitin and imaged every two min using confocal microscopy. The mNeonGreen, mRuby3, and Merged channels for the 0 min, 22 min and 58 min time points are shown. (B,C) Quantification of the nuclear fluorescent emission for the experiment shown in (A). In (B) each data point represents the ratio of the average mNeonGreen and mRuby3 emission intensities within four regions of interest (ROIs) corresponding to cell nuclei. In (C) each data point represents the average of the mNeonGreen or mRuby3 emission intensities within four regions of interest (ROIs) corresponding to cell nuclei. For (B,C) the data was normalized by dividing each value in the time-course by the 0 min value. The shaded background on each graph indicates when the sample was exposed to a given treatment. During the first 10 min of each experiment the samples were incubated in pure water. Error bars indicate standard deviation. Scale bar= 20 µm. Videos are available as Movies S11 and S12.

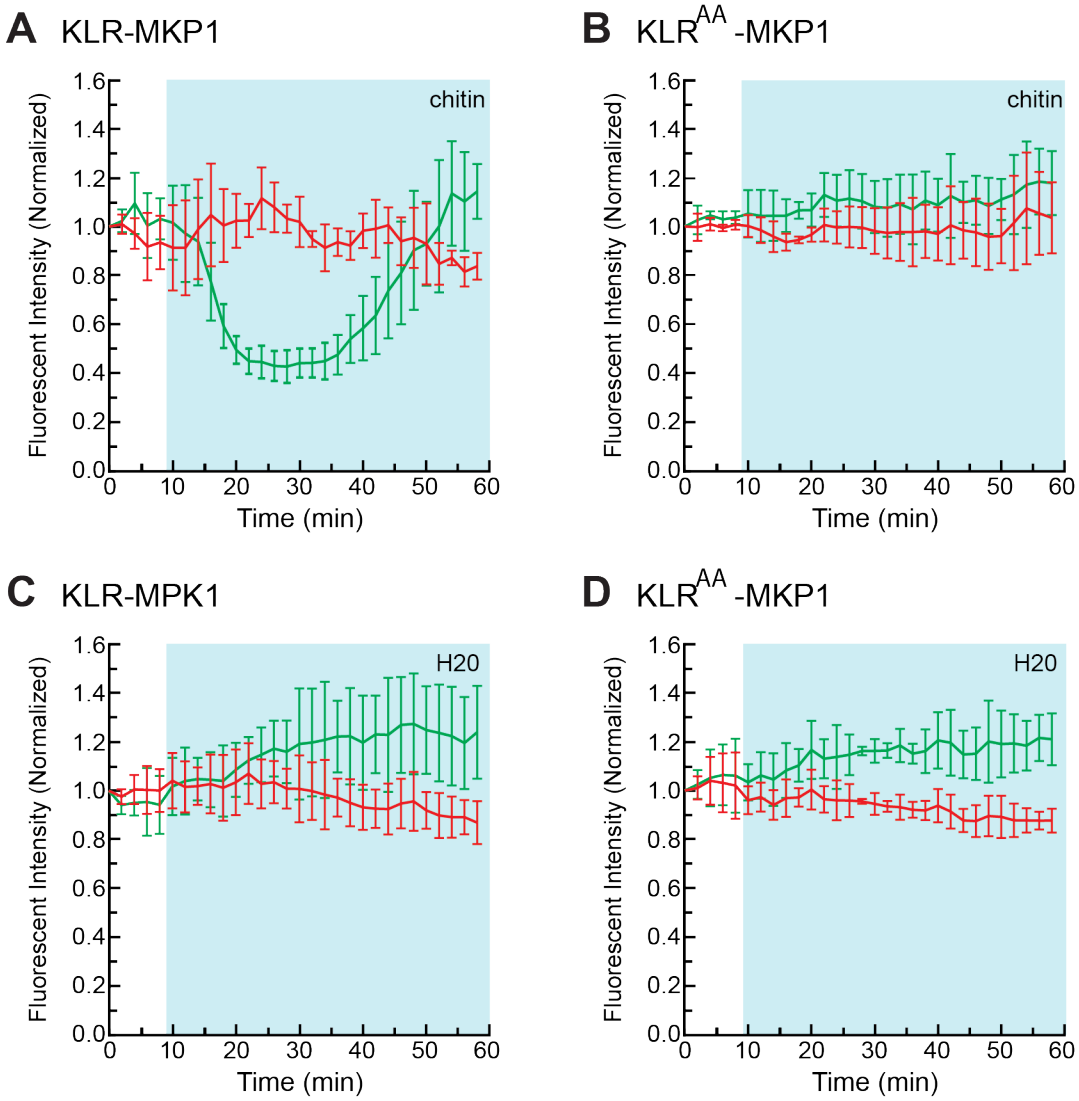

Figure S3. KLR-MKP1 exhibits a transient reduction in nuclear mNeonGreen fluorescence in response to chitin. The data presented in this figure is a different representation of the same measurements shown in Figure 4. The same ROIs used to collect the quantitative image data in Figure 4 were used for this figure. In this figure, each data point represents the average of the mNeonGreen or mRuby3 emission intensities within four regions of interest (ROIs) corresponding to cell nuclei. The data was normalized by dividing each value in the time-course by the 0 min value. The shaded background on each graph indicates when the sample was exposed to a given treatment. During the first 10 min of each experiment the samples were incubated in pure water. Error bars indicate standard deviation. Videos are available as Movies S13-S16.

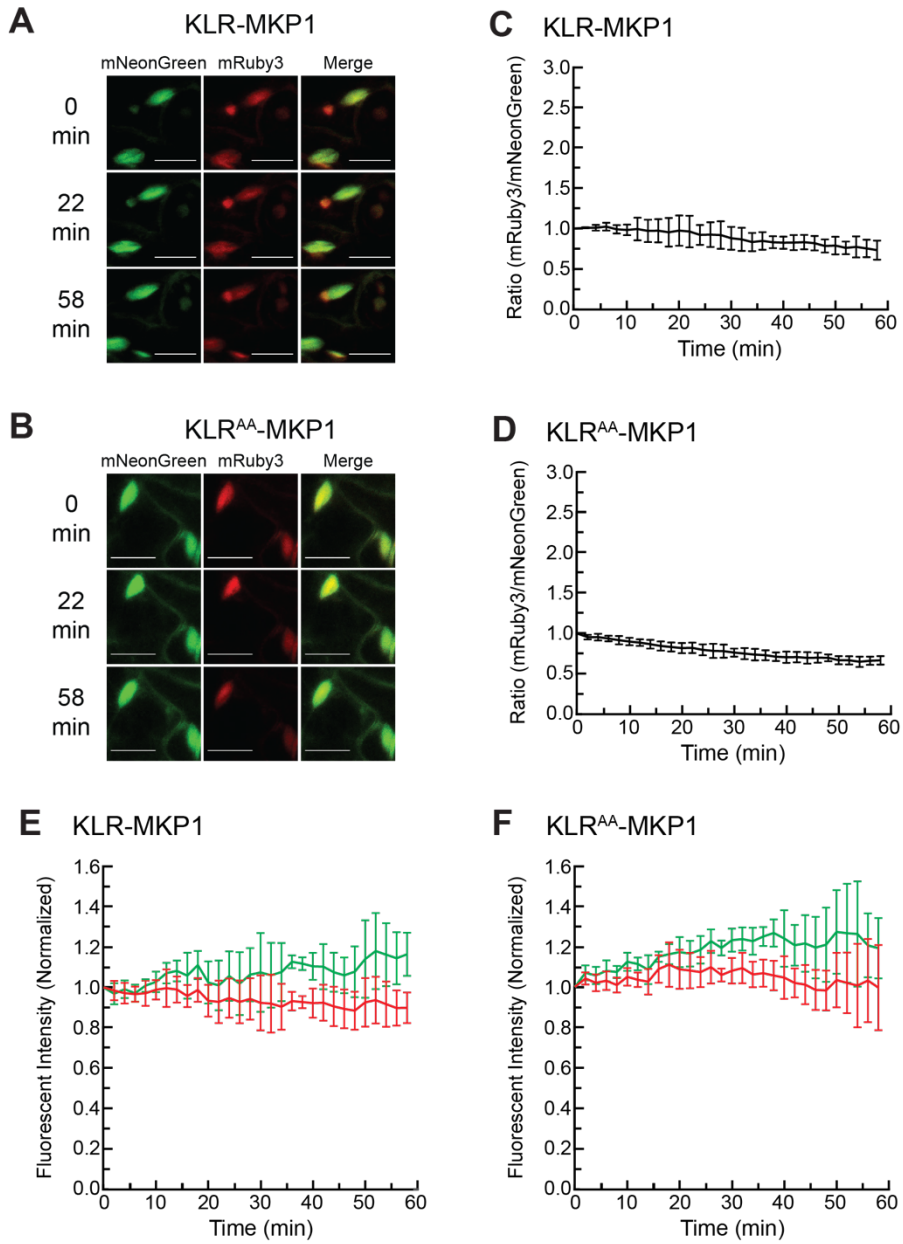

Supplementary Figure 4. Behavior of KLR-MKP1 and KLRAA-MKP1 in the absence of a treatment. (A,B) Arabidopsis cotyledons expressing KLR-MKP1 or KLRAA-MKP1 were incubated in 200 µl pure water and imaged every two min using confocal microscopy. The mNeonGreen, mRuby3, and Merged channels for the 0 min, 22 min and 58 min time points are shown for each experiment. (C-F) Quantification of the nuclear fluorescent emission for the experiments shown in (A,B). In (C,D) each data point represents the ratio of the average mNeonGreen and mRuby3 emission intensities within four regions of interest (ROIs) corresponding to cell nuclei. In (E,F) each data point represents the average of the mNeonGreen or mRuby3 emission intensities within four regions of interest (ROIs) corresponding to cell nuclei. In (C-F) the data was normalized by dividing each value in the time-course by the 0 min value. The shaded background on each graph indicates when the sample was exposed to a given treatment. During the first 10 min of each experiment the samples were incubated in pure water. Error bars indicate standard deviation. Scale bar= 20 µm. Videos are available as Movies S17-S20.

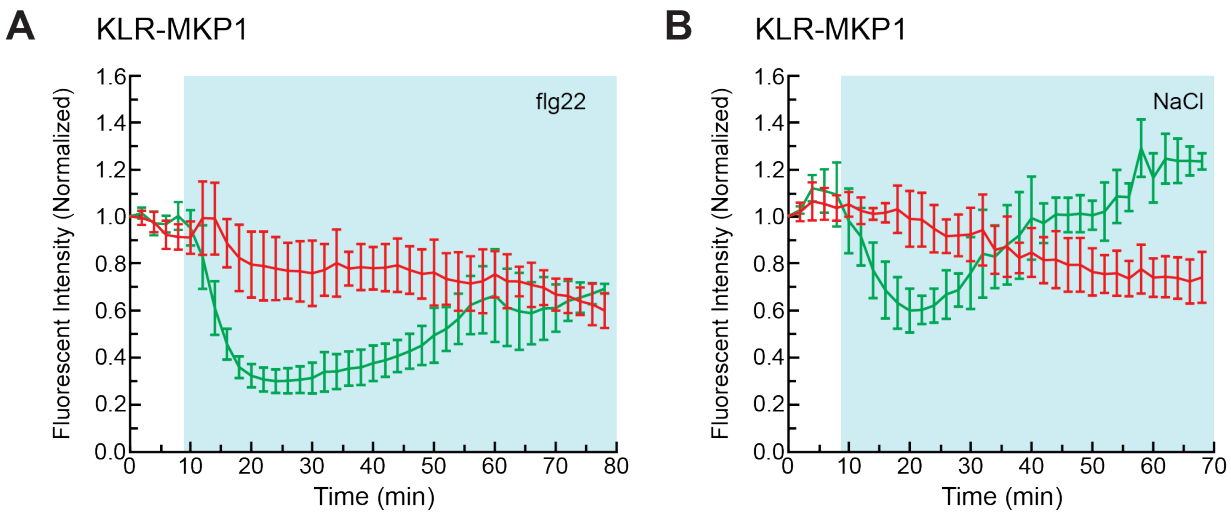

Figure S5. KLR-MKP1 exhibits a transient reduction in nuclear mNeonGreen signal in response to flg22 and NaCl. The data presented in this figure is a different representation of the same measurements shown in Figure 5. The same ROIs used to collect the quantitative image data in Figure 5 were used for this figure. In this figure, each data point represents the average of the mNeonGreen or mRuby3 emission intensities within four regions of interest (ROIs) corresponding to cell nuclei. The data was normalized by dividing each value in the time-course by the 0 min value. The shaded background on each graph indicates when the sample was exposed to a given treatment. During the first 10 min of each experiment the samples were incubated in pure water. Error bars indicate standard deviation. Videos are available as Movies S21 and S22.

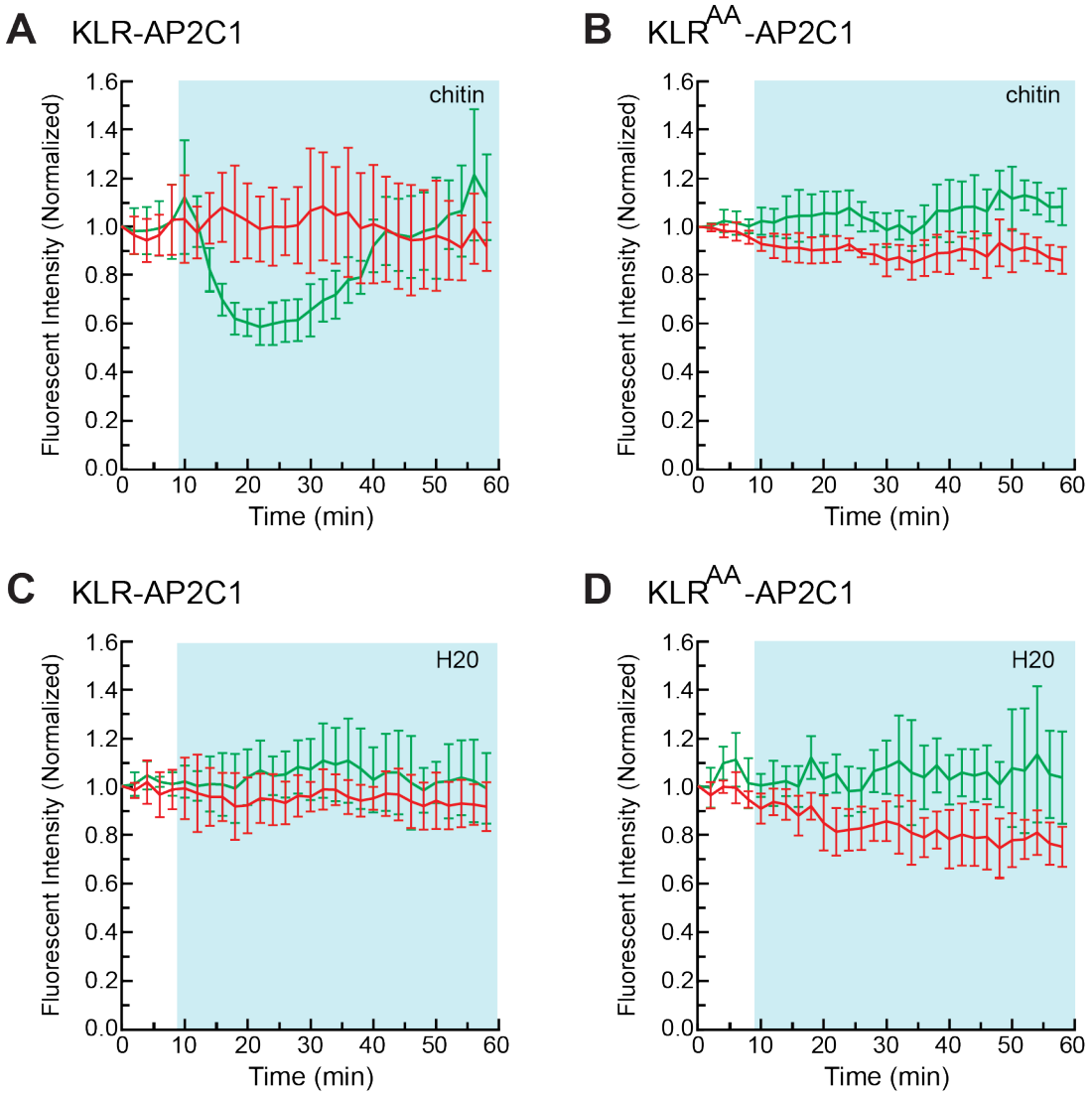

Figure S6. KLR-AP2C1 exhibits a transient decrease in nuclear mNeonGreen signal in response to chitin. The data presented in this figure is a different representation of the same measurements shown in Figure 6. The same ROIs used to collect the quantitative image data in Figure 6 were used for this figure. In this figure, each data point represents the average of the mNeonGreen or mRuby3 emission intensities within four regions of interest (ROIs) corresponding to cell nuclei. The data was normalized by dividing each value in the time-course by the 0 min value. The shaded background on each graph indicates when the sample was exposed to a given treatment. During the first 10 min of each experiment the samples were incubated in pure water. Error bars indicate standard deviation. Videos are available as Movies S23-S26.

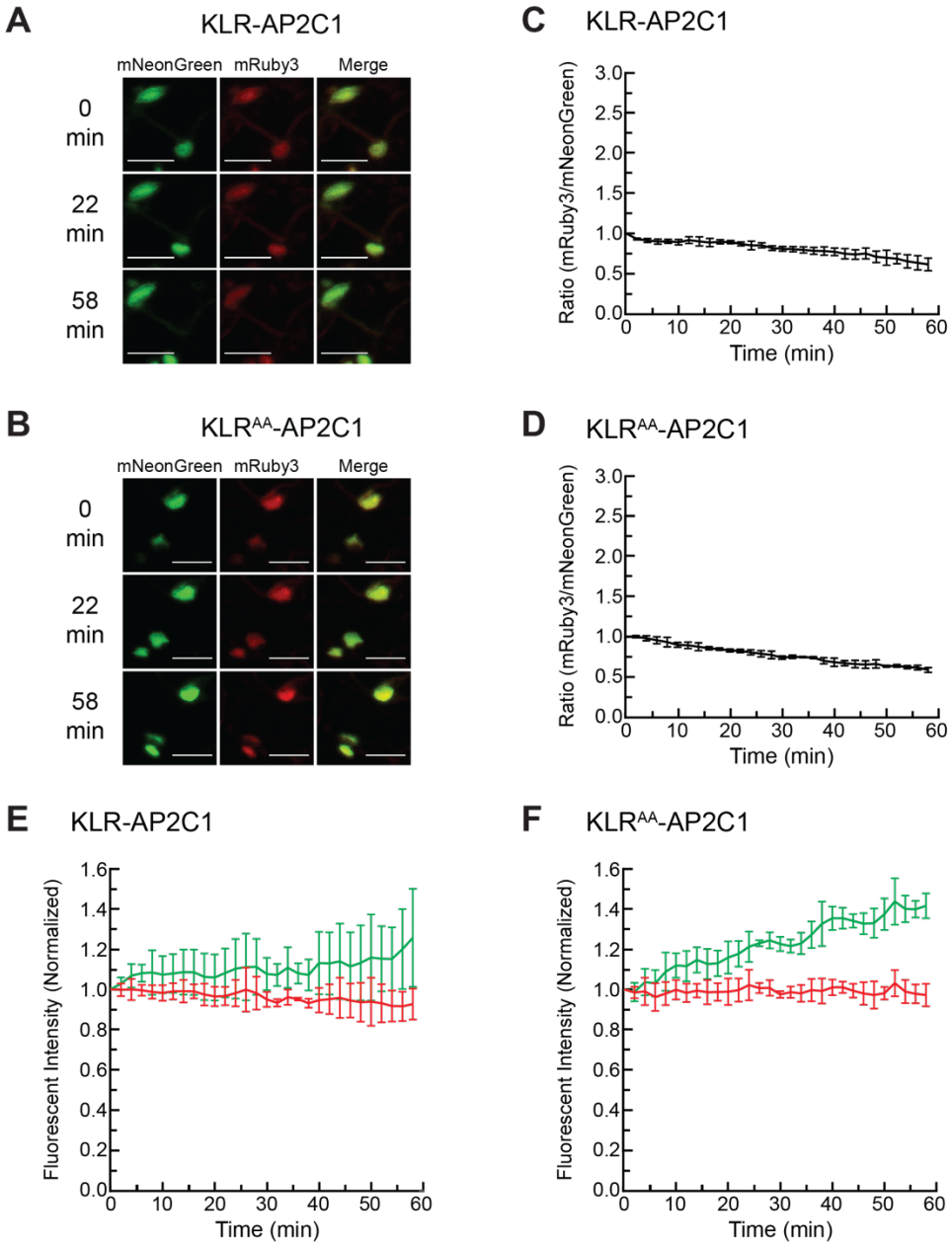

Supplementary Figure 7. Behavior of KLR-AP2C1 and KLR^{AA}-AP2C1 in the absence of a treatment. (A,B) Arabidopsis cotyledons expressing KLR-AP2C1 or KLRAA-AP2C1 were incubated in 200 µl water and imaged every two min using confocal microscopy. The mNeonGreen, mRuby3, and Merged channels for the 0', 22' and 58' time points are shown for each experiment. (C-F) Quantification of the nuclear fluorescent emission for the experiments shown in (A,B). In (C,D) each data point represents the ratio of the average mNeonGreen and mRuby3 emission intensities within four regions of interest (ROIs) corresponding to cell nuclei. In (E,F) each data point represents the average of the mNeonGreen or mRuby3 emission intensities within four regions of interest (ROIs) corresponding to cell nuclei. In (C-F) the data was normalized by dividing each value in the time-course by the 0 min value. The shaded background on each graph indicates when the sample was exposed to a given treatment. During the first 10 min of each experiment the samples were incubated in pure water. Error bars indicate standard deviation. Scale bar = 20 µm. Videos are available as Movies S27-S30.

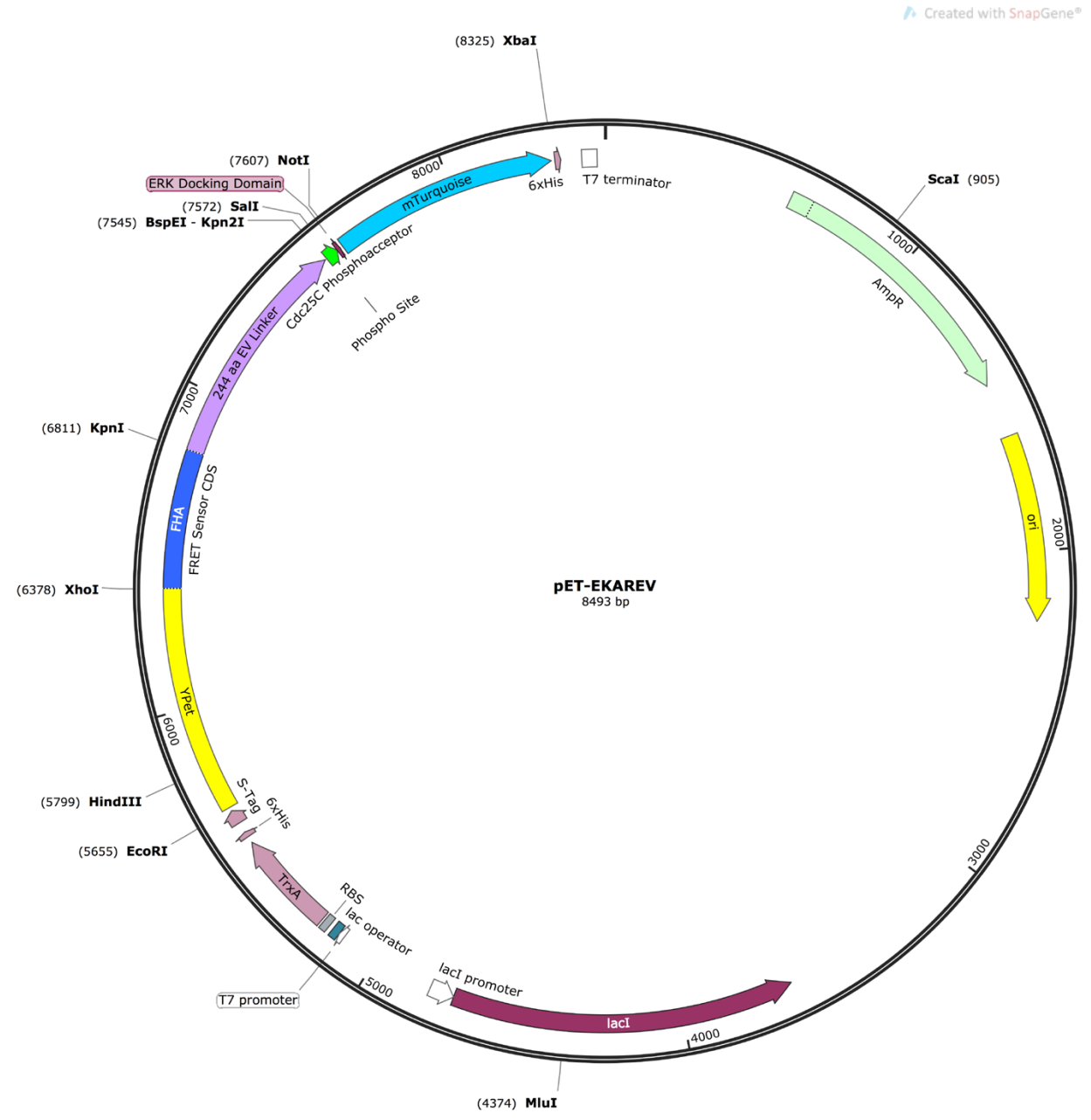

Figure S8. Plasmid map for pET-EKAREV

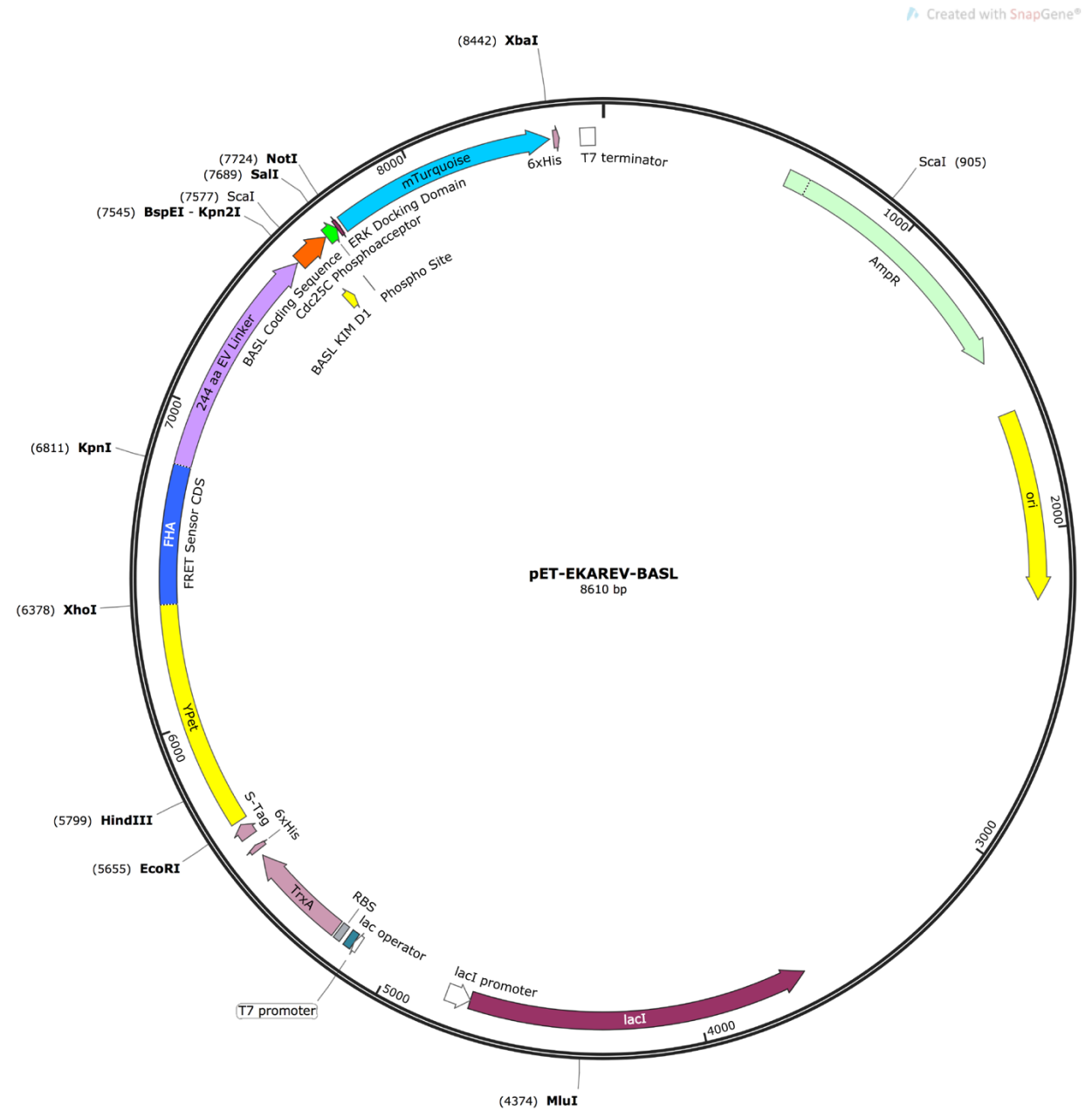

Figure S9. Plasmid map for pET-EKAREV-BASL

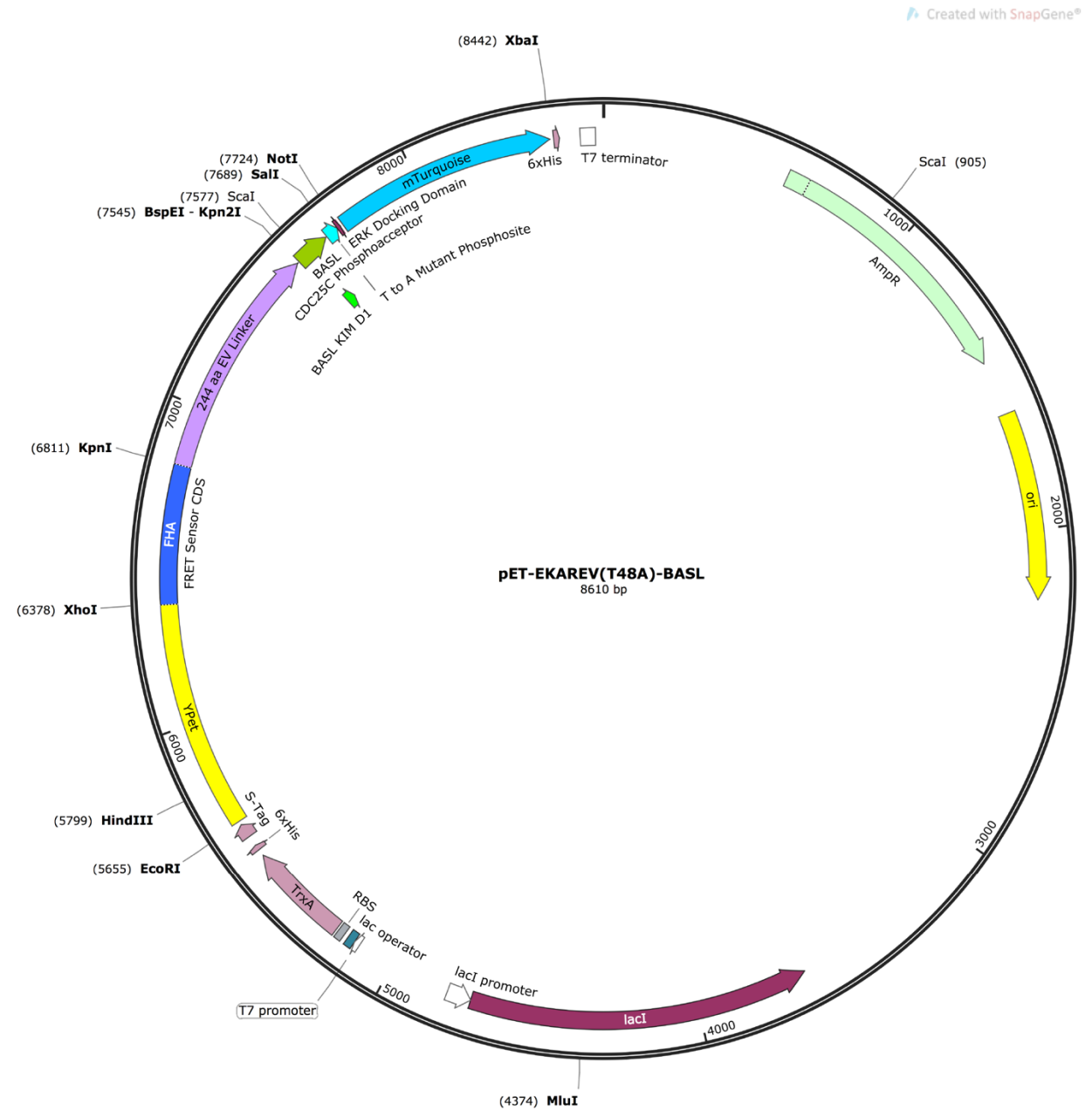

Figure S10. Plasmid map for pET-EKAREV(T48A)-BASL

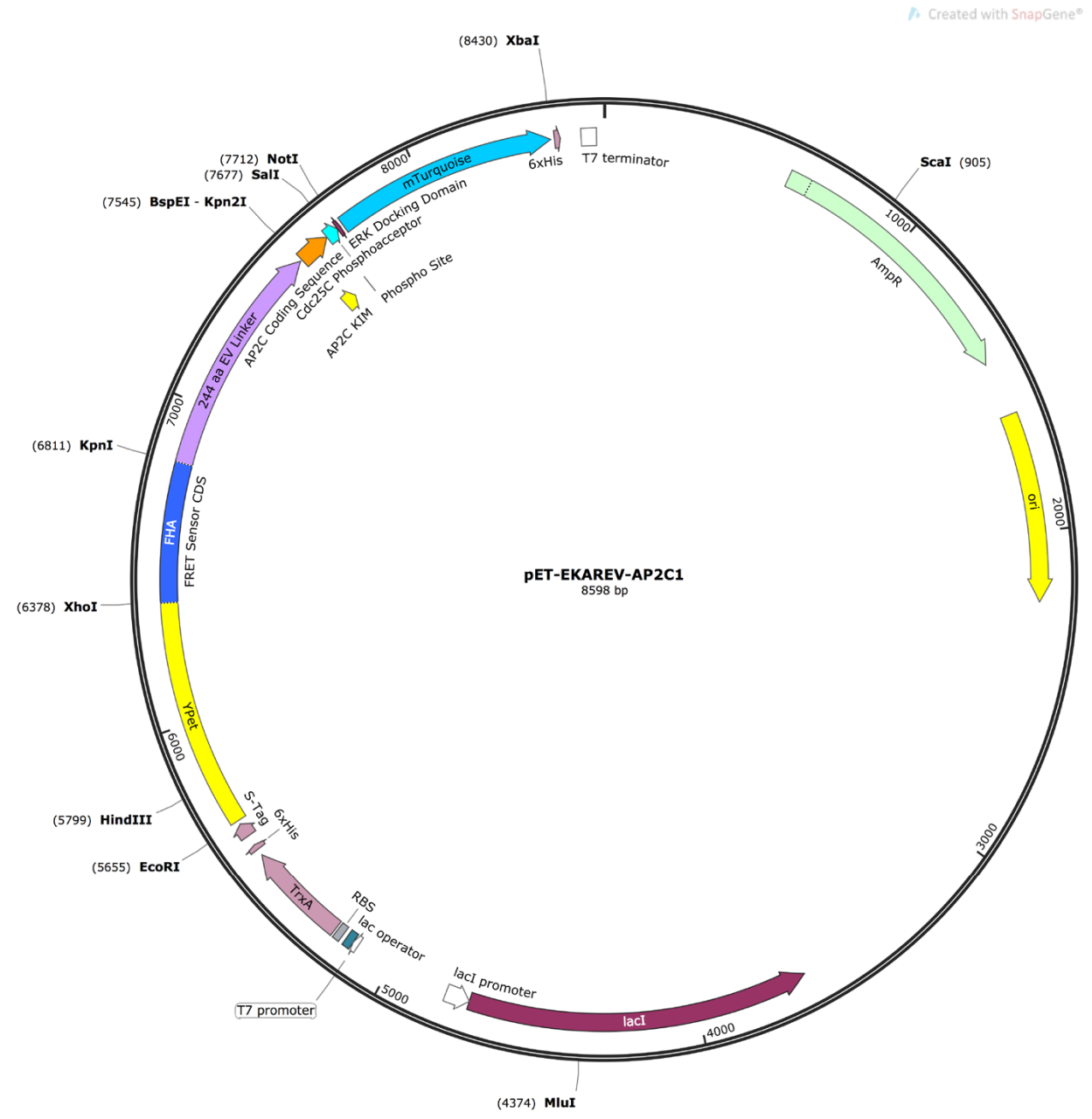

Figure S11. Plasmid map for pET-EKAREV-AP2C1

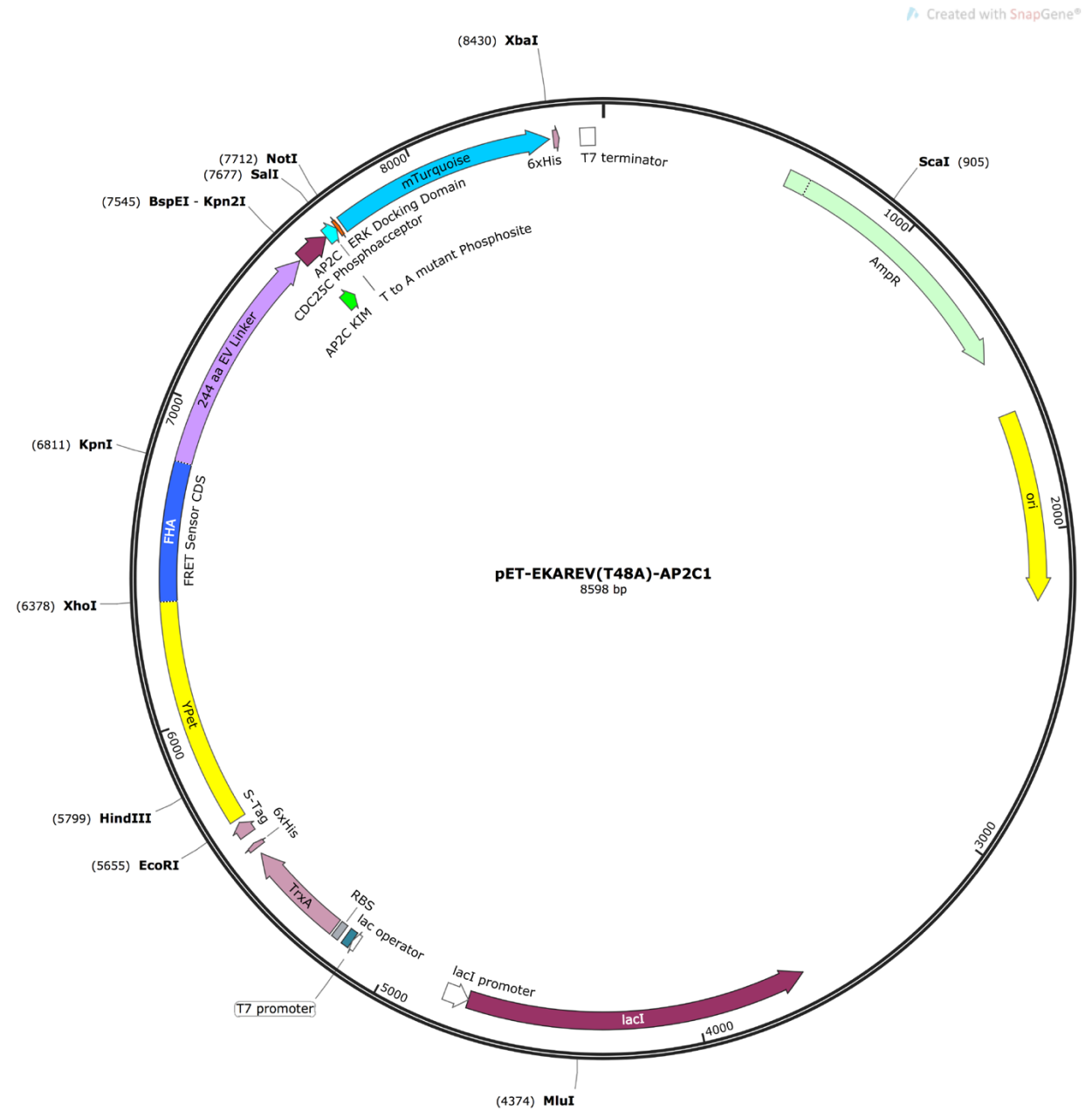

Figure S12. Plasmid map for pET-EKAREV(T48A)-AP2C1

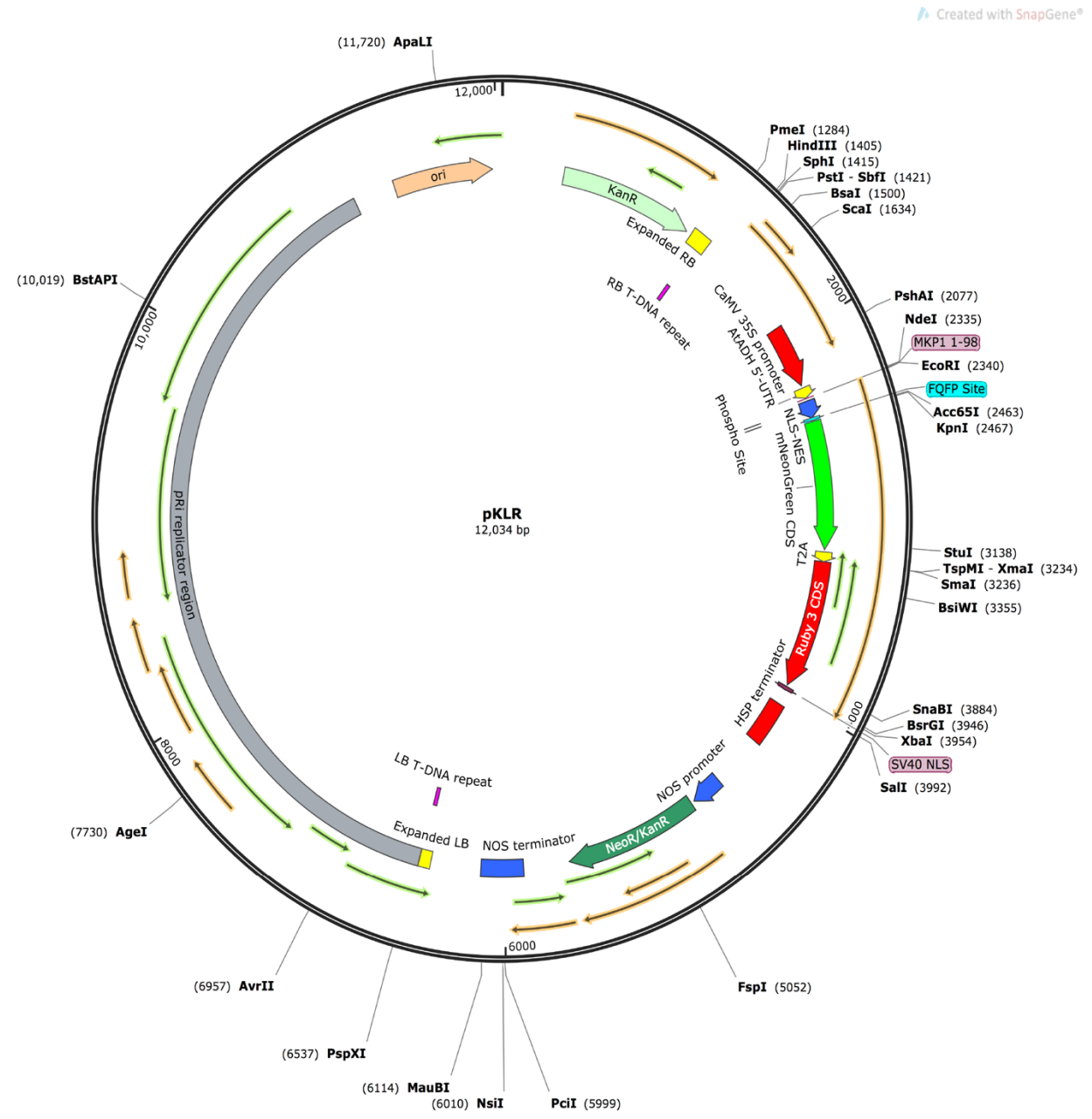

Figure S13. Plasmid map for pKLR

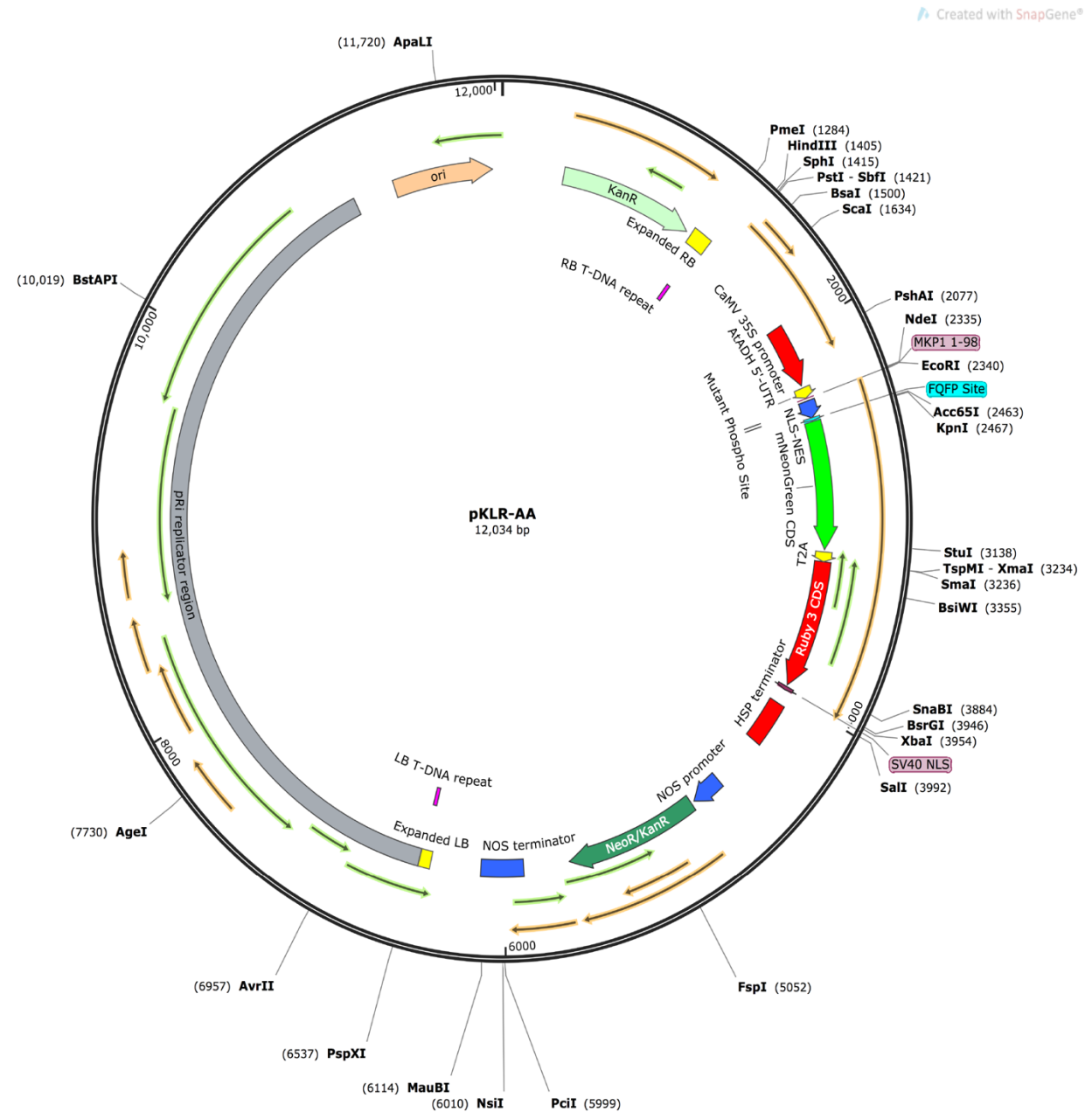

Figure S14. Plasmid map for pKLR-AA

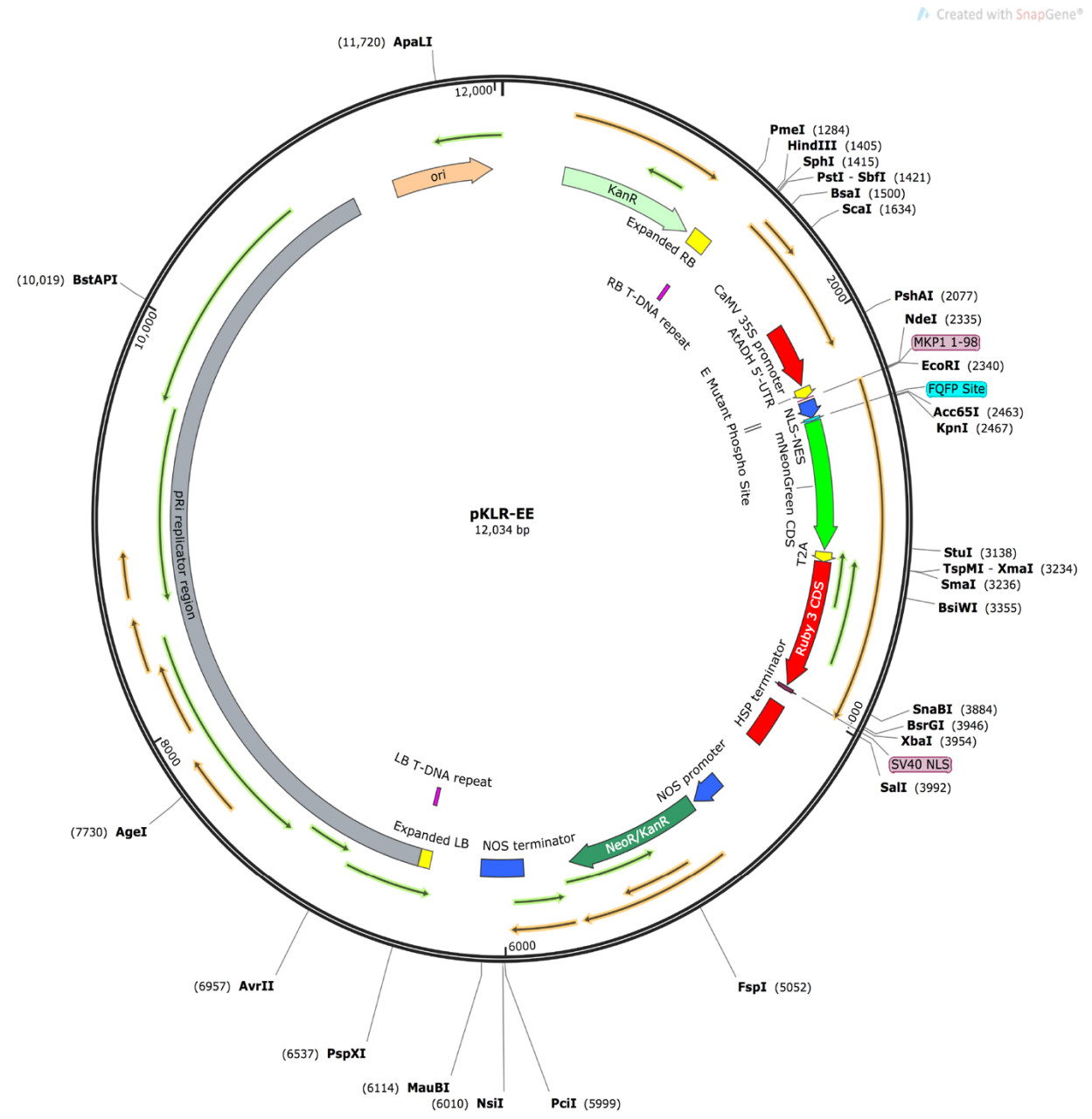

Figure S15. Plasmid map for pKLR-EE

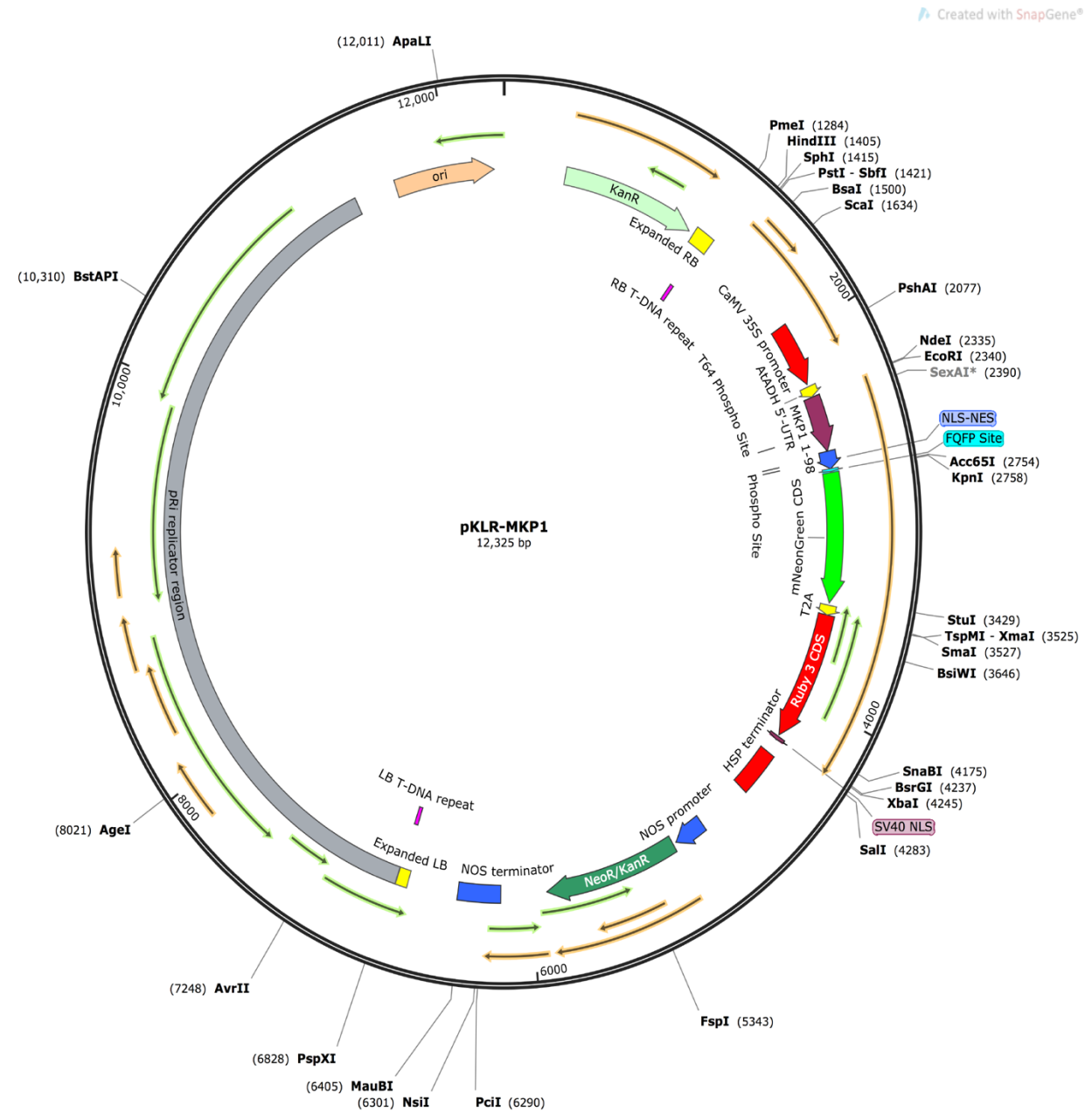

Figure S16. Plasmid map for pKLR-MKP1

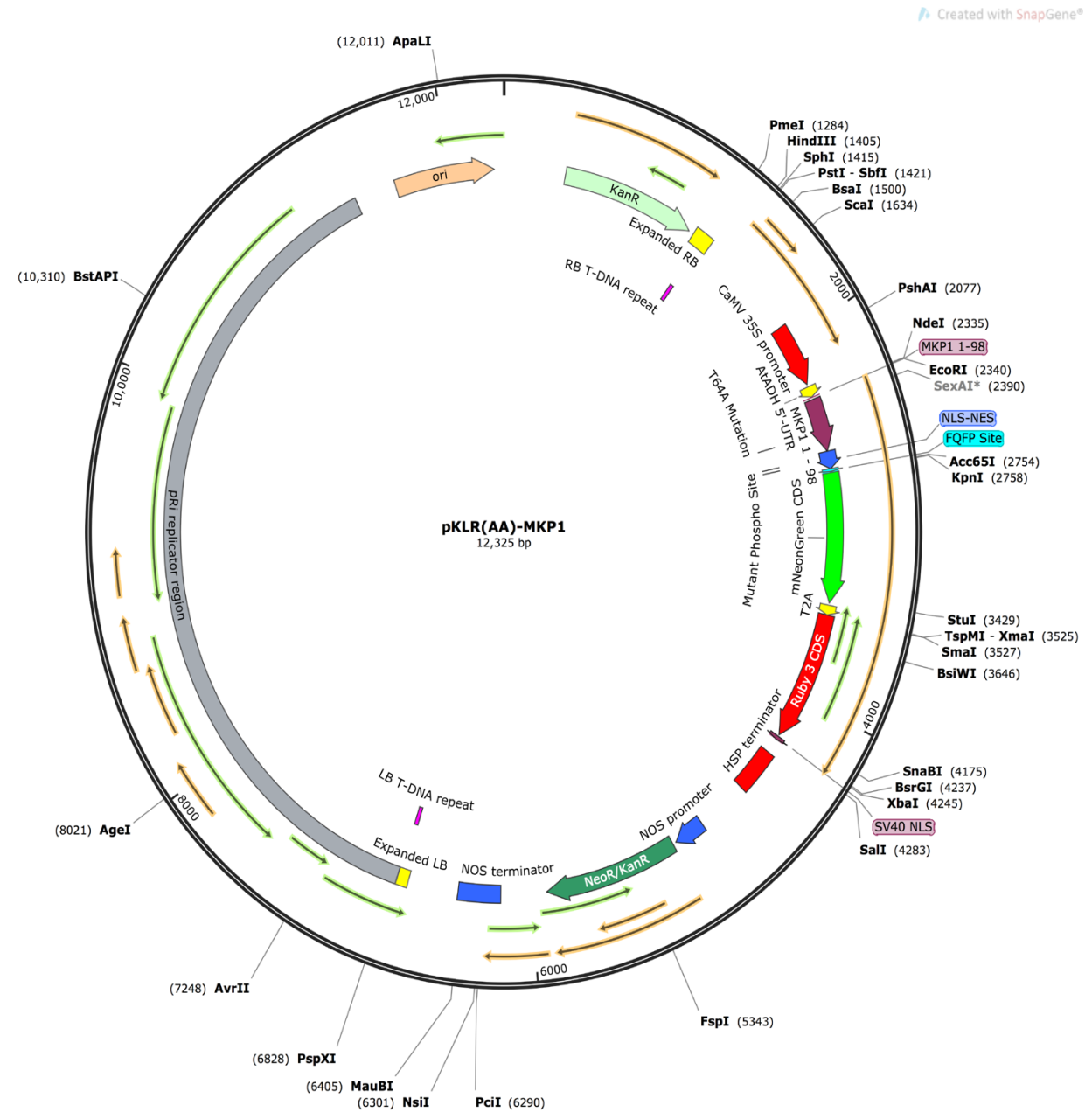

Figure S17. Plasmid map for pKLR(AA)-MKP1

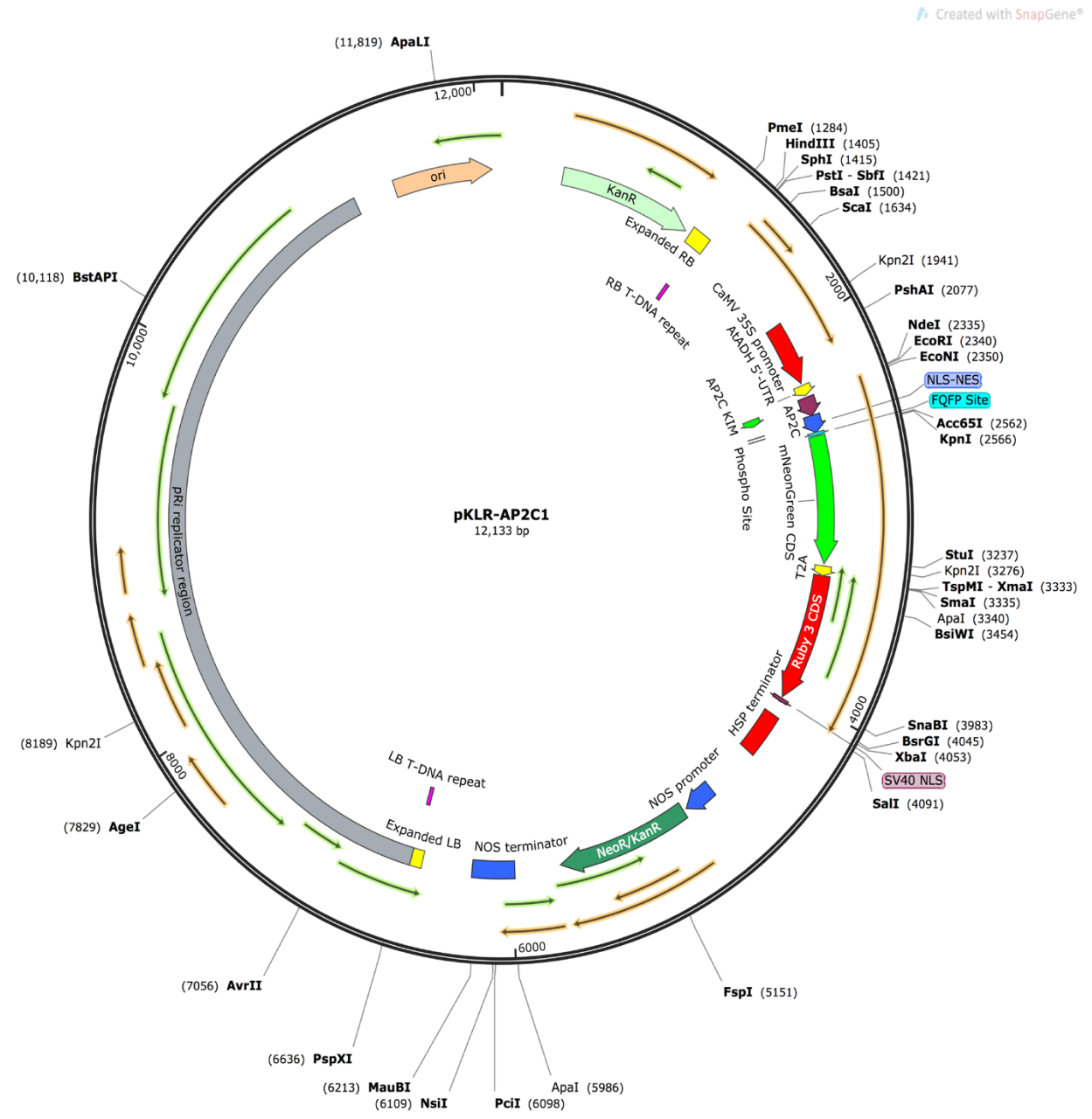

Figure S18. Plasmid map for pKLR-AP2C1

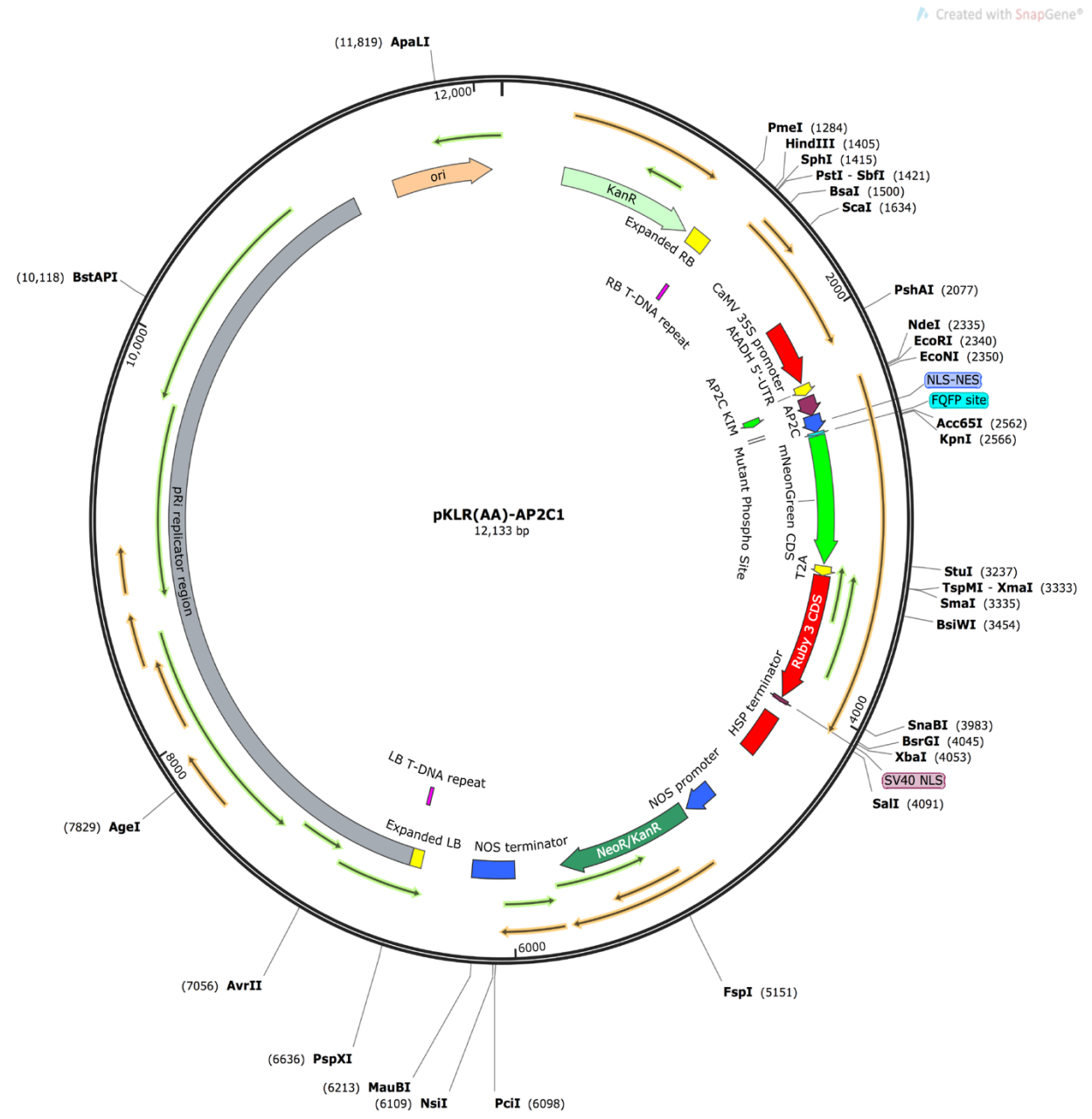

Figure S19. Plasmid map for pKLR(AA)-AP2C1

Chapter 5: Summary, Future Directions and Conclusions

Abstract

The development of two genetically encoded fluorescent biosensors for studying kinase activity in Arabidopsis provides a base for further elucidation of kinase spatiotemporal kinetics. Future topics of study will address whether the translocation biosensor KLR can report MAPK activity, and if so, which MAPK isoforms can interact with this biosensor. Additionally, the ability of KLR and SOMA to act as indicators of kinase activity can be further explored. One of the methods I utilized to apply these biosensors to interrogating the signaling processes underlying plant growth and development was through application of the HybriWell^{TM}. This device provides the means to create dosage-curve responses for a number of abiotic and biotic stress elicitors, which would generate MAPK activity profiles in response to these treatments and provide additional information on how external stimuli are translated into downstream responses with plant cells. While these experiments would provide information on how MAPKs respond to abiotic and biotic stressors, these fluorescent biosensors can also be utilized to address the role of MAPKs in other biological processes, such as growth and development. Both KLR and SOMA can be utilized in long-term confocal experiments to document MAPK kinetics during the plant life cycle. Finally, the creation of the plant MAPK docking domain trap provides the means for efficiently expanding the current pool of plant MAPK biosensors. Future work with this assay would focus on developing fluorescent biosensors with MAPK isoform input specificity.

Chapter 5: Summary and Future Directions

Summary

Ultimately, the aim of this dissertation work was to develop a suite of tools that would allow documentation of the dynamic activities of plant Mitogen-activated Protein Kinases (MAPKs) in fine detail. Achieving this goal would provide us with the means by which to further elucidate the mechanisms by which MAPKs regulate various plant biological processes. For that purpose, I developed and assessed genetically encoded fluorescent-based biosensors targeted towards Arabidopsis MAPKs. The real-time high resolution and spatiotemporal clarity offered by these reporters can provide novel insights into the complex kinetics of the regulation of these kinases, which in turn can enrich our understanding of the regulatory mechanisms that govern their activity and allow signaling networks to run smoothly.

Chapter 2 of my thesis described a novel method for performing live-cell imaging of plant tissue using confocal microscopy (Vang et al., 2018). Experimentation found that a commercially available device called a HybriWell^{TM} can maintain plant tissue in a relatively stress-free and steady-state environment during imaging. Additionally, the design of this apparatus permits the application of chemical treatments to the samples by exchanging the fluid surrounding the sample with a new solution. These traits result in an ideal tool for adding multiple successive chemical treatments to Arabidopsis plants expressing MAPK fluorescent biosensors during imaging, which can in turn be used to interrogate the response of said biosensors to chemical treatments containing MAPK activators.

Chapter 3 of my thesis described the first published genetically encoded fluorescent biosensor for studying MAPK activation in Arabidopsis, a FRET-based reporter named Sensor Of MAPK in Arabidopsis (SOMA) (Zaman et al., 2019). Through utilization of *in vitro* and *in vivo* experiments, I provided compelling evidence that SOMA is sensitive to the activity of the Arabidopsis MAPKs. I also documented the response of SOMA to known abiotic and biotic elicitors of MAPK activation in Arabidopsis. While the patterns of change in the FRET efficiency of SOMA in response to these stress treatments were consistent with the published literature (Droillard et al., 2004; Wan et al., 2004; Ichimura et al., 2006; Meszaros et al., 2006; Dóczi et al., 2007; Suarez-Rodriguez et al., 2007; Yu et al., 2010; Yamada et al., 2016), I also documented what seemed to be previously unobserved heterogeneity in MAPK kinetics within Arabidopsis cotyledon epidermal cells at the tissue, cellular, and subcellular levels. As such, this body of work provided proof-of-principle data establishing SOMA as the first fluorescence biosensor for reporting MAPK activation kinetics in living Arabidopsis plants, while also exploring how this tool could be used to further contribute to the body of knowledge for plant MAPK signaling.

Chapter 4 of my thesis is focused on my work developing methods to facilitate the generation of new plant MAPK fluorescent biosensors (Seitz & Krysan, under review). The first generation of any technology is never optimal, and while SOMA was a valuable first step in establishing plant MAPK fluorescent biosensors, there is always an insatiable need for improved tools. Based on the experience that I gained developing the first plant kinase fluorescent biosensor, my aim was to develop an experimental pipeline that would make building the second generation of plant kinase biosensors more efficient. My approach to this challenge was to first develop an *in vitro* method to identify plant MAPK docking domains. Although docking

domains are a critical component of previously described kinase biosensors (Harvey et al., 2008; Fosbrink et al., 2010; Oldach & Zhang, 2014; González-Vera & Morris, 2015), MAPK docking domains have not been well characterized functionally in plants (Nakagami et al., 2005; Feilner et al, 2005; Pitzschke et al., 2009; Singh et al., 2012; Pitzschke, 2015). I therefore established a plant MAPK docking domain trap to address the need for an efficient functional assay for characterizing plant MAPK docking domains. Inserting known plant MAPK docking domains into this pre-optimized FRET-based backbone resulted in FRET-based biosensors that displayed significant increases in FRET efficiency *in vitro* when active MAPK isoforms were present. While I only assessed the validity of this plant MAPK docking domain trap with known plant MAP docking domains, it is my expectation that this tool also has the potential to be able to identify novel plant MAPK docking domains by performing targeted screening of additional candidate sequences.

The other technical advance described in Chapter 4 is the development of the first fluorescent translocation biosensor for studying MAPKs in Arabidopsis, which we named a Kinase Localization Reporter (KLR). Phosphomimetic mutations in the synthetic bipartite Nuclear Localization Signal/Nuclear Exclusion Signal (bNLS/NES) domain of KLR caused it to exhibit a change in subcellular localization, suggesting that the phosphorylation status of the bNLS/NES module could regulate KLR subcellular localization. Additionally, inserting different plant MAPK docking domains into the KLR backbone (including a docking domain that had performed favorably in the plant MAPK docking domain trap) resulted in biosensors that displayed changes in subcellular localization *in vivo* in response to chemical treatments known

to activate MAPKs in Arabidopsis, further supporting the hypothesis that KLR can function as an Arabidopsis kinase activity reporter.

Combining the two tools described above produces a pipeline in which plant MAPK docking domains can be identified using the *in vitro* docking domain trap assay. These docking domains can then be directly used *in vivo* as new FRET kinase biosensors, or employed in the KLR backbone to produce a kinase localization reporter for use *in vivo*. This pipeline can therefore be utilized to expand the pool of available plant MAPK biosensors in a rapid and efficient manner, which in turn should increase the opportunities for applying these tools to documenting MAPK activation kinetics in living plant tissues and cells.

Future Directions

The work described in this thesis has focused on the development of novel tools that allow plant scientists to visualize the activation of MAPKs in living plant cells and tissues. Although I was able to perform several pilot proof-of-principle experiments demonstrating the potential of these new tools as elucidators of plant signaling pathways, the main focus of my work was on the technical aspects of these fluorescent biosensors. Two potential next phases in the experimental progression of this project are: (1) further validation and optimization of these tools as reporters of plant MAPK kinetics, and (2) applying these biosensors to a specific signaling pathway of interest to determine what new insights can be gained through the application of this technology. The remainder of this chapter will explore a number of possible next steps that could be taken to address these two aims and to follow-up on the advances reported in this thesis.

Additional characterization of the kinase translocation biosensor KLR

My initial work with KLR suggests that it may function as a *bona fide* MAPK biosensor *in vivo*. The evidence that KLR may be functioning as a plant kinase reporter can be summarized as follows: (1) phosphomimetic mutations to KLR result in the biosensor changing subcellular localization from nuclear to cytoplasmic. (2) In the absence of a plant MAPK docking domain, KLR does not exhibit a shift in localization when plant cells expressing KLR are exposed to chitin, a treatment known to activate plant MAPKs. (3) If a plant MAPK docking domain is added to KLR, the resulting biosensor rapidly changes its subcellular localization when plant cells expressing the reporter are treated with chitin. (4) If the known phosphoacceptor sites in KLR are mutagenized to alanine residues, the subcellular localization of KLR does undergo a redirection in response to chitin, even when a plant MAPK docking domain is present. Taken together, these results all strongly support the conclusion that KLR is functioning as a plant kinase sensor, and that those kinases are potentially MAPKs. However, additional experimentation is needed to fully prove this hypothesis.

The method we previously utilized to demonstrate that the FRET sensor SOMA was reporting MAPK activity *in vivo* involved an analog-sensitive variant of MAPK6 (Bishop et al., 2000; Berriri et al., 2012; Zaman et al., 2019). In those experiments, I demonstrated how application of a chemical inhibitor specific for an engineered MPK6 variant blocked the increase in FRET efficiency observed for SOMA when the samples were treated with NaCl. Considering the success of this experiment, it could serve as a potential means to determine which kinases are targeting KLR. By introducing KLR into the analog-sensitive MPK6 background and treating

this line with NaCl, we may be able to determine if MPK6 is responsible for the NaCl-induced subcellular localization changes displayed by KLR. Additionally, as analog sensitive variants of MPK3 and MPK4 are now also available (Leissing et al., 2016), similar experiments could be performed with those lines to further explore the input specificity of KLR. Favorable results from these experiments would strongly indicate that KLR is capable of being phosphorylated by MAPKs, and thus can serve as an indicator of MAPK activity in *Arabidopsis thaliana*.

Generating biosensor response curves for SOMA and KLR in response to select abiotic and biotic stressors

One common method for utilizing fluorescent biosensors involves generating biosensor response curves (Ritz et al., 2015; Greenwald et al., 2018; Hicks et al., 2020) (Figure 1). By exposing the biosensor to pre-specified amounts of a signal that elicit a certain, well-defined response, researchers can characterize many aspects of the biosensor, such as the range between the maximum and minimum fluorescent output (dynamic range) or the lowest concentration of the target which can be detected from the background response (limit of detection) (Hicks et al., 2020). The shape of these curves can also provide insight into the steady-state behavior of the signaling system the biosensor is measuring (Ferrell, 1996). Enzymatic activity can be typically categorized into either graded (also known as Michaelin or hyperbolic sensitivity) or switch-like (also known as ultrasensitivity) (Goldbeter & Koshland, 1981; Koshland et al., 1982; Ferrel, 1996; Michaelis & Menten, 2007). A graded response is characterized by a gradual increase in activity that follows a generally linear relationship with the strength of the input signal (Figure 1A). In contrast, a switch-like response does not initially

respond to low levels of a stimuli until a certain concentration threshold is met, upon which the enzyme displays a strong respond that reaches maximal response quickly (Figure 1B). Graded responses are common in signaling pathways that require a proportional response to the strength of the signal, such as pathways that maintain homeostasis, while switch-like responses tend to characterize networks that are responsible for control of cell fate (Atay & Skotheim, 2017).

While most MAPK responses have been characterized as switch-like (Huang & Ferrell, 1996; Ferrell & Machleder, 1998; Bagowski et al., 2003; Xiong & Ferrell, 2003; Zhang et al., 2013), as the three-tier cascade arrangement of MAPK proteins acts as a natural translator of graded signal inputs into a switch-like response, graded responses have also been reported for several systems and model organisms (Whitehurst et al., 2004; MacKeigan et al., 2005; Santos et al., 2007; Perrett et al., 2013; Conlon et al., 2016). As such, generating dose-response curves for SOMA and KLR in response to select abiotic and biotic treatments would allow us to further characterize MAPK behavior within these stress and defense signaling pathways, while also providing insight into the potentially unique characteristics of MAPK towards each input signal, such as the amplitude or duration of the response or patterns of bistability or oscillations.

Examples of abiotic stressors known to activate MAPKs in Arabidopsis that could be investigated this way include wounding, osmotic stress, heat stress, cold stress, UV-light stress, and heavy metal stress (Ichimura et al., 2000; Teige et al., 2004; Nakagami et al., 2005; Xing et al., 2007; Sinha et al., 2011; Smékalová et al., 2014). Examples of biotic MAPK activators that could be investigated in this way include microbe-associated molecular patterns (MAMPs) such as flagellin-22, chitin, elongation factor Tu (EF-Tu) or peptidoglycan (Nühse et al., 2000; Gómez-

Gómez et al., 2000; Asai et al., 2002; Kunze et al., 2004; Zipfel et al., 2006; Miya et al., 2007; Gust et al., 2007; Willmann et al., 2011; Newman et al., 2013) or damage-associated molecular patterns (DAMPs) such as putative cytosolic peptides (Peps) or oligogalacturonides (Norman et al., 1999; Yamaguchi et al., 2006, 2010; Ferrari et al., 2007; Brutus et al., 2010; Krol et al., 2010; Galletti et al., 2011; Bartels et al., 2013; Hou et al., 2019). Generating these biosensor response curves could potentially provide further insight into the spatiotemporal dynamics of plant MAPK activation and how said kinetics are utilized to translate external abiotic and biotic stress signals into the appropriate downstream response(s).

Utilizing SOMA and KLR to document the MAPK kinetics regulating growth and development

As discussed previously, MAPKs have been implicated in numerous plant cellular processes, including those associated with growth and development (Xu & Zhang, 2015). One such pathway is that which controls the development of stomata, the microscopic pores on the epidermis of leaf cells that allow for gas exchange (Schroeder et al., 2001). Increased activity of the Arabidopsis MAPKs MPK3 and MPK6 has been documented at several key stages within the stomatal differentiation pathway, suggesting these kinases may act as gatekeepers during this process (Wang et al., 2007; Lampard et al., 2009). Additionally, MPK3 and MPK6 have been shown to regulate several of the proteins involved in this process, including the transcription factor SPEECHLESS (SPCH) (Lampard et al., 2008) and the scaffolding protein SCREAM (SCRM) (Putarjunan et al., 2019; Larue & Zhang, 2019), while Arabidopsis MAPK MPK4 was shown to phosphorylate the transcription factor MUTE in a proteomic assay (Popescu et al., 2009).

Exploring MAPK kinetics within this system would likely offer further insights into how the spatiotemporal aspects of MAPK behavior influence cellular fate and function.

To investigate the role of MAPKs within the stomatal differentiation pathway, I would suggest using SOMA and/or KLR to perform a long-term, live-cell imaging analysis of epidermal cells of young cotyledons. Focusing on fluorescence emission changes within primordial cells as they develop into mature guard cells should allow creation of a MAPK activation “map”, pinpointing fluctuations in MAPK activity or localization and determining if they correspond to initiation or completion of specific developmental stages. If this experiment is successful, it would be instructive to simultaneously monitor spectrally-distinctly labeled MUTE, FAMA, or SPCH proteins within the same tissue as the fluorescent biosensor. As these transcription factors function as master regulations of a specific stage of stomata development and are each expressed at a distinct stage in the guard cell developmental cycle (Lampard & Bergmann, 2007), quantifying expression and degradation of these proteins while simultaneously documenting MAPK activity within the same cellular circumstances would offer valuable temporal and spatial context to the interactions between these signaling components.

In addition to their involvement in stomatal differentiation, genetic studies have recently reported that the MAPKs MPK3 and MPK6 also play a critical role in driving the initial cell divisions that occur during lateral root production in Arabidopsis (López-Bucio et al., 2014; Zhu et al., 2019; He & Meng, 2020). A similar approach to that described above for analyzing stomatal development could also be used to look for evidence of MAPK activation during lateral root development. These experiments have the potential to address prominent questions related to the regulation of developmental pathways in plants, such as an improved

understanding of the intensity and duration of MAPK activation that is necessary for developmental progression, as well as revealing the exact cells in which kinase activation occurs. Generating these kinase activation "maps" would provide critical temporal and spatial information within these developmental timelines, further elucidating the mechanisms by which MAPKs regulate these biological processes.

Develop isoform-specific MAPK biosensors

The plant MAPK docking domain trap described in Chapter 4 possesses the potential to be the foundation for an experimental strategy aimed at developing isoform-specific MAPK biosensors. Reporters which possess affinity for multiple MAPK isoforms and measure the integrated sum of several kinase activities may reflect the reality of the numerous shared substrates that comprise signaling processes within the cell. However, determining the extent to which specificity exists within these systems requires the development of tools capable of detecting measuring said specificity. MAPK isoform-specific fluorescent biosensors would provide the means to document specific MAPK activity within a pathway, addressing topics such as pathway selectivity and redundancy. Additionally, MAPK isoform-specific biosensors could be multiplexed within the same plant tissue, which could further enhance the opportunities to document interplay between signaling networks.

Developing isoform-specific MAPK sensors would require a panel of constitutively active plant MAPKs that one could use for rapid *in vitro* testing of candidate docking domains to search for variants that demonstrated a strong gain in FRET efficiency in the presence of only a single MAPK isoform. One approach to developing isoform-specific sensors would involve

mutagenizing specific amino acid residues within candidate docking domains in an attempt to confer MAPK input specificity. Although only a few dozen plant MAPK substrate has been experimentally characterized (Zhang et al., 2018; Dóczi et al., 2018), the majority of these have possessed known plant MAPK docking domains, and in several cases publications indicated that the ability of the substrate to facilitate MAPK binding is dependent on key residues within the plant MAPK docking domain sequence (Schweighofer et al., 2007; Zhang et al., 2015; Putarjunan et al., 2019). Mutagenizing theses residues within the context of a fluorescent biosensor could therefore be used to manipulate plant MAPK docking domain affinity and could potentially provide a way to confer sensor specificity towards specific MAPK isoforms.

Another method to produce isoform-specific MAPK sensors would be to use plant MAPK docking domains from substrate proteins that have been shown to be MAPK isoform specific from other publications. There exist several surveys that have compiled MPK3/MPK6 substrates based on yeast-two-hybrid, protein microarrays, phosphoproteomics, or *in silico* screening (Feilner et al., 2005; Sörrenson et al., 2012; Rayapuram et al., 2017; Dóczi et al., 2018), although many of these still need to be verified *in vivo*. It should also be noted that although these proteins have been characterized as MPK3/6 substrates, in the large majority of cases it is not clear where the actual plant MAPK docking domain resides within the substrate amino acid sequence, and roughly a third of the identified plant MAPKs substrates do not possess a known MAPK docking domain (Dóczi et al., 2018). Unlike the case with animal MAPK docking domains (Whisenant et al., 2010; Gordon et al., 2013; Zeke et al., 2015), there currently exists no computational tools for predicting plant MAPK docking domains, so empirical testing with a functional assay, such as the plant MAPK docking domain trap described in Chapter 4, is

necessary. The experimental approach would therefore be to take candidate substrate proteins that show a strong preference for either MPK3 alone or MPK6 alone and then systematically clone portions of that substrate protein into the docking domain trap to identify potential docking domains. If successful, we would find a docking domain that drives a strong MAPK-dependent increase in FRET efficiency in an isoform-specific manner. Although not as well characterized, this method could also be utilized for candidate substrate proteins that exhibit a strong preference for other MAPKs isoforms, such as MPK4 or MPK10. Additionally, data accumulated from these docking domain trap assays could provide the foundation for building a computational tool to predict candidate plant MAPK docking domains *in silico*.

Concluding Remarks

In this this dissertation I have discussed the work I performed to develop two separate types of genetically encoded fluorescent biosensors for studying kinase activation in plants. While further testing is necessary to parse the extent to which these reporters can be targeted by specific plant kinases, they remain important first steps in establishing genetically encoded fluorescent biosensors as viable tools within the plant MAPK research community. The adoption and spread of these tools should be further facilitated by our experimental pipeline for efficient engineering of plant MAPK biosensors. Broadly, future work on these tools will be two-pronged: one approach focused on optimization and assessment, the other on utilizing fluorescent biosensors to investigate the spatiotemporal aspects of MAPKs behavior in both environmental stress response and developmental pathways.

References

Asai, T.; Tena, G.; Plotnikova, J.; Willmann, M.R.; Chiu, W.L.; Gómez-Gómez, L.; Boller, T.; Ausubel, F.M.; Sheen, J. MAP kinase signalling cascade in Arabidopsis innate immunity. *Nature*. **2002**, *415*, 977-983.

Atay, O.; Skotheim, J. M. Spatial and temporal signal processing and decision making by MAPK pathways. Dynamic signal processing by MAPK pathways. *The Journal of Cell Biology*. **2017**, *216*, 317-330.

Bagowski, C. P.; Besser, J.; Frey, C. R.; Ferrell Jr, J. E. The JNK cascade as a biochemical switch in mammalian cells: ultrasensitive and all-or-none responses. *Current Biology*. **2003**, *13*, 315-320.

Bartels, S.; Lori, M.; Mbengue, M.; van Verk, M.; Klauser, D.; Hander, T.; Böni, R.; Robatzek, S.; Boller, T. The family of Peps and their precursors in Arabidopsis: differential expression and localization but similar induction of pattern-triggered immune responses. *Journal of Experimental Botany*. **2013**, *64*, 5309-5321.

Berriri, S.; Garcia, A.V.; dit Frey, N.F.; Rozhon, W.; Pateyron, S.; Leonhardt, N.; Montillet, J.L.; Leung, J.; Hirt, H.; Colcombet, J. Constitutively active mitogen-activated protein kinase versions reveal functions of Arabidopsis MPK4 in pathogen defense signaling. *The Plant Cell*. **2012**, *24*, 4281-4293.

Bishop, A.C.; Ubersax, J.A.; Petsch, D.T.; Matheos, D.P.; Gray, N.S.; Blethrow, J.; Shimizu, E.; Tsien, J.Z.; Schultz, P.G.; Rose, M.D.; Wood, J.L. A chemical switch for inhibitor-sensitive alleles of any protein kinase. *Nature*. **2000**, *407*, 395-401.

Brutus, A.; Sicilia, F.; Macone, A.; Cervone, F.; De Lorenzo, G. A domain swap approach reveals a role of the plant wall-associated kinase 1 (WAK1) as a receptor of oligogalacturonides. *Proceedings of the National Academy of Sciences*. **2010**, *107*, 9452-9457.

Buchler, N. E.; Louis, M. Molecular titration and ultrasensitivity in regulatory networks. *Journal of Molecular Biology*. **2008**, *384*, 1106-1119.

Conlon, P.; Gelin-Licht, R.; Ganesan, A.; Zhang, J.; Levchenko, A. Single-cell dynamics and variability of MAPK activity in a yeast differentiation pathway. *Proceedings of the National Academy of Sciences*. **2016**, *113*, 5896-5905.

Dóczi, R.; Bögre, L. The quest for MAP kinase substrates: gaining momentum. *Trends in Plant Science*. **2018**, *23*, 918-932.

Dóczi, R.; Brader, G.; Pettkó-Szandtner, A.; Rajh, I.; Djamei, A.; Pitzschke, A.; Teige, M.; Hirt, H. The Arabidopsis mitogen-activated protein kinase kinase MKK3 is upstream of group C mitogen-activated protein kinases and participates in pathogen signaling. *The Plant Cell*. **2007**, *19*, 3266-3279.

Droillard, M. J.; Boudsocq, M.; Barbier-Brygoo, H.; Laurière, C. Involvement of MPK4 in osmotic stress response pathways in cell suspensions and plantlets of *Arabidopsis thaliana*: activation by hypoosmolarity and negative role in hyperosmolarity tolerance. *FEBS Letters*. **2004**, *574*, 42-48.

Feilner, T.; Hultschig, C.; Lee, J.; Meyer, S.; Immink, R.G.; Koenig, A.; Possling, A.; Seitz, H.; Beveridge, A.; Scheel, D.; Cahill, D.J. High throughput identification of potential Arabidopsis mitogen-activated protein kinases substrates. *Molecular & Cellular Proteomics*. **2005**, *4*, 1558-1568.

Feilner, T.; Hultschig, C.; Lee, J.; Meyer, S.; Immink, R.G.; Koenig, A.; Possling, A.; Seitz, H.; Beveridge, A.; Scheel, D.; Cahill, D.J. High throughput identification of potential Arabidopsis mitogen-activated protein kinases substrates. *Molecular & Cellular Proteomics*. **2005**, *4*, 1558-1568.

Ferrari, S.; Galletti, R.; Denoux, C.; De Lorenzo, G.; Ausubel, F. M.; Dewdney, J. Resistance to *Botrytis cinerea* induced in Arabidopsis by elicitors is independent of salicylic acid, ethylene, or jasmonate signaling but requires PHYTOALEXIN DEFICIENT3. *Plant Physiology*. **2007**, *144*, 367-379.

Ferrell, J. E. Tripping the switch fantastic: how a protein kinase cascade can convert graded inputs into switch-like outputs. *Trends in Biochemical Sciences*. **1996**, *21*, 460-466.

Ferrell, J. E.; Machleder, E. M. The biochemical basis of an all-or-none cell fate switch in Xenopus oocytes. *Science*. **1998**, *280*, 895-898.

Fosbrink, M.; Aye-Han, N. N.; Cheong, R.; Levchenko, A.; Zhang, J. Visualization of JNK activity dynamics with a genetically encoded fluorescent biosensor. *Proceedings of the National Academy of Sciences*. **2010**, *107*, 5459-5464.

Galletti, R.; Ferrari, S.; De Lorenzo, G. Arabidopsis MPK3 and MPK6 play different roles in basal and oligogalacturonide- or flagellin-induced resistance against *Botrytis cinerea*. *Plant Physiol.* **2011**, *157*, 804–814.

Goldbeter, A.; Koshland, D. E. An amplified sensitivity arising from covalent modification in biological systems. *Proceedings of the National Academy of Sciences*. **1981**, *78*, 6840-6844.

Gómez-Gómez, L.; Boller, T. FLS2: an LRR receptor–like kinase involved in the perception of the bacterial elicitor flagellin in Arabidopsis. *Molecular Cell*. **2000**, *5*, 1003-1011.

González-Vera, J. A.; Morris, M. C. Fluorescent reporters and biosensors for probing the dynamic behavior of protein kinases. *Proteomes*. **2015**, *3*, 369-410.

Gordon, E.A.; Whisenant, T.C.; Zeller, M.; Kaake, R.M.; Gordon, W.M.; Krotee, P.; Patel, V.; Huang, L.; Baldi, P.; Bardwell, L. Combining docking site and phosphosite predictions to find new substrates: identification of smoothelin-like-2 (SMTNL2) as a c-Jun N-terminal kinase (JNK) substrate. *Cellular Signaling*. **2013**, *25*, 2518-2529.

Greenwald, E. C.; Mehta, S.; Zhang, J. Genetically encoded fluorescent biosensors illuminate the spatiotemporal regulation of signaling networks. *Chemical Reviews*. **2018**, *118*, 11707-11794.

Gust, A.A.; Biswas, R.; Lenz, H.D.; Rauhut, T.; Ranf, S.; Kemmerling, B.; Götz, F.; Glawischnig, E.; Lee, J.; Felix, G.; Nürnberger, T. Bacteria-derived peptidoglycans constitute pathogen-associated molecular patterns triggering innate immunity in Arabidopsis. *Journal of Biological Chemistry*. **2007**, *282*, 32338-32348.

Harvey, C. D.; Ehrhardt, A. G.; Cellurale, C.; Zhong, H.; Yasuda, R.; Davis, R. J.; Svoboda, K. A genetically encoded fluorescent biosensor of ERK activity. *Proceedings of the National Academy of Sciences*. **2008**, *105*, 19264-19269.

He, Y.; Meng, X. MAPK Signaling: Emerging Roles in Lateral Root Formation. *Trends in Plant Science*. **2020**, *25*, 126-129.

Hicks, M.; Bachmann, T. T.; Wang, B. Synthetic Biology Enables Programmable Cell-Based Biosensors. *ChemPhysChem*. **2020**, *21*, 132-144.

Hou, S.; Liu, Z.; Shen, H.; Wu, D. Damage-associated molecular pattern-triggered immunity in plants. *Frontiers in Plant Science*. **2019**, *10*, 646.

Huang, C. Y.; Ferrell, J. E. Ultrasensitivity in the mitogen-activated protein kinase cascade. *Proceedings of the National Academy of Sciences*. **1996**, *93*, 10078-10083.

Ichimura, K.; Casais, C.; Peck, S. C.; Shinozaki, K.; Shirasu, K. MEKK1 is required for MPK4 activation and regulates tissue-specific and temperature-dependent cell death in Arabidopsis. *Journal of Biological Chemistry*. **2006**, *281*, 36969-36976.

Ichimura, K.; Mizoguchi, T.; Yoshida, R.; Yuasa, T.; Shinozaki, K. Various abiotic stresses rapidly activate Arabidopsis MAP kinases ATMPK4 and ATMPK6. *The Plant Journal*. **2000**, *24*, 655-665.

Koshland, D. E.; Goldbeter, A.; Stock, J. B. Amplification and adaptation in regulatory and sensory systems. *Science*. **1982**, 220-225.

Krol, E.; Mentzel, T.; Chinchilla, D.; Boller, T.; Felix, G.; Kemmerling, B.; Postel, S.; Arents, M.; Jeworutzki, E.; Al-Rasheid, K.A.; Becker, D. Perception of the Arabidopsis danger signal peptide 1 involves the pattern recognition receptor AtPEPR1 and its close homologue AtPEPR2. *Journal of Biological Chemistry*. **2010**, *285*, 13471-13479.

Kunze, G.; Zipfel, C.; Robatzek, S.; Niehaus, K.; Boller, T.; Felix, G. The N terminus of bacterial elongation factor Tu elicits innate immunity in Arabidopsis plants. *The Plant Cell*. **2004**, *16*, 3496-3507.

Lampard, G. R.; Bergmann, D. C. A shout-out to stomatal development: how the bHLH proteins SPEECHLESS, MUTE and FAMA regulate cell division and cell fate. *Plant Signaling & Behavior*. **2007**, *2*, 290-292.

Lampard, G. R.; Lukowitz, W.; Ellis, B. E.; Bergmann, D. C. Novel and expanded roles for MAPK signaling in Arabidopsis stomatal cell fate revealed by cell type–specific manipulations. *The Plant Cell*. **2009**, *21*, 3506-3517.

Lampard, G. R.; MacAlister, C. A.; Bergmann, D. C. Arabidopsis stomatal initiation is controlled by MAPK-mediated regulation of the bHLH SPEECHLESS. *Science*. **2008**, *322*, 1113-1116.

Larue, H.; Zhang, S. SCREAM in the making of stomata. *Nature Plants*. **2019**, *5*, 648-649.

Leissing, F.; Nomoto, M.; Bocola, M.; Schwaneberg, U.; Tada, Y.; Conrath, U.; Beckers, G. J. Substrate thiophosphorylation by Arabidopsis mitogen-activated protein kinases. *BMC Plant Biology*. **2016**, *16*, 1-11.

López-Bucio, J.S.; Dubrovsky, J.G.; Raya-González, J.; Ugartechea-Chirino, Y.; López-Bucio, J.; de Luna-Valdez, L.A.; Ramos-Vega, M.; León, P.; Guevara-García, A.A. *Arabidopsis thaliana* mitogen-activated protein kinase 6 is involved in seed formation and modulation of primary and lateral root development. *Journal of Experimental Botany*. **2014**, *65*, 169-183.

MacKeigan, J. P.; Murphy, L. O.; Dimitri, C. A.; Blenis, J. Graded mitogen-activated protein kinase activity precedes switch-like c-Fos induction in mammalian cells. *Molecular and cellular biology*. **2005**, *25*, 4676-4682.

Mészáros, T.; Helfer, A.; Hatzimasoura, E.; Magyar, Z.; Serazetdinova, L.; Rios, G.; Bardóczy, V.; Teige, M.; Koncz, C.; Peck, S.; Bögre, L. The Arabidopsis MAP kinase kinase MKK1 participates in defence responses to the bacterial elicitor flagellin. *The Plant Journal*. **2006**, *48*, 485-498.

Michaelis, L.; Menten, M. L. Die kinetik der invertinwirkung. *Universitätsbibliothek*. Johann Christian Senckenberg. **2007**.

Miya, A.; Albert, P.; Shinya, T.; Desaki, Y.; Ichimura, K.; Shirasu, K.; Narusaka, Y.; Kawakami, N.; Kaku, H.; Shibuya, N. CERK1, a LysM receptor kinase, is essential for chitin elicitor signaling in Arabidopsis. *Proceedings of the National Academy of Sciences*. **2007**, *104*, 19613-19618.

Nakagami, H.; Pitzschke, A.; Hirt, H. Emerging MAP kinase pathways in plant stress signalling. *Trends in Plant Science*. **2005**, *10*, 339-346.

Nakagami, H.; Pitzschke, A.; Hirt, H. Emerging MAP kinase pathways in plant stress signalling. *Trends in Plant Science*. **2005**, *10*, 339-346.

Newman, M. A.; Sundelin, T.; Nielsen, J. T.; Erbs, G. MAMP (microbe-associated molecular pattern) triggered immunity in plants. *Frontiers in Plant Science*. **2013**, *4*, 139.

Norman, C.; Vidal, S.; Palva, E. T. Oligogalacturonide-mediated induction of a gene involved in jasmonic acid synthesis in response to the cell-wall-degrading enzymes of the plant pathogen *Erwinia carotovora*. *Molecular Plant-Microbe Interactions*, **1999**, *12*, 640-644.

Nühse, T. S.; Peck, S. C.; Hirt, H.; Boller, T. Microbial elicitors induce activation and dual phosphorylation of the *Arabidopsis thaliana* MAPK 6. *Journal of Biological Chemistry*. **2000**, *275*, 7521-7526.

Oldach, L.; Zhang, J. Genetically encoded fluorescent biosensors for live-cell visualization of protein phosphorylation. *Chemistry Biology*. **2014**, *21*, 186-197.

Perrett, R. M.; Fowkes, R. C.; Caunt, C. J.; Tsaneva-Atanasova, K.; Bowsher, C. G.; McArdle, C. A. Signaling to Extracellular Signal-regulated Kinase from ErbB1 Kinase and Protein Kinase C FEEDBACK, HETEROGENEITY, AND GATING. *Journal of Biological Chemistry*. **2013**, *288*, 21001-21014.

Pitzschke, A. Modes of MAPK substrate recognition and control. *Trends in Plant Science*. **2015**, *20*, 49-55.

Pitzschke, A.; Schikora, A.; Hirt, H. MAPK cascade signalling networks in plant defence. *Current Opinion in Plant Biology*. **2009**, *12*, 421-426.

Popescu, S. C.; Popescu, G. V.; Bachan, S.; Zhang, Z.; Gerstein, M.; Snyder, M.; Dinesh-Kumar, S. P. MAPK target networks in *Arabidopsis thaliana* revealed using functional protein microarrays. *Genes & Development*. **2009**, *23*, 80-92.

Putarjunan, A.; Ruble, J.; Srivastava, A.; Zhao, C.; Rychel, A.L.; Hofstetter, A.K.; Tang, X.; Zhu, J.K.; Tama, F.; Zheng, N.; Torii, K.U. Bipartite anchoring of SCREAM enforces stomatal initiation by coupling MAP kinases to SPEECHLESS. *Nature Plants*. **2019**, *5*, 742-754.

Ritz, C.; Baty, F.; Streibig, J. C.; Gerhard, D. Dose-response analysis using R. *PloS one*. **2015**, *10*, e0146021.

Santos, S. D.; Verveer, P. J.; Bastiaens, P. I. Growth factor-induced MAPK network topology shapes Erk response determining PC-12 cell fate. *Nature cell biology*. **2007**, *9*, 324-330.

Schroeder, J. I.; Allen, G. J.; Hugouvieux, V.; Kwak, J. M.; Waner, D. Guard cell signal transduction. *Annual Review of Plant Biology*. **2001**, *52*, 627-658.

Schweighofer, A.; Kazanaviciute, V.; Scheikl, E.; Teige, M.; Dóczi, R.; Hirt, H.; Schwanninger, M.; Kant, M.; Schuurink, R.; Mauch, F.; Buchala, A. The PP2C-type phosphatase AP2C1, which negatively regulates MPK4 and MPK6, modulates innate immunity, jasmonic acid, and ethylene levels in Arabidopsis. *The Plant Cell*. **2007**, *19*, 2213-2224.

Singh, R.; Lee, M.O.; Lee, J.E.; Choi, J.; Park, J.H.; Kim, E.H.; Yoo, R.H.; Cho, J.I.; Jeon, J.S.; Rakwal, R.; Agrawal, G.K. Rice mitogen-activated protein kinase interactome analysis using the yeast two-hybrid system. *Plant Physiology*. **2012**, *160*, 477-487.

Sinha, A. K.; Jaggi, M.; Raghuram, B.; Tuteja, N. Mitogen-activated protein kinase signaling in plants under abiotic stress. *Plant Signaling & Behavior*. **2011**, *6*, 196-203.

Smékalová, V.; Doskočilová, A.; Komis, G.; Šamaj, J. Crosstalk between secondary messengers, hormones and MAPK modules during abiotic stress signalling in plants. *Biotechnology Advances*. **2014**, *32*, 2-11.

Sörensson, C.; Lenman, M.; Veide-Vilg, J.; Schopper, S.; Ljungdahl, T.; Grøtli, M.; Tamás, M.J.; Peck, S.C.; Andreasson, E. Determination of primary sequence specificity of Arabidopsis MAPKs MPK3 and MPK6 leads to identification of new substrates. *Biochemical Journal*. **2012**, *446*, 271-278.

Suarez-Rodriguez, M.C.; Adams-Phillips, L.; Liu, Y.; Wang, H.; Su, S.H.; Jester, P.J.; Zhang, S.; Bent, A.F.; Krysan, P.J. MEKK1 is required for flg22-induced MPK4 activation in Arabidopsis plants. *Plant physiology*. **2007**, *143*, 661-669.

Teige, M.; Scheikl, E.; Eulgem, T.; Dóczi, R.; Ichimura, K.; Shinozaki, K.; Dangl, J.L.; Hirt, H. The MKK2 pathway mediates cold and salt stress signaling in Arabidopsis. *Molecular Cell*. **2004**, *15*, 141-152.

Vang, S.; Seitz, K.; Krysan, P. J. A simple microfluidic device for live cell imaging of Arabidopsis cotyledons, leaves, and seedlings. *Biotechniques*. **2018**, *64*, 255-261.

Wan, J.; Zhang, S.; Stacey, G. Activation of a mitogen-activated protein kinase pathway in Arabidopsis by chitin. *Molecular Plant Pathology*. **2004**, *5*, 125-135.

Wang, H.; Ngwenyama, N.; Liu, Y.; Walker, J. C.; Zhang, S. Stomatal development and patterning are regulated by environmentally responsive mitogen-activated protein kinases in Arabidopsis. *The Plant Cell*. **2007**, *19*, 63-73.

Whisenant, T.C.; Ho, D.T.; Benz, R.W.; Rogers, J.S.; Kaake, R.M.; Gordon, E.A.; Huang, L.; Baldi, P.; Bardwell, L. Computational prediction and experimental verification of new MAP kinase docking sites and substrates including Gli transcription factors. *PLoS Comput Biol*. **2010**, *6*, e1000908.

Whitehurst, A. W.; Robinson, F. L.; Moore, M. S.; Cobb, M. H. The death effector domain protein PEA-15 prevents nuclear entry of ERK2 by inhibiting required interactions. *Journal of Biological Chemistry*. **2004**, *279*, 12840-12847.

Willmann, R.; Lajunen, H.M.; Erbs, G.; Newman, M.A.; Kolb, D.; Tsuda, K.; Katagiri, F.; Fliegmann, J.; Bono, J.J.; Cullimore, J.V.; Jehle, A.K. Arabidopsis lysin-motif proteins LYM1 LYM3 CERK1 mediate bacterial peptidoglycan sensing and immunity to bacterial infection. *Proceedings of the National Academy of Sciences*. **2011**, *108*, 19824-19829.

Xing, Y.; Jia, W.; Zhang, J. AtMEK1 mediates stress-induced gene expression of CAT1 catalase by triggering H2O2 production in Arabidopsis. *Journal of Experimental Botany*. **2007**, *58*, 2969-2981.

Xiong, W.; Ferrell, J. E. A positive-feedback-based bistable 'memory module' that governs a cell fate decision. *Nature*. **2003**, *426*, 460-465.

Xu, J.; Zhang, S. Mitogen-activated protein kinase cascades in signaling plant growth and development. *Trends in Plant Science*. **2015**, *20*, 56-64.

Yamada, K.; Yamaguchi, K.; Shirakawa, T.; Nakagami, H.; Mine, A.; Ishikawa, K.; Fujiwara, M.; Narusaka, M.; Narusaka, Y.; Ichimura, K.; Kobayashi, Y. The Arabidopsis CERK 1-associated kinase PBL 27 connects chitin perception to MAPK activation. *The EMBO Journal*. **2016**, *35*, 2468-2483.

Yamaguchi, Y.; Huffaker, A.; Bryan, A. C.; Tax, F. E.; Ryan, C. A. PEPR2 is a second receptor for the Pep1 and Pep2 peptides and contributes to defense responses in Arabidopsis. *The Plant Cell*. **2010**, *22*, 508-522.

Yamaguchi, Y.; Pearce, G.; Ryan, C. A. The cell surface leucine-rich repeat receptor for AtPep1, an endogenous peptide elicitor in Arabidopsis, is functional in transgenic tobacco cells. *Proceedings of the National Academy of Sciences*. **2006**, *103*, 10104-10109.

Yu, L.; Nie, J.; Cao, C.; Jin, Y.; Yan, M.; Wang, F.; Liu, J.; Xiao, Y.; Liang, Y.; Zhang, W. Phosphatidic acid mediates salt stress response by regulation of MPK6 in *Arabidopsis thaliana*. *New Phytologist*. **2010**, *188*, 762-773.

Zaman, N.; Seitz, K.; Kabir, M.; George-Schreder, L.S.; Shepstone, I.; Liu, Y.; Zhang, S.; Krysan, P.J. A Förster resonance energy transfer sensor for live-cell imaging of mitogen-activated protein kinase activity in Arabidopsis. *The Plant Journal*. **2019**, *97*, 970-983.

Zeke, A.; Bastys, T.; Alexa, A.; Garai, Á.; Mészáros, B.; Kirsch, K.; Dosztányi, Z.; Kalinina, O.V. Reményi, A. Systematic discovery of linear binding motifs targeting an ancient protein interaction surface on MAP kinases. *Molecular Systems Biology*. **2015**, *11*, 837.

Zhang, M.; Su, J.; Zhang, Y.; Xu, J.; Zhang, S. Conveying endogenous and exogenous signals: MAPK cascades in plant growth and defense. *Current Opinion in Plant Biology*. **2018**, *45*, 1-10.

Zhang, Q.; Bhattacharya, S.; Andersen, M. E. Ultrasensitive response motifs: basic amplifiers in molecular signalling networks. *Open Biology*. **2013**, *3*, 130031.

Zhang, Y.; Wang, P.; Shao, W.; Zhu, J. K.; Dong, J. The BASL polarity protein controls a MAPK signaling feedback loop in asymmetric cell division. *Developmental Cell*. **2015**, *33*, 136-149.

Zhu, Q.; Shao, Y.; Ge, S.; Zhang, M.; Zhang, T.; Hu, X.; Liu, Y.; Walker, J.; Zhang, S.; Xu, J. A MAPK cascade downstream of IDA–HAE/HSL2 ligand–receptor pair in lateral root emergence. *Nature Plants*. **2019**, *5*, 414-423.

Zipfel, C.; Kunze, G.; Chinchilla, D.; Caniard, A.; Jones, J. D.; Boller, T.; Felix, G. Perception of the bacterial PAMP EF-Tu by the receptor EFR restricts Agrobacterium-mediated transformation. *Cell*. **2006**, *125*, 749-760.

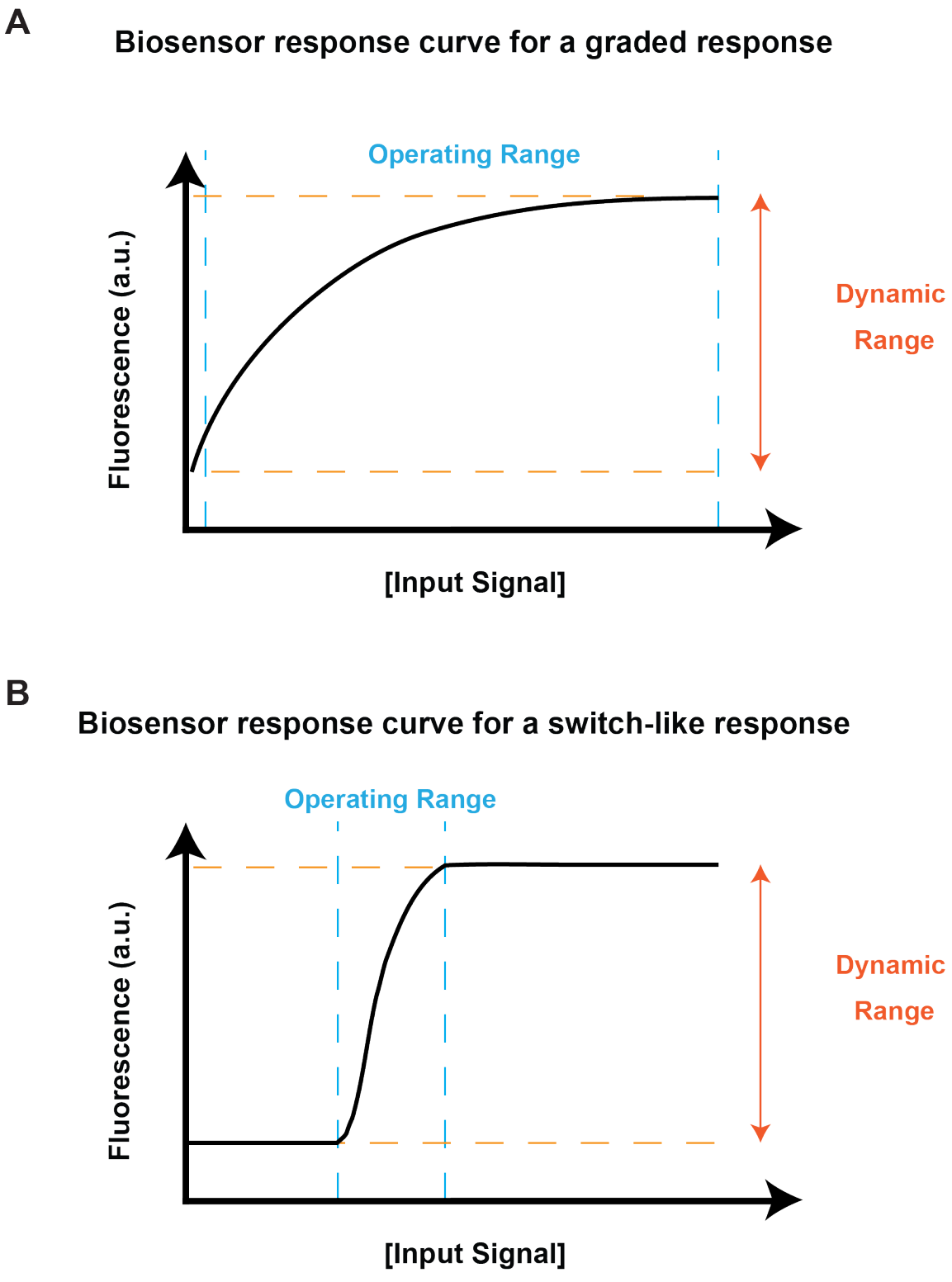

Figure 1. Typical biosensor response curves for a graded or switch-like response. The dynamic range is ratio between the maximum and minimum biosensor output expression. The operating range gives the concentrations of target which can be detected through a change in the output. (a.u.) indicates arbitrary units.